COUPLED CHANNEL ALPHA DECAY THEORY FOR EVEN- AND ODD-MASS LIGHT AND HEAVY NUCLEI

Elizabeth A. Rauscher
(Ph.D. thesis)

February, 1978

Prepared for the U. S. Department of Energy
under Contract W-7405-ENG-48

COUPLED CHANNEL ALPHA DECAY THEORY FOR EVEN- AND ODD-MASS LIGHT AND HEAVY NUCLEI

Elizabeth A. Rauscher

Nuclear Science Division
Lawrence Berkeley Laboratory
University of California
Berkeley, California 94720

ABSTRACT

The detailed mechanism of alpha decay and its implications about the structure of nuclear matter has been a study of much interest over the last fifty years. We have examined four major approaches to the theoretical calculation of alpha decay widths for light and heavy, even- and odd-mass nuclei. Application of the microscopic shell model rate theory as well as macroscopic models utilizing the coupled channel formalism have been studied.

Use of the R-matrix and S-matrix theories have been applied in order to overcome problems involving dependency on the connection radius and nuclear potential parameters of the relative and absolute alpha decay widths.

We calculate the alpha decay branching ratios for the 3^- and 5^- states to the ground state decay of the ^{212m}Po isomeric state to the spherically symmetric daughter ^{208}Pb. Improved fit to experiment is achieved by considering a smaller connection radius and also by using the

coupled channel formalism of the radial Schrödinger equation for the two-channel $\ell = 18$ and $\ell = 15$ waves in which the coupling is primarily due to collective octupole vibrational field.

Since the coupled channel formalism appears to be useful in understanding some features of the alpha decay problem, we extend this calculation to alpha decay of odd-mass nuclei. We examine the relationship of daughter excitation by alpha emission and inelastic alpha scattering on daughter nuclei. Again, an exact numerical coupled-channel integration treatment is applied to the alpha decay of the odd-mass spheroidal nuclei, ^{253}Es and ^{255}Fm, both ground state $7/2^+$. The only non-central coupling of importance between an emitted alpha particle and rotational final states in the daughter nucleus involves the intrinsic quadrupole moment of the daughter. Relative intensity show a reasonable fit but these are still an underestimation to the decay of the 9/2 states and overestimates the intensity to the 11/2 states.

Because of the dependence of the calculated intensity ratios on the nuclear connection radius, and the failure of earlier alpha decay theories to reproduce the absolute alpha decay rate widths and, in some cases, the relative widths, we have developed a new formalism for alpha decay. This formation utilizes the time-dependent perturbation method to develop an expression for the alpha decay width based on the unified reaction theory or R-matrix theory. The new expression does not depend on the radial boundary conditions, but dependence on the nuclear potential well depth remains.

We examine the resonance compound nuclear decay process in terms of the energy and partial angular momentum wave dependence of the complex

scattering matrix elements. It is of interest to examine the S-matrix formalism for a few quasi-elastic channels in terms of the detailed qualitative properties of the structure of the S-matrix. The role of the alpha clustering in the nuclear surface and interior and in terms of the alpha (α,α') scattering process is discussed as well as other implications of the alpha decay process on the properties of nuclear matter. It is believed that extensive evolution of the alpha decay mechanism will lead to a better understanding of nuclear structure, the nuclear potential, and of nuclear forces.

TABLE OF CONTENTS

I. INTRODUCTION

Application of the coupled channel formalism is made for the alpha decay of even and odd mass (spherical and spheroidal) light and heavy nuclei.

In the second section of this paper, we will examine the alpha decay of the high spin, $J = 18^+$ state of ^{212m}Po to the ground state and various excited states of the spherically symmetric daughter ^{208}Pb as a simple barrier penetration problem. We apply the microscopic "shell model" rate theory neglecting coupling effects and find that both the experimental 1% alpha branch to the 3^-, first excited state of ^{208}Pb, and the 2% alpha branch to the second 5^- state are underestimated for a nuclear connection radius of $R = 9.5f$. Choosing a connection radius of $R = 7.5f$ results in a satisfactory agreement for the branching to the 5^- state but leaves over an order of magnitude discrepancy for the branching to the 3^- state.[1]

Coupled channeling is introduced to attempt to rectify this discrepancy.[2,3] Radial Schrödinger equations for two-channel $\ell = 18$ and $\ell = 15$ waves coupled to the collective octupole vibrational field are inwardly numerically integrated. For $R \geqq 7.5f$ the intensity to the 3^- level is still underestimated for the parameters we used. (Detailed examination of the role of the connection-matching radius will be presented in the fourth section of this paper.)

Since it is felt that the coupled channel formalism holds great promise in comprehending the mechanism of alpha decay we have extended this calculation to alpha decay of odd-mass nuclei as well as examined

the relationship of daughter excitation by alpha emission and inelastic alpha scattering on daughter nuclei.

We have examined vibrational coupling in the second section of this paper and in the third section we will examine the coupled channel formalism for odd-mass nuclei with rotational final states of excitation.

In Section III of this paper, an exact numerical coupled-channel integration treatment is applied to the alpha decay of odd-mass spheroidal nuclei. The only non-central coupling of importance between an emitted alpha particle and rotational final states in the daughter nucleus involves the intrinsic quadrupole moment of the daughter. The nuclei ^{253}Es and ^{255}Fm are ideal cases to examine since alpha transitions to the favored bands are well known and angular distribution data from low temperature nuclear alignment is available.[4]

Two commonly used approximations were examined in detail: First, that near the nuclear surface there is zero projection of orbital angular momentum of favored alpha waves along the cylindrical symmetry axis of the daughter nucleus[5] and second, that the intensity of each alpha-particle ℓ-wave is proportional to the product of a squared Clebsch-Gordon coefficient and the calculated spherical barrier penetrability factor.[6] It is found that neither approximation holds within experimental error, and $m_\ell \neq 0$ alpha wave components must be introduced at the nuclear surface to give agreement with experimental intensities for both $\ell = 2$ and $\ell = 4$ waves.

To attempt to rectify the problems of the dependence of the calculated intensity ratios on the connection radius, we use the time-dependent perturbation method (presented in the first part of Section IV).

With this method, a new expression for the alpha decay width is introduced. Because of the failure of earlier alpha decay theories to reproduce the absolute alpha decay rate widths and, in some cases, the relative widths, a new formalism for alpha decay has been developed based on the unified reaction theory or R-matrix theory.[7] This theory, which uses shell model wave functions, and utilizes the time-dependent perturbation method, is independent of the nuclear radius matching parameter and the boundary conditions at infinity.[8] Previous microscopic alpha decay theories appear to deal improperly with the problem of the mismatch at the nuclear radius of logarithmic derivatives of the alpha wave functions in inner and outer regions.[9] The new proposed theory has the advantage over the previous ones in that it makes it possible to calculate the absolute value of the decay rate with reasonable accuracy, which was not previously possible. Both single-level and coupled-channel calculations have been made.

Although the problem of the discontinuities at the matching radius appear to be eliminated by the R-matrix approach, it is found that the results of the calculations performed for the ^{212}Po and ^{210}Po ground state decays are sensitive to the well-depth parameter of the alpha-nucleus potential. A real part well-depth of about V_o = -120 MeV gives good agreement with the absolute values of experimental decay rates.[10] In Section IV we briefly discuss the time dependent reaction theory and its drawbacks. Again the model depends on optical model well-depth parameters.

In Section II and III, the coupled channel calculations lead to an emphasis on the uncertainty in the radius parameter, whereas the R-matrix approach, presented in Section IV, emphasizes the uncertainty in the

well-depth parameter. A third approach is detailed in Section V, where we relate the R-matrix approach to the collision theory, or S-matrix approach. With the formalism dependent on the calculation of a resonant alpha decay in terms of the complex scattering matrix elements, the extreme sensitivity to Woods-Saxon parameters is reduced, and it then becomes possible to calculate absolute decay widths with this method. We examine the effects on the resonance width with various strengths of the absorbative part of the Woods-Saxon nuclear potential.

The calculation of resonance cross section alpha decay widths in terms of the complex elements of the (α,α) and (α,α') scattering matrix is examined. It appears that it is fruitful to explore a model where we may be able to determine the alpha-wave particle-wave decay width in terms of a resonance process which is calculated in terms of the S-matrix for elastic and inelastic scattering. In this model the resolution of the problem of the mix-match in the nuclear radius at the inner classical turning point appears to be overcome.

The real and imaginary S-matrix elements in the angular momentum or ℓ-plane are calculated for a few quasi-elastic channels (elastic and several alpha particle removal channels).

The early success of the H.Bethe[11] and G.Gamow alpha cluster models[12] as well as the R. G. Thomas[13] and A.Mang[14] microscopic models are discussed in the context of this new approach in which we calculate absolute decay widths in terms of the resonance widths of the complex elements of the scattering matrix in the ℓ-plane. We examined in detail the role of the (α,α') scattering process, the alpha cluster on the nuclear surface assumption and the calculation of coupled channel few level alpha decay

width. The early models of Gamow, which were quite successful, were based on the assumption of the alpha cluster retaining its identity in the nuclear box well. The new S-matrix alpha scattering capture and emission also implies the alpha cluster model as a viable one.

Important consequences of the theory are a better understanding of the (1) alpha cluster formation, (2) compound nucleus formation, (3) some mechanics of alpha decay, (4) possible nuclear transfer mechanisms, (5) absorption processes to inelastic channels, and (6) the role of the nuclear potential depth V_o and nuclear radius R_o in the theory of alpha decay.

II. MICROSCOPIC AND MACROSCOPIC ALPHA DECAY RATE THEORY FOR ^{212m}Po

A. Previous Alpha Decay Models

We start from the shell model rate theory of H. J. Mang[14] and simple barrier penetrability calculation. Macroscopic theory in its ordinary form of a particle in a potential well yields alpha decay rates roughly proportional to a Coulomb barrier penetration factor arising from the solution of a separate Schrödinger equation for each alpha group of given ℓ-value. Preston early considered[15] the effects of the coupling arising from the electromagnetic field associated with transitions between various states of the daughter nucleus; these considerations led to sets of coupled, second-order, linear differential equations in the present case where we are considering coupling in the nuclear barrier region.

The coupling effects have been studied extensively for the rotational states of deformed nuclei, where such effects are predominantly due to the large collective E2 transition strengths and the small energy differences between various rotational states.[16] The magnitude of the coupling terms for alpha particles outside the range of nucleon forces is uniquely related to the reduced electric transition probability (where nucleon forces can be neglected) between the states is being considered (see Ref. 16, Eq. (6.3).

The one-body alpha decay theory, even when augmented with the inter-channel coupling treatment, is inadequate for calculating absolute alpha intensities and is even unable to explain the relative intensities of alpha decay to the various excited states of the daughter nucleus.[17] The "microscopic" or shell-model theoretical approach of Mang has proved

remarkably successful in calculating alpha relative intensities in spherical nuclei (Bi, Po region) without regard to interchannel coupling[18] and in spheroidal nuclei,[19] taking such coupling into account by Fröman's matrix method.[20] It is necessary to specify a nuclear surface, characterized by a radius R_o, where the alpha wave function of the inner region joins that of the outer which we term the connection radius. It is fortunate that relative decay rates of the theory do not usually appear to be highly sensitive to the exact choice of R_o.[18] It is found in the present work that the relative intensity ratios of excited states to ground are sensitive to the choice of R_o. Also we have examined problems of connection radius matching in an earlier paper.[3] In Section IV of this paper we will consider the possible resolution of the intensity ratio dependence on R_o.

B. Choice of Optical Model Parameters

The present case involves the region of spherical nuclei where the shell-model theoretical method without interchannel coupling has difficulty with the relative alpha intensities and where the results appear sensitive to the choice of R_o. This case is the remarkable super-high-spin isomer of ^{212}Po, which we now believe to be spin 18, even parity, on the basis of recent shell-model calculations.[21] The experimental alpha decay energies and intensities[22] for ^{212m}Po are summarized in Fig. 1.

This alpha emitter is unusual in that the angular momentum values in the alpha decay are so high. Suppose we take the following alpha-nuclear potential, which is the real part of a potential used for optical model fits of alpha elastic scattering angular distributions, which we

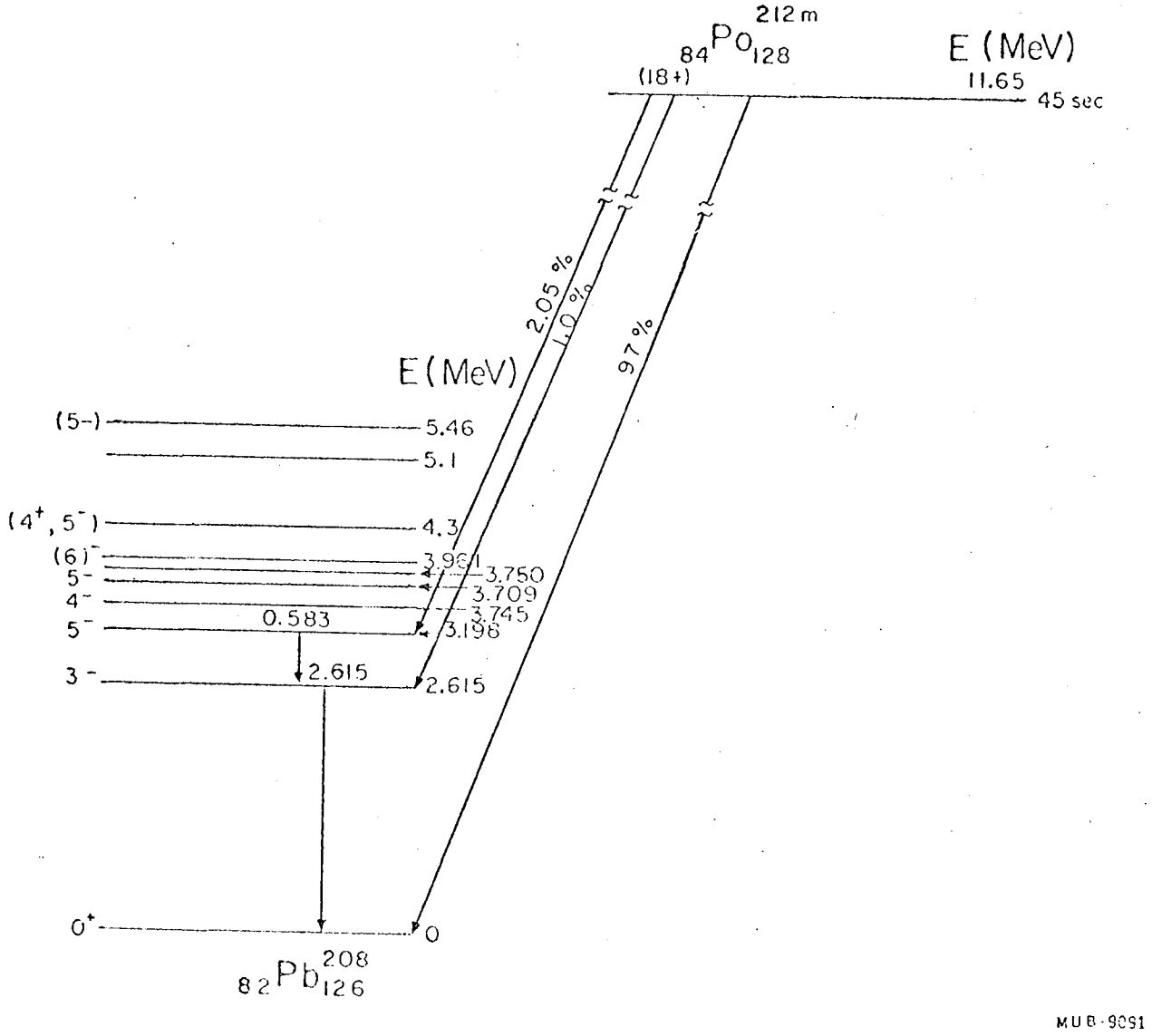

Fig. 1. Energy levels of ^{208}Pb and the alpha decay scheme of ^{212m}Po (cf. ref. 22). Their work favors very deep potentials of the order of 200 MeV. Earlier work was performed with the more shallow potentials since most scattering experiments were interpreted in this manner. The McFadden-Satchler[24] work encouraged us to proceed with the investigation of the case of deeper well depths.

will examine further in Section IV.

$$V_N(r) = \frac{-V_o}{1 + \exp \frac{r - r_o A^{1/3} - a}{d}} \qquad (1)$$

with V_o = 35.0 MeV, R_o = 1.17 f, a = 2.17 f, and d = 0.576 f. (We will examine other choices for these parameters in Sections III and IV.) The resulting effective potentials in the radial wave equation for various alpha partial waves are plotted in Fig. 2. The alpha decay energy of ^{212m}Po is 11.65 MeV, and we see that we are confronted with the unusual situation of the absence of an inner classical turning point for the $\ell = 18$ partial wave, because the inner minimum potential energy is more than 27 MeV. The same is true of the lower energy groups to the 3^- and 5^- excited states.

The alpha-decay barrier width and hence barrier penetrability, as calculated using realistic optical potentials is undefined, that is, both the nucleon connection radius, R_o, and potential well depth, V_o, cannot be simultaneously determined. We introduce both the time-dependent perturbation method similar to the one used by H. Feshbach,[23] which will be presented in Section IV.

If we used a Woods-Saxon nuclear potential with well depth V_o exceeding 50 MeV, the inner turning points would reappear, but the arbitrariness of the problem remains. We attempt to rectify this in Section IV. Optical-model analyses for alpha scattering have been unable to determine very well the potential in the nuclear interior, because alpha particles have such short mean free path in nuclear matter that alpha scattering does not sample the nuclear interior but only the

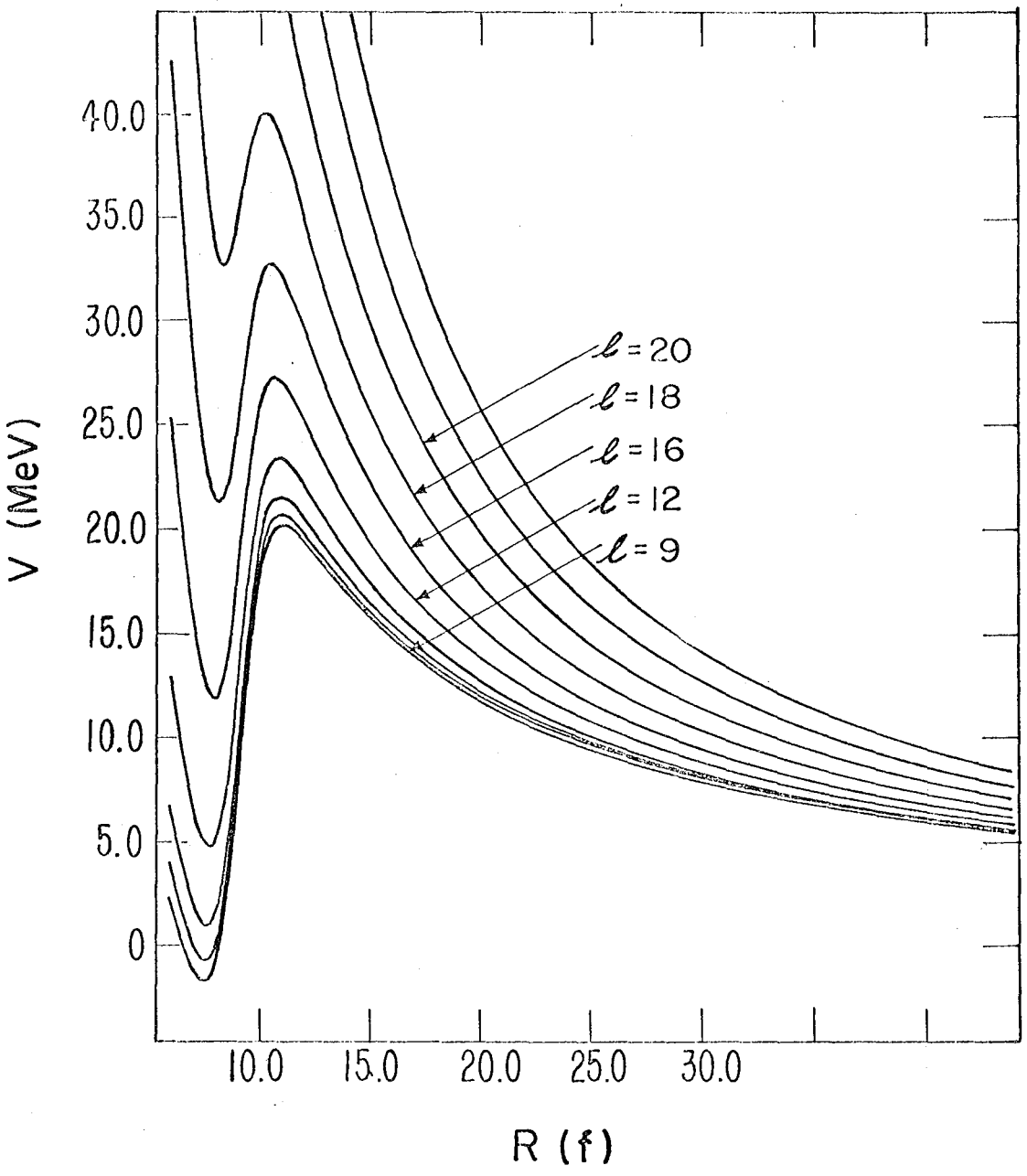

XBL 783-2443

Fig. 2. Potential energy (including centrifugal term) for various alpha partial waves on ^{208}Pb, is given as

$$V(R) = \frac{2Ze^2}{R} + \frac{\hbar^2(\ell + 1/2)^2}{2\mu R^2} - V_0\left[1 + \exp\frac{R - r_0A^{1/3} - a}{d}\right]^{-1}$$

with optical model parameters $V_0 = 35$ MeV, $r_0 = 1.17$ f, $a = 2.17$ f, and $d = 0.576$ f.

surface region. This fact lends credence to the alpha particle cluster model in which the alpha particle is considered to have a specific identity on the nuclear surface.

It appears from the R-matrix and S-matrix approach (presented in Section IV) that there is consistence with the thorough alpha optical-model analysis of L. McFadden and G. R. Satchler.[24]

C. Alpha Decay Theory Neglecting Channel Coupling

Let us first apply simple microscopic alpha decay rate theory without channel coupling to this case. For the 3^- first excited state of ^{208}Pb, calculations based on the random phase approximation (RPA) have been performed by H. V. Gillet, A. M. Green and E. A. Sanderson.[31] The RPA method admixes two-particle-two-hole (2p-2h) states into the ground state wave function of ^{208}Pb, and 3p-3h states into the 3^- state function in addition to the 1p-1h states. Since the ground state core correlations were not included in the ^{212m}Po wave functions[21] we shall use, the use of the ^{208}Pb wave functions obtained by the usual Tamm-Dancoff shell theory which are more consistent with the present calculation.

Two different shell model wave functions for the 3^- state of ^{208}Pb are considered here. One is calculated by W. T. Pinkston,[26] and another is by W. W. True and W. T. Pinkston.[27] The former does not reproduce the correct energy, but in the latter model True succeeded in getting a nice agreement by taking into account twenty 1p-1h configurations. True included the $4s_{1/2}$, $2g_{7/2}$, and $3d_{3/2}$ neutron levels in his particle configurations, while they were neglected in the shell model calculations[21] on ^{212}Po. Among the many configurations in ^{212m}Po involving the above neutron

orbitals, only the following four configurations can have spin 18: $[(i_{13/2})^2(g_{7/2})^2]$, $[(i_{13/2})^2(g_{9/2}g_{7/2})]$, $[(i_{13/2})^2(i_{11/2}g_{7/2})]$ and $[(i_{13/2})^2(d_{5/2}g_{7/2})]$. (The proton configuration is written first, then the neutron.) Since the amounts of the mixing of those components in the isomeric state would be very small, we may use True's 3^- state wave function as is, without mixing, for our calculations. To facilitate comparison with earlier alpha rate calculations of H. D. Zen[14] we list the principal components with greater than 1% contribution to parent and daughter wave functions in Table 1.

Adopting the approximation of the small alpha size limit, as in Ref. 29, we get the following expression from Ref. 29 for the reduced amplitude, γ_α, at the radius, R,

$$\gamma_\alpha = \frac{\hbar^2}{2\mu}\sqrt{2}\int\left\langle (j_1 j_2)J_p(j_3 j_4)J_n JM\right| \cdot \chi_\alpha \sum_m (LjM - mm|JM)Y_{LM-m}(\hat{R}) \times |j_4, j_5^{-1}; jm\rangle$$

$$\times\, dx_N dx_\alpha d\Omega_R = C\, 2 N_{j_1 j_2} N_{j_3 j_4} \sum_{J_n'} (-)^{(j_2 - 1_2 - 1/2) + (j_5 - 1_5 - 1/2)}$$

$$\times \sqrt{[j_1][j_2][j_3][j_5][J_n][J_n'][j]} \times (j_1 j_2 1/2 - 1/2\ J_p 0)(j_3 j_5 1/2$$

$$-\ 1/2|J_n' 0)(J_p J_n' 00|L0) \times (-)^{j_4 + j_5 + J_n + J_n'} W(j_3 j_4 J_n' j; J_n j_5) W(j J_n' J J_p J_n L)$$

$$\times\, R_1(R)\ R_2(R)\ R_3(R)\ R_5(R)$$

where C is a constant independent of nuclear structure, $R_i(a)$ is the value of the i^{th} particle wave function at the radius R; and $[j_1]$ stands stands for $2j_1 + 1$; and N_{ij} is

TABLE 1. Parent and daughter wave functions for ^{212m}Po and ^{208}Pb (Ref. 22).

$$\chi_{18^+}(^{212m}\mathrm{Po}) = -0.810\,|\,(h_{9/2})^2_8\,(g_{9/2}i_{11/2})_{10}\rangle$$
$$-0.570\,|\,(h_{9/2}f_{7/2})_8\,(g_{9/2}i_{11/2})_{10}\rangle$$
$$+0.104\,|\,(h_{9/2})^2_3\,(i_{11/2})^2_{10}\rangle + 24 \text{ smaller components}$$

$$\chi_{3^-}(^{208}\mathrm{Pb})\,(\text{Ref. 26}) = -0.124|f^{-1}_{5/2}\,g_{9/2}\rangle_N + 0.616\,f^{-1}_{5/2}\,i_{11/2}\rangle_N$$
$$+0.737|d^{-1}_{3/2}\,h_{9/2}\rangle_P + 0.237\,s^{-1}_{1/2}\,f_{7/2}\rangle_P$$
$$+ 1 \text{ component } (< 0.1)$$

$$\chi_{3^-}(^{208}\mathrm{Pb})\,(\text{Ref. 27}) = -0.166|f^{-1}_{5/2}\,g_{9/2}\rangle_N + 0.431|p^{-1}_{3/2}\,g_{9/2}\rangle_N$$
$$+0.528|d^{-1}_{3/2}\,h_{9/2}\rangle_P + 0.396|f^{-1}_{5/2}\,i_{11/2}\rangle_N$$
$$-0.120|p^{-1}_{1/2}\,d_{5/2}\rangle_N + 0.375|s^{-1}_{1/2}\,f_{7/2}\rangle_P$$
$$-0.151|d^{-1}_{3/2}\,f_{7/2}\rangle_P + 0.182|f^{-1}_{7/2}\,g_{9/2}\rangle_N$$
$$+0.227|i^{-1}_{13/2}\,j_{15/2}\rangle_N + 0.183|p^{-1}_{1/2}\,g_{7/2}\rangle_N$$
$$+0.135|f^{-1}_{5/2}\,g_{7/2}\rangle_N + 9 \text{ components } (< 0.1)$$

$$\chi_{5^-}(^{208}\mathrm{Pb})\,(\text{Ref. 27}) = -0.801|p^{-1}_{1/2}\,g_{9/2}\rangle_N - 0.131|f^{-1}_{5/2}\,g_{9/2}\rangle_N$$
$$+0.250|p^{-1}_{1/2}\,i_{11/2}\rangle_N + 0.320|s^{-1}_{1/2}\,h_{9/2}\rangle_P$$
$$+0.144|p^{-1}_{3/2}\,g_{9/2}\rangle_N + 0.225|d^{-1}_{3/2}\,h_{9/2}\rangle_P$$
$$+0.171|f^{-1}_{5/2}\,i_{11/2}\rangle_N - 0.185|d^{-1}_{3/2}\,f_{7/2}\rangle_P$$
$$+0.105|p^{-1}_{3/2}\,g_{3/2}\rangle_N + 11 \text{ components } (< 0.1)$$

$$N_{ij} = \sqrt{2} \qquad \text{for} \quad i \neq j$$
$$N_{ij} = 1 \qquad \text{for} \quad i = j \tag{3}$$

The radial wave functions of J. Blomqvist and S. Wahlborn,[30] evaluated at a radius R = 9.5 f, are used for numerical calculation. The results of these numerical calculations are summarized in Table 2.

The usual definition of barrier penetrability factor is given as $[F_\ell^2(R_0) + G_\ell^2(R_0)]^{-1}$, where F and G are the regular and irregular Coulomb functions, or their continuations in the presence of a nuclear potential. For the cases in this calculation, $F_\ell^2 \ll G_\ell^2$, and F_ℓ^2 are ignored. The first order WKB approximation for this penetrability is as follows:

$$\frac{1}{G_\ell^2(R_0)} \approx \frac{k_\ell}{\xi_\ell} \exp\left[-2\int_R^{R_t} \frac{2\mu(V_\ell - Q)}{\hbar}\, dr\right] \tag{4}$$

where

$$\xi_\ell = \frac{[2\mu(V_\ell(R)) - Q]^{1/2}}{\hbar} \quad .$$

We define a "zeroth order" penetrability factor differing in that it drops the pre-exponential factor to avoid problems with the singularity in this term. The first order WKB approximation at the inner classical turning point has a singularity when $2\mu(V_\ell(k))$ approaches Q in the ξ_ℓ term. The barrier penetrability factor in this form is distinguished by the superscript zero, and is simply the exponential function of argument twice the WKB (Wentzel, Kramers, Brillouin) integral from outer turning point, R_t, integrated into the radius R.

TABLE 2. Shell-model theoretical alpha-reduced transition matrix elements and their squares (radius R = 9.5f).

Decay Mode	ℓ	$\gamma_{\alpha\ell}$	$\gamma^2_{\alpha\ell}$
$^{212m}Po(18^+) \rightarrow {}^{308}Pb(0^+)$	18	+0.556	0.309
$\rightarrow {}^{208}Pb(3^-)$ (Ref. 26)	15	-0.2039	0.0416
$\rightarrow {}^{208}Pb(3^-)$ (Ref. 27)	15	-0.0720	0.0052
	17	+0.0326	0.0011
	19	+0.0005	0.0000
	21	-0.0000	0.0000
$\rightarrow {}^{208}Pb(5^-)$ (Ref. 27)	13	+0.3284	0.1078
	15	+0.0156	0.0002
	17	-0.0020	0.0000
	19	+0.0001	0.0000
	21	-0.0001	0.0000
	23	intrinsically forbidden	

$$P_\ell^{(0)}(Q,R) = \exp\left[-2\int_R^{R_t} \frac{2\mu(V_\ell - Q)}{\hbar}\right] \qquad (5)$$

where V_ℓ is the sum of Coulomb and nuclear potentials

$$V_\ell(r) = \frac{2Ze^2}{r} + \frac{\hbar^2(\ell + 1/2)^2}{2\mu r^2} - V_N(r) \qquad (6)$$

where $V_N(r)$ as defined by Eq. (1), with the same parameters (35 MeV nuclear potential) as used for Fig. 2. In Table 3 the penetrability factors are given according to Eq. (5) for all possible partial waves to the 0^+, 3^-, and 5^- states of ^{208}Pb, evaluated at several values of the lower limit of R. Also given are the s-wave penetrabilities for ^{212}Po ground state decay. To give some feeling for effect on the absolute penetrabilities associated with the uncertainties in the nucleon potential, we compare the penetrabilities in Table 3 with some calculated with the deeper potential of k. The parameters for Poggenberg's theoretical calculation, which appears to be more realistic upon further calculation, see Section III, Table 4, are V_o = -74.0 MeV, r_o = 1.17 f, a = 1.6 f, and d = 0.565 f for Eq. (1) here. For example, comparing for ℓ = 17, R_o = 9.5 f, and Q_ℓ = 9.291 MeV, the P_ℓ in Table 4 is about 30% smaller. Other comparisons give similar results for the P_ℓ's for the deeper potential.

By definition of the reduced width, γ_ℓ^2 the partial decay rate is (R. G. Thomas[31])

$$\lambda_\ell = \frac{2\gamma_\ell^2}{\hbar} \frac{\xi_\ell}{(F_\ell^2 + G_\ell^2)} \approx \frac{2\gamma_\ell^2 k_\ell}{\hbar} P_\ell^{(0)} \qquad (7)$$

TABLE 3. "Zeroth-order-WKB" barrier penetration factors at various radii $V_0 = 35$ MeV.

Q_α (MeV)	ℓ	R_0(f) 6	7	7.5	8	9.5
			Isomer Decay			
11.906	18	6.640(-24)	9.725(-22)	7.338(-21)	4.394(-20)	9.293(-18)
9.291	15	1.984(-25)	1.245(-23)	6.310(-23)	2.591(-22)	2.497(-20)
9.291	17	2.867(-28)	3.623(-26)	2.604(-25)	1.513(-24)	3.240(-22)
9.291	19	3.148(-31)	7.850(-29)	7.846(-28)	6.284(-27)	2.899(-24)
9.291	21	2.598(-34)	1.262(-31)	1.732(-30)	1.883(-28)	1.837(-26)
8.720	13	3.060(-24)	9.832(-23)	3.533(-22)	1.026(-21)	4.784(-20)
8.720	15	5.474(-27)	3.609(-25)	1.895(-24)	8.080(-24)	8.655(-22)
8.720	17	7.612(-30)	1.006(-27)	7.425(-27)	4.446(-26)	1.041(-23)
8.720	19	7.897(-33)	2.048(-30)	2.094(-29)	1.721(-28)	8.359(-26)
8.720	21	6.091(-36)	3.061(-33)	4.288(-32)	4.770(-31)	4.988(-28)
8.720	23	< (-38)	3.397(-36)	6.467(-35)	9.642(-34)	2.091(-30)
			Ground State Decay			
8.720	0	*	*	*	*	4.295(-14)

*Penetrability at inner turning point of 9.124 f is 2.706×10^{-14}.

TABLE 4. "Zeroth-order-WKB" barrier penetration factors at inner t.p. of 9.5f, $V_0 = 74.0$ MeV.

	Q_α = 11.906 MeV		Q_α = 9.291 MeV		Q_α = 8.720 MeV		Q_α = 8.950 MeV	
	R_0(f) i.t.p.	P_ℓ	R_0(f) i.t.p.	P_ℓ	R_0(f) i.t.p.	P_ℓ	R_0(f) i.t.p.	P_ℓ
ℓ=18	8.368	3.209(-19)						
	9.5	8.305(-18)						
ℓ=13					8.712	6.196(-21)		
					9.5	4.218(-20)		
ℓ=15			8.573	1.898(-21)	8.551	5.978(-23)		
			9.5	2.217(-20)	9.5	7.697(-22)		
ℓ=17			8.374	1.100(-22)	8.349	3.168(-25)		
			9.5	2.901(-22)	9.5	9.334(-24)		
ℓ=19			8.087	3.265(-26)	8.053	8.455(-28)		
			9.5	2.615(-24)	9.5	7.754(-26)		
ℓ=21			7.5*	2.932(-28)	7.5	6.799(-31)		
			9.5	1.668(-26)	9.5	4.534(-28)		
ℓ-23					7.5	5.970(-34)		
					9.5	1.912(-30)		
ℓ=0							9.220	2.498(-14)
							9.5	3.596(-14)

*The inner turning point is <6.0f for the ℓ=21 and ℓ=23 waves.

or are proportional to the product of γ_ℓ^2 from Table 1, $P_\ell^{(0)}$ at 9.5 f in the last column of Table 3, and the wave number, k_ℓ. It is readily seen that the theory predicts that partial waves of higher ℓ than the lowest value are never more than a few tenths of a percent. If we ignore higher partial waves, the theory predicts an alpha intensity ratio as follows at R of 9.5 f for the references listed after each calculated result.

$$\frac{I(18^+ \xrightarrow{15} 3^-)}{I(18^+ \xrightarrow{18} 0^+)} = 4.0 \times 10^{-5} \quad \text{(Ref. 27)}, \quad \text{or} \tag{8a}$$

$$= 3.2 \times 10^{-4} \quad \text{(Ref. 26)},$$

to be compared with the experimental ratio of 1.0×10^{-2} or even a factor of 100 off.

In a similar fashion we theoretically get the following

$$\frac{I(18^+ \xrightarrow{13} 5^-)}{I(18^+ \xrightarrow{18} 0^+)} = 1.5 \times 10^{-3} \quad \text{(Ref. 27)} \tag{8b}$$

to be compared with the experimental ratio of 2.1×10^{-2} which is in better agreement, again over a factor of 10 off.

Before we turn to channel coupling in an attempt to understand these very serious discrepancies, let us consider the effect of a smaller connection radius, R. Because of the very high ℓ values involved, there is a considerable sensitivity to the value of the connection radius R for the predicted intensity ratios. Using the Blomqvist-Wahlborn radial functions for R = 7.5f instead of 9.5f and the same parameters otherwise as for calculations of Table 1, we find only moderate changes in the ratio $\gamma^2(18^+ \xrightarrow{13} 5^-)/\gamma^2(18^+ \xrightarrow{18} 0^+)$, specifically a decrease of 29% for the wave function of Ref. 27 and an increase of 15% for that of Ref. 26 in

going from 9.5f to 7.5f and for the ratio $\gamma^2(18^+ \xrightarrow{13} 5^-)/\gamma^2(18^+ \xrightarrow{18} 0^+)$ there is an increase of 16%.

By inspection of Table 3, one sees that the relative values of barrier penetrability change very markedly for a similar change of radius R. We get the following revised theoretical intensity ratios at R = 7.5f.

$$\frac{I(18^+ \xrightarrow{15} 3^-)}{I(18^+ \xrightarrow{18} 0^+)} \approx 1.0 \times 10^{-4} \text{ (Ref. 33)} \quad \text{or} \quad \text{(9a)}$$

$$\approx 1.3 \times 10^{-3} \text{ (Ref. 32)}$$

$$\frac{I(18^+ \xrightarrow{13} 5^-)}{I(18^+ \xrightarrow{18} 0^+)} \approx 1.9 \times 10^{-2} \text{ (Ref. 33)} \quad \text{(9b)}$$

which gives us a factor of 10 in the correct direction.

We see that the latter theoretical intensity ratio (decay to 5^-) is completely in agreement with experiment for R = 7.5f, but the theoretical relative intensity to the 3^- state is still one or two orders of magnitude too small, depending on which daughter wave functions are used.

Note also that in the paper of N. Glendenning and K. Harada[21] that the microscopic alpha rate calculations gave too large an isomeric decay rate relative to ground decay rate, i.e., a discrepancy factor of 45 at R = 9.5f and 18 at R = 9.0f. J. O. Rasmussen has given formulas[16] for microscopic theory with R inside the inner turning point; using this approach and considering that the effective penetrability factor is approximately constant at 2.7×10^{-14} for ground decay for R < 9.124f (see Table 3), perfect agreement with experiment is obtained around R = 8f, and at smaller radii the disagreement is of the opposite sense,

that is, theory becomes larger than the experimental rates. Here we have assumed the ratios of γ^2 values to be nearly independent of the radius.

The indications are that a joining radius R in the neighborhood of R = 7.5 to 8.5f is more nearly correct with the shell-model nuclear wave functions employed. However, even with the R values in this vicinity, the underestimate of decay intensity to the 3^- state still remains serious. Our difficulty is probably consistent with the results of H. D. Zeh,[28] who found for several combinations of unmixed shell-model initial and final states, that the theoretical fraction of alpha decay to the 3^- was too low. Two of his three combinations, giving agreement with theory are only minor contributors in the configuration-mixed wave functions we used (for protons and neutrons respectively), but one, namely $|(h_{9/2})^2_{8P}(g_{9/2}{}^i{}_{11/2})_{10N}\rangle_{18}$ initial and $|d^{-1}_{3/2}h_{9/2}\rangle_P$ final would be given large weight in our wave functions. Perhaps the main reason that there is a discrepancy has less to do with our use of the fewer term 3^- level wave functions of Ref. 26 but relates to the fact that the $|d^{-1}_{3/2}h_{9/2}\rangle_P$ configuration has a larger relative amplitude than the 3^- level (Ref. 26) wave function (see Table 1).

It may be possible to use our theory, microscopic or macroscopic match to experiment, to help illustrate the proper optical model well depth and radius parameters.

D. Alpha Rate Theory with Electromagnetic Coupling

We propose here to explore the possibility that interchannel coupling due to the collective electric octupole transition in ^{208}Pb affects significantly the theoretical decay rate to the 3^- state. We consider at first

only the two channels $\ell = 18$ and $\ell = 15$. The wave function is of form

$$\Psi_M = \frac{u_{18}(r)}{r} Y_{18}^M(\omega)\chi_0^0 + \frac{u_{15}(r)}{r} \sum_m (15\ 3\ m\ M-m|18\ M) Y_{15}^m\ \chi_3 M-m \tag{10}$$

where $\chi_j^{M_j}$ is the daughter nuclear wave function and Y_ℓ^m is the spherical harmonic of the alpha angular position. Upon substitution into the Schrödinger equation and integration over all variables except r we get the following coupled radial equations to be solved for the case where $r \gtrsim 12f$ or the alpha particle is outside the range of nuclear forces

$$\frac{d^2u_{18}}{dr^2} - \left\{ \frac{2\mu}{\hbar^2}\left[\frac{2Ze^2}{r} - Q_{18}\right] + \frac{18\times19}{r^2}\right\} u_{18} = K_{03}u_{15} \tag{11a}$$

$$\frac{d^2u_{15}}{dr^2} - \left\{ \frac{2\mu}{2}\left[\frac{2Ze^2}{r} - Q_{15}\right] \frac{15\times16}{r^2}\right\} u_{15} = K_{03}u_{18}\ , \tag{11b}$$

where u_ℓ is r times the radial function of the ℓ^{th} partial wave, μ is the reduced mass, Q_ℓ is the alpha decay energy. The E3 reduced transition probability, B(E3) is calculated[32] to be $4.8\times10^4\ e^2f^6$ from the experimentally measured half life of 3×10^{-11} sec for the 3^- state. The electromagnetic coupling constant, K_{03}, is given (Ref. 16, Eq. 6.3) in general for distances $r > R_0$ as

$$K^\lambda_{\ell I_f \ell' I_f'}(r) = (-)^{I_f' - I} \frac{2\mu}{\hbar^2} \frac{2e\left[(2\ell+1)(2\ell'+1)4\pi(2I_f'+1)B_{I_f' \to I_f}(E\lambda)\right]^{1/2}}{r^{\lambda+1}(2\lambda+1)}$$

$$\times\ (\ell\ell'00|\lambda0)\ W(\ell I_f \ell' I_f';\ I\lambda)\ . \tag{12}$$

Following, in our Eq. (32) for nuclear coupling, we later discuss the choice of sign associated with the reduced electric transition probability between the computed final states $[B(E\lambda)]^{1/2}$, where $(\ell\ell'00|\lambda 0)$ is the Clebsch Gordon coefficient and $W(\ell I_f \ell' I_f'; I\lambda)$ is the Racah coefficient. We choose the method[33] of inward numerical integration with boundary conditions at large distance restricted by the experimental relative intensities. We will discuss this point more extensively when we turn to the odd-mass coupled channel calculation for ^{253}Es and ^{255}Fm. Extensive examination indicates that none of the usual analytical approximations to solution of these equations seems suitable, since the diagonal energy differences become large on either side of the crossover distance. The complete set of four linearly independent solutions is computed by the four boundary conditions at 40.0f given in Table 5. The quantities G_L and F_L denote the standard irregular and regular Coloumb functions, respectively, with the arguments η and ρ defined as $\rho = kr$ and $\eta = 2Ze^2\mu/\hbar^2 k$ for reduced mass, μ and wave number $k = (2\mu Q_\ell)^{\frac{1}{2}}/\hbar$ appropriate to the decay energy, Q_ℓ in each case.[16] The general solution may be expressed as a linear combination of these basis solutions. The general solution for the uncoupled equations can be written as $u_\ell(\eta,\rho) = G_\ell(\eta,\rho) + iF_\ell(\eta,\rho)$.

The desired solutions for the alpha decay problem behave asymptotically like outgoing Coulomb waves, although there may be additional phase shifts δ_{18} and δ_{15} arising from the channel coupling. We can express this behavior for large radii in the following linear combinations.

$$u_{18} \rightarrow A[G_{18}(k_{18}r) + iF_{18}(k_{18}r)]e^{i\delta_{18}} \tag{13a}$$

$$u_{15} \rightarrow B[G_{15}(k_{15}r) + iF_{15}(k_{15}r)]e^{i\delta_{15}} \tag{13b}$$

TABLE 5. Boundary conditions for the coupled equations.

	Set I	Set II	Set III	Set IV
u_{18}	G_{18}	F_{18}	0	0
$\frac{du_{18}}{dr}$	$k_{18}\frac{dG_{18}}{d\rho}$	$k_{18}\frac{dF_{18}}{d\rho}$	0	0
u_{15}	0	0	G_{15}	F_{15}
$\frac{du_{15}}{dR}$	0	0	$k_{15}\frac{dG_{15}}{d\rho}$	$k_{15}\frac{dF_{15}}{d\rho}$

The solutions are to be joined at the nuclear surface with quasi-stationary state solutions, in which the real components vastly dominate over the imaginary components, and A and B are normalization constants which we will evaluate.

Let us denote the components of the basis set of solutions as $u_{18}^{(I)}$, $u_{15}^{(I)}$, $u_{18}^{(II)}$, $u_{15}^{(II)}$, etc., for the four boundary conditions. Then the above conditions at the nuclear surface are essentially expressed on additional constants by the equations for both ℓ values setting the imaginary components to zero,

$$\begin{aligned} \mathrm{Im}(u_\ell) &= A[\sin \delta_{18} u_\ell^{(I)}(R_0) + \cos \delta_{18} u_\ell^{(II)}(R_0)] \\ &+ B[\sin \delta_{15} u_\ell^{(III)}(R_0) + \cos \delta_{15} u_\ell^{(IV)}(R_0)] = 0 \end{aligned} \quad (14)$$

The other two equations necessary to solve for the four real quantities A, B, δ_{18}, and δ_{15} may be either supplied near the nuclear surface by a microscopic nuclear model, or in the approach we use a large-distance boundary condition phenomenologically fixed by experimental alpha decay rates.

Let λ_{18} and λ_{15} be the partial decay constants (sec^{-1}) for the two alpha groups. Then we equate the constants to the probability flux through a sphere at large R.

$$\lambda_{18} = u_{18}^* \frac{4\pi}{\mu} \frac{\hbar}{i} \frac{du_{18}}{dr} \quad (15a)$$

$$\lambda_{15} = u_{15}^* \frac{4\pi}{\mu} \frac{\hbar}{i} \frac{du_{15}}{dr} \quad (15b)$$

where u_{18}^* is the complex conjugate of u_{18} and u_{15}^* is the complex conjugate of u_{15}. Substituting from Eqs. (13a) and (13b) into Eqs. (15a) and (15b)

and using the asymptotic forms for the Coulomb functions we obtain

$$\lambda_{18} = 4\pi A^2 \frac{\hbar k_{18}}{\mu} = 4\pi A^2 v_{18} \tag{16a}$$

$$\lambda_{15} = 4\pi B^2 \frac{\hbar k_{15}}{\mu} = 4\pi B^2 v_{15} \tag{16b}$$

where v_{18} and v_{15} are the velocities of the respective alpha groups at infinity ($r = \infty$). From the experimental values of λ's and v's we calculate in the asymptotic region the following values of A and B.

$$A = 2.2 \times 10^{-12} \quad f^{-\frac{1}{2}} \tag{17a}$$

$$B = 2.3 \times 10^{-13} \quad f^{-\frac{1}{2}} \tag{17b}$$

E. Alpha Rate Theory Including Electromagnetic and Nuclear Force Coupling

If we wish to continue the alpha wave functions into the region of the nuclear force field, we must make more specific assumptions about models, which will involve including the nuclear coupling terms. For the electric 2^{λ}-pole coupling terms, we can assume that there are source currents on a sphere in the nuclear surface region. Then the coupling potential, with radial dependence of $r^{-\lambda-1}$ outside the nuclear surface region joins continuously at the sphere to an r^{λ} dependence inside this region.

The most fundamental form of the nuclear potential for the alpha particle involves summing over various nucleon-nucleon coordinates in a microscopic model, but a simpler approximate procedure that may be adequate for collective "shape vibrational" states would be to describe the alpha nuclear potential in terms of collective shape coordinates. Consider in

the case of ^{208}Pb and an alpha particle a shape-dependent nuclear surface potential

$$V_\alpha(r,\theta,\phi,\alpha_{3\nu}) = \frac{-V_0}{1 + \exp\left[\frac{r - R(\theta,\phi,\alpha_{3\nu})}{d}\right]} \tag{18}$$

with an expansion of the form

$$R(\theta,\phi,\alpha_{3\nu}) = R_0\left[1 + \sum_\nu \alpha_{3\nu}\, Y^*_{3\nu}(\theta,\phi)\right] \tag{19}$$

We consider the first-excited 3^- state of ^{208}Pb as the first octupole shape oscillation excitation and have earlier derived[34] the coupled radial equations for alpha decay for the ground state of ^{212}Po. An alpha cluster is assumed to form somewhere in the nuclear interior but octupole coupling does not occur until the alpha cluster reaches the matching radius. At R the alpha cluster exchanges angular momentum and energy with the daughter nucleus. (The angular momentum exchanged, as stated before, can be even or odd, as $\ell^\pi = 0, 3^-, 4^+, 5^-$, where π is the parity of the phonon state or mode of oscillations.) Nuclear coupling is assumed to occur in a narrow region around R.

The time average of the octupole permanent deformation is zero, as $\langle\alpha_{3\nu}\rangle = 0$, where $\alpha_{3\nu}$ is the collective coordinate since there is no prolate or oblate, permanent deformation in ^{208}Pb since it is doubly magic in Z and N. Lead, ^{208}Pb, has no rotational bands, but several excited states seem to have collective character as shape oscillations about an equilibrium sphere.

We can consider the node as ripples moving around on the surface, or, looking along a radial direction, we can imagine an undulating or

oscillating surface. There is a net effect of $\langle \alpha_{3\nu}{}^2 \rangle \neq 0$, where the coupling occurs in this "deformed" coupling region. (Of course, we have a similar picture for $\ell = 4$, the 4^+ level where there are four nodes.)

In any case, it is pictured that the alpha leaves the parent at the point of the connection radius R and at this point the parent nucleus becomes the daughter; that is to say, that the barrier "belongs" to the daughter. The coupling of angular momentum or "sharing" occurs between the alpha particle and the daughter, ^{208}Pb. This is essentially the picture presented earlier in Ref. 40 (see Fig. 3).

The macroscopic coupled equations in Ref. 34 are modified for the case of the high-spin isomer calculations of this paper. T. Tamura has also given[2] very comprehensive and general formulations of the problem. Aside from differences in notation our formulas are identical to the appropriate special cases of his. Therefore, we proceed from the derivations in T. Tamura's work.

To include the nuclear potential coupling in our Eqs. (11a,b) it is only necessary to add to the electromagnetic coupling term (12) the nuclear coupling term given by Tamura's Eq. (27), although we must multiply his coupling matrix element by $i^{\ell-\ell'} = (-)^{(\ell-\ell')/2}$ since the ordinary spherical harmonics Y_ℓ^m are used here and he uses $i^\ell Y_\ell^m$.

$$(-)^{\frac{\ell-\ell'}{2}} \langle \ell j I | V_{coupl} | \ell' j' I' \rangle = (-)^{\frac{\ell-\ell'}{2}} \sum_{t,\lambda} v_\lambda^{(t)}(r) \langle I \| Q_\lambda^{(t)} \| I' \rangle A(\ell j I, \ell' j I', \lambda J) \tag{20}$$

In the present special case of Eqs. (11a,b), the alpha spin s is zero, the multipolarity $\lambda = 3$, $\ell = j = 18$, $\ell' = j' = 15$, the total angular momentum $J = 18$, the final nuclear spin states are $I = 0$, $I' = 3$, and the tensorial

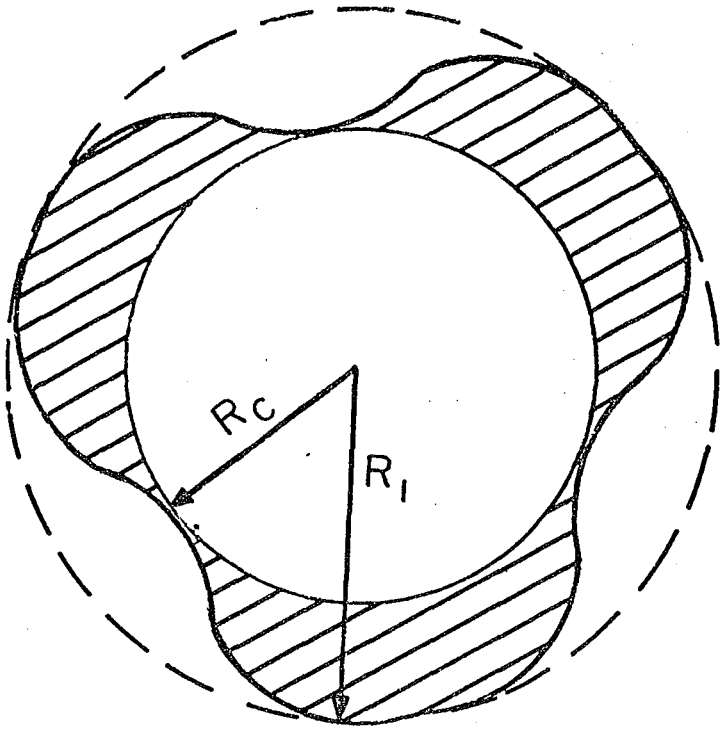

MU-35096

Fig. 3. The mechanism by which the channel mixing or coupling between the recoil-excited states and the ground state, is represented by the change in momentum and energy of the emitted alpha particle through the exchange of a phonon, or a quasi-particle of integral spin, between it and the recoil nucleus "flipping" the ^{208}Pb nucleus between the 0^+ and 3^- states. That is, the emitted alpha can induce, through phonon exchange, a change in the daughter's spatial distribution from that of a sphere to that of a three-nodal deformation of higher energy and angular momentum, sometimes termed a pear-shaped λ^2 for $\lambda = 3$ octupole collective deformation.

rank t = 1 is considered.

Therefore, from Tamura's Eq. (29.2), assuming the $\ell\ell'$ therein is a typographical error for $\hat{\ell}\hat{\ell}'$ from these equations,

$$A(18\ 18\ 0,\ 15\ 15\ 3;\ 3\ 18\ 0) = i\left(\frac{31}{4\pi \cdot 7}\right)^{\frac{1}{2}} (18\ 15\ 00|30) \qquad (21)$$

The Racah coefficient in Tamura's equation for the present case has a zero as one argument, and it is replaced above by the equivalent algebraic factor.

In Bohr's model[35] of irrotational vibrations of a uniformly charged spherical nucleus, the reduced electric matrix elements are given in terms of surface phonon oscillator constants. From this relationship we can express the reduced matrix element as follows:

$$\left|\langle I \| Q_3^{(1)} \| I' \rangle\right|^2 = (2I + 1)\, B(E3;\ I \to I') \left(\frac{4\pi}{3ZeR_e^3}\right)^2 \qquad (22)$$

where R_e is the radius of the equivalent uniformly charged sphere of around ~7.5f. This equation differes from that of Tamura's[3] footnote 18a only by the squared factor.

His $v_\lambda^{(1)}(r)$ factor is given in his Eq. (13.1); in the present case the nuclear potential is purely real and becomes just the first term of his Eq. (13.1). Thus it is taken that $v_3^{(1)}(r)$ as just R_0 times the first radial derivation of the real Woods-Saxon potential designated V_{nuc}; the coupling term is very nearly a Gaussian peaking on the nuclear surface, which can be compared to H. J. Mang and J. O. Rasmussen.[36]

Finally, combining the above expressions we get the nuclear coupling term to add to the electromagnetic coupling term of our Eq. (12):

$$K_{nuc}(r) = -R_0 \frac{dV_{nuc}}{dr}\left(\frac{4\pi}{3ZeR_e^3}\right)^2 \gamma[B(E3;\ 0 \to 3)]^{1/2}\left(\frac{31}{4\pi \cdot 7}\right)^{1/2}(18\ 15\ 00|30) \tag{23}$$

where we insert a factor γ to allow for possible deviations from the completely vibrational model.

It should be understood that the relationship between $B(E\lambda)$ and the electric coupling matrix element in (12) is exact in the long-wave-length limit. (If the distances over which the alpha-nuclear coupling is effective are not small compared to the wave length of the photon of energy equal to the nuclear transition energy, then a more complicated expression based on a retarded potential would be necessary. For the present case, the reduced wave length $\lambda\!\!\!^{-}$ of a 2.615 MeV photon is 75f and integrations were carried only from 40f inward.) However, the relationship of Eq. (23) is model-dependent, depending on the assumption that the 3^- excitation of ^{208}Pb is an octupole oscillation of a nuclear fluid of constant proton-to-neutron ratio. The factor γ might be less than unity if the microscopic description gave a predominant share of excitation to protons, and, conversely, the factor γ could be greater than unity if the 3^- excitation was predominantly neutron-excitation.[37]

We note that the signs of the nuclear and electromagnetic coupling terms are everywhere opposite to one another. This result accords with the qualitative argument that an excursion of the nuclear surface toward the alpha near the nucleus produces a lowered nuclear potential energy and a more repulsive electrostatic potential energy.

There is a subtle point to be noted regarding the proper sign of the square root of B(E3) in Eqs. (12) and (23). In Section II.B of this paper the microscopic wave functions used for the 3^- state of ^{208}Pb are given.

The choice of overall sign of these wave functions is completely arbitrary. However, once the choice is made the sign of the electric octupole matrix element is fixed, determining the sign of the coupling term of Eq. (23); also the choice fixes the sign of the reduced alpha width to the 3^- state. With the arbitrary choice of phases for the parent 18^+ and daughter 3^- wave function, as listed in Section II.B, the $\gamma_{\alpha L}$ values have the signs shown in Table 1 and we must take the plus sign for the electric octupole matrix element $[B(E3)]^{1/2}$ in Eqs. (12) and (23). Thus, the final theoretical results of a coupled-equation calculation with the microscopic boundary condition are, as they must be, independent of choice of phase of the shell model wave functions.

F. Numerical Solutions of Coupled Equations for the ^{212m}Po Decay

Presented here are the results of inward numerical integrations of the two coupled radial equations [(11a) and (11b)], where the coupling matrix element K_{03} is the sum of electromagnetic [Eq. (12)] and nuclear [Eq. (23)] terms. Three cases are considered. The nuclear potential of Eqs. (18) was used with V_0 = 35.0 MeV, d = 0.576 f, and R_0 = 9.10 f. A model-dependence factor γ of 2.7 was used in order to see the effect of very strong surface coupling. A second calculation was made with $\gamma = 1$, and a third with V_0 = 74.0 MeV, d = 0.565 f, and R_0 = 8.53 f and $\gamma = 2.7$ as above. The electric coupling term has radial dependence r^{-4} outside of R_e = 7.5 f and r^3 inside [cf. Tamura's Eq. (13.1)].

The boundary conditions of Table 5 were used, and the resulting amplitudes near the nuclear surface for the four linearly independent basis solutions are given in Tables 6, 7, and 8. In the absence of

TABLE 6. Basis sets of wave amplitudes for the 2-channel case.

$\gamma = 2.7$, $V_0 = 35.0$ MeV

B. C.*	ℓ	Radius 6.1 f	7.1	8.1	9.1	10.1
I	18	-5.6182×10^{11}	-5.5269×10^{10}	-7.0778×10^{9}	-6.8428×10^{8}	-6.7685×10^{7}
II	18	3.6619×10^{11}	3.6024×10^{10}	4.6134×10^{9}	4.4617×10^{8}	4.4133×10^{7}
III	18	1.2860×10^{13}	1.2634×10^{12}	1.5828×10^{11}	1.1994×10^{10}	4.5038×10^{8}
IV	18	-1.7562×10^{10}	-1.7254×10^{9}	-2.1616×10^{8}	-1.6374×10^{7}	-6.1319×10^{6}
I	15	2.7410×10^{11}	3.9089×10^{10}	5.9410×10^{9}	4.6448×10^{8}	1.6724×10^{7}
II	15	-1.7865×10^{11}	-2.5477×10^{10}	-3.8719×10^{9}	-3.0255×10^{8}	-1.0844×10^{7}
III	15	-6.4028×10^{12}	-9.1594×10^{11}	-1.4368×10^{11}	-1.5061×10^{10}	-1.6346×10^{9}
IV	15	8.7445×10^{9}	1.2509×10^{9}	1.9624×10^{8}	2.0577×10^{7}	2.2346×10^{6}

*For Boundary Conditions (see Table 5).

TABLE 7. Basis sets of wave amplitudes for the 2-channel case.

$\gamma = 1.0$; $V_0 = 35.0$ MeV

B. C.	ℓ	6.1	7.1	8.1	9.1	10.1
I	18	-2.259 (11)	-2.300 (10)	-3.622 (9)	-5.415 (8)	-6.611 (7)
II	18	1.473 (11)	1.500 (10)	2.362 (9)	3.533 (8)	4.315 (7)
III	18	3.173 (12)	3.195 (11)	4.500(10)	4.027 (9)	1.553 (8)
IV	18	-4.330 (9)	-4.360 (8)	-6.139 (7)	-5.485 (6)	-2.098 (5)
I	15	6.466 (10)	9.708 (9)	1.700 (9)	1.572 (8)	5.847 (6)
II	15	-4.212 (10)	-6.325 (9)	-1.107 (9)	-1.021 (8)	-3.746 (6)
III	15	-1.905 (12)	-2.953 (11)	-6.321(10)	-1.143(10)	-1.594 (9)
IV	15	2.602 (9)	4.034 (8)	8.636 (7)	1.563 (7)	2.179 (6)

TABLE 8. Basis sets of wave amplitudes for the 2-channel case.

$\gamma = 2.7$; $V_0 = 74.0$ MeV

B.C.	ℓ	6.1	7.1	8.1	9.1	10.1
I	18	-8.2561(10)	-5.7765(10)	-1.0881(10)	-7.2861(8)	-6.8738(7)
II	18	5.3812(10)	3.7650(10)	7.0916(9)	4.7507(8)	4.4857(7)
III	18	1.9023(12)	1.3343(12)	2.5390(11)	1.2849(10)	3.6252(8)
IV	18	-2.5980(9)	-1.8222(9)	-3.4677(8)	-1.7541(7)	-4.9300(5)
I	15	2.9143(10)	4.7744(10)	1.0307(10)	5.1116(8)	1.3568(7)
II	15	-1.8995(10)	-3.1118(10)	-6.7180(9)	-3.3297(8)	-8.7831(6)
III	15	-6.7788(11)	-1.1043(12)	-2.3540(11)	-1.6049(10)	-1.6605(9)
IV	15	9.2580(8)	1.5028(9)	3.2149(8)	2.1925(7)	2.2701(6)

coupling, solutions II and IV based on the regular solutions should be extremely small, and indeed could not be calculated by inward integration, since rounding errors would grow exponentially in the barrier region. However, with coupling present the variations of magnitude of all wave amplitudes is not so great, and the significance of the final results should not be seriously altered by rounding errors. The program was checked by running calculations with coupling turned off and demanding that solutions based on the regular F_ℓ Coulomb function boundary conditions be much less than those based on irregular G_ℓ.

Using the experimental decay rates of ^{212m}Po to ground and 3^- state and Eqs. (17a), (17b), and (14), phase shifts due to coupling were solved. There are two acceptable sets: $\delta_{18} = 33°10'$ with $\delta_{15} \approx 0$ and $\delta_{18} = 213°10'$ with $\delta_{15} \approx 0$. The phase shifts are essentially the same for the calculation with different V_0, for the phase shifts are mainly determined by coupling strength and potential energies in the vicinity of the outer classical turning point.

With these phases we calculate the real parts of the acceptable solutions by the appropriate linear combination of basis solutions as follows:

$$\mathrm{Re}(u_\ell) = A[u_\ell^{(I)} \cos\delta_{18} - u_\ell^{(II)} \sin\delta_{18}] + B[u_\ell^{(III)} \cos\delta_{15} - u_\ell^{(IV)} \sin\delta_{15}] \tag{24}$$

The amplitudes are normalized by the absolute decay rates such that when squared and multiplied by Δr in f one gets the absolute probability of finding the alpha between spherical surfaces at r and $r + \Delta r$. The square of the amplitude multiplied by $R_0/4\pi$ is the dimensionless quantity called

"surface probability" and tabulated at 9.3f for even-even ground state transitions in Table 8 of I. Perlman and J. O. Rasmussen.[37]

To display the effects of coupling on the wave amplitudes we have plotted the ratios u_{18}/u_{15} in Figs. 4 and 5 at various radial distances. The three coupled solutions are shown along with the ratio for no coupling, and in the lower part of the graph we show the ratios given by the microscopic shell-model calculation (Table 1). One sees that even with coupling, the microscopic theory gives too low u_{15} amplitude at the larger radii, but it appears that a choice of a small R_0 value reduces the discrepancy markedly. The most favorable situation occurs for the cases of the deepest potential (74 MeV) and the strongest surface coupling ($\gamma = 2.7$). There is, surprisingly, not much difference at radii less than 8f between the amplitude ratios of the $\delta_{18} = 33°$ and $\delta_{18} = 213°$ solutions for the deep potential and strong coupling.

One is restrained from inward extrapolation of the γ_ℓ ratios in Figs. 4 and 5 to get apparent complete agreement at $R \sim 6$f, for several reasons: 1) Inside the exponential tail region of the nucleon wave functions the γ_ℓ values will greatly fluctuate and microscopic alpha theory has not been formulated for R in this region. 2) From Tables 9, 10 and 11 it is evident that the solutions imply alpha probabilities in excess of unity for the volume outside 6f, and the solutions at such small radius must therefore have no physical significance.

Tables 9, 10 and 11 give the values of the real parts of the $\ell = 18$ and $\ell = 15$ coupled alpha waves at various radial distances for the two-phase choices satisfying experimental intensities and for the three different choices of nuclear potential parameters. Upon further examination it appears that the choice of parameters in Table 11 is the most realistic.

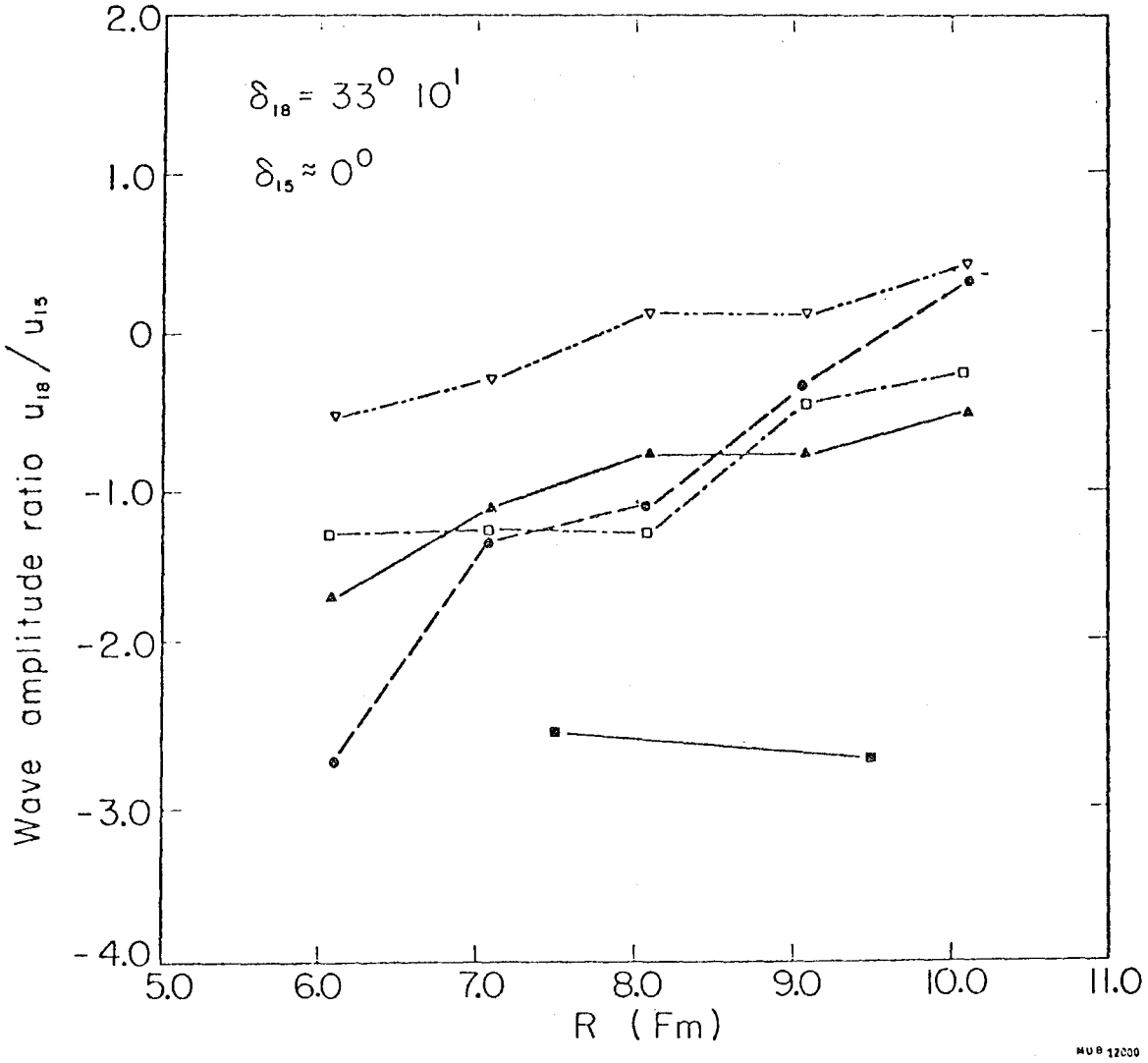

Fig. 4. Wave amplitude ratio u_{18}/u_{15} for 33°10' solutions as a function of radial distance (——▲——) are given for the uncoupled potential V_0 = 35 MeV; – – – □ – – – is the coupled $\gamma = 2.7$, V_0 = 35 MeV case, and – – – – ▽ – – – – the coupled $\gamma = 1.0$, V_0 = 35 Mev; – –●– – is for the coupled $\gamma = 2.7$, V_0 = 74 MeV, and ■——■ is the γ_{18}/γ_{15} ratio uses shell model wave functions of Refs. 21 and 26.

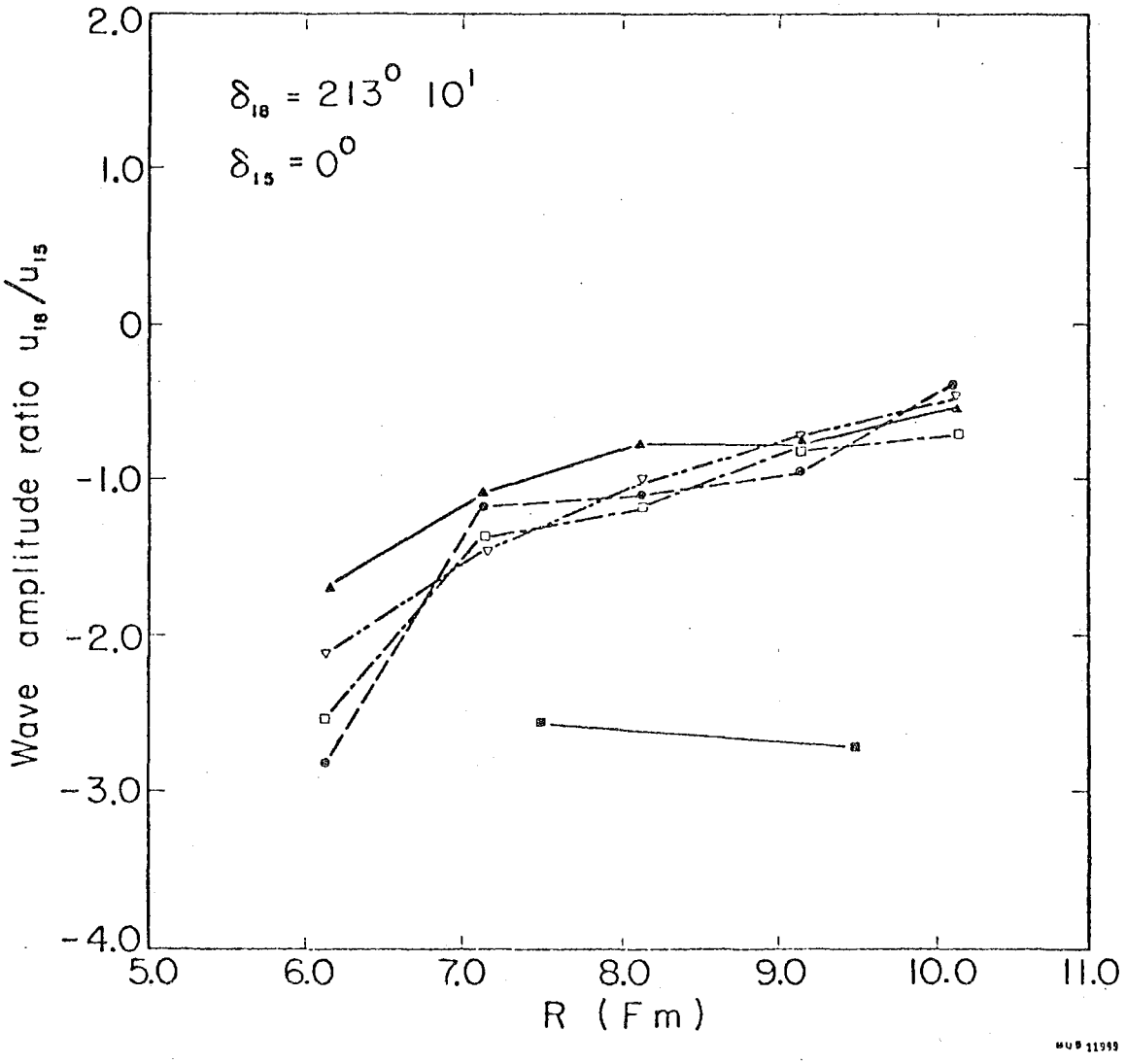

Fig. 5. Wave amplitude ratio u_{18}/u_{15} for 213°10' solutions as a function of radial distance. —▲— are given for the uncoupled potential $V_0 = 35$ MeV; – – –□– – – is the coupled $\gamma = 2.7$, $V_0 = 35$ MeV case, and – – – – ▽ – – – – the coupled $\gamma = 1.0$, $V_0 = 35$ MeV; – –●– – is for the coupled $\gamma = 2.7$, $V_0 = 74$ MeV; and ■——■ is from Refs. 21 and 26 using γ_{18}/γ_{15} ratio shell model wave functions.

TABLE 9. Real part of alpha wave amplitudes near the nucleus for $V_0 = 35.0$ MeV and $\gamma = 2.7$.

	$\delta_{18} = 33°10'$ $\delta_{15} = 0°$			$\delta_{18} = 213°10'$ $\delta_{15} = 0°$		
R	Re (u_{18})	Re (u_{15})	Ratio	Re (u_{18})	Re (u_{15})	Ratio
6.1 f	1.49 (0)	-1.18 (0)	-1.26	4.43 (0)	-1.77 (0)	-2.51
7.1 f	1.35(-1)	-1.08(-1)	-1.25	4.25(-1)	-3.14(-1)	-1.35
8.1 f	1.79(-2)	-1.43(-2)	-1.24	5.50(-2)	4.87(-2)	-1.13
9.1 f	9.60(-4)	-2.24(-3)	-0.429	4.56(-3)	-4.68(-3)	-0.97
10.1 f	-7.89(-5)	-3.32(-4)	-0.238	2.82(-4)	-4.20(-4)	-0.67

TABLE 10. Real part of alpha wave amplitudes near the nucleus for $V_0 = -35.0$ MeV and $\gamma = 1.0$.

	$\delta_{18} = 33°10'$ $\delta_{15} \approx 0°$			$\delta_{18} = 213°10'$ $\delta_{15} \approx 0°$		
R	Re (u_{18})	Re (u_{15})	Ratio	Re (u_{18})	Re (u_{15})	Ratio
6.1 f	1.35(-1)	-2.67(-1)	-0.51	1.29 (0)	-6.07(-1)	-2.12
7.1 f	1.30(-2)	-4.25(-2)	-0.306	1.34(-1)	-9.35(-2)	-1.43
8.1 f	8.2 (-4)	-1.00(-2)	+0.082	1.98(-2)	-1.90(-2)	-1.04
9.1 f	-2.09(-4)	-2.22(-3)	+0.094	2.07(-3)	-2.94(-3)	-0.70
10.1 f	-1.43(-4)	-3.51(-4)	+0.404	2.12(-4)	-5.19(-4)	-0.408

TABLE 11. V_0 = -74.0 MeV and γ = 2.7.

	$\delta_{18} = 33°10'$ $\delta_{15} \approx 0°$			$\delta_{18} = 213°10'$ $\delta_{15} \approx 0°$		
R	Re (u_{18})	Re (u_{15})	Ratio	Re (u_{18})	Re (u_{15})	Ratio
6.1	2.18(-1)	-8.00(-2)	-2.72	6.54(-1)	-2.32(-1)	-2.82
7.1	1.68(-1)	-1.28(-1)	-1.31	4.44(-1)	-3.80(-1)	-1.17
8.1	2.99(-2)	-2.69(-2)	-1.11	8.71(-2)	-8.11(-2)	-1.07
9.1	8.40(-4)	-2.35(-3)	-0.36	4.68(-3)	-5.05(-3)	-0.93
10.1	-9.65(-5)	-3.69(-4)	0.26	1.56(-4)	-4.19(-4)	-0.37
11.1	-1.93(-5)	-4.91(-5)	0.34	1.06(-5)	-5.02(-5)	-0.21
12.1	-2.91(-6)	-7.26(-6)	0.46	1.21(-6)	-7.28(-6)	-0.17
13.1	-4.88(-7)	-1.24(-6)	0.39	1.92(-7)	-1.24(-6)	-0.16
14.1	-9.36(-8)	-2.40(-7)	0.39	3.64(-8)	-2.40(-7)	-0.14
15.1	-2.08(-8)	-5.27(-8)	0.39	8.18(-9)	-5.27(-8)	-0.16
16.1	-5.21(-9)	-1.86(-8)	0.28	2.29(-9)	-1.86(-8)	-0.12

G. Discussion of the Results for the ^{212m}Po Alpha Decay

By no means can we claim a satisfactory explanation of the large (1.0%) alpha decay group from ^{212m}Po to the first excited state of ^{208}Pb. It may well be that the lack of octupole core polarization in the initial wave function is a major cause of the remaining discrepancy. It does, however, seem clear that the connection radius R_0 of microscopic alpha decay theory should be chosen significantly smaller than the values hitherto used (8 - 10 f). If a smaller R_0 is chosen then the strong alpha-channel coupling involving major collective shape oscillational modes must be taken into account, for our numerical calculations here show substantial effects from coupling to the octupole mode. Not only is the ratio of amplitudes to ground and excited states affected, but also the absolute decay rates will be affected. Since we have not resolved the alpha branching ratio problem, we shall not try to use our numerical solutions for quantitative absolute decay rate calculations. Suffice it to note qualitatively that there are substantial effects of channel coupling on theoretical absolute rates. Note in Tables 9, 10 and 11 that the total alpha probabilities ($|u_{18}|^2 + |u_{15}|^2$) at small radii are usually about an order of magnitude larger for the 213° cases than for the 33° cases. This result means that the effective barrier penetrability in the 213° cases is an order of magnitude smaller than for the 33° cases. The effect of the surface coupling potential is to raise the effective barrier for both partial waves in the 213° cases and to lower the barrier for 33° cases.

As mentioned earlier in Section II.B, Glendenning and Harada calculated theoretical alpha decay ratios between the ^{212m}Po isomer and the ground state, finding the theoretical relative rate for the isomer

too fast by a factor of about 45 for $R_0 = 9.5$ f or about 18 for $R_0 \approx 9.0$ f. We noted in Section II.B that their apparent discrepancy factor may reverse for $R_0 < 8$ f. A careful recalculation of the decay rate ratio of isomer and ground state might provide the basis to decide between the 213° case and the 33° case. The ground state decay rate is also affected by channel coupling but less so than the isomer.

The alpha decay theory applied to high-spin isomers, such as ^{212m}Po and ^{211m}Po, is deserving of further study for the light it may shed on fundamentals of the theory. We have argued above for joining bound and open-channel solutions at smaller radii than previous practice; however, such will aggravate the problem of the usual mismatch at R_0 of logarithmic derivatives of the alpha amplitude in inner and outer regions. There is clearly a need to reformulate alpha theory along the lines of Feshbach's "unified theory of nuclear reactions,"[23] where the arbitrary division of space into inner and outer regions need not be made.

We are encouraged enough by the results of the coupled channel method for even mass nuclei to extend our use of it to the alpha decay of odd mass nuclei. In the next section, we present calculations for the coupled channel alpha decay theory for odd madd nuclei ^{253}Es and ^{255}Fm.

III. ODD-MASS COUPLED-CHANNEL ALPHA DECAY THEORY

A. Alpha Decay of Spheroidal Nuclei ^{253}Es and ^{255}Fm

When a spheroidal nucleus undergoes alpha decay, the noncentral electromagnetic field permits exchange of energy between internal nuclear excitation and the external alpha particle. The noncentral couplings of greatest importance involve collectively enhanced rotational E2 transitions in deformed nuclei. Starting with boundary conditions set at the spheroidal nuclear surface, the formal problem involves propagation of the alpha particle wave function outward through the anisotropic barrier to some distance where coupling effects are negligible.

Although other researchers have performed the numerical integration of coupled channel equations for the alpha decay of even-even spheroidal nuclei (see Section II of this paper) there has been little analogous work on the alpha decay of odd-mass nuclei. In the latter case, an alpha particle wave of a given orbital angular momentum ℓ may branch to more than one energy level of the daughter nucleus. Thus for the favored alpha decay of ^{233}U, R. R. Chasman and J. O. Rasmussen[38] considered the decay of the s wave to the 5/2 level and the branching of the d wave to the 5/2, 7/2 and 9/2 levels of ^{229}Th. Channel coupling effects are most significant for the case of a relatively weak wave, such as the highly hindered g wave, coupled to a strong wave such as the s wave. Therefore, we have extended the work of Chasman and Rasmussen by considering the branching of the s, d, and g waves in the favored alpha decays of both ^{253}Es and ^{255}Fm. Favored alpha decays are those decays in which the quantum numbers of the odd nucleon are the same for both the parent and daughter.

The nuclei ^{253}Es and ^{255}Fm, both having spin 7/2, are ideal cases for applying an exact numerical treatment because alpha transitions to the favored bands of the daughters have been well studied,[39-42] and angular distribution data from low temperature nuclear alignment experiments are available.[4] If we include the branching of the $\ell = 0$, 2, and 4 partial waves, then nine coupled second-order differential equations must be solved for favored decays to the five lowest levels (7/2, 9/2, 11/2, 13/2, 15/2) of the daughter rotational band. The $\ell = 6$ contributions have been taken into account in an approximate way[7] (see Fig. 6a for the partial alpha decay scheme for ^{253}Es and Fig. 6b for the partial decay scheme for ^{255}Fm).[43]

The results of the numerical integration test two commonly used assumptions. The first is that near the nuclear surface the favored alpha waves have zero projection of orbital angular momentum along the cylindrical symmetry 3-axis of the daughter nucleus. Subject to this $m_\ell = 0$ constraint, we wish to determine if the coupled channel treatment can reproduce both the angular distribution data and the experimental relative intensities to the spin 7/2, 9/2, 11/2, 13/2, and 15/2 states of the daughter. The second assumption to be tested is that the relative intensities of a given ℓ-wave are given by the square of a Clebsch-Gordan coefficient times the calculated spherical barrier penetrability for the alpha group (formula of Bohr, Fröman and Mottelson (BFM)).[6] Experimental data show deviations from the BFM expression for favored decay. It is of great interest to determine whether a careful coupled channel treatment of the barrier penetration explains the deviations while retaining the first assumption above.

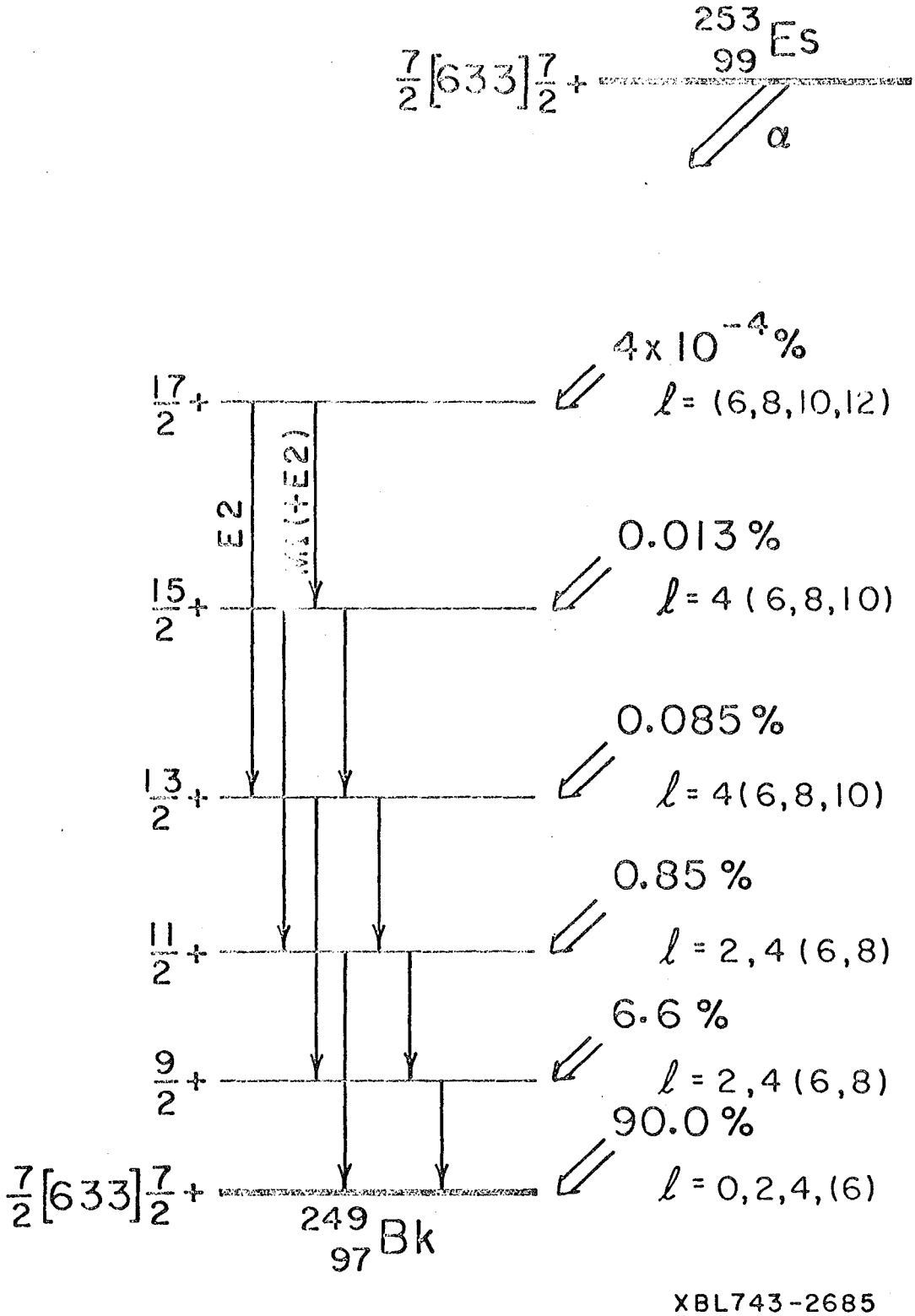

Fig. 6a. Partial alpha decay scheme for ^{253}Es adapted from refs. 40 and 41. The intensities to each daughter level and the permitted alpha particle angular momentum values are shown. The ℓ values in parenthesis are not included in the coupled channel calculation since their contribution is very small. In ref. 1 the ℓ partial waves are included in an approximate manner.

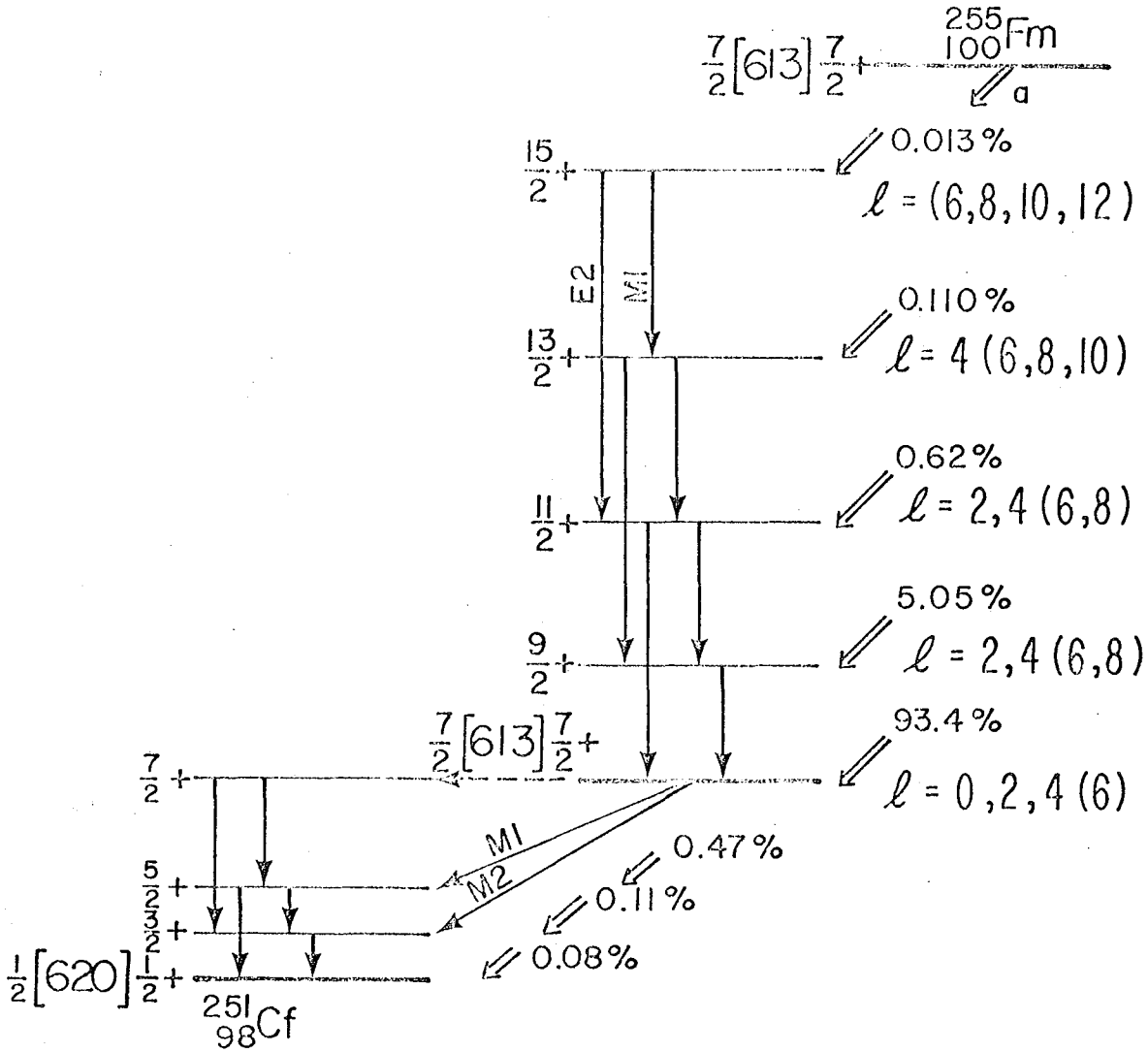

Fig. 6b. Partial decay scheme for ^{255}Fm as adapted from ref. 42. The favored alpha decays populate a rotational band built on the 7/2[613] state. The intensities to each given level of the daughter and the alpha particle angular momentum values are shown.

B. Mathematical Formalism for the Alpha Decay of ^{253}Es and ^{255}Fm

The formalism for alpha decay in the presence of a non-central field is given by I. Perlman and J. O. Rasmussen.[37] A multipole expansion is made for the Coulombic potential energy outside the nuclear surface. The zero-order term is the central Coulombic term.

The E2 interaction contributes the first important coupling term. For nuclei with large hexadecapole deformations, E4 coupling may also be important;[44,45] however, both ^{249}Bk and ^{251}Cf have small hexadecapole deformation. The coupled differential equations can be written in the radial separation variable[1,43] as

$$u''_{I_d,\ell} - \frac{2\mu}{\hbar^2}\left(\frac{2Ze^2}{r} + \frac{\hbar^2\ell(\ell+1)}{2\mu r^2} - Q_{I_d}\right)u_{I_d,\ell} = \sum_{I'_d,\ell'} K^2_{I_d\ell\, I'_d\ell'}\, u_{I'_d,\ell'} \,. \tag{25}$$

which is a generalized form of Eqs. (11a) and (11b) of Ref. 43 where I_d and ℓ are the total angular momentum of the daughter and of the alpha particle in a given decay channel, M is the reduced mass, Z is the charge of the daughter nucleus, Q_{I_d} is the effective Q value for the alpha particle with electron screening and daughter recoil energy corrections, and the $K^2_{I_d\ell I'_d\ell'}$ are the matrix elements of the quadrupole coupling operator which is proportional to the product of the intrinsic nuclear quadrupole moment Q_o of the daughter times $P_2(\cos\theta)$ divided by r^3, where r is the radial separation variable. For ^{249}Bk the value for Q_o was taken to be the same as that for the parent, ^{253}Es; namely, 13.1 b.[46] For ^{251}Cf and ^{255}Fm we used approximately the same value, namely, 13.0 b.

Explicit expressions for the quadrupole coupling matrix element

were given for alpha decay in Ref. 4 and Ref. 6 and for optical model scattering applications and decay, see Refs. 2 and 3.

As before, the general solutions of the uncoupled differential equations can be written as $u_\ell(\eta,\rho) = G_\ell(\eta,\rho) + iF_\ell(\eta,\rho)$ where G_ℓ and F_ℓ are the irregular and regular Coulomb functions[47] respectively. Solutions of the coupled differential equations approach the Coulomb functions asymptotically at large radius.

In general, the phase of an oscillating coupled-channel solution in the far region will differ from the phase of the corresponding Coulomb function. This phase difference is referred to as the quadrupole phase shift, $\Phi_{I_d\ell}$. Although phase shifts do not affect intensity calculations, they do affect angular distributions through the interference terms between alpha wave components of differing ℓ going to the same final state I_d. For notational convenience we sometimes use the single index j or k in place of the pair (I_d,ℓ), where j = 1 through 9 denote respectively, (I_d,ℓ) = (7/2, 0), (7/2, 2), (7/2, 4), (9/2, 2), (9/2, 4), (11/2, 2), (11/2, 4), (13/2, 4) and (15/2, 4).

Here we have a set of nine second-order coupled differential equations which can be transformed into a set of eighteen first-order coupled differential equations having eighteen linearly independent solutions or, equivalently, nine complex solutions. Because the physically meaningful solutions decrease exponentially going outward through the barrier, it is not possible to obtain stable solutions by outward numerical integration. Instead we use Coulomb functions as starting conditions at 150 f, a radius sufficiently large that the coupling forces are small, and integrate inward as we discussed in detail in our ^{212m}Po alpha decay case. The

solutions of interest then increase in the direction of integration and remain stable. For the k^{th} linearly independent set of solutions, we initialize the k^{th} function and its derivative with the value of the complex Coulomb function corresponding to that channel and the remaining channels are initialized to zero. We label the resulting linearly independent set of complex solutions as $u_{jk}(r) = g_{jk}(r) + if_{jk}(r)$, representing the j^{th} channel of the k^{th} linearly independent solution.[48]

Any general solution of the coupled differential equations may be expressed as a linear combination of the solutions just described; that is, the general solution for the j^{th} channel may be written as

$$\Psi_j(r) = \sum_{k=1}^{9} c_k u_{jk}(r) \tag{26}$$

where the coefficients $c_k = a_k + ib_k$ are complex numbers. Because an alpha particle is assumed to exist in a quasi-stationary state prior to emission, the imaginary part of each wave function Ψ_j must essentially vanish near the nuclear surface. Using nuclear model constraints, which will be discussed in the next Section III.C, values for the real parts of the wave functions at the nuclear surface can be obtained. Then the set of nine complex simultaneous equations, $\Psi_j(r)$, can be solved for the coefficients c_k.

The system of simultaneous equations is conveniently represented in the matrix equation

$$\underset{\sim}{U}\,\underset{\sim}{C} = \underset{\sim}{\Psi} \tag{27}$$

where the matrix elements u_{jk} of the 9×9 complex matrix U are the amplitudes of the linearly independent solutions on or near the nuclear surface. The elements of the column vector $\underset{\sim}{C}$ are the unknown complex coefficients c_k,

and the elements of the column vector $\underset{\sim}{\Psi}$ are the purely real nuclear model surface amplitudes. The problem is solved by inverting the U matrix

$$\underset{\sim}{C} = \underset{\sim}{U}^{-1} \underset{\sim}{\Psi} \tag{28}$$

The intensity of a given partial wave is the product of the square of the wave function amplitude and the velocity which goes as $Q_\alpha^{1/2}$. From the c_k values thereby obtained, and in view of the starting conditions of the pure Coulomb functions, the relative alpha partial wave intensities ϑ_k are

$$\vartheta_k = |c_k|^2 Q_\alpha^{1/2} = (a_k + b_k) Q_\alpha^{1/2} \tag{29}$$

where Q_α is the alpha decay energy in that channel. The quadrupole phase shifts ϕ_k are

$$\phi_k = \arg c_k = \tan^{-1}(b_k/a_k) \tag{30}$$

The most general way to present the results of the numerical integration is as the complex matrix $\underset{\sim}{U}^{-1}$ (the inverse of the complex 9×9 matrix $\underset{\sim}{U}$). The matrix elements of $\underset{\sim}{U}$ are the amplitudes of the linearly independent solutions on a spherical surface near the nucleus. These matrices reduce to unit matrices for vanishing nuclear quadrupole moment. Operation with U^{-1} on a vector representing boundary conditions on a sphere near the nuclear surface will yield partial wave amplitudes and quadrupole phase shifts at large distances. If boundary conditions are fixed on the spheroidal nuclear surface, then a Fröman matrix can be used to transform them to boundary conditions on a sphere at 10 f. The real and imaginary components of the 9×9 matrix $\underset{\sim}{U}^{-1}$ have been given in Refs. 12 and 13.

C. Numerical Results for the Odd-Mass Coupled Channel Cases

In the similar work of J. O. Rasmussen and E. R. Hansen[49] on even-even ^{242}Cm favored alpha decay, the boundary conditions for the real part of the solutions could be imposed by demanding agreement with experimental relative transition intensities to the rotational levels in ^{238}Pu. Because of partial-wave branching in odd-mass nuclei, however, the relative intensity data are inadequate. In our present formulation, there are nine real solutions, so after normalization eight boundary conditions must be specified. The experimental data provide only four relative alpha intensities going to the five daughter levels, and there are no direct experimental measurements of the partial wave amplitudes or relative phases contributing to each alpha transition. The low-temperature angular distribution data provide two experimental numbers, the coefficients of the $P_2(\cos\theta)$ and $P_4(\cos\theta)$ terms in the angular distribution function, but they do not uniquely determine relative partial wave amplitudes and phases.[43]

1. Deviation from BFM spherical barrier penetrability

Because there are insufficient experimental data to completely fix the boundary conditions, nuclear model constraints are used as well. We use the fundamental assumption underlying the "leading order intensity relationships" of the strong coupling model[2,50] that near the nuclear surface the projection of any partial wave's angular momentum along the cylindrically-symmetric 3-axis of the daughter nucleus, m_ℓ, has a value of $K_d \pm K_p$, where K_d and K_p are the projections of the daughter and parent total nuclear angular momentum on the 3-axis. For $(K_d + K_p) > \ell$ only one value of m_ℓ is allowed; for favored alpha decay $m_\ell = 0$ and $K_d = K_p = K$.

The condition of only $m_\ell = 0$ components on a sphere of radius R_0 near the nucleus provides six boundary conditions, tying together the components of a given ℓ-wave in proportion to Clebsch-Gordan coefficients. A. Bohr, P. O. Fröman, and B. R. Mottelson[6] and F. Asaro, S. G. Thompson, F. S. Stephens, and I. Perlman[40] have, in some applications, constrained the relative s, d and g wave intensities to the average of nearest neighbor even-even nuclei, but such a constraint is not as fundamental as the $m_\ell = 0$ constraint. The remaining two boundary conditions are left as free parameters which we denoted as α_2, the ratio of total d wave to s wave amplitude at R_0, and α_4, the ratio of total g wave to s wave amplitude at R_0. Therefore, the nine elements of the column vector wave function of Eq. (28) at R_0 are given as follows:

$$\Psi_j(R_0) = \alpha_\ell \langle \ell I_p 0K | I_d K \rangle \tag{31}$$

Here we use the trivial normalization condition, $\alpha_0 = 1$. The real part of the wave function decreases exponentially going outward through the barrier region and oscillates in the far region.

Having chosen these boundary conditions, the numerical integration of the coupled differential equations permits us to test two assumptions of the strong coupling model as usually applied. The first is that near the nuclear surface only $m_\ell = 0$ alpha partial waves occur. Subject to this $m_\ell = 0$ constraint, we wish to determine if the coupled channel treatment can reproduce both the experimental relative intensities to the five lowest rotational levels of the daughter nucleus and the angular distribution data. This $m_\ell = 0$ condition is equivalent to Bohr and Mottelson's "leading-order intensity relations." The second assumption is the usual

approximate treatment of anisotropic barrier penetrability, in which the relative intensity of an ℓ-wave to a given level is calculated as a Clebsch-Gordan coefficient squared times a spherical barrier penetrability factor for the alpha group.[6] This approximation, originally due to BFM, is exact either when $m_\ell = 0$ or in the limits of infinite moment-of-inertia or for vanishing nuclear quadrupole moment, $Q_o = 0$.

It is interesting to compare the BFM predictions with intensity data for favored decay in several odd-mass deformed nuclei. In Fig. 7 we have plotted the ratios of hindrance factors of second to first excited states. The hindrance factors are from the compilation of Y. A. Ellis and M. R. Schmorak.[51] If these alpha groups were purely $\ell = 2$, the ratio would, by the BFM intensity relations, equal the indicated ratio of squared Clebsch-Gordan coefficients. Actually the ratio points are lower limits for the desired $\ell = 2$ intensity ratio, since the small correction for $\ell = 4$ components would raise them.

2. Deformation parameter specifications of boundary conditions with and without the $m_\ell = 0$ surface constraint

Let us now consider for ^{253}Es and ^{255}Fm the determination of the two free parameters α_2 and α_4. The value for α_2 is largely determined by the requirement that the alpha intensity to the $9/2^+$ daughter level be reproduced, because this level receives the largest d-wave component In general there are two values for α_2, one positive and one negative, that give satisfactory agreement with experiment. The sign of the anisotropy in the alpha particle angular distributions for both ^{253}Es and ^{255}Fm requires that the s and d waves be in phase, that is, that they interfere constructively near the nuclear poles. Therefore only positive values

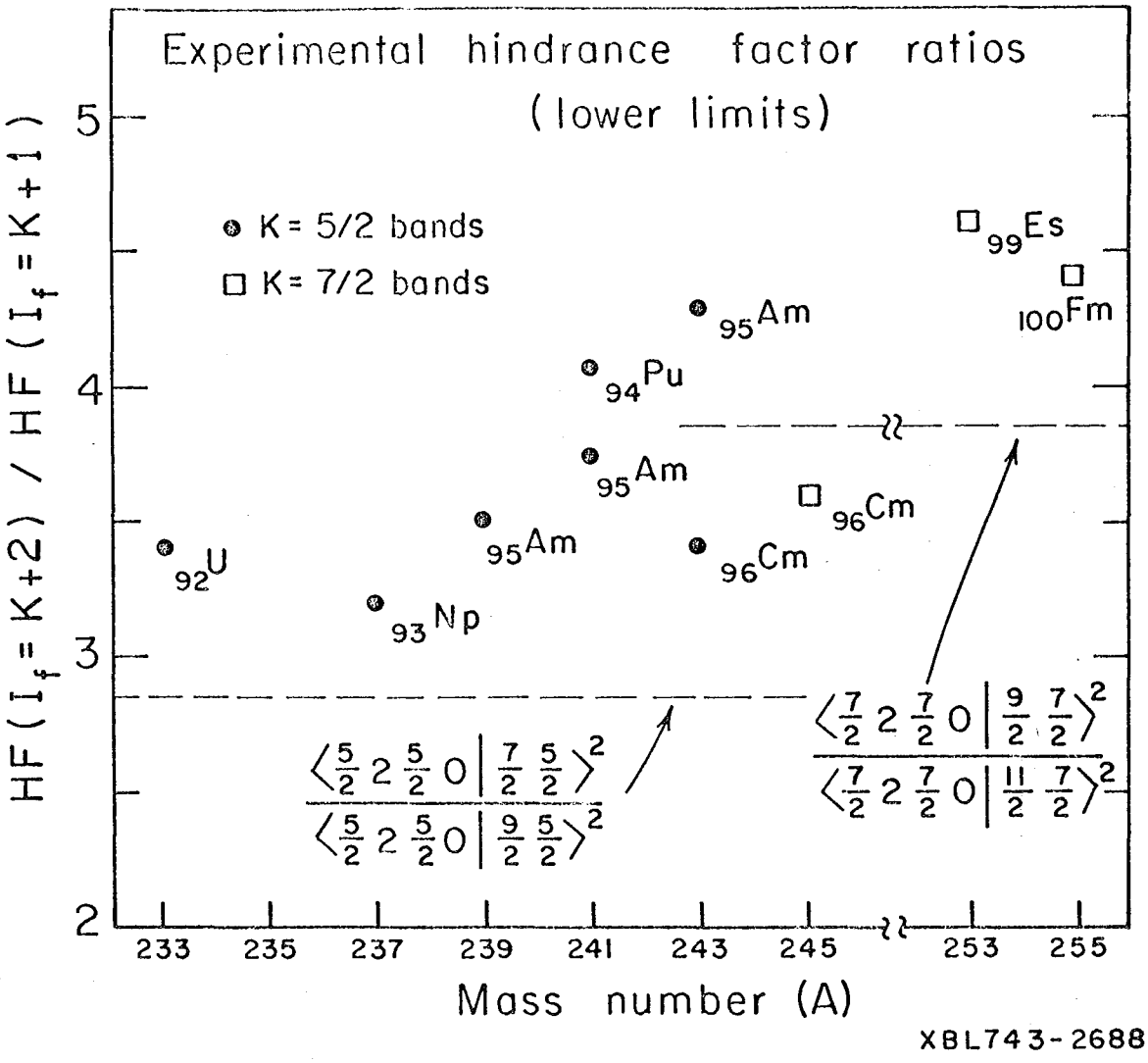

Fig. 7. Ratio of the hindrance factor of the second excited level to that of the first excited level in the favored alpha decay band of odd-mass nuclei.[51]

for α_2 are acceptable.

In like manner the alpha intensity to the $13/2^+$ level largely determines the value for α_4. The phase of the g wave is less well determined by the angular distribution data, but the ^{253}Es angular distribution data and alpha decay systematics suggest that the g wave is out of phase. Therefore only negative values for α_4 are acceptable.

From microscopic theory using Nilsson functions the values of both α_2 and α_4 can be estimated. J. K. Poggenburg[19,52] calculated partial wave amplitudes on a Nilsson coordinate surface to be 1.035, 0.309, and -0.376 respectively for the $\ell = 0$, 2 and 4 waves of ^{253}Es and 1.008, 0.361, and -0.387 for ^{255}Fm. Applying a Fröman matrix of argument B = 1.36, which is approximately correct* for the transformation from the Nilsson surface to a sphere near the nuclear radius, we obtain $\alpha_0:\alpha_2:\alpha_4 = 1 : 0.81 : -0.10$ for ^{253}Es and $1 : 0.85 : -0.09$ for ^{255}Fm.

Using the $\underset{\sim}{U}^{-1}$ matrix and Eqs. (29) and (31) for the relative intensities, we applied a least-squares fitting procedure, allowing the surface amplitude ratios of d to s waves (α_2) and g to s waves (α_4) to vary.

The values of α_2 and α_4 were obtained by minimizing the weighted root-mean-square logarithmic differences between the theoretical and

---

*In the work of Poggenburg,[19] it was determined that a Fröman matrix argument of B = 0.9 was optimum for propagating the Legendre expanded wave function on a Nilsson stretched coordinate surface out to a spherical surface outside the barrier. In coupled channel work of Rasmussen and Hansen[49] on ^{242}Cm it was determined that the Fröman argument of B = -0.455 was appropriate for propagation from a sphere near the nucleus but just beyond the range of nuclear potential out to a sphere at large distance. Since Fröman arguments are additive, we thus take the argument for propagation across the nuclear surface to be the difference 0.9-(-0.455) ≈ 1.36. We approximated the Fröman matrix by interpolation from Fröman's tables.[53]

experimental intensities. The weighting reflected the uncertainties in the experimental intensities. The best fits to the experimental intensities are obtained with $\alpha_0:\alpha_2:\alpha_4 = 1.0 : 0.8580 : -0.0977$ for ^{253}Es and $\alpha_0:\alpha_2:\alpha_4 = 1 : 0.7918 : -0.1794$ for ^{255}Fm. The agreement of these amplitude ratios with those above calculated from microscopic theory is reasonable.

These fits are plotted in the left-hand bars of Figs. 8a and 8b. The right-hand bars refer to calculations with the $m_\ell = 0$ constraint removed, and they will be discussed in Section III.C. The nuclear orientation results do not explicitly enter the least-squares fitting, but because of them only the region of positive α_2 was searched.

The logarithmic histogram display is chosen to show the predicted ℓ-mix within various alpha groups, but one should not be misled by the apparent large $\ell = 4$ crosshatched area which results from using a logarithmic and not a linear scale.

The partial wave intensities, Coulomb phase shifts, and quadrupole phase shifts corresponding to the least-squares solutions are summarized in Tables 12 and 13 for ^{253}Es and ^{255}Fm, respectively. The pure Coulomb phase shifts are given by[47]

$$\sigma_\ell = \arg \Gamma(\ell + 1 + i\eta) \qquad (32)$$

We shall discuss primarily the ^{253}Es results; however, the general comments are applicable also to the ^{255}Fm results.

Examination of the best fits to the intensities for both ^{253}Es and ^{255}Fm reveals a systematic discrepancy. The experimental intensity ratio between the second and first excited states in the rotational band of the daughter is significantly larger than predicted for both nuclei. These

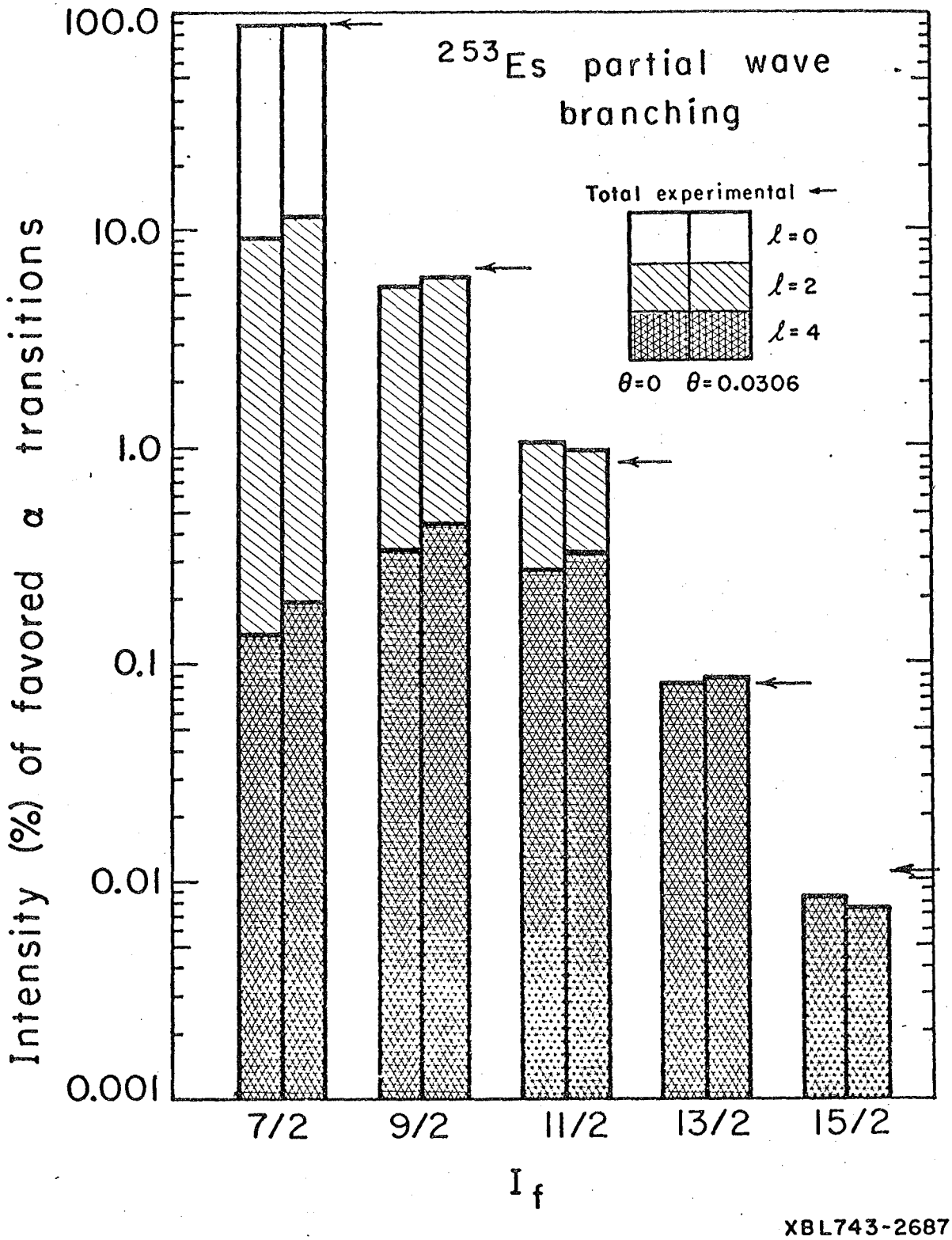

Fig. 8a. Favored band alpha branching calculations for ^{253}Es compared with experiment (arrows). The left-hand bars represent coupled-channel, logarithmic least-squares fits with the constraint $m_\ell = 0$. The right-hand bars are fits with an additional parameter, the tilt angle θ, varied (see text).

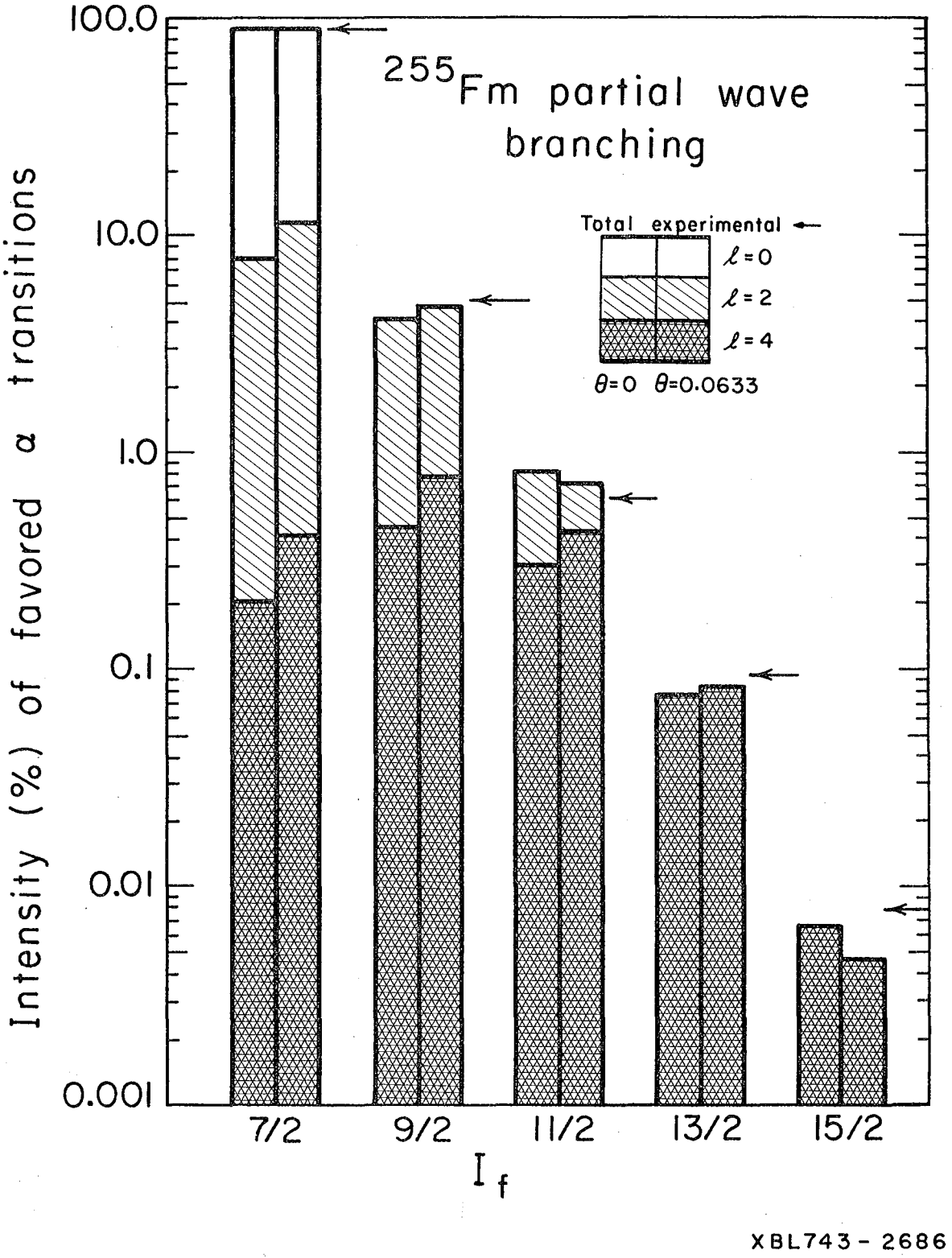

Fig. 8b. The same as in Fig. 8a, except it is the favored band alpha branching calculation for ^{255}Fm.

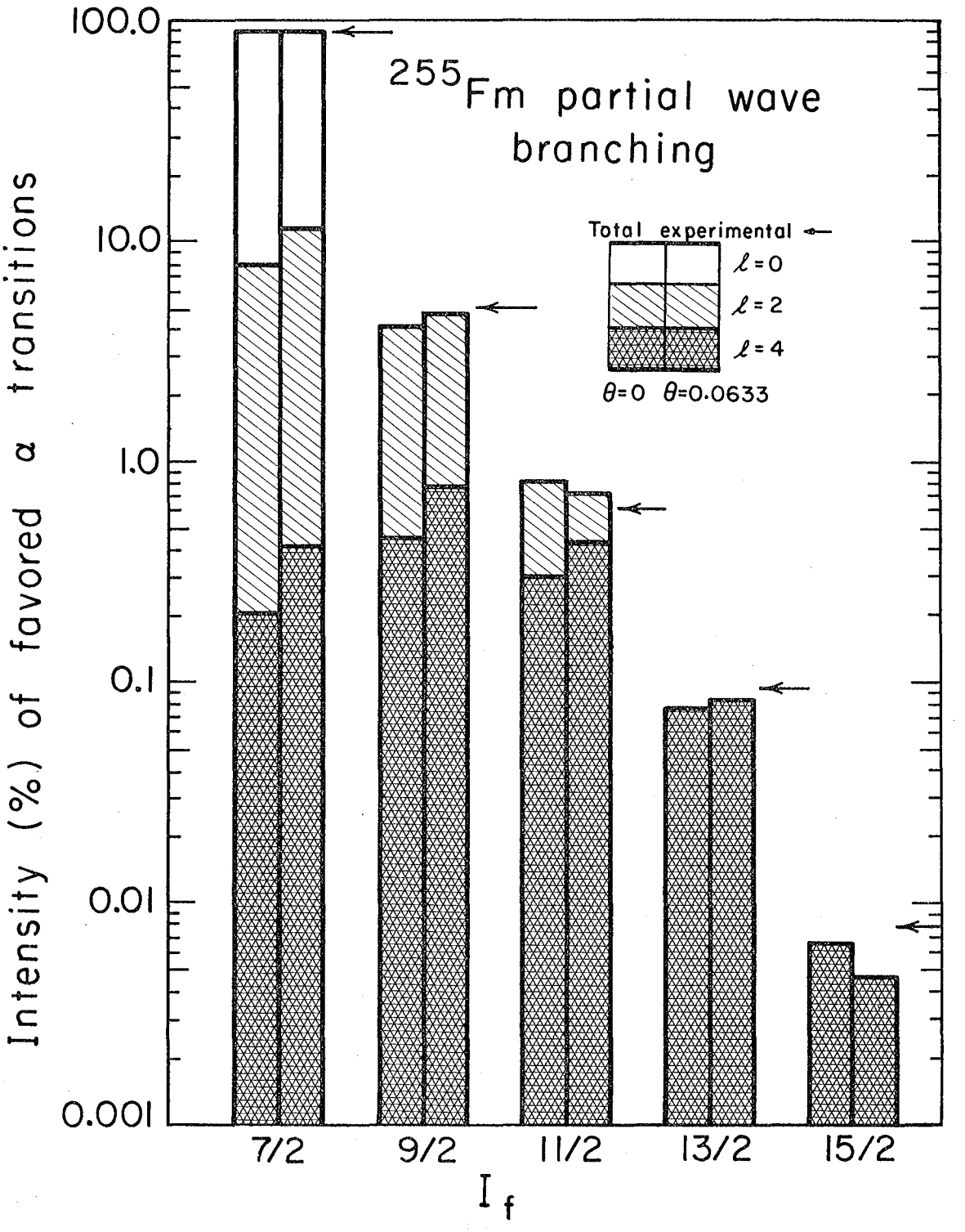

Fig. 8b. The same as in Fig. 8a, except it is the favored band alpha branching calculation for ^{255}Fm.

TABLE 12. ^{253}Es partial wave intensities, quadrupole phase shifts, and Coulomb phase shifts obtained by numerical integration ($\alpha_0 = 1$, $\alpha_2 = 0.8580$, $\alpha_4 = -0.0977$).

I_d,π	ℓ	Partial wave intensity	Experimental intensity with i-wave subtracted (%)	Quadrupole phase shift (radians)	Coulomb phase shift (radians)
$7/2^+$	0	81.7983		-0.021	50.803
	2	8.9034		-0.130	53.81
	4	0.1355		0.127	56.659
	sum	90.8372	89.8		
$9/2^+$	2	5.2180		-0.159	54.047
	4	0.3383		0.138	56.891
	sum	5.5564	6.6		
$11/2^+$	2	0.7788		-0.193	54.338
	4	0.2723		0.151	57.183
	sum	1.0511	0.845		
$13/2^+$	4	0.0848	0.0810	0.167	57.537
$15/2^+$	4	0.0085	0.011	0.184	57.963

TABLE 13. ^{255}Fm partial wave intensities, quadrupole phase shifts and Coulomb phase shifts obtained by numerical integration ($\alpha_0 = 1$, $\alpha_2 = 0.7918$, $\alpha_4 = -0.1794$).

I_d,π	ℓ	Partial wave intensity	Experimental intensity with i-wave subtracted (%)	Quadrupole phase shift (radians)	Coulomb phase shift (radians)
$7/2^+$	0	86.1522		-0.007	49.495
	2	7.5837		-0.136	52.505
	4	0.2035		0.110	55.343
	sum	93.9393	93.4		
$9/2^+$	2	3.9054		-0.179	52.807
	4	0.4433		0.122	55.646
	sum	4.34487	5.05		
$11/2^+$	2	0.5004		-0.226	53.180
	4	0.3013		0.134	56.021
	sum	0.8017	0.62		
$13/2^+$	4	0.0787	0.097	0.146	56.471
$15/2^+$	4	0.0066	0.008	0.158	56.994

states are populated primarily by d waves, and no combination of initial $\ell = 0$, 2, 4 ratios reproduces the experimental intensity ratio if the $m_\ell = 0$ constraint in the nuclear frame is maintained. This same systematic deviation from BFM theory has been noted for favored bands of many alpha emitters as was shown in Fig. 6, but it is only now clear that the coupled channel treatment does not remove the discrepancy. As a result, we conclude that some d-wave component with $m_\ell \neq 0$ must be included near the nucleus.

Table 14 compares the $\ell = 4$ branching prediction of our coupled-channel theory with the BFM formula[6] as applied by K. Poggenburg[19] and by F. Asaro, S. G. Thompson, F. S. Stephens and I. Perlman[40] where they used a square-well model to calculate alpha penetrabilities, while Poggenburg used an optical model nuclear potential. It can be seen that our coupled channel results are very close to the earlier BFM approximation, thus confirming the theoretical validity of approximating alpha branching at infinity by the product of the barrier penetrability times the square of the appropriate Clebsch-Gordan coefficient. However, there is a regime of higher $\ell = 4$ wave hindrance where the channel coupling results in deviations from the BFM branching approximation. In Fig. 9, $\ell = 4$ branching ratios are plotted as a function of α_4 with $\alpha_2 = 0.89$. The values at $\alpha_4 = -0.101$ are given in Table 12. In the vicinity of $\alpha_4 = 0.2$ the hindrance factors are highest, and the deviations from the BFM branching approximation are substantial. But channel coupling does not affect the accuracy of the simple Clebsch-Gordan branching expressions for $\ell = 4$ until higher $\ell = 4$ hindrance factors are encountered than those in ^{253}Es or ^{255}Fm.

TABLE 14. Comparison among theories of calculated branching ratios for the $\ell = 4$ groups from ^{253}Es.

I_d	BFM-sharp barrier (F. Asaro et al)[40]	BFM-sloping barrier (K. Poggenburg)[19]	Coupled-channel (this work)
7/2	(1)	(1)	(1)
9/2	2.57	2.486	2.499
11/2	2.10	1.994	2.010
13/2	0.65	0.632	0.626
15/2	0.065	0.063	0.063

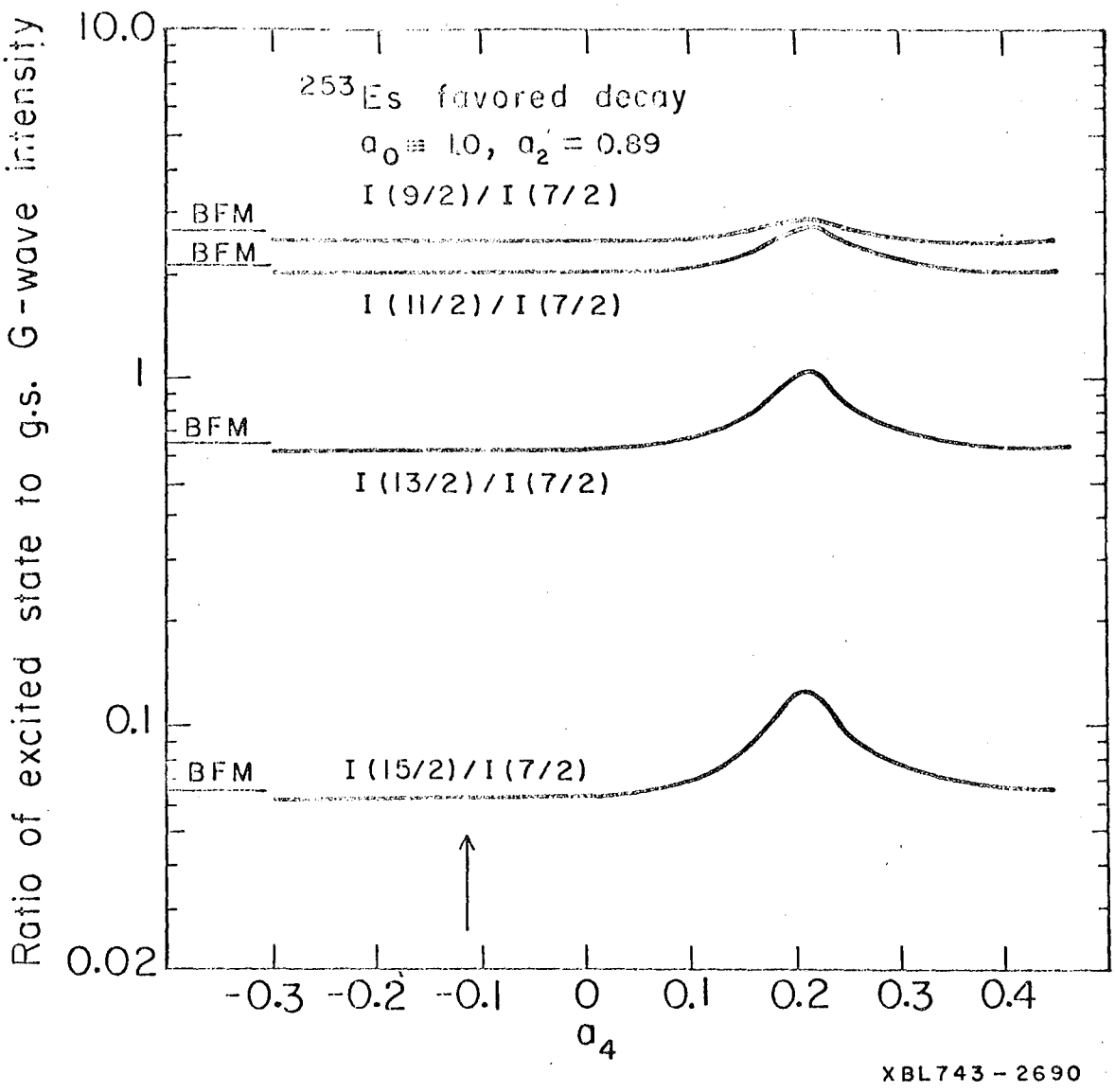

Fig. 9. Logarithm of the calculated ratios of $\ell = 4$ partial waves as a function of α_4, with α_2 fixed at 0.89. The coupled channel calculations are for ^{253}Es with $m_\ell = 0$ constraint. The BFM ratios (Clebsch-Gordan coefficients squared) are shown at left.

3. Checks on the accuracy of the coupled channel computer calculations

Several numerical tests on the computer programs were performed. The regular and irregular Coulomb functions were integrated inward from 150 f to 10 f with coupling turned off, i.e., with $Q_0 = 0$. The irregular solutions agreed with pure Coulomb functions to within a few tenths of a percent. The uncoupled regular solutions, which should be exponentially decreasing going into the barrier, were not stable inside the barrier, but they were smaller than the irregular solutions by a factor of 10^5, which is more than sufficiently accurate for this problem. The radial integration interval was varied by an order of magnitude to insure that accuracy was not limited by choice of mesh size.

In order to check the completeness and accuracy of the quadrupole coupling matrix elements, the rotational energy and the centrifugal energy of each group were set equal to zero. The regular Coulomb function $F_0(\eta,\rho)$ with η and ρ appropriate for the $I_d = 7/2$ channel was integrated inward from 150 f with $Q_0 = 13.1$ b. The d and g waves were found to branch in the ratio of Clebsch-Gordan coefficients as they should.

A relative penetrability can be approximated by the ratio of the uncoupled regular function at 10 f to the uncoupled regular function at 150 f squared. Each squared ratio was divided by the corresponding penetrability given by K. Poggenburg,[19] who used a Fröman matrix to calculate penetrabilities. The resulting quotients should be, and were, approximately equal.

D. Inclusion of $m_\ell \neq 0$ Favored Alpha Decay Components

We have shown that a careful coupled-channel barrier treatment does not correct the BFM formula deviations visible in Fig. 6, under the constraint that the surface alpha wave function contains only $m_\ell = 0$ components. The systematic deviation of hindrance factor ratios from Clebsch-Gordan coefficient ratios must be explained in terms of $m_\ell \neq 0$ admixtures.

Gamma vibrational phonon ($\ell = 2$, $m_\ell = 2$) admixtures into actinide element nuclear wave functions have been calculated by Soloviev and co-workers,[54,55] but these admixtures seem too small to change the d-wave branching to the degree required to fit intensity patterns and nuclear orientation data.

There are insufficient data to completely determine all $m_\ell \neq 0$ amplitudes. In general, four experimental intensity ratios are known, and when $m_\ell = 0$, two adjustable parameters α_2 and α_4 are derived by a least-square fit. Then there are only two remaining degrees of freedom. If we introduce $m_\ell \neq 0$ amplitudes in a formulation that has two or more adjustable parameters, the problem becomes completely determined or over-determined, and a least-squares fitting procedure cannot be used to derive parameter values. We have therefore attempted to introduce $m_\ell \neq 0$ amplitudes in a formulation with only one new adjustable parameter.

It was proposed that a one-parameter constraint be used for introduction of $m_\ell \neq 0$ components from consideration that the mass of the alpha particle is not negligible compared to that of the daughter nucleus.[56] While the alpha particle is within the nucleus (as a cluster), it is part of the system of spheroidal symmetry with symmetric top inertial properties.

When the alpha particle leaves the surface suddenly, the principal axes of the core will be suddenly shifted by a tilt angle θ. We represent the nuclear core inertial system classically by mass distributed along the body-fixed symmetry z' axis (see Fig. 10), or a diatomic molecule model such that the moment-of-inertia has the experimental value $\mathcal{J}$ and $\mathcal{J}^{-1} = m_\alpha R^2/J$. We then consider the removal of alpha particle mass at the nuclear radius at a particular angle ϕ in the body fixed y-z plane. (Equivalently we may add alpha particle mass at $-\phi$.) The new principal inertial axes are rotated from the old by angle θ, given by

$$\sin 2\theta = 1/\mathcal{J} \sin 2(\phi - \theta) \tag{33}$$

Since in the mass $A \sim 250$ region $\mathcal{J}^{-1} = m_\alpha R^2/J \approx 0.11$, which is $\ll 1$, we can make a small θ expansion approximation of the above tilt equation to give

$$\theta \approx 1/\mathcal{J} \left\{ \sin 2\phi (1 + 1/\mathcal{J} \cos 2\phi)^{-1} \right\} \tag{34}$$

We assume that the appropriate average alpha emission angle ϕ, in the nuclear frame, should refer to the alpha wave outside the barrier. Thus, as an approximation we may estimate $\langle \phi \rangle$ directly from hindrance factors of even-even neighbors. For nuclei with the maximum $\ell = 4$ hindrance factors ($A \sim 244$) we believe $\langle \phi \rangle$ to have the value of the first zero of $P_4(\cos\phi)$, or $\phi \sim 30°$. The trend in hindrance factors is such that $\langle \phi \rangle$ is a monotonically increasing function of mass number throughout the actinide region, and at the highest masses for which alpha fine structure has been measured, the rising $\ell = 2$ hindrance factor has not yet gone through a maximum. Hence $\langle \phi \rangle < 55°$, the zero of $P_2(\cos\phi)$. If we take for $\langle \phi \rangle$ an approximate value for ^{253}Es, and ^{255}Fm of $\phi \approx 45°$, we can solve Eq. (34)

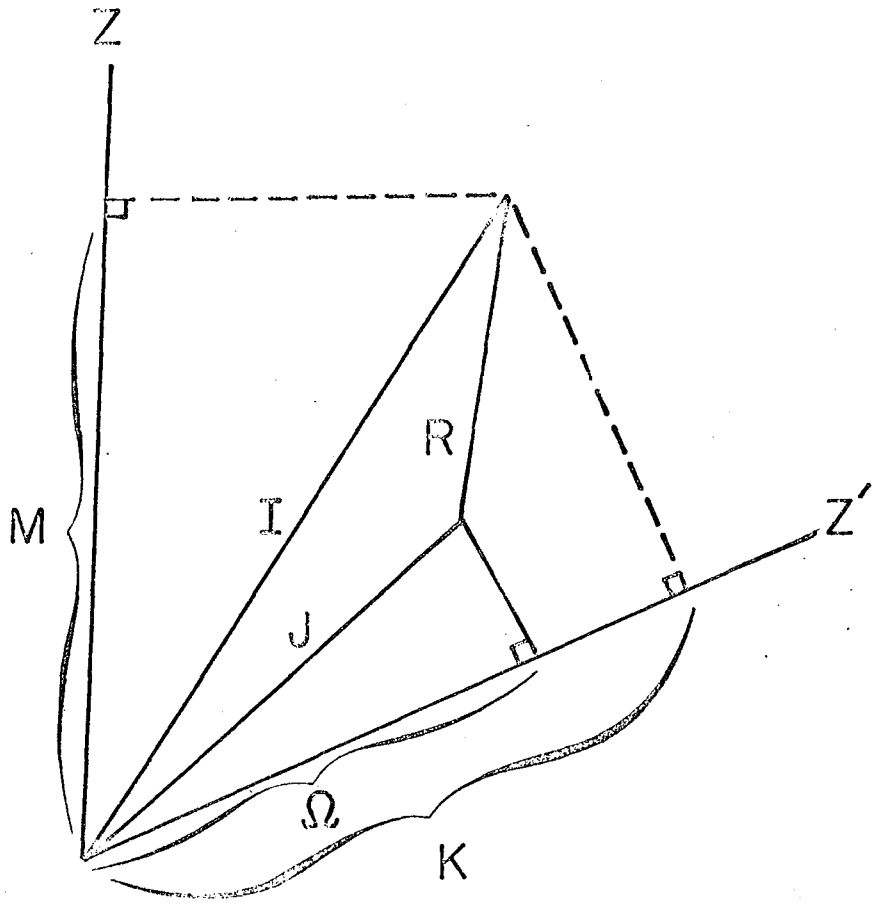

XBL 783-2439

Fig. 10. Vectoral diagram of nuclear spin vectors and projections. The external orientation direction is Z and the nuclear symmetry axis is Z', I is the nuclear spin with projection K on the axis of symmetry. The resultant from the last odd nucleon or total of odd nucleons is denoted as $\vec{R}$ and is the vectoral addition of $\vec{I}$ and $\vec{J}$ and the projection of $\vec{J}$ on the nuclear symmetry axis Z'; and M is the projection of I on the external direction, Z. For favored alpha $K_i = K_f$ and for the ground state rotational band $I = R = K$ and the ground state for even-even nuclei is zero, $I = 0$, so that $J^\pi = 0^+$.

to get tan $2\theta \approx 0.11$ or $\theta \approx 0.05$. Thus, we would take the favored alpha wave amplitude of $m_\ell = 0$ at the surface and rotate the coordinate system, generating $m_\ell \neq 0$ components in the new frame (see Ref. 1 for further details).

With our numerical solutions of the coupled-channel equations we have made a weighted least-squares determination of the best values of α_2, α_4, and θ to fit the experimental intensities. The original two-parameter least-squares fits, i.e., with the constraint $\theta = 0$ for $m_\ell = 0$, were presented in Section D, and Figs. 7 and 8 also show the fits with θ unconstrained.

The optimum α_2, α_4, and θ values for ^{253}Es are 0.891, -0.117, and 0.0306 radians, respectively. The corresponding values for ^{255}Fm are 0.828, -0.250, and 0.0633. Our one additional parameter θ can be seen from Figs. 7 and 8 to have improved the 11/2 : 9/2 branching ratio ($\ell = 2$), and the least-squares θ values are in satisfactory agreement with the estimate of tilt of principal axes during alpha decay. The 15/2 : 13/2 branching ratio ($\ell = 4$) is not in very good agreement with theory, but the weak $\ell = 4$ groups may be affected by our truncation of the coupled-channel equations to exclude $\ell \geq 6$. (See Section III.F for an analysis of the effect of the $\ell = 6$ wave on the results of our coupled channel calculation.)

E. Additional Discussion of the Relaxation of the $m_\ell = 0$ Condition

We have formulated a derivation in terms of a model of $\ell = 2$ favored alpha hindrance factor ratios from the leading-order Clebsch-Gordan intensity relations, due to a recoil term in the core rotational inertial

system. The effect is to introduce $m_\ell \neq 0$ components into the favored alpha wave function at the nuclear surface. Although we solved the nine coupled channel equations only for parent spin 7/2, we can reasonably infer a similar behavior for the several $I_i = 5/2$ cases plotted in Fig. 6. As the mass number increases the mean alpha emission angle $\langle \phi \rangle$ in the nuclear frame shifts from small values toward 45 or 50° for the mass, A ~ 250 region, the deviations should monotonically increase, as they do for the spin 5/2 cases.

With the coupled channel equations we have calculated the quadrupole phase shifts, which affect the interference terms in angular distribution experiments involving favored alpha decay. It would be interesting to have experimental α-γ angular correlation studies to test our predicted angular momentum mixtures and phase shifts for decay to excited rotational band members. The low-temperature nuclear orientation experiments could not resolve individual alpha groups and were thus mainly sensitive to the composition of the alpha group or to the band head. In the next section we discuss the effect of not including the $\ell = 6$ partial wave components in the coupled channel calculations.

F. The Effect of Exclusion of the $\ell = 6$ Partial Waves from the Coupled Channel Calculation

In order to limit the number of coupled differential equations to be solved, the $\ell = 6$ and higher angular momentum waves were excluded from our analysis. The hindrance factor for the $\ell = 6$ wave of the nearest neighbor Cf isotope is approximately 1000, whereas the hindrance factor for the $\ell = 4$ wave is[51] approximately 30. Therefore, the $\ell = 6$ wave cannot

noticeably affect the $\ell = 4$ branching. Because the $\ell = 6$ wave was excluded from the theoretical analysis, an approximate i-wave component was subtracted from the experimental intensities before making the comparison with theory. This was done as follows: I. Ahmad[41] has measured the alpha intensities to the $17/2^+$ and $19/2^+$ levels of ^{253}Es (see Table 15). These levels are populated by $\ell = 6$ and higher angular momentum waves only, and we assumed that the higher ℓ waves are much weaker than the i-wave. The $\ell = 6$ penetrability factor for alpha decay to the $17/2^+$ level, which was obtained by extrapolating Poggenburg's penetrabilities,[19] was multiplied by the appropriate squared Clebsch-Gordan coefficient in order to obtain a relative theoretical intensity which was normalized to Ahmad's experimental intensity. The process was then reversed to obtain the i-wave component to the lower spin states of the favored rotational band. The results are given in Table 15.

For ^{255}Fm alpha decay the experimental intensity to the $17/2^+$ level is unknown; therefore, we assumed that Poggenburg's calculations correctly predict the relative i-wave component. We believe this approximation is permissible because the correction is, in any case, small, and the correction has a significant effect only on the $13/2^+$ and $15/2^+$ intensities, which already have small weighting factors in the fitting routine. While it is true that any error in this extrapolation from Poggenburg will to some degree be reflected in our fit of α_4, our major fitting difficulty is in reproducing the ratio between the $9/2^+$ and $11/2^+$ intensities, which is not strongly affected by either α_4 or the correction. Our corrections to the ^{255}Fm experimental intensities are also given in Table 15.

TABLE 15. Correction factors for the i partial wave.

	^{253}Es		^{255}Fm	
I_d^π	Experimental intensity[41] (%)	$\ell = 6$ component (%)	Experimental intensity[41] (%)	$\ell = 6$ component (%)
$7/2^+$	90.0	0.0002	93.4	0.0003
$9/2^+$	6.6	0.0014	5.05	0.0022
$11/2^+$	0.85	0.0037	0.62	0.0040
$13/2^+$	0.085	0.0039	0.110	0.0129
$15/2^+$	0.013	0.0018	0.013	0.0049
$17/2^+$	0.0004	(0.0004)		
$19/2^+$	0.00012			

The reliability of our i-wave correction for ^{255}Fm decay is indicated by applying the same method to ^{253}Es. The subtracted components would then be 0.0001, 0.0016, 0.0031, 0.0060 and 0.0033 for the $7/2^+$ through $15/2^+$ levels. The differences between these values and the ones given in Table 15 suggest that the i-wave, like the d wave, may be more skewed toward the lower levels of the rotational band than the BFM branching relation predicts.

G. Discussion of Odd-Mass Coupled Alpha Decay Theory

We have performed a coupled channel calculation for the odd-mass nuclei ^{253}Es and ^{255}Fm which both have $7/2^+$ ground states. We have found a more improved fit to the experimental values than the BFM or K. Poggenburg results. Using the $m_\ell = 0$ assumption and not excluding the $\ell = 6$ partial wave contributions, we find that there is an underestimation of the $9/2^+$ level in which the largest contributor is from the $\ell = 2$ wave and the $11/2^+$ level is overestimated, in which the largest contributions occur from the $\ell = 4$ wave, compared to the $\ell = 4$ contribution to other levels.

Our analysis is improved by including the $\ell = 6$ partial waves in an approximate manner and also including a term, depending on relaxing the $m_\ell = 0$ condition. The systematic deviation of the hindrance factor ratios determined from the Clebsch-Gordan coefficient ratios are explained in terms of the admixtures of the $m_\ell \neq 0$ terms. We consider the effects of the alpha particle components which effect the spheroidal symmetry. The principal axis is shifted as the alpha particle is emitted. Improved fits are derived from the inclusion of gamma vibrational admixtures $\ell = 2$, $m_\ell = 2$ (see Section III.C for further discussion).

Our analysis of both the even mass and odd mass alpha decay theory has demonstrated the sensitive dependence of this formalism on the Woods-Saxon parameters and also the inexact nature of the BFM and $m_\ell = 0$ assumption. The uncertainty of the matching radius and optical model parameters prohibits us from calculating absolute decay rates; see Section II. We examine some new approaches to alpha decay theory which we hope will yield model independence of the nuclear matching parameter and the well depth of the optical model parameter.

In the next section, we utilize the time dependent reaction theory of H. Feshbach[7,23] to calculate alpha decay rates in terms of the R-matrix of real optical model potential in the absence of channel coupling. In Section V we calculate the alpha decay rate in terms of resonant decay width in the R- and S-matrix theory including channel coupling with a complex nuclear potential. The attempt of S-matrix resonant theory approach is to be able to calculate absolute decay rate which is independent of the nuclear optical model parameters.

IV. UNIFIED REACTION THEORY OF ALPHA DECAY FOR ^{212}Po AND ^{210}Po

A. Application of the R-Matrix Theory to the Alpha Decay Problem

In this section we examine in detail methods of avoiding the inherent problems of matching radius dependence of the coupled channel alpha decay theory presented in Sections II and III.

The alpha decay problem has been an illusive one. Many approaches have been taken, since the H. A. Bethe[11] and G. Gamow[12] models of an alpha cluster which is trapped in a nuclear potential well. Microscopic shell model calculations gave great impetus to the alpha decay problem. This type theory was developed by R. G. Thomas[13,31] and A. M. Lane and F. G. Thomas[8] and H. Mang,[18,57] and it has been quite successful but there are cases where it has failed to correctly predict the alpha decay, relative as well as absolute, rates; but a major failing of these alpha decay theories has been their inability to calculate absolute alpha decay widths.

A new theory of alpha decay is presented in this section, in which the nuclear radius parameter is not used explicitly. A similar expression for the decay width, as in the unified reaction theory of H. Feshbach, A. K. Kerman and R. H. Lemmer,[58] is derived based on the time-dependent perturbation method and it overcomes the inadequacies of previous alpha decay theories. It is pointed out that the new decay formula makes it possible to calculate even the absolute value of the decay rate. In this theory, the alpha decay process is interpreted as the transition due to the perturbation which is caused by the difference between four times the

nucleon-nucleus and alpha-nucleus potentials. The method of numerical calculation is illustrated for the case of a simple alpha decay.

Many alpha decay rate calculations, based on the nuclear shell model, have been performed and they reproduce the experimental fine structures of decay rates fairly well, as far as the relative intensities are concerned.[14,16] Therefore, the basic formula used in the decay rate calculations, which is the well known expression for the resonance level width in R-matrix theory, seems to be useful.

The applicability of the one-level formula in R-matrix theory to the alpha decay problem was shown by R. G. Thomas,[31] and he suggested the possibility of using shell model microscopic calculations of the alpha decay rate. H. Mang[18,31] was the first to perform practical microscopic calculations for the alpha decay rates. He derived the basic formula by generalizing Casimir's time-dependent alpha decay theory,[59] and then used it in his calculations. If the boundary condition that assures the continuity of the internal and the external alpha particle wave functions is introduced into Mang's formula, it becomes identical with Thomas' formula.

However, there are two shortcomings in these microscopic calculations based on the one-level formula. First, we must introduce the nuclear radius, which divides the space sharply into internal and external regions. The barrier penetrability, relevant to alpha decay, is very sensitive to the radius parameter. For that reason many theoretical calculations have been performed only for the determination of relative intensities, but not for the calculation of absolute decay rates. Second, the shell model wave function used for the parent nucleus does not satisfy the

boundary condition, which we normally impose upon a compound state in R-matrix theory. Fortunately, the energies of the emitted alpha particle are much lower than the height of the Coulomb barrier and these energies lie in a narrow range of between 5 and 10 MeV, so that the error due to this defect would be nearly constant. Strictly speaking, however, this defect certainly brings some errors even into the theoretical predictions of the absolute intensities.

In the next two sections of this paper (IV.B and IV.C) the effects of channel coupling were studied for coupling between the vibrational states in spherical daughter and the rotational states of a spheroidal daughter nuclei. It was found that the channel coupling affects the alpha particle barrier penetrability significantly.[3] For the decay with channel coupling, however, it is not desirable to calculate the decay rate microscopically based on the usual Mang[18,31] formula, since the coupling potential localizes at the nuclear surface and the defect of the introduction of the nuclear radius becomes a serious problem.

Recently we[10] studied the alpha decay of ^{212m}Po, taking into account the effects of collective octupole coupling, and found that the conventional microscopic theory does not explain the large alpha decay group to the first excited state of ^{208}Pb. A major cause of discrepancy may be attributed to the lack of octupole core polarization in the wave function for ^{212m}Po. However, it is also the case that the conventional theory is not satisfactory in describing this isomeric state decay. Because the very high angular momentum of the emitted alpha particle makes the predicted intensity ratio very sensitive to the choice of the

the radius parameter.

The purpose of this section is to derive a new decay formula in which the radius parameter and the boundary condition are not used at all. In order to make clear the comparison of the new formula with the old one, we shall proceed along Mang's formulation[57] as far as possible, but giving up the approximations he used. In the new decay formula we can take into account the channel coupling, in a manner that is not artificial, but we will not take up this subject here in order to simplify our discussions.

B. Lane and Thomas One-Level R-Matrix Formula

The new theory of alpha decay, in which we calculate the decay rate for the resonance level width in R-matrix theory, is compared to the one-level formula. R. G. Thomas demonstrated the applicability of the one-level formula in R-matrix to the alpha decay problem.[31] If the boundary conditions, which assures the continuity of the internal and external alpha particle wave functions is introduced into H. J. Mang's[18,31] formula, his formula becomes identical with Thomas's formula. We will give more details of Mang's theory in the next Section, IV.C. We need not specify the nuclear-radius parameter explicitly which divides the space sharply into internal and external regions. Theoretical calculations have been, in the past, performed only for the relative intensities, and not for absolute decay rates because the barrier penetrability is very sensitive to the radius parameter. We have traded the arbitrariness in R_o for an arbitrariness in the real part of the well depth parameter V_o which we will explore in more detail in this section.

A. M. Lane and R. G. Thomas have presented an extensive and detailed

discourse on R-matrix theory. The analytical form of the R-matrix and the interpretation of the properties, as the reduced width amplitudes in the Breit-Wigner energy resonances expression, is given in Ref. 8. The reduced width is defined as the alpha decay width divided by the barrier penetration factor.

The R-matrix in general is calculated in terms of the logarithmic derivatives, of the form,

$$L_c = \left(\frac{\rho_c u_c'}{u_c}\right)_{r_c} \tag{35}$$

where u_c is the outgoing and where L_c depends on the channel radius $\rho_c = (r_c \hbar^2/2u_c)^{1/2}$ and $u_c' \equiv (du_c/dr)$. The radial wavefunctions can be expressed in terms of the regular and irregular Coulomb wave functions, $u_c = G_c + iF_c$ (note that usually the definition of channel includes angular momentum, ℓ).

The diagonal form of the S-matrix can be expressed in terms of a phase shift as $U = e^{-2i\phi}$ for pure elastic scattering [where for pure Coulomb phase shifts $\phi = \tan - 1(F/G)$]. The S-matrix, or scattering matrix, is given by

$$S = U^{-1} VU \tag{36}$$

where U is a unitary symmetric matrix, and

$$V = 1 + 2iP^{1/2}(1 - RL)^{-1} RP^{1/2} \tag{37}$$

where R is the symmetrical R-matrix, L is the logarithmic derivative and P is the barrier penetration matrix, or $P = \rho/(F^2 + G^2)$ at nuclear radius, R_o and $\rho = kr$ for wave number k and radius r of the alpha particle in the

asymptotic region. These expressions hold for each partial wave ℓ and we have omitted the channel subscripts.[29] Equation (37) shows the form relationship of the R-matrix and S-matrix function. We can write the expression for alpha decay constant λ_ℓ in terms of the reduced width of Thomas,[31] γ_ℓ as

$$\lambda_\ell = \frac{2\gamma_\ell^2}{\hbar} \left(\frac{\rho}{F_\ell^2 + G_\ell^2} \right)_{r=R_o} \tag{38}$$

(we have included the partial wave subscript, ℓ). The recent paper by H. M. A. Radi, A. A. Shihab-Eldin, and J. O. Rasmussen present a brief and very useful review of the alpha decay problem with a discussion of the decay process for doubly odd nuclei.[59]

The R-matrix can be separated into two parts in the one-level R-matrix, $R = R_o + R'$, or

$$R' = \sum_\lambda \frac{\gamma_\lambda \times \gamma_\lambda}{E_\lambda - E} \tag{39}$$

where the R' part is similar to Wigner's resonance form and R^o comes from contributors not included in the λ sum singularities which occur at $E = E_\lambda$. The usual form of the R-matrix still depends upon the potential parameters and this is why we plan to turn to the S-matrix approach[8] which we presented in Section V of this paper. The scattering formalism is discussed in Section V.E.

In Eq. (39), which is the one-pole approximation for the R-matrix in terms of the reduced width γ_λ, E_λ is the resonance energy. The γ_λ are related to the real parts of the radial wave function as $\gamma_\lambda = (\hbar^2/2\mu r_c)^{1/2} u_\lambda$. We have associated poles in the S-matrix (see Section V.A.2). The pole

terms in Eq. (39) can be used to construct the resonance decay cross section. Distant pole terms are considered to give rise to a background contribution (see Section V.I.).

Causality and unitary are handled naturally and efficiently in the R- and S-matrix formations. In our Ref. 3 we base our calculations on the generalization of the Casimir time-dependent alpha decay theory[60] and introduce a new radial partial wave defined such that the R-matrix and decay width no longer depend on the channel radius and therefore we are able to attempt to calculate absolute decay widths.

C. Derivation of the Decay Width Formula

1. Mang microscopic shell-model time-dependent alpha decay rate theory

H. Mang[18] developed a theory to take into account the influence of nuclear structure on alpha decay. The theory was successful enough in explaining the fine structure of alpha decay in the Po region, it led to further exploration of this type of model. The relative intensities of transitions which lead to various states (ground and excited) in the daughter nucleus and the coefficients of alpha-gamma angular correlations were obtained with reasonable agreement with experimental values.

In Ref. 57, H. Mang derives the expression for the decay constant which is then applied to discuss the ground-state transitions of even-mass and odd-mass alpha emitters in the region of ^{208}Pb. The nuclear wave functions are approximated by shell model wave functions and reasonable agreement is obtained with experimental data.[18,57] In an earlier version of Ref. 57 (see Ref. 61), derivations of the formulas for deformed nuclei

are also given. The present derivation of the alpha decay width is similar to H. Mang's of Refs. 57 and 61.

2. Time-dependent Schrödinger equation: Decomposition of the Hamiltonian, parent, daughter wave, and alpha wave functions (in the asymptotic condition)

We start from the time-dependent Schrödinger equation for a system of A nucleons (Z protons and N neutrons)

$$H\psi(1 \ldots A,t) = i\hbar \frac{\partial \psi(1 \ldots A,t)}{\partial t} \tag{40}$$

The time-dependent wave function of the parent nucleus $\Psi_{JM}(1 \ldots A,t)$ is expanded in the following form

$$\Psi_{JM}(1 \ldots A,t) = a(t)\ \Phi_{JM}(1 \ldots A) + \sum_i \int d\varepsilon\ b_i(\varepsilon,t)\theta^i_{JM} \tag{41}$$

where Φ_{JM} is the bound state wave function and θ^i_{JM} is the channel wave function; see Eq. (62) which defines the parameter b_i.

The channel wave function θ^i_{JM} is given by

$$\theta^i_{JM} = A\left\{\chi_\alpha\left[Y_\ell(\hat{R})\ \phi_{J\sigma}(\vec{x}_N)\right]_{JM} \varphi_\ell(\varepsilon,R)\right\} \tag{42}$$

where A is the antisymmetrization operator and the superscript i stands for the set of quantum numbers $(j\sigma\ell)$. The wave functions χ_α and $\varphi_\ell(\varepsilon,R)$ $Y^m_\ell(\hat{R})$ describe the internal and center-of-mass motion of the alpha particle respectively, and $\phi^{M-m}_{j\sigma}$ is the daughter nucleus wave function. The square bracket is used to denote the angular momentum addition, and for Clebsch-Gordon coefficient, $C(\ell jJ;m\ M-m)$,

$$\left[Y_\ell\ \phi_{j\sigma}\right]_{JM} = \sum_m C(\ell jJ;m\ M-m)\ Y^m_\ell(\hat{R})\ \phi^{M-m}_j(\vec{x}_N) \tag{43}$$

Introducing this expression for Ψ into the Schrödinger equation (40) we get a system of coupled integro-differential equations for amplitudes $a(t)$ and $b_i(\varepsilon,t)$. But this system of equations decouples and becomes rather simple if one more approximation is introduced. We shall discuss some of these approximations, but first, we introduce the Hamiltonian for our problem.

The Hamiltonian H is decomposed into four parts,

$$H = H_N + H_\alpha - \frac{\hbar^2}{2\mu}\nabla^2_{\vec{R}} + V_{\alpha N} \tag{44a}$$

for
$$V_{\alpha N} = \sum_{i=1}^{4}\sum_{k=5}^{A} v_{ik} \quad , \tag{44b}$$

where H_N and H_α are the internal Hamiltonians of the daughter nucleus and of the alpha particle, respectively and the alpha nucleon potential can be written in terms of a two-body potential, v_{ik}. The wave functions $\phi_{j\sigma}$ and χ_α satisfy the following eigenvalue equations;

$$\begin{aligned} H_N\,\phi_{j\sigma} &= E(j\sigma)\phi_j \\ H_\alpha\,\chi_\alpha &= E(\alpha)\chi_\alpha \quad . \end{aligned} \tag{45}$$

The alpha particle wave function $\varphi_\ell(\varepsilon,R)$ is defined as the solution of the equation

$$\frac{\hbar^2}{2\mu}\left(-\nabla^2_{\vec{R}} + \frac{\ell(\ell+1)}{R^2}\right)\varphi_\ell(R) + U_\alpha(R)\,\varphi_\ell(R) = \varepsilon_\ell\varphi_\ell(R) \tag{46}$$

and is normalized as follows:

$$\int \varphi_\ell(\varepsilon,R)\varphi_\ell(\varepsilon',R)R^2dR = \delta(\varepsilon-\varepsilon') \tag{47}$$

The one body potential $U_\alpha(R)$ for the alpha particle should be determined so as to be consistent with Eq. (55) which appears later. One obtains an integro-differential equation of the type from Eq. (55):

$$\left\{ \frac{\hbar^2}{2\mu} \nabla^2_{\vec{R}} + \varepsilon_L - V_D(\vec{R}) \right\} \varphi_\ell(\vec{R}) = \int K(\vec{R},\vec{R}') \, \varphi_\ell(\vec{R}') d\vec{R}' \qquad (48)$$

Unfortunately, the evaluation of nonlocal potential $K(\vec{R},\vec{R}')$ in terms of $V_{\alpha N}$, $\phi_{j\sigma}$ and χ_α, being possible in principle, cannot be carried out in practice because of the large number of nucleons involved and the vast number of exchange terms resulting in different integral types contributing to $K(\vec{R},\vec{R}')$. The effects of the nonlocal term $K(\vec{R},\vec{R}')$ is usually approximated by using a local velocity-dependent potential, such as for $U_\alpha(R)$ in Eq. (46). In practical calculations, we use the real part of alpha-nucleus optical potential for $U_\alpha(R)$ as a first approximation, which is determined phenomenologically by the analyses of alpha scattering experiments. However, it should be noted that the effects of the dissociation and the distortion of the alpha particle are not contained in $U_\alpha(R)$; therefore $U_\alpha(R)$ is given by the first term of the optical potential, $\langle \chi_\alpha[Y_\ell \, \phi_{j\sigma}] \, | V_{\alpha N} | \, \chi_\alpha[Y_\ell \, \phi_{j\sigma}] \rangle$, and the exchange terms.

Because of the normalization condition of Eq. (47), we must solve Eq. (46) with the following conditions. Let us define the new radial wave function, $u_\ell(R)$ by

$$\varphi_\ell(R) = (-2i)^{-1} \sqrt{\frac{2}{\pi}} \, \frac{1}{\hbar} \sqrt{\frac{\mu}{k_\ell}} \, \frac{1}{R} \, u_\ell(R) \quad , \qquad (49)$$

where k_ℓ is the wave number of the alpha particle in the asymptotic region for large R_o. Then the boundary condition is expressed as $u_\ell(R) = 0$ at

$R = 0$ and the asymptotic form is given by

$$u_\ell(R) \xrightarrow[\lim R \to \infty]{} u_\ell^{(-)} - n_\ell \, u_\ell^{(+)} \tag{50}$$

The incoming and outgoing waves, $u_\ell^{(-)}$ and $u_\ell^{(+)}$ obey the well known expression

$$u_\ell^{(\pm)} = G_\ell \pm i \, F_\ell$$

where F and G are the regular and irregular Coulomb functions. The scattering amplitude η_ℓ is related with phase shift δ_ℓ as

$$\eta_\ell = \exp(2i \, \delta_\ell) \tag{52}$$

and is determined by smoothly joining the interior wave function at the matching radius to its asymptotic form of the wave function. If we join the interior wave function to the outgoing wave only, the energy ε_L becomes complex (discrete) and the integration in Eq. (47) gives an infinite value. The solution for the amplitudes $a(t)$ and $b_i(\varepsilon,t)$, defined in Eq. (41), will be given in Eqs. (61), (62) and (68). Using those expressions we can prove that the total wave function $\Psi_{JM}(1 \ldots A,t)$ has only outgoing waves at the resonance energy, so long as the decay width is small.

D. Real Bound State Wave Functions

Before proceeding further, let us discuss the bound state wave function Φ_{JM}. H. Casimir[60] and H. J. Mang[57] gave in their papers that the orthogonality condition

$$\langle \Phi_{JM} | \sum_i \int d\varepsilon \, b_i(\varepsilon,t) \; \theta^i_{JM} \rangle = 0 \tag{53}$$

is necessary to get unique solutions for the coefficients $a(t)$ and $b_i(\varepsilon,t)$.

It is possible to prove that the orthogonality condition, Eq. (53), is satisfied for time, t going to infinity, i.e., for the "asymptotic wave packet states,"[62] but not for all values of t. It would be natural to assume that Φ_{JM} is given by the usual shell model calculation,

$$(H_{shell} - E)\ \Phi_{JM} = 0 \tag{54}$$

where H_{shell} is the shell-model Hamiltonian. Since the wave functions Φ_{JM} and θ^i_{JM} are eigenfunctions of different Hamiltonians, they are not expected to be orthogonal to each other [see Eq. (42) and (43)]. As we shall see in Eqs. (81) and (82), the final expression for the alpha width is given in the form of the transition matrix element between Φ_{JM} and θ^i_{JM}. As in the case of rearrangement collisions, the lack of orthogonality of Φ_{JM} and θ^i_{JM} brings some arbitrariness into the expression of the alpha width.[63] But we avoid this arbitrariness by defining the perturbation which causes the alpha transition to vanish as R becomes infinite.

Since Φ_{JM} and θ^i_{JM} are not eigenfunctions of H, let us denote the expectation values of H with respect to these eigenfunctions as E_o and E as

$$\langle \Phi_{JM} | H | \Phi_{JM} \rangle = E_o \tag{55}$$

and

$$\int d\varepsilon\ \langle \theta^i_{JM} | H | \theta^i_{JM} \rangle = E = E(j\sigma) + E(\alpha) + \varepsilon_\ell \tag{56}$$

We note that the nondiagonal matrix elements between open channel wave functions vanish because the channel coupling is neglected in this section (IV)(see Sections II and III, in which channel coupling is included).

$$\int d\varepsilon\ \langle \theta^i_{JM} | H | \theta^j_{JM} \rangle = 0 \qquad \text{for } i \neq j \tag{57}$$

Inserting Eq. (41) into Eq. (40), we get

$$i\hbar \frac{\partial a}{\partial t} \Phi + i\hbar \sum_i \int d\varepsilon \frac{\partial b_i}{\partial t} \theta^i = H\left(a\Phi + \sum_i \int d\varepsilon\, b_i \theta^i\right) \tag{58}$$

(Note that the subscript JM of Φ_{JM} and θ^i_{JM} is dropped from the following equations.) The following two equations are derived directly from Eq. (58),

$$i\hbar \frac{\partial a}{\partial t} + i\hbar \sum_i \int d\varepsilon \frac{\partial b_i}{\partial t} \langle \Phi | \theta^i \rangle = aE_o + \sum_i \int d\varepsilon\, b_i \langle \Phi | H | \theta^i \rangle \tag{59a}$$

$$i\hbar \frac{\partial a}{\partial t} \langle \theta^i | \Phi \rangle + i\hbar \frac{\partial b_i}{\partial t} = a\langle \theta^i | H | \Phi \rangle + b_i E \quad . \tag{59b}$$

Since Φ and θ^i, the bound state and channel wave function, respectively, have very little overlap in the alpha decay problem, $\langle \Phi | \theta^i \rangle$ and $\langle \Phi | H | \theta^i \rangle$ will be very small quantities.

For the two groups of nucleons, as a daughter nucleus and an alpha particle [see Eq. (45) and (46)], we have $\phi_{j\sigma}$ and χ_α as the internal wave functions of the daughter and nucleus, respectively.

If $\phi_{j\sigma}\, \phi_{j'\sigma'}$ and $\chi_\alpha \chi_{\alpha'}$ are bound state solutions, then the following holds

$$\langle \chi_{\alpha'} \psi_{\sigma'} | V_{\alpha N} | \psi_\alpha \psi_\sigma \rangle = \delta_{\sigma\sigma'}\, \delta_{\alpha\alpha'} V(R) \tag{60}$$

for $R > R_o$ with R_o the matching radius. The meaning of this relation is always that when the alpha particle and the daughter nucleus are well separated in space the interaction between them is described by a simple potential. Furthermore, V(R) approaches the Coulomb potential $\frac{2(Z-2)e^2}{R}$ rapidly. For most purposes, therefore, it will be sufficient to use

$\frac{2(Z-2)e^2}{R}$ instead of V(R) and $R_o \approx 8.5$ f from scattering data on most natural alpha emitters (the charge Z is the parent nuclear charge). These considerations led us to give the form of $\psi(1 \ldots A,t)$ in Eq. (41) (see Ref. 57). If we denote coefficients a and b_i as

$$a = \alpha(t) \exp\left(-i \frac{E_o t}{\hbar}\right) \tag{61}$$

$$b_i = \beta_i(t) \exp\left(-i \frac{E_o t}{\hbar}\right) \tag{62}$$

again $\partial\alpha/\partial t$ and $\partial\beta_i/\partial t$ are very small quantities for the alpha decay problem for the asymptotic consideration considered above.

Therefore, we may use the following approximations in Eqs. (59) and (60):

$$i\hbar \sum_i \int d\varepsilon \frac{\partial b_i}{\partial t} \langle \Phi | \theta^i \rangle \approx E_o \sum_i \int d\varepsilon \, b_i \langle \Phi | \theta^i \rangle \tag{63}$$

$$i\hbar \frac{\partial a}{\partial t} \langle \theta^i | \Phi \rangle \approx E_o a \langle \theta^i | \Phi \rangle \tag{64}$$

Then, Eqs. (59) and (60) become

$$i\hbar \frac{\partial \alpha}{\partial t} = \sum_i \int d\varepsilon \, b_i \langle \Phi | H - E_o | \theta^i \rangle \tag{65}$$

$$i\hbar \frac{\partial \beta_i}{\partial t} = (E - E_o)\beta_i + \alpha \langle \theta^i | H - E_o | \Phi \rangle \tag{66}$$

These equations are the same as Eqs. (3a),(3b) in Ref. 59; therefore, we can write solutions as

$$\alpha = \exp\{-i(\Delta - i\Gamma/2)t/\hbar\} \tag{67}$$

$$\beta_i = \frac{\exp\{-i(\Delta - i\Gamma/2)t/\hbar\} - \exp\{-i(E - E_o)t/\hbar\}}{\Delta - i\Gamma/2 - (E - E_o)} \langle \theta^i | H - E_o | \Phi \rangle \qquad (68)$$

$$\Delta = \sum_i P \int \frac{\left| \langle \Phi | H - E_o | \theta^i \rangle \right|^2}{\Delta - (E - E_o)} \, d\varepsilon \qquad (69)$$

$$\Gamma = 2\pi \sum_i \left| \langle \Phi | H - E_o | \theta^i \rangle \right|^2_{E = E_o + \Delta} \qquad (70)$$

where the energy difference Δ is defined in Eq. (69) in terms of the principal value P and is small. The problem of determining the decay constant is now reduced to the calculation of the matrix element $\langle \Phi | H - E_o | \theta^i \rangle$ at $E = E_o$, since the energy shift Δ is very small and can be neglected in the alpha decay problem.

E. Alpha Decay Width Formula

Let us decompose Φ into two parts by using the following projection operators

$$\Phi = P\Phi + Q\Phi \qquad (71)$$

where

$$P = \sum_i |\chi_\alpha[Y_\ell \ \phi_{j\sigma}]\rangle \langle \chi_\alpha[Y_\ell \ \phi_{j\sigma}]| \qquad (72)$$

$$Q = 1 - P \qquad (73)$$

It is to be noticed that

$$P\Phi = \sum_i |\chi_\alpha[Y_\ell \phi_{j\sigma}]\rangle \ \langle \chi_\alpha[Y_\ell \phi_{j\sigma}]|\Phi\rangle \qquad (74)$$

$$= \sum_i |\gamma_\ell(R)\chi_\alpha \ [Y_\ell \ \phi_{j\sigma}]\rangle \qquad (75)$$

where $\gamma_\ell(R)$ is the conventional reduced alpha amplitude. Let us define H_o as follows.

$$H_o = H_N + H_\alpha - \frac{\hbar^2}{2\mu} \nabla^2_{\vec{R}} + U_\alpha(R) \tag{76}$$

$$H = H_o + V_{\alpha N} - U_\alpha(R) \tag{77}$$

where $U_\alpha(R)$ is the one body alpha-nucleus potential defined in Eq. (46); in other words, $\langle Q\Phi | U_\alpha(R) | \theta^i \rangle = 0$. Then, the matrix element $\langle \Phi | H - E_o | \theta^i \rangle$

$$\langle \Phi | H - E_o | \theta^i \rangle = \langle \Phi | H_o - E_o | \theta^i \rangle + \langle \Phi | V_{\alpha N} - U_\alpha | \theta^i \rangle \quad , \tag{78}$$

using

$$H_o | \theta^i \rangle = E | \theta^i \rangle \quad . \tag{79}$$

Let us rewrite the expression for the decay width as

$$\Gamma = 2\pi \sum_i \Gamma_i \tag{80}$$

where the partial width Γ_i is given by

$$\Gamma_i = 2\pi \left| \langle \Phi | V_{\alpha N} - U_\alpha | \theta^i \rangle \right|^2_{E=E_o} \tag{81}$$

$$\Gamma_i = 2\pi \left| \langle \Phi | V_{\alpha N} | \theta^i \rangle - \sum_\ell \langle \gamma_\ell(R) | U_\alpha | \varphi_\ell(R) \rangle \right|^2_{E=E_o} \tag{82}$$

In Eq. (82) the partial width Γ_i is given by the transition matrix element between the bound shell model wave function and the channel wave function and the perturbation which causes the alpha transition is given by $V_{\alpha N} - U_\alpha$. The partial width is expressed in terms of the bound state Φ, channel wave function θ, and alpha particle wave function φ_ℓ.

F. Four Nuclear States in the Real Bound-State Wave Function

In Eq. (82) we have expressed the partial decay width Γ_i in terms of Φ (bound state wave functions). We can discuss models of Φ in terms of the comparison of states. The state of the four nucleons included in Φ has the following five possible components:

1) separated four nucleons ,

2) 2-particle cluster + separated two nucleons ,

3) 2-particle cluster + 2-particle cluster ,

4) 3-particle cluster + one nucleon (but does not have α cluster component) ,

5) 4-cluster or the reduced alpha width $\gamma_\ell(R)$.

Since $V_{\alpha N}$ is the sum of two-body forces, we may express the general character of the new formula, Eq. (82), the alpha barrier width, as

$$\Gamma_\alpha \propto (\text{formation probability of 3-particle cluster}) \times \left|\langle (\text{3-particle cluster + one nucleon}) \mid V_{\alpha N} \mid \alpha \text{ cluster} \rangle\right|^2 \quad (83)$$

but in the ordinary formula, $\Gamma_\alpha \propto$ (formation probability of α cluster) (see Fig. 11 as a schematic illustration).

We usually define the reduced width by dividing the decay width by the barrier penetrability calculated at some radius. However, the reduced width, calculated by the ordinary formula, depends only on the configurations of four nucleons inside the nucleus, and does not depend on the energy of the decaying alpha particle. Furthermore, in the ordinary formula the angular momentum dependence of the reduced width appears only through the geometrical factors. These are due to the neglect of the boundary condition required in R-matrix theory. On the contrary, our

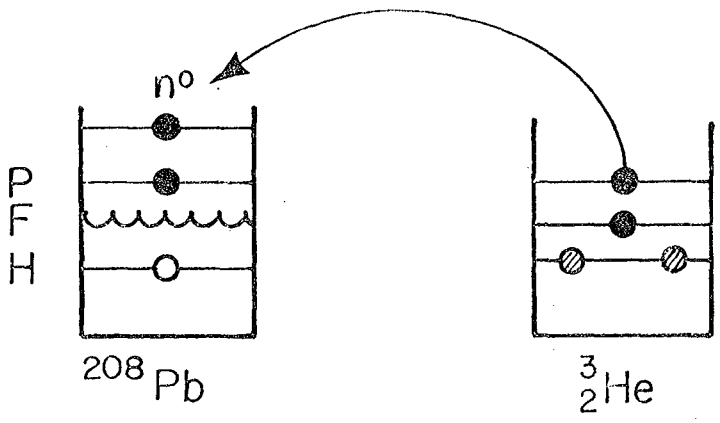

XBL 783-2446

Fig. 11. A schematic representation of the capture of a neutron (dark circle) in the ^{208}Pb alpha decay daughter nuclear potential well from a ^{4}He (alpha) particle, leaving a ^{3}He proton cluster (protons are denoted by cross-hatched circles). The captured neutron excites a particle-hole state in the ^{208}Pb nucleus. (The particle, neutron is termed P, the Fermi level F, and hole state as H.) Higher order exchange terms may also be considered, such as two-particle and two-hole states.

reduced width depends dynamically on the energy and the angular momentum of the decaying alpha particle, through $\varphi_\ell(\varepsilon,R)$ in the transition matrix element.

The new formula, Eq. (82), for the decay width has a great advantage since it does not depend on the radius parameter and the boundary condition. So, in principle we shall be able to calculate even the absolute value of the decay width by this formula. On the other hand, Eq. (82) requires us to do fairly difficult numerical calculations. D. H. Wilkinson[64] raised the question concerning the structure of the nuclear surface, especially on the formation of alpha cluster at the surface. In the next section the method of calculation is illustrated for two cases of simple alpha decay.

G. Practical Treatment of the Unified Alpha Decay Theory for ^{212}Po to ^{208}Pb and ^{210}Po to ^{206}Pb

Let us consider the ^{212}Po and ^{210}Po ground state alpha decays. There are two kinds of the matrix elements in Eq. (82). The calculation of the second term is straightforward, since $\gamma_o(R)$ is just the reduced amplitude, which is calculated with the ordinary formula. In order to calculate the first matrix element, we expand the parent nucleus wave function in terms of the daughter nucleus wave functions, $\{\phi_n\}$,

$$\Phi_o = \sum_{mn} a_{mn} \psi_m(1\ 2\ 3\ 4)\ \phi_n \quad , \tag{84}$$

for the index m which specify the state of four nucleons and index n which specify the daughter nucleus and for expansion coefficients a_{mn}.

To get some feeling for the practical calculation using Eq. (82), let us consider the ^{212}Po (ground state) decay to ^{208}Pb (ground state) as the simplest case without channel coupling. Using the approximation of Eq. (49), we get from Eq. (82),

$$\Gamma = 2\pi \left| \langle \Phi_o | V_{\alpha N} | \chi_\alpha [Y_o^o \phi_o] \varphi_o(R) \rangle - \langle \gamma_o(R) | U_\alpha | \varphi_o(R) \rangle \right|^2 \qquad (85)$$

where Φ_o and φ_o are shell model wave functions for the ground states of ^{212}Po and ^{208}Pb, respectively.[3,21] There are two kinds of matrix elements in the absolute value square bracket. We shall discuss each term of Eq. (85) separately.

To calculate the second term in Eq. (85), we may use the real part of the alpha-nucleus optical potential, U_i^{opt}, for $\langle \chi_\alpha [Y_o^o \phi] \mid V_{\alpha N} \mid \chi_\alpha [Y_o^o \phi_o] \rangle$, where $\gamma_o(R)$ is the reduced amplitude which is easily calculated with ordinary formula. The radial behavior of $\gamma_o(R)$, U_i^{opt}, and $\varphi_o(R)$ are given schematically in Fig. 12.

To calculate the first term in Eq. (85), we expand the parent nucleus wave function Φ_o in terms of the daughter nuclear wave functions $\{\phi_n\}$, as mentioned before in Eq. (84), to obtain Eq. (83). We may use the approximation in which $\langle \phi_o | \sum_{k=5}^{A} v_{ik} | \phi_o \rangle$ is replaced by the real part of the i^{th} nucleon-nucleus optical potential U_i^{opt} and $\langle \phi_n | \sum_{k=5}^{A} v_{ik} | \phi_o \rangle$,

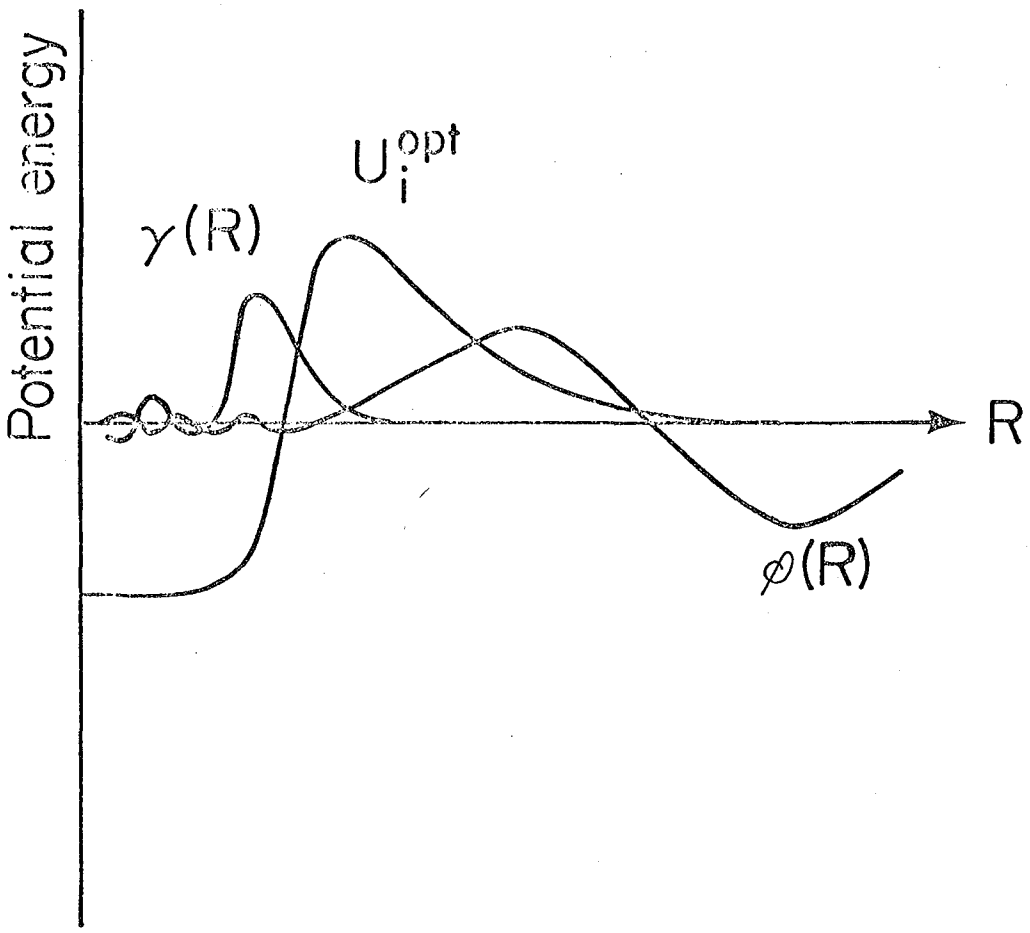

XBL 783-2447

Fig. 12. A schematic representation of the radial behavior of $\gamma(R)$, $U_i^{opt}(R)$, and $\phi(R)$ are plotted.

with $n \neq 0$ neglected because the latter are generally much smaller than the former. Then, the first term becomes

$$\langle \Phi_o | V_{\alpha N} | \chi_\alpha [Y_o^o \phi_o] \varphi_o(R) \rangle = \langle \sum_m a_{mo} \psi_m (1\ 2\ 3\ 4) | \sum_{i=1}^{4} U_i | \chi_\alpha Y_o^o \phi_o(R) \rangle \tag{86}$$

Hereafter, we shall consider only the $\langle \psi_m(1\ 2\ 3\ 4) | U_1 | \chi_\alpha Y_o^o \phi_o(R) \rangle$ term; we drop the opt superscript from U_i^{opt} and denote as U_i. The states of particles 2, 3 and 4 should be the same in the initial and the final states of this matrix element, since U_1 depends only on the coordinate of particle 1. Taking this fact into account, we divide the calculation of $\langle \psi_m(1\ 2\ 3\ 4) | U_1 | \chi_\alpha Y_o^o \phi_o(R) \rangle$ into the following three steps.

The internal wave function of the alpha particle is assumed to be

$$\chi_\alpha \propto \exp(-\frac{\beta}{4} \sum r_{ij}^2)\ S_{oo}(12)\ S_{oo}(34) =$$

$$= \left(\frac{2\beta^3}{\pi^3}\right)^{3/4} \exp\left[-\frac{\beta}{2}\left(\frac{3}{2}\eta^2 + \frac{4}{3}\rho^2 + \xi^2\right)\right] S_{oo}(12)\ S_{oo}(34) \tag{87}$$

where the coordinates are defined by H. Mang[14]

$$\vec{\xi} = \vec{r}_3 - \vec{r}_4 \quad , \qquad \vec{R}_2 = \frac{1}{2}(\vec{r}_3 + \vec{r}_4)$$

$$\vec{\rho} = \vec{r}_2 - \vec{R}_2 \quad , \qquad \vec{R}_3 = \frac{1}{3}(\vec{r}_2 + \vec{r}_3 + \vec{r}_4) \tag{88}$$

$$\vec{\eta} = r_1 - R_3 \quad , \qquad \vec{R} = \frac{1}{4}(\vec{r}_1 + \vec{r}_2 + \vec{r}_3 + \vec{r}_4) \ ,$$

and S_{oo} is the spin singlet function for each nucleon pair. The value of the parameter β used in the present study is $\beta = 0.217\ f^{-2}$, and we have the normalization constant

$$N = \left(\frac{32\pi^3}{\beta^3}\right)^{3/4} = 5.5 \times 10^3\ f^{9/2} \tag{89}$$

The notations $\psi_a(1)$, $\psi_b(2)$, $\psi_c(3)$, and $\psi_\alpha(4)$ are used for each nucleon in $\psi_m(1\ 2\ 3\ 4)$, respectively.

First, transforming the neutron pair wave function in $\psi_m(1\ 2\ 3\ 4)$ into the wave functions of $\vec{\xi}$ and $\vec{R}_2$, we have

$$[\psi_c(3)\ \psi_\alpha(4)]_{J_n} = \sum_{n_2 \ell_2 N_2 \ell_2} T_{n_2 \ell_2 N_2 \ell_2}\ [\phi_{n_2 \ell_2}(\vec{\xi})\ \phi_{N_2 \ell_2}(\vec{R}_2)]_{J_n} \qquad (90)$$

Only the $\ell_2=0$ term has a non-zero overlap with $\chi_\alpha(\vec{\xi})$, and the integration with respect to $\vec{\xi}$ leads to

$$\sum_{n_2 N_2} T_{n_2\, 0\, N_2 \ell_2} \langle \phi_{n_2 0}(\vec{\xi}) | \chi_\alpha(\vec{\xi}) \rangle\ \phi_{N_2 \ell_2}(\vec{R}_2) \qquad (91)$$

Second, transforming $\psi_b(2)\ \phi_{N_2 \ell_2}(\vec{R}_2)$ into the wave functions of $\vec{\rho}$ and $\vec{R}_3$, we have

$$[\psi_b(2)\ \phi_{N_2 \ell_2}(\vec{R}_2)]_{J'} = \sum_{n_3 \ell_3 N_3 \ell_3} T_{n_3 \ell_3 N_3 \ell_3}\ [\phi_{n_3 \ell_3}(\vec{\rho})\ \phi_{N_3 \ell_3}(\vec{R}_3)]_{J'} \qquad (92)$$

Only the $\ell_3=0$ term has a non-zero overlap with $\chi_\alpha(\vec{\rho})$, and the integration with respect to $\vec{\rho}$ results in

$$\sum_{n_3 N_3} T_{n_3\, 0\, N_3 \ell_3} \langle \phi_{n_3 0}(\vec{\rho}) | \chi_\alpha(\vec{\rho}) \rangle\ \phi_{N_3 \ell_3}(\vec{R}_3) \qquad (93)$$

Third, expanding $\chi_\alpha(\vec{\eta})\phi_\alpha(\vec{R})$ in terms of the bound state wave functions $\phi_{N_3 \ell_3}(\vec{R}_3)$, we have

$$[\chi_\alpha(\vec{\eta})\varphi_\alpha(\vec{R})]_o = \sum_{N_3\ell_3} \langle \phi_{N_3\ell_3}(\vec{R}_3) \,|\chi_\alpha(\vec{\eta})\phi_\alpha(\vec{R})\rangle \;\; \phi_{N_3\ell_3}(\vec{R}_3)$$

$$\equiv \sum_{N_3\ell_3} \varphi_{N_3\ell_3}(1) \;\; \phi_{N_3\ell_3}(\vec{R}_3) \tag{94}$$

Therefore the final expression for the matrix element becomes

$$\langle \psi_m(1\ 2\ 3\ 4)\,|U_1|\chi_\alpha Y_o^o \varphi_o(R)\rangle$$

$$= C \sum_{n_2N_2n_3N_3} T_{n_2\,0\,N_2\ell_2}\; T_{n_3\,0\,N_3\ell_3}\; \langle \psi_a(1)\,|U_1\varphi_{N_3\ell_3}(1)\rangle$$

where C is some geometrical factor. Similarly, we can calculate the matrix element of U_i^{opt}, for i = 2,3,4.

To get some feeling for the practical calculation with the new formula, we performed the numerical calculations using the point-size approximation for the internal wave function of the alpha particle. The expression for the alpha width becomes simple in this case, and is written as

$$\Gamma_\alpha = 2\pi \left| \frac{1}{2}\,\hat{j}_p\,\hat{j}_n\,N_\alpha(4\pi)^{-3/2}\;(-)^{\ell_p+\ell_n} \int [2(U_p+U_n) - U\alpha]\; R_p^2\, R_n^2\, \varphi_\alpha\; r^2 dr \right|^2 \tag{96}$$

where R_p and R_n are the wave functions of the bound states of the proton and neutron, respectively, and $\hat{j}$ stands for $\sqrt{2j+1}$. Under the same approximation, the ordinary formula gives

$$\Gamma_\alpha = 2P_o\left(\frac{\hbar^2 R_o}{2\mu}\right) \left| \frac{1}{2}\,\hat{j}_p\,\hat{j}_n\,N_\alpha(4\pi)^{-3/2}\;(-)^{\ell_p+\ell_n}\; R_p(r=R_o)\; R_n(r=R_o) \right|^2 \tag{97}$$

where P_o is the penetrability defined by R. G. Thomas[37] and R_o is the nuclear radius. It should be noted that the same geometrical factors

appear in both formulas.

Pure configurations for ^{212}Po and ^{210}Po were assumed. The nucleon-nucleus potentials U_p and U_n are assumed to be of a Woods-Saxon type and their parameters are taken from Ref. 29. For the nucleon wave functions R_p and R_n, the eigenfunctions calculated from those potentials are used. Eigenfunctions of a Woods-Saxon potential for single particle levels around ^{208}Pb is given in Ref. 30. The assumed configurations and the potential parameters are listed in Tables 16 and 17.

TABLE 16. The configurations for ^{212}Po, ^{210}Po and ^{206}Po

Element	Protons	Neutrons
^{212}Po	$(h_{9/2})^2_0$	$(g_{9/2})^2_0$
^{210}Po	$(h_{9/2})^2_0$	--
^{206}Pb	--	$(P_{1/2})^{-2}$

TABLE 17. Parameters of nucleon-nucleus potentials (taken from Ref. 36).

V_p (MeV)	V_n (MeV)	r_o (f)	a (f)	λ	r_c (f)
58	44	1.27	0.67	32	1.27

It is well known that considerable ambiguities exist in the value of the parameter for the alpha-nucleus optical potentials. Several potentials, which give the same phase shifts, will also give the same

calculated scattering cross section. L. McFadden and G. R. Satchler,[24] and also W. J. Thompson, G. E. Crawford, and R. H. Davis[65] have made detailed analyses of the scattering of alpha particles and studied these ambiguities. From Table 3 in Ref. 30 we constructed four sets: the potentials #3, #2, and #1, for the Bi target element, and #3 for the Au target, and used these to calculate our $U_\alpha(r)$. Since the imaginary parts are not needed for our present purpose, only the real parameter values of the four sets are listed in Table 18.

TABLE 18. Parameters of alpha-nucleus potentials (taken from Ref. 24).

Set	V_α (MeV)	r_o (f)	a (f)	r_c (f)	χ^2
(A)	177.3	1.342	0.569	1.3	0.144
(B)	124.7	1.380	0.566	1.3	0.142
(C)	58.8	1.454	0.560	1.3	0.142
(D)	168.7	1.378	0.517	1.3	0.137

The alpha wave functions $\phi_\alpha(r)$, distorted by these $U_\alpha(r)$, are calculated using the computer code WAFFLE.[66] In Figs. 13a and 13b we plotted $r\phi_\alpha(r)/\sqrt{P_o}$ for ^{212}Po and ^{210}Po, respectively, where P_o is the penetrability, e^{-2G}. It is seen that the numbers of the half wave-length in the nuclear well are 13, 11 and 5 for the set (A), (B) and (C), respectively. Set (D) produces the same number of nodes as set (A), but the positions of the nodes are shifted slightly. Various potentials and the products of the four nucleon wave functions are plotted in Fig. 14.

Numerical integrations of $\int U(r)\, R_p^2(r)\, R_n^2(r)\, \phi_\alpha(r) r^2 dr$ are made with the integration mesh of 0.1 f. In Table 19 we present the calculated results for ^{212}Po and ^{210}Po decays.

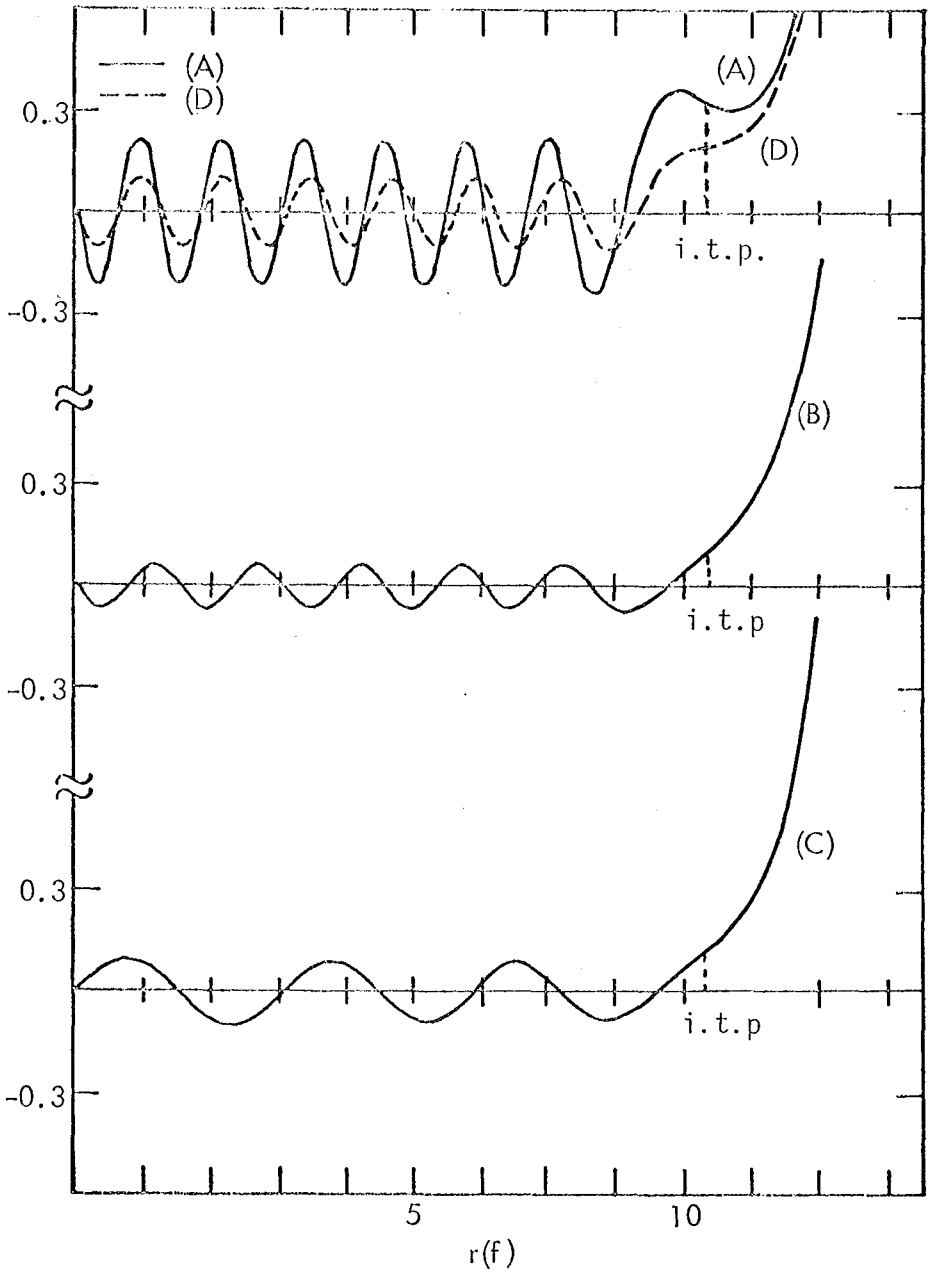

XBL783-2444

Fig. 13a. The alpha particle wave functions $\phi_\alpha(r)$ for ^{212}Po decay are illustrated for the potentials (A), (B), (C), and (D). For convenience the quantities $r\phi_\alpha(r)/\sqrt{P_o}$ are plotted, in which P_o is the penetrability. The notation i.t.p means the inner classical turning point. The unit of the ordinate scale is $f^{-1/2}$ $MeV^{-1/2}$.

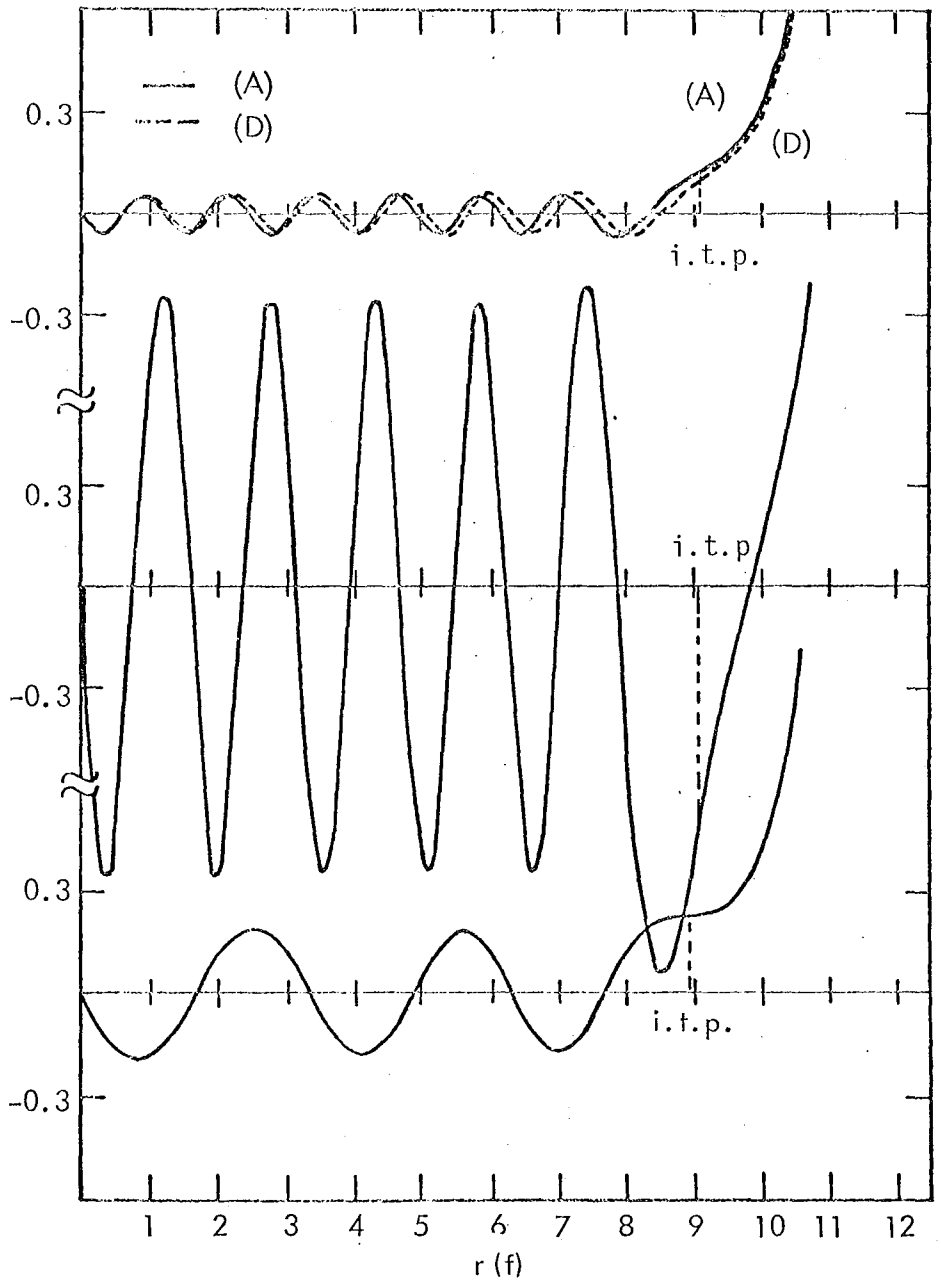

XBL 783-2451

Fig. 13b. The alpha particle wave function for ^{210}Po decay are plotted. The others are the same as in Fig. 12.

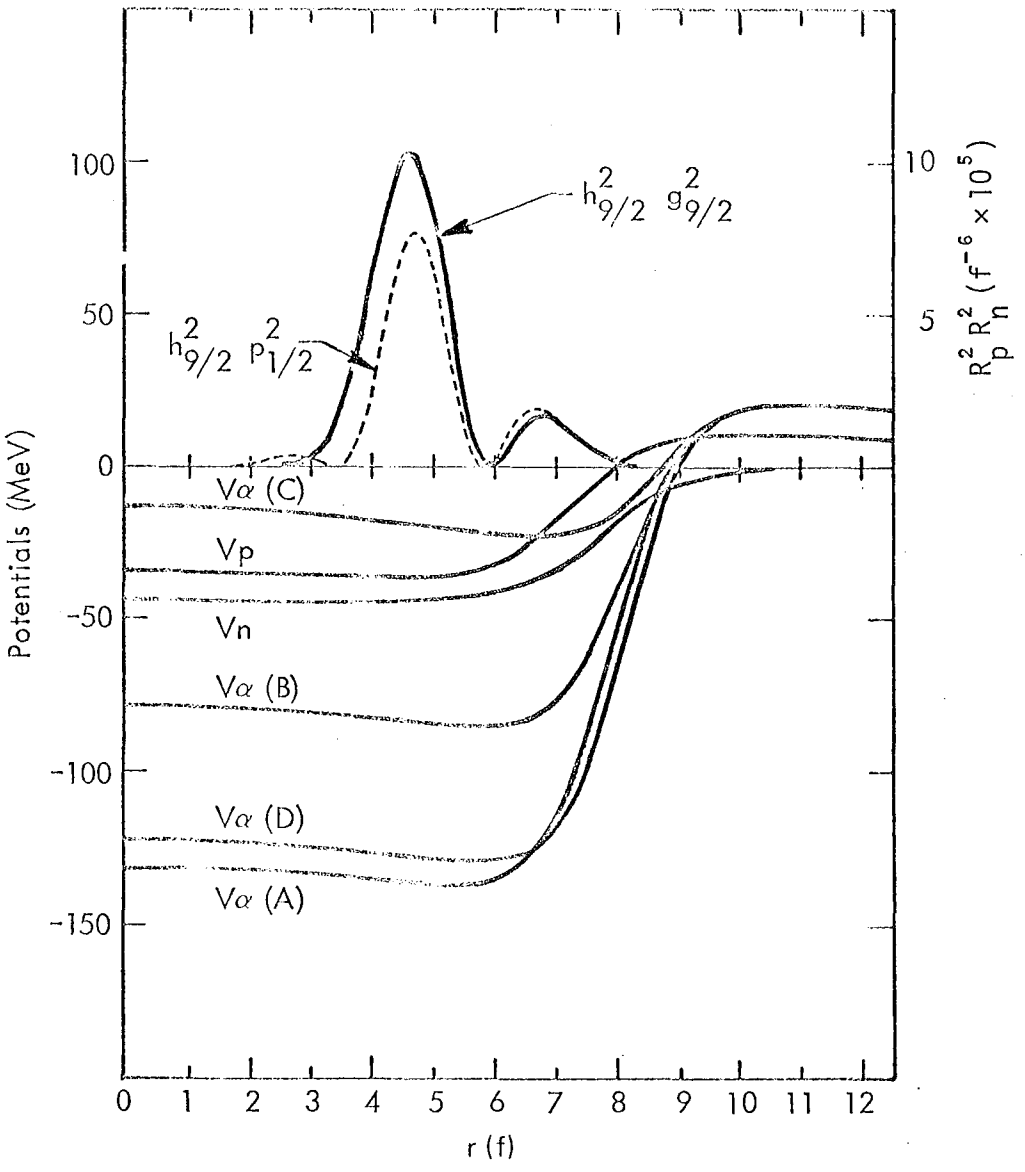

XBL783-2450

Fig. 14. Various potentials and the products of the four nucleon wave functions R_n^2 R_p^2 are plotted.

TABLE 19. Absolute decay widths for ^{212}Po and ^{210}Po alpha decays.

I. ^{212}Po with E_α = 8.81 MeV

	Present				Experiment	Ordinary*
	(A)	(B)	(C)	(D)		
P_o	0.39×10^{-13}	0.39×10^{-13}	0.30×20^{-13}	0.43×10^{-13}	--	--
Γ_α (MeV)	1.4×10^{-16}	3.3×10^{-15}	4.8×10^{-15}	1.0×10^{-18}	1.5×10^{-15}	$\sim10^{-22}$
Γcal./Γexp.	0.92×10^{-1}	2.2	3.2	0.68×10^{-3}	--	$\sim10^{-7}$

II. ^{210}Po with E_α = 5.33 MeV

	Present				Experiment	Ordinary*
	(A)	(B)	(C)	(D)		
P_o	0.66×10^{-26}	0.65×10^{-26}	0.45×10^{-26}	0.78×10^{-26}	--	--
Γ_α	3.5×10^{-32}	6.5×10^{-27}	2.3×10^{-26}	3.8×10^{-30}	3.8×10^{-29}	$\sim10^{-36}$
Γcal./Γexp.	0.92×10^{-3}	1.7×10^{2}	6.2×10^{2}	0.10	--	$\sim10^{-7}$

* R_o = 10 f is used in the ordinary formula.

From Table 19, it is seen that none of the potentials examined give completely satisfactory results for the absolute decay width and the best fit parameters for ^{212}Po is for case (B) and for ^{210}Po case (D) gives the best fit for Γ(cal.)/Γ(exp.).

Unfortunately, none of the potentials examined here give completely satisfactory results. In order to find useful parameters for $U_\alpha(r)$, we have to make a more systematic parameter search, taking configuration mixing into account. However, it should be noted that all four potential sets give the same penetrability and χ^2-values but they give different values for the alpha width. The results indicate that this kind of calculation is helpful is removing the ambiguities of the alpha-nucleus potential parameters.

The calculated magnitudes of the three overlap integrals $\int U_{p,n,\alpha}(r)\ R_p^2(r)\ R_n^2(r)\phi_\alpha(r)\ r^2dr$ are not proportioned to their well depths, $V_{p,n,\alpha}$. This suggests that the inner region, where the potential is flat, gives little contribution to the overlap integral due to the rapid oscillation of $\phi_\alpha(r)$, and the main contribution comes from the surface region. The density of four nucleons $R_p^2\ R_n^2$ at the nuclear surface is enhanced by configuration mixing, so that the mixing provides us with larger values for the decay widths. In this respect, the potentials (A) and (D) are expected to be superior to (B) and (C).

Absorption effects in the nucleon interior may mandate the use of an absorptive part of the nucleon potential. Inclusion of such a term would give an attenuation wave function in the nuclear interior (see Figs. 12 and 13). It has been suggested by S. D. Kadmenskii, V. E. Kalachits, and A. A. Martynov[66] that the alpha wave functions in the nuclear interior

region should attenuate to zero at the nuclear origin and that the use of this boundary condition constraint will yield better fits to absolute decay rates and give us less dependence on the nuclear well depth parameter (see Table 18). Although we have eliminated the ambiguities connected with the choice of the effective cut-off radius, R_o, of the nuclear force, we still have dependence on other nuclear potential parameters, particularly the well depth felt by the alpha particle in the nucleon potential, V_α.

H. Concluding Remarks on the Application of the Unified Reaction Alpha Decay Theory Applied to ^{212}Po and ^{210}Po Alpha Decay

By making use of the time-dependent perturbation method, we have been able to get a new expression for the alpha decay width. The new formula is presented in a form which is independent of the nuclear radius parameter and the boundary condition. Previous microscopic alpha decay theories inevitably neglect the problem of the mismatch at the nuclear radius, of logarithmic derivatives of the alpha wave functions in the inner and outer regions. The new theory has an advantage over the previous ones, in this respect, and makes it possible to calculate the alpha decay rates in a more rigorous way.[67]

Our formula [Eq. (82)] has the same form as the general expression for the level width which is given by Feshbach in his unified theory of nuclear reactions.[23] His theory has been applied often to the interpretation of the nuclear reaction in which the incident particle is a nucleon,[58] but it has not ever been applied to the reaction induced by a composite particle. Furthermore, there is a remarkable difference between the alpha

decay and the nuclear reaction with respect to the excitation energy of the compound (parent) nucleus. The compound state Φ_s in nuclear reaction is generally very complicated and it is difficult to know to what extent Φ_s contains the so-called doorway state, which can be depicted as the two particle-one hole configuration for the nucleon-induced reaction. On the contrary, the corresponding state, Φ_{JM} in alpha decay, is the ground state or the low-lying excited state of a parent nucleus, and is known in the sense of the current nuclear shell model. Unfortunately, at present there are considerable ambiguities in the parameter values of the potential. Equation (82) contains the one-body alpha-nucleus potential in it. M. Rogenberg and L. Wilets[67] give a discussion about the magnitude of the alpha potential which may be useful for application to this present problem. Further parametric sources may yield improved results and reduce the ambiguities in the calculation of the alpha width.

Although we have eliminated the dependence of the alpha decay width on the nuclear cut-off radius, R_o, we still have ambiguities with the nucleon well depth. We have more properly isolated the oscillating interior solutions to the exterior exponential solutions at the nucleon radius, R_o. We have considered only the real part of the nucleon potential and have excluded channel coupling.

To more properly apply boundary conditions in the nucleon interior for the attenuation of the alpha wave functions, we will include channel coupling and introduce the complex absorptive part of the Woods-Saxon potential. The coupling of a particular alpha wave to other channels by the absorptive part of the optical model potential will cause damping of the interior solutions, so that as r approaches zero, $\varphi_\ell(r)$ also goes to

zero.[66] The inclusion of channel coupling in a complex potential may free us from the alpha decay width dependence on the well depth parameter.

In the next section, we examine in detail a resonance S-matrix coupled channel model in a complex nucleon potential, in which we calculate the alpha decay resonance width from the energy position of resonance loops in the complex S-matrix plane "Argand" diagrams.

V. ELASTIC AND INELASTIC COUPLED CHANNEL ALPHA SCATTERING THEORY AND RESONANCE DECAY WIDTH

A. Introduction to Reaction Theory and Compound Nuclear Formation

1. Historical background

In 1937, H. A. Bethe[11] presented a quantitative description of nuclear reactions in terms of the compound nucleus mechanism suggested earlier by N. Bohr.[68] The time-dependent perturbation theory of V. H. Weisskopf and E. P. Wigner,[69] applied to atomic systems for resonance absorption model with subsequent emission of optical radiation, was adopted to nuclear reactions by G. Breit and E. P. Wigner[70] and G. Breit.[71] In this model, the nuclear reaction proceeds via an isolated, long-lived intermediate resonance states and gives excellent fits to observed cross sections. This intermediate state proceeds through a compound nucleus. The strong nuclear force leads to a sharing of the available energy by all the nucleons and the long life is due to the small probability of the energy being concentrated in a mode that corresponds to disintegration by an "open" or energetically allowed channel.

The P. L. Kapur and R. E. Peierls[72] model is formulated in terms of a complete set of "formal" states of all particles defined in a volume of nuclear size with fixed boundary conditions on the nuclear surface. This model is readily adaptable to the compound nuclear description which is done by identifying the complete set of formal states with the states of the compound nucleus. These boundary conditions are energy-dependent and complex and the boundary conditions of Kapur and Peierls can be made explicit by use of the Wigner energy-independent boundary conditions. The Kapur and Peierls energy dependence is equivalent to the presence of

the level shift factor which occurs explicitly in the Wigner formulation.

In expanding on the work of Kapur and Peierls, E. P. Wigner and L. Eisenbud[73] introduced the concept of the R-matrix in 1947, in which the physical parameters of the theory are interpreted in terms of their physical significance. The reaction theory can account for both compound nuclear formation and "direct reaction" models, in which direct scattering occurs without changing the internal structure of the two groups of nucleons.

Reaction theories divide configuration space into two regions: the internal region in which the nucleons interact strongly and form a nearly stable configuration identified as the compound nucleus state; the external region of channels corresponding to various ways in which the compound nucleus can disintegrate. In the external region channel coupling is non-nuclear but can be Coulombic or centrifugal. The dividing surface between the internal and external region is taken to be the various channel radii, r_c, which is roughly equal to what is usually identified with the nuclear radius, R_o. A complete set of wave functions for the internal region are obtained as solutions to the Schrödinger equation and homogeneous boundary conditions at the channel radii.

Model dependence comes into the picture in the internal region when the wave function, derived from the expansion in a complete set and the form of the nucleon potential, utilized and in the external region by the use of the wave functions for the description of the disintegrating system in each channel.[7] The external region of configuration space contains the regions wherein the nucleons are grouped into two well separated stable clusters so that we consider the wave functions in the asymptotic region.

To more accurately describe the interaction between two complex nuclei, the potential would, most likely, be a function of more than the separation of their centers. Parametrization of the changes of shape or internal parameters should be included. For the present simple assumptions, we eliminate most of the coupled equations except those describing the elastic and a few inelastic channels. This leads to the effective potential in the remaining equations.

2. The R-matrix theory and decay process

In the R-matrix theory, we can define a set of states of all nucleons in which we can calculate the cross section. To calculate the cross section in terms of these state parameters, intermediate quantities are calculated, in terms of which the R-matrix is expressed. One of these quantities is the U-matrix or collision matrix. Other such intermediate parameters are the logarithmic derivative on the nuclear surface and the angular distribution of fragments. In the R-matrix theory the term "strong absorption model" is identified with those models in which the chance of collision without compound nucleus formation is very small, such as for high-energy scattering. We have found that compound nucleus formation does not occur at relativistic energies involving alpha and ^{12}C projectiles at various light and medium-light target elements.[74] The present model is applicable to lower energies due to compound nucleus formation; also higher energies require the inclusion of a large number of partial wave channels beyond the calculational abilities of modern computers.

The collision matrix U(E) is defined as the amplitude of the outgoing waves of a pair of nuclei or groupings of nuclei, bombarded against each

other with energy E, resulting from unit flux of bombardment. It follows that the cross section σ is proportional to $|U|^2$. The quantity U is a particularly useful quantity because of its ability to express the two very general physical principles: the conservation of probability flux (unitarity), and time-reversability (Poincare' invariance), which impose restrictions on the reaction theory. The collision matrix U must be unitary and symmetric. The matrices R and U are nondiagonal and the R-matrix depends on E, r_c (approximately the nucleon radius) as well as the boundary conditions. Although the general form of R is unknown, its energy dependence, given by E. P. Wigner and L. Eisenbud, is of a simple one-pole form [see Eq. (39) in Section IV.B].

$$R(E) = \sum_{\lambda} \frac{\gamma_\lambda^2}{E_\lambda - E} \tag{98}$$

The label λ runs over a complete set of states, the γ_λ's are called "reduced width amplitudes," and the γ_λ's and E_λ depend on the nuclear radius and boundary conditions. The E_λ are the energy eigenvalues of the states λ, and are the energies of the physically observed quasi-bound "resonance" states with singularities occurring at $E = E_\lambda$. In applying the R-matrix theory to a reaction proceeding through a resonance level, only one term in the sum over λ is kept and this leads to the well known "one level" cross section formula formulated by Breit and Wigner.

A third major principle obeyed by the R and U matrices is that of causality which states that two nuclei cannot be scattered before they interact. Causality leads to the analyticity form of the R- and U-matrix. The U-matrix should be independent of the nuclei radius.[62]

We define the channel radius of a pair of nucleon clusters, r_c, as the minimum radial distance of separation of the pair at which neither one experiences any polarizing or strong interaction force from the other. In the most simple prescription, $r_c = R_o(A_1^{\frac{1}{3}} + A_2^{\frac{1}{3}})$ where R_o is independent of A_1 and A_2. The interior region is defined as that region where $R < r_c$. G. Breit[75] defined the concept of channel for each split $A = (A_1, A_2)$ as separate from the others by a region of zero probability, so that a given pair of nuclei in their channels cannot change directly into another pair or channel configuration. Such a change must take place indirectly through the interior region.

Again, we can define a derivative quantity in terms of the radial wave functions, $u(r_c)$, as $L_\lambda = (r\, d\, u_\lambda/u_\lambda\, dr)_{r=r_c}$, which is defined on the nuclei surface [see Eq. (35) in Section V]. One of the boundary conditions is that the logarithmic derivatives, L_λ is real, fixed and independent of the states λ. We can relate the Green's function to the reciprocal of the logarithmic derivative $u(r) = G(r,r_c)(r_c\, d\, u/dr)_{r=r_c}$ where we have the resonant form

$$G(r,r_c) = \frac{\hbar^2}{2\mu r_c} \sum_\lambda \frac{u_\lambda(r)\, u_\lambda(r_c)}{E_\lambda - E} \tag{99a}$$

The Green's function relates to the value of the wave function in the internal region to its derivative on the surface. The R-matrix function is defined as

$$R = G(r_c,r_c) = \sum_\lambda \frac{\gamma_\lambda^2}{E_\lambda - E} \tag{99b}$$

and $\gamma_\lambda = (\hbar^2/2\mu r_c)^{\frac{1}{2}}$. $u_\lambda(r_c)$ is the reduced width amplitude, so that R

is equal to the reciprocal of "r_c" times the logarithmic derivative of u at r, $R = u(r_c)/r_c(du/dr)_{r=r_c}$.

A. M. Saperstein[76] examines the radius-free reaction theory. The Wigner R-matrix formalism leads to energy-independent parameters as opposed to the Kapur-Peierls formalism in which the transition matrix has energy-dependent resonance parameters. The R-matrix is expressed as a sum of resonance terms and the transformation between the R-matrix and the transition matrix is given in detail in Ref. 76. See also Section V.J.1 for the relationship of the R-matrix and S-matrix poles.

3. Weidenmüller S-matrix theory and the relationship of the R-matrix and S-matrix to decaying states

H. A. Weidenmüller[77] presents a detailed discussion of the analytic properties of the S-matrix in the multi-channel coupled Schrödinger equation formulation. Resonance phenomena in the reaction cross section is related to the structure of the S-matrix near a resonance pole in the complex energy and momentum plane. It is demonstrated that both the scattering wave functions and the elements of the S-matrix are dominated by the "wave function" for the decaying state in the vicinity of such a pole. The elements of the S-matrix are functions on a Riemann surface, the properties of which Weidenmüller presents in detail.

The explicit expression for the S-matrix is presented in terms of a specific form of Green's theorem integral on the topological surface defined as the nuclear surface. The S- and R-matrix can be related via the logarithmic derivative on the nuclear surface. The theory is applied to two-channel elastic and inelastic scattering. The physical interpretation of the Breit-Wigner resonance formula is discussed in the framework

of Weidenmuller's formulation. This model would allow us to examine in detail the relationship of resonance decay to the S-matrix pole position in the complex plane and the detailed structure of the Riemannian manifold.

We examined the S-matrix for the two-channel case as an initial approximate solution. The results were encouraging enough for us to proceed further with the S-matrix resonance model calculation.

4. Feshbach reaction theory and the R- and S-matrix calculation of alpha decay rates

In this "classic" unified theory of nuclear reactions, H. Feshbach[7] presents a reaction theory in which poles in the scattering matrix are identified with resonance states in nuclear reactions. A new derivation of the Breit-Wigner formula is given in which the concept of channel radius is not utilized and the model is extended to cases of overlapping resonances. The energies for levels of the compound nucleus (which are complex in the Kapur and Peierls[72] formalism), the overlap integrals between the compound nuclear wave functions (in the internal region), and the wave functions in the external region corresponding to a specific exit channel can be used to calculate the amplitudes for various reactions. The reaction widths are proportional to the square of the overlap integrals. We can calculate the overlap of the compound nuclear states with the wave functions for a particular disintegration mode. The complex scattering amplitude of the "complex potential model" can be obtained from the diagonal entrance channel components of the transition matrix. H. Feshbach identified the real and imaginary parts of the scattering amplitudes which satisfies a dispersion-type relation with poles which identified with resonances in nuclear reactions.

The R- or S-matrix can be formulated in terms of the incident and decaying states, relating this overlap with the decay width and decay time.

Resonant decay cross sections are associated with the pole strength function derived from the ratio of the reduced width to the energy level spacing.[13] With the generalized one-level collision matrix of Wigner and Eisenbud,[73] one can associate the decay width(in which the resonance energy is associated with a pole in the transition matrix).[31] The transition matrix can easily be expressed in terms of the scattering matrix. A comparison between the single level approximation of the R-matrix and S-matrix theory is derived from many channel scattering. The single level approximation for the R-matrix is approximatey valid at energy E, if and only if there exists a pole of the S-matrix in the vicinity of E. With increasing width of the resonances, the disagreement between the single level approximation given by the R-matrix theory and a single pole approximation for the S-matrix increases. This is because the resonance parameters of the R-matrix theory are implicitly energy-dependent (in the Kapur and Peierls model) while those of the S-matrix are not. The approximate R-matrix must preserve the unitarity of the S-matrix.

Agreement between the absolute resonance width calculated from the R-matrix and S-matrix is optimum for narrow resonances. In Ref. 78 the criterion of the comparison of the R- and S-matrix calculation of the resonance width is given, including the discussion of the choice of the boundary conditions.

Although the application of resonance theory to alpha decay is not new, some of the previous attempts have overlooked the important effects of the boundary conditions on the decay rate.[31] The decay rate can be related to the resonance width of a metastable state by the "golden rule" of

$$\Gamma = \hbar/\tau \quad , \tag{100}$$

which we used also in Section IV.

The possibility of relating the absolute decay width of resonance decay of a compound nuclear state to the poles in the complex elements of the scattering matrix is of interest in illucidating a reasonable model of nuclear internal states. In a picture utilizing this method of calculating the decay width, it may allow us to calculate reasonably accurate absolute widths, which are not extremely sensitive to the nuclear optical model parameters.

Our formalism of the nuclear reaction theory for alpha decay will be similar to the treatment of Lane and Thomas,[8] and we will utilize their notation. In this formalism of alpha decay, where the alpha decay rate or decay width for alpha decay can be identified with a scattering event, one identifies a resonance width with a pole in the S-matrix. When the real and imaginary parts of the energy-dependent S-matrix elements are plotted and these are identified with a loop which appears in the unit phase circle, the residue of the pole of this loop can be identified with the energy of the compound nuclear resonance state.

B. Formulation of the Solution of Coupled Equations for Scattering from an Even Nucleus

1. Detailed formalism of the coupled channels

First we divide the states into the natural and unnatural parity states. The natural parity states are defined as those with parity, $\pi = (-)^J$. Let there be n+1 total states to be considered, including the ground state. We assign to each five quantum numbers, E_s, λ_s, P_s, J_s, π_s, where $s = 1, \ldots n$, and P is a convenient label which for vibrational states could be the phonon number.

The initial nuclear state is $P_1 = 0$, $J_1 = 0$ nuclear spin, and $\pi_1 = +1$ parity. Consider an incident wave of orbital angular momentum ℓ; since $J_1 = 0$, the channel spin is ℓ. The target nucleus can be directly coupled only to natural parity states; the channels to which the incident channel can be coupled directly are those for which

$$\ell' = |\ell - J_s|, \; |\ell - J_s| + 2, \; \ldots \; (\ell + J_s) \; , \tag{101}$$

where s spans over all the natural parity states.

To solve for each ℓ lying in some specified range $\ell_1 \leq \ell \leq \ell_2$ we start from the coupled radial Schrödinger wave equations with radial wave function solutions $u^{\ell}_{\ell o}(r)$

$$\left(\frac{d^2}{dr^2} - \frac{\ell(\ell+1)}{r^2} + k_o^2\right) u^{\ell}_{\ell o}(r) = u^{\ell}_{\ell o}(r) \; V^{\ell}_{\ell o, \ell o}(r) + \sum_{\ell'' = |\ell - J|}^{\ell + J} v^{\ell}_{\ell'' J}(r) \; V^{\ell}_{\ell o, \ell'' J}(r) \tag{102a}$$

$$\left(\frac{d^2}{dr^2} - \frac{\ell'(\ell'+1)}{r^2} + k_J^2\right) u^{\ell}_{\ell' J}(r) = u^{\ell}_{\ell o}(r) \; V^{\ell}_{\ell' J, \ell o}(r) + \sum v^{\ell}_{\ell'' J}(r) \; V^{\ell}_{\ell' J, \ell'' J}(r) \tag{102b}$$

There are then a set of N coupled equations for ℓ'', ℓ''' and so forth, where $\ell' = |\ell - J|$ to $(\ell + J)$ in steps of two, as do the sums. Thus for each ℓ, there are J+2 coupled equations. The Coulomb part of the interaction of the form $V_{\ell' J, \ell'' J}$ in the external region is given by the form

$$V_c(r) = \frac{4\mu Z e^2}{\hbar^2 r} \tag{103}$$

where μ is the reduced mass, $\mu = M_\alpha M_N / (M_\alpha + M_N) = 4M_N(4 + M_N)$, where M_α is the mass of the alpha particle and M_N is the mass of the daughter nucleus. (This formalism can be made general only for the division of

the nucleons as (A_1,A_2).) In this problem we assume one of the clusters to be an alpha particle.

The wave number of the alpha cluster is given as $k_\alpha = (2\mu E_\alpha/\hbar^2)$ and the relative velocity is given as $v_\alpha = \hbar k_\alpha/\mu$. The Coulomb parameter is then given as $\eta_c = 2Ze^2/\hbar v_\alpha$ for the alpha-daugher interaction and the Coulomb phase shift is given as $\sigma_\ell = \arg\Gamma(1 + \ell + i\eta_c)$. The dimensionless radial parameter corresponding to the dimensionless Coulomb parameter η_c is given as $\rho_\alpha = k_\alpha r$. The center of mass energy is then $E_{cm} = \mu E_{lab}/\mu_\alpha$ $\mu E_{lab}/4$. The real part of the interaction potential used in our calculation can be written as the sum of three terms: $V_{Re}(r) = V_\ell(r) + V_c(r) + V_N(r)$, or the centrifugal barrier penetration energy $V_\ell(r) = \ell(\ell+1)\hbar^2/2\mu r^2$, the Coulomb potential, $V_c(r)$, and the nucleon Woods-Saxon potential.

The Coulomb potential for the alpha-nucleon system, separated by r for an electrostatically sharp boundary at R_o on a uniform charge sphere, is given by

$$V_c(r) = \begin{cases} \dfrac{2Ze^2}{r} & \text{for } r > R_o \\ \left[3 - \left(\dfrac{r}{R_o}\right)\right]^2 \dfrac{2Ze^2}{R_o} & \text{for } r < R_o \end{cases} \tag{104}$$

where R_o is defined as the nuclear radius. It is assumed that the nuclear and Coulomb radii are approximately equal.

The nuclear potential of the Woods-Saxon form is given by

$$V_N(r) = \frac{V_o}{[1 + \exp\ (r - R_o)/a]} \tag{105a}$$

where $R = rA^{1/3}$ and $R_o = r_o(2 + A^{1/3})$, and where A is the scattering target for an alpha particle.

In Fig. 1, we show a representative example of a plot of potential $V_{Re}(r)$ for the alpha-^{208}Pb nuclear system.

We introduce a complex part to the nucleon potential, of the form $iW/\{\exp[(r-\bar{R}_o)/\bar{a}]\}$ such that the nuclear potential, in general, is given by $V_N(r) = V_{Re}(r) + V_{Im}(r)$ or

$$V_N(r) = \frac{V_o}{1+e(r)} + \frac{iW}{1+\bar{e}(r)} \qquad (105b)$$

for $e(r) = \exp[(r-R_o)/a]$ and $\bar{e}(r) = \exp[(r-\bar{R}_o)/\bar{a}]$. The imaginary part of the nuclear potential is introduced to account for absorption into other channels. The total potential experienced by the interacting pair of nuclei (in this paper, one is an alpha particle) is V(r), which is complex because of the imaginary part of the nuclear potential.

A major assumption of the model is that the effective interaction potential for a few quasi-elastic channels (elastic and several inelastic) will describe our system of two complicated nuclei. It is assumed that the real part of the potential[3] is represented by a figure of the type shown in Fig. 1 for a local potential, for $V = V_N+V_C+V_\ell$. The modification potential by coupling to other channels is described by the introduction of a complex part of this potential. It may be that the potential is so strongly nonlocal and complicated in form for the region of overlap of the nuclear cluster that no simple parametrization such as presented here is adequate, but we feel that it is extremely useful to examine the use and limitations of this model.

For positive energy channels, the radial wave functions $\mu^{\ell}_{\ell',J}$ can be most parametrically identified with the representation in which we have incoming ($\mathcal{O}_\ell(r)$) and outgoing ($\mathcal{I}_\ell(r)$) which are known functions which can be expressed in general terms of J-type Bessel functions and the so-called collision matrix, U_ℓ (see Section V.A.2).

The boundary conditions for r = 0 are that $u^{\ell}_{\ell',J}$ and u^{ℓ}_{ℓ} approach zero. For the asymptotic region, r approaches infinity.

$$u^{\ell}_{\ell o}(r) \rightarrow U^{\ell}_{\ell o,\ell o}\ \mathcal{O}_{\ell}(r) - \mathcal{I}_{\ell}(r) \tag{106a}$$

$$u^{\ell}_{\ell' J}(r) \rightarrow U^{\ell}_{\ell o,\ell' J}\ \mathcal{O}_{\ell'}(r), \qquad \text{for } \ell' = |\ell - J| \text{ to } \ell + J \tag{106b}$$

Here $\mathcal{O}_{\ell}$ and $\mathcal{I}_{\ell}$ are known functions.[8] The constants U are unknown and are quantities to be determined.[62]

We will examine these boundary conditions on our N coupled equations in more detail, but first we shall examine the representation of the radial wave functions, $u^{\ell}_{\ell',J}$ and $u^{\ell}_{\ell o}$. In the next section we shall formulate the form of radial wave functions and the asymptotic conditions on u_{ℓ}.

2. Asymptotic conditions of the radial wave functions

The radial wave function μ_{ℓ} can be expressed as a linear combination as $u_{\ell} \sim U_{\ell}\mathcal{O}_{\ell} - \mathcal{I}_{\ell}$ in the asymptotic region. We can unite the outgoing wave as $\mathcal{O}_{\ell} = G_{\ell} + iF_{\ell}$ and the incoming wave as $\mathcal{I}_{\ell} = G_{\ell} - iF_{\ell}$. We use the linearly independent Coulomb solutions which are *regular* (F_{ℓ}) and *irregular* (G_{ℓ}) at the origin. The Wronskian of this pair is

$$F_{\ell}'G_{\ell} - G_{\ell}'F_{\ell} = 1 \tag{107}$$

which holds for all $\rho = kr$.[79] We can unite $F_{\ell} = \rho j_{\ell}(\rho)$ and $G_{\ell} = (-)^{\ell}\ (\pi\rho/2)^{\frac{1}{2}} j_{\ell-\frac{1}{2}}(\rho)$, for $\rho = kr$ for the Bessel function[8] j_{ℓ}. In the asymptotic region and $\ell = 0$, $F_{\ell} \sim \sin\rho$ and $G_{\ell} \sim \cos\rho$.

We can write u_{ℓ} in terms of F_{ℓ} and G_{ℓ}. Then $u_{\ell} \sim U_{\ell}\mathcal{O}_{\ell} - \mathcal{I}_{\ell} = U_{\ell}(G_{\ell} + iF_{\ell}) - (G_{\ell} - iF_{\ell})$. Collecting real and imaginary terms, then

$u_\ell = G_\ell(U_\ell - 1) + iF_\ell(U_\ell + 1)$ which asymptotically goes to $u_\ell \sim \cos\rho_\ell(U_\ell - 1) + i \sin\rho_\ell(U_\ell + 1)$.

In Table 20 we demonstrate the asymptotic condition for $u \sim U\mathcal{Q}\text{-}\mathcal{V}$ for the computer program SCATER2, July scatter which we use to calculate our complex coupled-channel differential equations which we discuss in more detail in later subsections of this section.[80] (Note that the coupling term is turned on in Table 20.)

TABLE 20. A check on the asymptotic condition of the magnitude of the $U\mathcal{Q}\text{-}\mathcal{V}$ term, giving comparison to those calculated by July SCATER2.

	$U\mathcal{Q}\text{-}\mathcal{V}$		u(SCATER)	
R	Re	Im	Re	Im
10.35	-3.8862×10^{1}	3.2410×10^{1}	-2.5530×10^{-6}	1.9959×10^{-4}
19.95	-1.8474×10^{-2}	3.0443	-1.3055×10^{-2}	3.0426
29.95	1.1244×10^{-2}	-2.9319×10^{-1}	1.0309×10^{-2}	-2.9104×10^{-1}
39.95	9.4782×10^{-4}	1.6129	8.0748×10^{-4}	1.6136
51.95	6.3798×10^{-4}	1.7343	6.3798×10^{-4}	1.7343

As can be seen in Table 20, the radius R becomes larger, then u approaches the value of $U\mathcal{Q}\text{-}\mathcal{V}$ for both the real and imaginary parts of $U\mathcal{Q}\text{-}\mathcal{V}$ and u (SCATER2). We use $R_{min} = 0.05$, $R_{max} = 50.$, $\ell_1^{(min)} = 60$, $U_1 = (0.9916, 7.0219 \times 10^{-3})$, where the first term in the bracket is the real part of the scattering matrix and the second term is the imaginary part of the scattering matrix. In Section V.E we discuss the boundary conditions in further detail.

3. Enumeration of the parity states for the coupled equations

In order to satisfy the boundary condition at infinity (or large but finite r) it is necessary to obtain J+2 linearly-independent solutions by defining different boundary conditions.

Returning to our coupled Schrodinger equations Eqs. (102a) and (102b) , let the index s span, s = 1, ... m. For each J_s there are, for $\ell \geq J_s$, $J_s + 1$ channels ℓ', J_s to which the incident channel is coupled. We can enumerate these; let k=1 correspond to the incident channel ℓ, J_o. For the other natural parity levels, we have the representation in Table 21. In each case in Table 21, the parity of the final channel is

$$(-)^{\ell'}\pi_s = (-)^{\ell' + J_s} = (-)^{\ell} \qquad (108)$$

That is, they are parity conserving channels.

TABLE 21. Enumeration of natural parity states.

Channel number k	Nuclear state s	Nuclear spin J_s	Orbital angular momentum ℓ'
1	1	$J_1 = 0$	ℓ
2	2	J_2	$\lvert\ell - J_2\rvert$
3			$\lvert\ell - J_2\rvert + 2$
⋮			⋮
$J_2 + 2$			$\ell + J_2$
$J_2 + 3$	3	J_3	$\ell - J_3$
$J_2 + 4$			$\ell - J_3 + 2$
⋮			⋮
$J_2 + J_3 + 3$			$\ell + J_3$
⋮			⋮
$N_m \equiv 1 + \sum_{s=2}^{m} (J_s+1)$	m	J_m	$\ell + J_m$

For the unnatural parity states, we again require that the channel parity be the same as the incident channel parity $(-)^{\ell}$

$$(-)^{\ell} = (-)^{\ell'}\pi_s = -(-)^{\ell'+J_s} \tag{109}$$

In this case, we have

$$\ell' = |\ell - J_s| + 1,\ |\ell - J_s| + 3 \ldots \ell + J_s - 1 \tag{110}$$

and there are J_s such channels. See Table 22 for the enumeration of unnatural parity states.

TABLE 22. Enumeration of unnatural parity states.

Channel number k	Nuclear state s	Nuclear spin J_s	Orbital angular momentum ℓ'
$N_m + 1$	$m+1$	J_{m+1}	$\lvert\ell - J_{m+1}\rvert + 1$
$N_m + 2$			$\lvert\ell - J_{m+1}\rvert + 3$
⋮			⋮
$N_m + J_{m+1}$			$\ell + J_{m+1} - 1$
$N_m + J_{m+1} + 1$	$m+2$	J_{m+2}	$\lvert\ell - J_{m+2}\rvert + 1$
⋮			⋮
$N_m + J_{m+1} + J_{m+2}$			$\ell + J_{m+2} - 1$
⋮			⋮
$N = N_m + \sum_{s=m+1}^{n} J_s$	n	J_n	$\ell + J_n - 1$

Altogether there are N such states,

$$N = N_m + N_n \quad , \quad \text{for } N_m = 1 + \sum_{s=1}^{m}(J_s+1) \quad , \quad \text{and } N_n = \sum_{s=m+1}^{n} J_s \tag{111}$$

coupled channels (for channels of the same parity and same channel spin). The first N_m are directly coupled amongst themselves. More precisely, the incident channel is coupled directly to, and only to, the remaining members of the first N_m channels, and indirectly coupled to the other N_n channels.

C. Coupled Equations for Computer Calculations

We will now write our set of coupled differential equations in a more convenient form for calculational purposes. We will write the total interaction potential as a function, $D^{\ell}_{\ell' J}(r)$, which, in general, is complex. Let

$$D^{\ell}_{\ell' J}(r) = \frac{\ell'(\ell'+1)}{r^2} + V(r) + iW(r) + V_c(r) + V^{\ell}_{\ell', J; \ell', J}(r) - k_J^2 \tag{112}$$

in terms of the diagonal elements of the coupling potential, $V_{\ell' J; \ell' J}$ and where the quantities V, W, V_c and $V^{\ell}_{\ell' J, \ell' J}$ are all given as function of r. For ℓ' channel states, k_J^2 is the energy which depends on the nuclear state (designated by a given value of s in Tables 21 and 22. We discuss the detailed form of the coupling potential in Section V.D.

For each ℓ' value in the range $\ell_1' \leq \ell \leq \ell_2'$ (for $\ell_1 = \min \ell$ and $\ell_2 = \max \ell$), we want to solve the set of N coupled equations,

$$\frac{d^2}{dr^2} u^{\ell}_{\ell o}(r) = D^{\ell}_{\ell o}(r)\, u^{\ell}_{\ell o}(r) + \sum_{\ell'' = |\ell - J_s|}^{\ell + J_s} \sum_{s=1}^{n} V^{\ell}_{\ell, o; \ell'', J_s}(r)\; u^{\ell}_{\ell'' J_s}(r) \tag{113}$$

$$\frac{d^2}{dr^2} u^{\ell}_{\ell' J_s}(r) = D^{\ell}_{\ell' J_s}\, u^{\ell}_{\ell' J_s} + V^{\ell}_{\ell' J_s; \ell 0}\, u^{\ell}_{\ell o} + \sum_{\ell''} \sum_{s' \neq s} V^{\ell}_{\ell' J_s; \ell'' J_{s'}}\, u^{\ell}_{\ell'' J_{s'}}$$

where $\ell' = |\ell - J_s|$ to $(\ell + J_s)$ in steps of two, s runs s = 1,n and $N = 1 + \sum_{s=1}^{n} (J_s + 1)$, see Table 23. By use of the notational charges given in Table 23, we can write out our set of differential equations, represented in Eq. (113) above for each ℓ as

$$\begin{aligned}
\frac{d^2}{dr^2} u_1 &= D_1 u_1 + \sum_{k=2}^{N} V_{1;k}\, u_k \\
\frac{d^2}{dr^2} u_2 &= D_2 u_2 + \sum_{k\neq 2} V_{2;k}\, u_k \\
&\vdots \\
\frac{d^2}{dr^2} u_N &= D_N u_N + \sum_{k=1}^{N-1} V_{N;k}\, u_k
\end{aligned} \tag{114}$$

the terms of the form, $V^{\ell}_{\ell' J_s;\ell'' J_s}$ in Eq. (113), or $V_{N;k}$ in Eq. (114) are the coupling potential functions.

TABLE 23. Relationship of angular momentum and nuclear indices.

k = 1	⟷	ℓ	J = 0	s = 0
k = 2	⟷	$\ell' = \lvert\ell - J_1\rvert$	J_1	s = 1
k = 3	⟷	$\ell' = \lvert\ell - J_1\rvert + 2$	J_1	s = 1
	⋮			
$k = J_1 + 1$	⟷	$\ell' = \ell + J_1$	J_1	s = 1
$k = J_1 + 2$	⟷	$\ell' = \lvert\ell - J_2\rvert$	J_2	s = 2
	⋮			
k = N	⟷	$\ell' = \ell + J_n$	J_n	s = n

For convenience we introduce indices k and p for k = 1,N, where $N \equiv J+2$ and $p = 2,N$; then

$$\begin{aligned} k = 1 &\rightarrow \ell \\ k = 2 &\rightarrow |\ell - J|, J \end{aligned} \tag{115}$$

In this form, we can calculate the integration routine in terms of a set of differential equations. In Section V.E we set up these N second-order equations as 2N first order equations. For convenience we introduce new indices p and k in order to write out the form we use for solution in Section E. We define a channel in terms of the index, p. The coupled equations are, for each value of the entrance channel

$$u_1''(r) = D_1(r)u_1(r) + (2\mu/\hbar^2)\sum_{k=2}^{N_{max}} V_{1,k}(r)\, u_k(r) \tag{116a}$$

$$u_p''(r) = D_p(r)u_p(r) + (2\mu/\hbar^2)\sum_{k\neq p}^{N} V_{p,k}(r)\, u_k(r) \tag{116b}$$

for $p = 2,\ldots N$ and where the total complex reaction potential function is D_p, and the coupling potential function is $V_{p,k}$.

The total potential function has the form

$$D_p(r) = \frac{\ell'(p)[\ell'(p)+1]}{r^2} - k_p^2 + \frac{2\mu}{\hbar^2}\left(V(r) + iW(r) + V_c(r)\right) \tag{117}$$

Here $\ell'(p)$ designates the value of ℓ' corresponding to the p^{th} channel, called the channel index and k_p^2 is its energy which depends on the number state and which is the same for all p corresponding to the same nuclear state (elastic) for a given value of s in Tables 21 and 22.

In this notation for our channel indices, our differential equations have the form

$$\left(\frac{d^2}{dr^2} - \frac{\ell(\ell+1)}{r^2} + k_o^2\right) u_1 = \sum_{p=1}^{N} V_{1p}\, u_p \tag{118a}$$

$$\left(\frac{d^2}{dr^2} - \frac{\ell'(\ell'+1)}{r^2} + k_J^2\right) u_k = \sum_{p=1}^{N} V_{kp}\, u_p \tag{118b}$$

for k = 2,...N. We introduce the column vector of dimension N

$$\hat{u} = \begin{pmatrix} u_1 \\ u_2 \\ \vdots \\ u_N \end{pmatrix} \tag{119}$$

In Section V.E we discuss the boundary condition in terms of the radial wave functions for small radius,

$$\hat{u}_p(r) = \begin{pmatrix} \delta_{p1}\, r^{\ell} \\ \delta_{p2}\, r^{\ell'} \\ \delta_{p3}\, r^{\ell'} \\ \vdots \end{pmatrix} \tag{120}$$

for p = 1,N, where we choose radius as small, we generate N linearly-independent solutions. In the next section (V.D) we discuss the coupling potential in detail.

D. The Coupling Potential

In this section we present a detailed discussion of the form of the coupling term in the complex differential equations given in Eqs. (102a) and (102b). The coupling term accounts for the exchange of angular

momentum and spin between the various exit channels. All of the radial wave functions, $u_{\ell'J'}$, and most of the coupling potential terms, $V^{\ell}_{\ell'J',\ell''J'}$, are complex. The diagonal terms of $V^{\ell}_{\ell'J',\ell'J'}$ are complex while the off-diagonal terms are real. The off-diagonal terms express the exchange of ℓ and J. The diagonal terms correspond to "elastic" processes and the non-diagonal terms correspond to "inelastic processes." All potential terms are functions of the radial separation, r.

1. Symmetry relations of the potential coupling term

We can express the symmetry condition of $V^{\ell}_{\ell'J',\ell''J''}$ and $V^{\ell}_{\ell''J'',\ell'J'}$ as

$$V^{\ell}_{\ell'J',\ell''J''} = \delta_{\ell'\ell''}\,\delta_{J'J'}\,V(r) + e^{-\alpha n^2}\sum_{p=L_1}^{\bar{p}} r^p\,\Lambda^{\ell}_{p}(\ell'J'\ \ell''J'') \tag{121}$$

where $L_1 = |J' - J''|$ and $\bar{p} = J' + J'' + 2\mu$, where $\bar{\mu}$ depends on J' and J'' implicitly in the sum. The terms Λ^{ℓ}_{p} are real constants which depend on the nucleon structure and therefore depend on the nuclear model under consideration (see also Eq. (27)).

2. The coupling potentials $V_{p,k}$

Let us consider a particular p and k which correspond to $p \equiv P', J', \pi', \ell'$ and $k \equiv P'', J'', \pi'', \text{and } \ell''$. Then we have

$$V_{p,k}(r) \equiv V^{\ell}_{p,k}(r) = \int [Y^{*}_{\ell'}(\hat{r})\ \Phi^{*}_{p'J'\pi'}(\xi)]^{0}_{\ell}\ V(r,\xi) \times [Y_{\ell''}(\hat{r})\ \Phi_{p''J''\pi''}(\xi)]^{0}_{\ell}\ d\hat{r}\ d\xi \tag{122}$$

where the integration is taken over all the nuclear coordinates, designated by ξ, and over the direction $\hat{r} \equiv \theta,\phi$ of $\vec{r}$, the radial coordinate. The

nucleon wave functions are $\Phi_{P'J'\pi'}$. We can then expand $V(\bar{r},\xi)$ in multipoles,

$$V(\bar{r},\xi) = \sum_{LM} Y_L^M(\hat{r}) \; T_L^{M*}(r,\xi) \tag{123}$$

[see Eq. (128)]. Then we can unite $V_{p,k}$ from Eq. (122) above as

$$V_{p,k}^{\ell}(r) = \sum_{L} C_L^{\ell}(p,k) \; (P'J'\pi' \| T_L \| P''J''\pi'') \tag{124}$$

where

$$C_L^{\ell}(p,k) \equiv C_L^{\ell}(\ell'J';\ell''J'') = (-)^{\ell'-\ell+J''} \; W(\ell'J'\ell''J'';\ell L)\times(\ell' \| \gamma_L \| \ell'') \tag{125}$$

where $W(\ell'J'\ell''J'';\ell L)$ are Racah coefficients and γ_L are the reduced matrix elements. The form of the transition matrix and its reduced matrix elements depends on the specific nuclear model. We choose to look at the vibrational harmonic oscillator model for the coupling potential.

3. Coupling Potential in the Vibrational Model

In the vibrational model we can describe the nuclear surface as (see Section V.F also)

$$R = R_o\left(1 + \sum_{\lambda\mu} \alpha_{\lambda\mu} \, Y_{\lambda\mu}(\theta,\phi)\right) \tag{126}$$

We can expand about the spherical shape for the interaction as

$$\begin{aligned} V(r-R) &= V(r-R_o) - R_o \left(\frac{\partial V}{\partial \chi}\right)_{\chi=r-R_o} \sum \alpha_{\lambda\mu} \, Y_{\lambda\mu} + \frac{R_o^2}{2} \left(\frac{\partial^2 V}{\partial \chi^2}\right)_{\chi=r-R_o} \\ &\times \left(\sum \alpha_{\lambda\mu} \, \gamma_{\lambda\mu}\right)^2 + \ldots . = V(r-R_o) - R_o \frac{\partial V}{\partial r} \sum_{\lambda\mu} \alpha_{\lambda\mu} \, \gamma_{\lambda\mu} \\ &+ \frac{R_o^2}{2} \frac{\partial^2 V}{\partial r^2} \sum_{\lambda\lambda' LM} \sqrt{\frac{(2\lambda+1)(2\lambda'+1)}{4\pi}} \begin{pmatrix} \lambda & \lambda' & L \\ 0 & 0 & 0 \end{pmatrix} [\alpha_\lambda \, \alpha_{\lambda'}]_L^M \end{aligned} \tag{127}$$

The transition matrix can be expressed in terms of the expansion about a spherical surface shape,

$$T_L^{M*} \equiv -R_o \frac{\partial V}{\partial r} \alpha_{LM} + \frac{R_o^2}{2} \frac{\partial^2 V}{\partial r^2} \sum_{\lambda\lambda'} \sqrt{\frac{(2\lambda+1)(2\lambda'+1)}{4\pi}} \begin{pmatrix} \lambda & \lambda' & L \\ 0 & 0 & 0 \end{pmatrix} [\alpha_\lambda \alpha_{\lambda'}]_L^M (-)^L \tag{128}$$

We can define the reduced matrix element in two parts,

$$B_{p,k}^L \equiv (P'J'\pi' \| \alpha_L \| P''J''\pi'')$$

and (129)

$$E_{p,k}^L \equiv (P'J'\pi' \| \sum_{\lambda\lambda'} \sqrt{\frac{(2\lambda+1)(2\lambda'+1)}{4\pi}} \begin{pmatrix} \lambda & \lambda' & L \\ 0 & 0 & 0 \end{pmatrix} [\alpha_\lambda \alpha_{\lambda'}]_L^M \| P''J''\pi'')$$

The we can express the coupling potential as

$$V_{p,k}^{\ell}(r) = \sum_L C_L^{\ell}(p,k) \left\{ R_o \frac{\partial V(r)}{\partial r} B_{p,k}^L + \frac{R_o^2}{2} \frac{\partial^2 V(r)}{\partial r} E_{p,k}^L \right\} \tag{130}$$

where we express the matrices in terms of the indices p,k. The quantities $C_L(p,k)$, $B_{p,k}^L$ and $E_{p,k}^L$ can be considered at known constants which can be used as input to our coupled channel code. The $B_{p,k}^L$ defines the boundary conditions and the $E_{p,k}^L$ relates to energy. We can then unite the coupled equations in terms of these constants as

$$u_1''(r) = D_1(r)\, u_1(r) + \frac{2\mu}{\hbar^2} R_o \frac{\partial V(r)}{\partial r} \sum_{k=2}^{N} \mathcal{B}_{p,k}^{\ell}\, u_k(r)$$

$$+ \frac{2\mu}{\hbar^2} \frac{R_o^2}{2} \frac{\partial^2 V(r)}{\partial r^2} \sum_{k=2}^{N} E_{p,k}^{\ell}\, u_k(r) \tag{131}$$

and, in general, for any p,

$$u_p''(r) = D_p(r)\, u_p(r) + \frac{2\mu}{\hbar^2} R_o \frac{\partial V(r)}{\partial r} \sum_k^N \mathcal{B}^{\ell}_{p,k}\, u_k(r)$$

$$+ \frac{2\mu}{\hbar^2} \frac{R_o^2}{2} \frac{\partial^2 V(r)}{\partial r^2} \sum_k^N E^{\ell}_{p,k}\, u_k(r) \qquad (132)$$

for $p = 2,\ldots N$ and where

$$\mathcal{B}_{p,k} = \sum_L C^{\ell}_L(p,k)\, B^L_{p,k} \qquad (133)$$

recall that μ is the reduced mass.

In the next section, we will discuss the form of the input parameters to the coupled differential equations in the program SCATER2. In the following section we present a more detailed discussion of the deformation parameters and other parameters that are input to the code.[80]

E. Numerical Integration of the Coupled Differential Equations and Small and Large Radius Boundary Conditions

In this section we formulate the SCATER2 program numerical calculation of the scattering matrix and discuss the use of the boundary conditions applied. As stated before, SCATER2 was written in order to solve the coupled complex differential equations for coupling between the excited states of the target nucleus.

In principle, the integration proceeds from the nuclear origin. However, to avoid problems with singularities we integrate from small r_o, usually taken to be $r_{min} = 0.01$ f.

To avoid possible problems with overflow in the numerical calculation at larger radii, we do not assign an arbitrary boundary condition but fit the boundary conditions of the asymptotic form of the wave functions

to the corresponding Bessel functions. We discussed this form in terms of the expression of the outgoing wave, in terms of the regular and irregular Coulomb wave functions. Introducing a vector notation for a given solution of the N equations, we set the boundary condition

$$\hat{u}_p(\bar{r}) = \begin{pmatrix} \delta_{p1}(K_1\bar{r})^{\ell+1} / (2\ell+1)!! \\ \delta_{p2}(K_2\bar{r})^{\ell'(2)+1} / (2\ell'(2)+1)!! \\ \vdots \\ \delta_{pN}(K_N\bar{r})^{\ell'(N)+1} / (2\ell'(N)+1)!! \end{pmatrix} \tag{134}$$

where we define K_n^2 as

$$K_n^2 = p_n^2 - \frac{2\mu}{\hbar^2}\left(V + \frac{6Ze^2}{2R_c}\right) \tag{135}$$

where μ is the reduced mass and R_c is the Coulomb radius and the double factorial refers to the inclusion of odd terms only.

For each $\ell'(N)$, only one term in Eq. (134) is non-vanishing and $\bar{r}$ is a radius such that

$$\frac{(K_1\bar{r})^{\ell+1}}{(2\ell+1)!!} \simeq 10^{-35}$$

By solving the set of coupled equations N times, with initial conditions given above with $p = 1,\ldots N$, we get N sets of linearly-independent solutions

$$\hat{u}_p(r) = \begin{pmatrix} u_{1p}(r) \\ u_{2p}(r) \\ \vdots \\ u_{Np}(r) \end{pmatrix}, \quad p = 1,N \tag{136}$$

for a linear combination which can be chosen to satisfy the boundary condition at $R \equiv R_{max}$,

$$\sum_p \alpha_p \hat{u}_p(R) = \begin{pmatrix} U_1 \mathcal{O}_1 - \mathcal{I}_1 \\ \sqrt{p_1/p_2}\ U_2 \mathcal{O}_2 - \mathcal{I}_2 \\ \vdots \\ \sqrt{p_1/p_N}\ U_N \mathcal{O}_N - \mathcal{I}_N \end{pmatrix} \tag{137}$$

where the outgoing wave in terms of the regular and irregular Coulomb functions is $\mathcal{O}_k = [G_{\ell'(k)}(K_k,R) + iF_{\ell'(k)}(K_k,R)]$. The Eq. (136) and their first derivatives comprise the 2N inhomogeneous linear equations in the N coefficients, α and the N dimensional collision matrix elements, U.

$$\begin{aligned}
&\alpha_1 u_{11} + \alpha_2 u_{12} + \ldots\ldots + \alpha_N u_{1N} - U_1 \mathcal{O}_1 + 0 \ldots\ldots = -\mathcal{I}_1 \\
&\alpha_1 u_{21} + \alpha_2 u_{22} + \ldots\ldots + \alpha_N u_{2N} + 0 - U_2 \mathcal{O}_2 \ldots\ldots = 0 \\
&\alpha_1 u_{N1} + \alpha_2 u_{N2} + \ldots + \alpha_N u_{NN} + 0 \ldots\ldots - U_N \mathcal{O}_N = 0 \\
&\alpha_1 u'_{11} + \alpha_2 u'_{12} + \ldots + \alpha_N u'_{1N} - U_1 \mathcal{O}'_1 + 0 \ldots\ldots = -\mathcal{I}'_1 \\
&\qquad\vdots \\
&\alpha_1 u'_{N1} + \alpha_2 u'_{N2} + \ldots\ldots + \alpha_N u'_{NN} \quad \text{to} \quad - U_N \mathcal{O}'_N = 0
\end{aligned} \tag{138}$$

where u' denotes du/dr.

If one wants the actual solution with the appropriate asymptotic boundary conditions, it can now be obtained by using the initial condition

$$u(r) = \begin{pmatrix} \alpha_1 \, r^{\ell+1} / (2\ell+1)!! \\ \alpha_2 \, r^{\ell(2)+1} / (2\ell'(2)+1)!! \\ \vdots \\ \alpha_N \, r^{\ell'(N)+1} / [2\ell'(N)+1]!! \end{pmatrix} \tag{139}$$

Then we can impose the boundary condition in the asymptotic region for large r, by the use of

$$\sum_p \alpha_p \, \hat{u}_p(r) \underset{\lim R \to \infty}{=} \hat{u}_\infty(r) \equiv \begin{pmatrix} U_1 \, \mathcal{O}_\ell(r) - \mathcal{V}_\ell(r) \\ U_2 \, \mathcal{O}_{\ell'}(r) - \mathcal{V}_{\ell'}(r) \\ \vdots \\ U_N \, \mathcal{O}_{\ell'}(r) - \mathcal{V}_{\ell'}(r) \end{pmatrix} \tag{140}$$

These equations and their first derivatives give 2N equations in the N coefficient α_p and the N elements U_p. The entire procedure above is repeated for each ℓ in the range $\ell_1 \leq \ell \leq \ell_2$ and thus we obtain a rectangular array of the elements U_k^ℓ as the calculational output of the calculation.

F. Deformation Parameters in the Vibrational Coupled Channel Scattering Model

The complex coupling potential form that we consider for the alpha scattering and subsequent alpha decay of light nuclei is taken to be as formulated for the vibrational model. In this section we give a detailed

description of the vibrational model. We can calculate nuclear spectroscopic information from alpha particle scattering data. Using the model developed by N. Austern and J. S. Blair[81] for diffraction of arbitrary multipole excitation allows the amplitude for the ℓ^{th} outgoing particle wave to be complex.[82] We consider the strong absorption model for our alpha particle projectile where most of the absorption takes place on the nuclear surface.

N. Austern and J. S. Blair[81] present a theoretical model of the inelastic scattering amplitudes which is formulated in terms of derivatives of elastic scattering phase shifts. The role of the dependency on the optical model parameter is minimized. The relationship between the Blair model and the Fraunhofer diffraction model is, for elastic scattering for a black sphere, where the scattering amplitude is expressed in terms of J-type Bessel functions. The applicability of the model is best for strongly absorbed medium-energy projectiles such as alpha particles which excite collective states of the nuclear surface. The strong absorption condition simplifies the Green's functions that enter the calculation for higher order processes (not presently considered). The scattering amplitude, in the adiabatic approximation, is calculated in terms of the transition probability which is dependent upon the angular momentum derivative of the scattering phase shift coefficients. Then, of course, the differential cross section is calculated in terms of the absolute value of the amplitude squared. The elastic scattering amplitude has the form

$$f(\theta) = f_c(\theta) + \frac{i}{2k} \sum_{\ell=0}^{\infty} e^{2i\sigma_\ell} (2\ell + 1) \times (1 - \eta_\ell) P_\ell(\cos\theta) \qquad (141)$$

where $f_c(\theta)$ is the Coulomb amplitude, σ_ℓ is the Coulomb phase shift for the ℓ^{th} partial wave amplitude, [$\sigma_\ell = \arg\Gamma(\ell + \ell + 2\eta)$, where $\eta = 2Ze^2/\hbar v$, the Coulomb parameter]. The $p_\ell(\cos\theta)$ are the usual Legendre polynomials of order ℓ and k is the relative projectile target wave number. The Legendre polynomials for $\ell = 0, 1, 2$ are:

$$\begin{aligned} p_0(\cos\theta) &= 1 \\ p_1(\cos\theta) &= \cos\theta \\ p_2(\cos\theta) &= 3/2\ \cos^2\theta - \tfrac{1}{2} \end{aligned} \tag{142}$$

The derivatives of the scattering phase shift $\partial\eta_\ell/2\ell$ can be identified with the elements of the S-matrix.

In the case for the bombardment of spin-zero particles on the zero spin (ground state) of the target, we can extract the single and double excitation amplitudes from the coupled channel calculation of J. Wills.[83] If we consider the part of the wave function that belong to an excited state of the target, having spin I and projectile M_I, then the scattering amplitude for excitation of this state is the asymptotic amplitude of that part of the wave function,

$$f_{I,M_I} = \frac{-i}{2k} \sum_{\ell,\ell'} (4\pi)^{\frac{1}{2}}\ (2\ell+1)^{\frac{1}{2}}\ e^{i(\sigma_\ell+\sigma_{\ell'})}\ S^{\ell}_{\ell'I}\ \langle \ell' I,\ -M_I M_I | \ell, 0\rangle\ Y_{\ell'}^{-M_I}(\theta,0) \tag{143}$$

where σ_ℓ are the Coulomb phase shifts and $Y_{\ell'}^{-M_I}(\theta,0)$ are the usual spherical harmonics. The quantities in brackets are the Clebsch-Gordan coefficients. The coefficients $S^{\ell}_{\ell'I}$ are the S-matrix elements for excitation of the nuclear excited state with spin I, with initial projectile angular momentum ℓ and final angular momentum ℓ'. In our example we consider

the excitation of the excited states of ^{24}Mg, through bombardment of alpha particles. The nucleus is treated as permanently deformed. For the first excited state, I=2, the extended optical model potential which describes the projectile nucleus interaction is that which is appropriate for the rotational quadrupole excitation,

$$U(R,r) = U\left(r - R_o \left[1 - \beta_2 Y_2^o(\theta,0)\right]\right) \tag{144}$$

where θ is the polar scattering angle in the center-of-mass system, and $\phi = 0$. N. Austern and J. S. Blair[81] calculate the S-matrix elements for the case of ^{24}Mg. Using optical model parameters with a larger absorption term, W~50 MeV, for E_{lab} = 42 MeV and with V~90 MeV, plots are made for Re $S^{\ell}_{\ell'2}$ and Im $S^{\ell}_{\ell'2}$ vs. $\bar{\ell} = (\ell+\ell')/2$. We make similar such plots and compare results.

G. Coupling Matrix in Rotational Nuclei

The energy level structure of even mass spheroidal nuclei can be associated with contributions from collective vibrations of the nuclear surface as well as rotational degrees of freedom. These oscillations preserve the system's axial symmetry (as stated in Section II.E) and are described by the well known β and γ "permiate" quadrupole rotator degrees of freedom.

The shape of the nuclear surface in the body-fixed coordinate system is given by[53]

$$R(\theta,\phi) = R_o\left[1 + \sum_{\substack{\lambda > 0 \\ \nu \text{ even}}} \alpha_{\lambda\nu} Y_{\lambda\nu}\right] = R_o + \delta R \tag{145}$$

The angles of the spherical harmonics are in the frame of the body-fixed axis. The independent $\alpha_{\lambda\nu}$ can be written in terms of the deformation constants β_λ where λ is an integer.

$$\begin{aligned}
\alpha_{2,0} &= \beta_2 \cos \beta_1 \\
\alpha_{2,2} &= \alpha_{2-2} = 1/\sqrt{2}\ \beta_2 \sin \beta_1 \\
\alpha_{6,0} &= \beta_6 \\
\alpha_{6,\mu} &= 0\ , \qquad \mu \neq 0 \\
\alpha_{4,0} &= \beta_4 \cos \beta_3 \\
\alpha_{4,2} &= \alpha_{4,-2} = 1/\sqrt{2}\ \beta_4 \sin \beta_3 \cos \beta_5 \\
\alpha_{4,4} &= \alpha_{4,-4} = 1/\sqrt{2}\ \beta_4 \sin \beta_3 \sin \beta_5
\end{aligned} \tag{146}$$

so that β_2 and β_4 are the deformation parameters, β_1 corresponds to γ and β_3 and β_5 are azimuthal asymmetry parameters in the $\lambda = 4$ deformations. Expanding in a Taylor series about the spherical shape

$$V(r - R) = V(r - R_o) + \sum_{s=1}^{\infty} \frac{(-\delta R)^s}{s!} \frac{\partial^s V}{\partial r^s} \tag{147}$$

We can unite $(\delta R)^s$ in terms of spherical harmonics referred to as space fixed systems in terms of the deformation functions $\mathcal{O}^\lambda_{\mu\nu}$. For the first term we have

$$\frac{\delta R}{R_o} = \sum_{\lambda\nu} \alpha_{\lambda\nu} Y_{\lambda\nu} = \sum_{\lambda\nu} \alpha_{\lambda\nu} \sum_{\mu} \mathcal{O}^\lambda_{\mu\nu} Y_{\lambda\mu} \tag{148}$$

Or, in general, for any power of s, as

$$\left(\frac{\delta R}{R_o}\right)^s = \sum_{LK} \delta^s_{L,K} \sum_M \mathcal{D}^L_{MK} Y_{LM} \tag{149}$$

where $\delta^{(s)}_{L,K}$ is expressed in terms of an expansion of $\mathcal{D}^L_{MK}$ and Y_{LM} coupled by three j-symbols for $L = 0,2,4,6,8$, and for K even and $-L \leq K \leq L$, and from symmetry considerations $\delta_{L,K} = \delta_{L,-K}$. If we confine our attention to the K=0 and K=2 bands then we need only these terms in the expansion

$$V_{coup}(r-R) = V(r - R_o) + \sum_{LM} Y_{LM} \mathcal{D}^L_{MK} \left[\sum_s \frac{(-R_o)^s}{s!} \delta^{(s)}_{L,K} \frac{\partial^s V}{\partial r^s} \right] \tag{150}$$

the term in brackets, $F_{L,K}(r)$ is called the radial form factor,

$$F_{L,K}(r) = \sum_{s=1}^{\infty} \frac{(-R_o)^s}{s!} \delta^{(s)}_{L,K} \frac{\partial^{(s)} V}{\partial r^s}$$

for $L = 0,2,4,6,8$, etc. and $K \leq L$ and $K \leq 2$. Then Eq. (150) becomes

$$V_{coup}(r-R) = V(r - R_o) + \sum_{LM} Y_{LM} \left[\sum \mathcal{D}^L_{mK} F^{(r)}_{L,K} \right] \tag{153a}$$

We can then calculate the coupling matrix elements from the non-spherical concentration having the general form

$$V_{\ell J;\ell'' J''} = \langle Y_{\ell'} \Phi_{J'K';\ell 0} | V_{coup}(r-R) | Y_{\ell''} \Phi_{J''K'';\ell 0} \rangle$$

$$= \sum_L C_L(\ell' J';\ell'' J'') \sum_K \langle J'K' | \mathcal{D}^L_{MK} J''K'' \rangle F^{(r)}_{L,K} \tag{153b}$$

where $C^{\ell}_L(\ell' J';\ell'' J'')$ are the Clebsch-Gordan coefficients. The values of s, K, and J run as in Table 24(a), and L and K as in Table 24(b).

TABLE 24. The relationship of indices s, K, J, and L, K.

(a) Input indices for coupling potential

s	K	J
1	0	0
2	0	2
3	2	2
4	2	3

(b) Relationship of indices L and K

L	0	2	4	6	8
K	0	-2	-4	-6	-8
		0	-2	-4	-6
		2	0	-2	-4
			2	0	-2
			4	2	0
				4	2
				6	4
					6
					8

The differential cross sections involving populations of rotational bands of even-even deformed nuclei, up to and including $\lambda = 6$, are fitted with combinations of the β_λ deformation parameters. In this analysis it it assumed that the nucleus is a perfect rotor (i.e. stretching and volume changes are neglected).[84] The spin and parity of the rotationally deformed nuclei are given as $J^\pi = 0^+$, 2^+, 4^+, and 6^+. Some of the deformation parameters β_λ are represented schematically in Fig. 15.

If the deformation parameter β_2 is small it can be related to the intrinsic quadrupole moment, Q_o, by

$$Q_o = \frac{3}{\sqrt{5\pi}} (Z - 2) R_o^2 \beta_2 \qquad (154)$$

for the unformed nuclear charge distributions.[20]

The deformation parameter used for our ^{24}Mg calculation are given in Table 25.

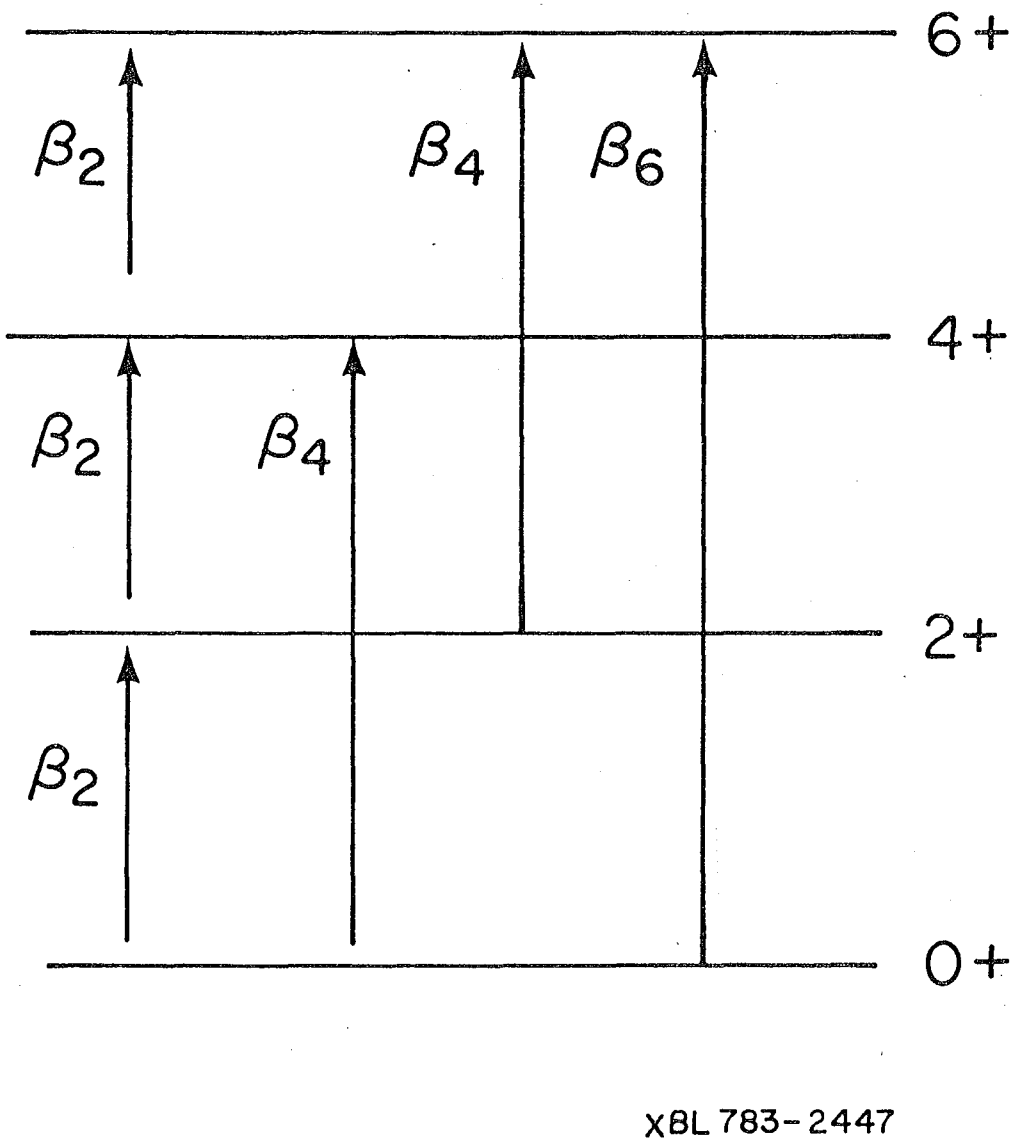

Fig. 15. Schematic relationship of the deformation parameters β_λ for λ even and for the rotational excitation of the ground state rotational band.

TABLE 25. Deformation parameters used in the ^{24}Mg calculation, β_λ.

$\beta(1)$	$\beta(2)$	$\beta(3)$	$\beta(4)$	$\beta(5)$	$\beta(6)$
0.29	0.35	1.571	0.12	0	0

H. The Nuclear Potential Parameters

For our ^{24}Mg case in our present calculation, the form of the complex nuclear potential is the same as in Eq. (105),

$$V_{Re}(r) = -V_o / \exp\left[1 + (r - R_o A^{1/3}) / a\right]$$

and (155)

$$V_{Im}(r) = -W / \exp\left[1 + (\bar{r} - \bar{r}_o A^{1/3}) / \bar{a}\right]$$

for a total potential $V = V_{Re}(r) + V_{Im}(r)$.

In Table 26 we present the parameters used and compare these to similar parameters brought to this researcher's attention.[24,85]

TABLE 26. Complex Woods-Saxon potential parameters:
(a) the parameters used in our calculation;
(b) parameters from Ref. 80.

	Real nuclear potential		Imaginary nuclear potential	
	Parameter	Value	Parameter	Value
(a)	V_o	-100. MeV	W	-1.0 or 0 MeV
	r_o	1.38 f	$\bar{r}_o$	1.40 f
	a	0.69 f	$\bar{a}$	0.58 f
	r_o^c	1.30 f		
(b)	V_o	-107.9 MeV	W	18.88 MeV
	r_o	1.26 f	$\bar{r}_o$	1.78 f
	a	0.76 f	$\bar{a}$	0.49 f
	r_o^c	1.28 f		

Further investigation of the effect on the position and width of resonance states will be made by varying the potential parameters and by use of the new potential parameter of Ref. 80. The present potential parameters are sufficient to demonstrate the existence and nature of the scattering-matrix resonance curves.

Note that in Ref. 85 the imaginary part of the potential used is W = 18.88 MeV, which is comparable to W = 18 MeV, used to fit the differential diffraction scattering cross section vs. angle.

I. Scattering Cross Sections and the Properties of the S-Matrix

The power of the S-matrix formalism comes in the analysis of the behavior of the S-matrix elements in the complex plane. The structure of the S-matrix gives us information about the detailed mechanism of compound nuclear formation resonance decay processes. The scattering and capture of nuclear projectiles can probe the nuclear interior. Problems arise because different competing processes occur in the nuclear interior. The detailed structure of the behavior of the properties of the S-matrix may illuminate the detailed mechanism of alpha decay and yield information about the properties of the nuclear force in the interior region; a goal of nuclear physics since its inception.[86]

The Yukawa force considered the interaction of nucleon pairs[87] but also of significance may be the formation and interaction of clusters. The carbon, $^{12}_{6}C$ nucleus has been modeled in terms of the cluster of three alpha particles, $^{4}_{2}He$ clusters.[88] The structure of the $^{24}_{12}Mg$ target can also be considered in terms of six alpha particle clusters or in terms of two carbon clusters. The question of interest is to what extent does

a nuclear cluster retain its identity on the nuclear surface or in the nuclear interior. This is certainly a relevant consideration to the early model of G. Gamow.[12] Cluster-cluster interaction would modify the apparent nuclear force and, in the case of alpha clusters, would effect spin terms in the nuclear force, since they are spinless as compared to the nucleons which are Fermions. These properties would effect the renormalization in terms of the Pauli principle requirement for renormalization of the nucleon wave functions. It is of interest then to examine the extent to which alpha clustering occurs. For example, the reactions involving alpha transfer, such as $^{16}O(\alpha,^{8}Be)^{12}C$ are utilized to measure the extent of alpha clustering in nuclei.[89] It is of interest here to see whether the compound nuclear state appears to be a reasonable model. We have utilized this model in developing the S- and R-matrix approaches. Let us consider the calculation of the elastic resonance reaction and total cross sections for a spinless target including Coulomb interactions.

We can calculate the resonance cross section from the expression for the amplitude, A^s, for each s as a function of the angle θ where $d\sigma_s$ is the general inelastic differential cross section

$$d\sigma_s(\theta) = \frac{1}{2} \sum_{mm'M'} |A^s_{m,m',M'}(\theta)|^2 \tag{156}$$

where the amplitude is given by

$$A^s_{m,m',M'}(\theta) = i\,\delta_{s,1}\,\delta_{m,m'}\,\delta_{M'0}\,C(\theta) + \frac{\sqrt{\pi}}{p_1} \sum_{\ell,j} \sqrt{2\ell+1}\; C^{\ell\ \frac{1}{2}\ j}_{0\ m\ m}$$

$$\times \sum_{\ell'j'} i^{\ell-\ell'}\, e^{i(\sigma_\ell+\sigma_{\ell'})} \left[U^{\ell}_{\ell'j'J_s} - \delta_{s,1}\right]$$

$$\times\ C^{j'\quad J_s\quad j}_{m-M',\ M',\ m}\ C^{\ell'\ \frac{1}{2}\ j'}_{m-M'-m',\ m',\ m-M'}\ Y^{m-M'-m'}_{\ell'}(\theta,0) \tag{157}$$

Here m and m' take two values each, $-\frac{1}{2}$ and $\frac{1}{2}$, and $-J_s \leq M \leq J_s$. The quantities $U^{\ell}_{\ell' j' J_s}$ are the scattering matrices; the Coulomb phase shifts are given as $\sigma_\ell + \sigma'_\ell$, and the C's are the Clebsch-Gordan coefficients for the spins and spin projections. The value of ϕ is taken as zero. The sum on $\sum_{\ell' j'}$ corresponds to the portion of the range of k that corresponds to the current value of s. The sum on $\sum_{\ell j}$ corresponds to the sum on ℓ as before for $j = \ell - \frac{1}{2}$ and $j = \ell + \frac{1}{2}$, and $\max j' = \max J_s + \ell_2 + \frac{1}{2}$ and therefore $\max \ell' = \max j' + \frac{1}{2}$, and max m index on $Y^m_{\ell'}$ is $\max J_s + 1$ and for all m such that $0 \leq m \leq \max \ell$. The spherical harmonics are of the form $Y^m_\ell(\theta) = P^m_\ell(\cos\theta) e^{im\theta}$.

We can also unite the polarization in terms of the amplitude and the cross section as

$$P_s(\theta) = \left\{ \tfrac{1}{2} \sum_{m,m',M'} (-)^{\frac{1}{2}-m'} \left| A^s_{m,m'M'} \right|^2 \right\} \Big/ d\sigma_s(\theta) \qquad (158)$$

Using the coupled channel SCATER2 code of N. K. Glendenning, we fit the scattering of the alpha particles on the ^{24}Mg target. The value of the physical parameters and numerical data used in the fit to the different cross sections are given in Table 27. These parameters can be compared to those of L. McFadden and G. R. Shatchler[24] who have performed an optical model analysis for the scattering of 24.7 MeV alpha particles off of a number of target nuclei. The target nuclei ^{24}Mg and ^{28}Ni have been studied in some detail. The fit to the differential cross section $d\sigma/d\sigma_R$ vs. angle in the center of mass system, $\theta_{c.m.}$ is best for $V \sim 100$ MeV for light target nuclei, and $V \sim 150$ to 200 MeV for heavier target nuclei which is consistent for our ^{24}Mg case, where the ratio $d\sigma/d\sigma_R$ is the elastic differentiated cross section over the Rutherford differential cross section in their plots.

TABLE 27. The parameters used in the fit of the cross section are given for the ^{24}Mg target and the alpha particle projectile.

Elements	Radius and ℓ value	Deformation	Nuclear potential
$E_{lab} = 50$ MeV	$R_{min} = 0.05$ f	$\beta(1) = 0.290$	V = -100.0 MeV
$M_T = 23.985$ target mass	$R_{max} = 19$ f	$\beta(2) = 0.350$	a = 0.690 MeV
$Z_T = 12$ target atomic no.	H = 0.01 step size	$\beta(3) = 1.571$	R_o = 1.380 MeV
$M_p = 4.0026$ projectile mass	$\ell_{1(min)} = 0$	$\beta(4) = 0.120$	W = -18.0 MeV
$Z_p = 2$ projectile atomic no.	$\ell_{2(max)} = 50$	$\beta(5) = 0$	$\bar{a}$ = 0.580 MeV
	θ = 1 angular interval	$\beta(6) = 0$	$\bar{R}_o$ = 1.40 MeV

We have plotted the S-matrix elements in three forms. The first is in terms of a quantity proportional to the transmission coefficient, or $\mathcal{T}_\ell = |1 - U_\ell|^2$, which is related to the total elastic or coherent cross section for each partial wave in the semiclassical picture

$$\sigma_{\substack{e\ell \\ total}} = \pi\lambda\!\!\!^{-2} \sum_\ell (2\ell + 1)\,|1 - U_\ell|^2 \tag{159}$$

where $\lambda\!\!\!^{-} = \frac{1}{2}\pi k$, and k is the wave number. The second quantity is proportional to the reaction cross section, $1 - |U_\ell|^2$; the reaction cross section is given by

$$\sigma_{react.} = \pi\lambda\!\!\!^{-2} \sum_\ell (2\ell + 1)(1 - |U_\ell|^2) \tag{160}$$

and using the fact that the square of the modulus $|1 - U_\ell|^2 = (1 - U_\ell)(1 - U_\ell)^*$ for the complex number U_ℓ, we can express the total cross section as

$$\sigma_{total} = \sigma_{e\ell} + \sigma_{react.} = \pi\lambda\!\!\!^{-2} \sum_\ell 2(2\ell + 1)(1 - \mathrm{Re}U_\ell) \tag{161}$$

Fig. 16. The dimensionless ratio of the differential cross section for alpha scattering from the ^{24}Mg, $d\sigma/d\Omega$(mb/sr) to the Rutherford differential cross section $d\sigma_R/d\Omega$ is plotted vs. the center-of-mass scattering angle $\theta_{c.m.}$ in degrees. The spins and parities of the rotational spectra are also given. The experimental data points are fit with Glendenning coupled channel code.

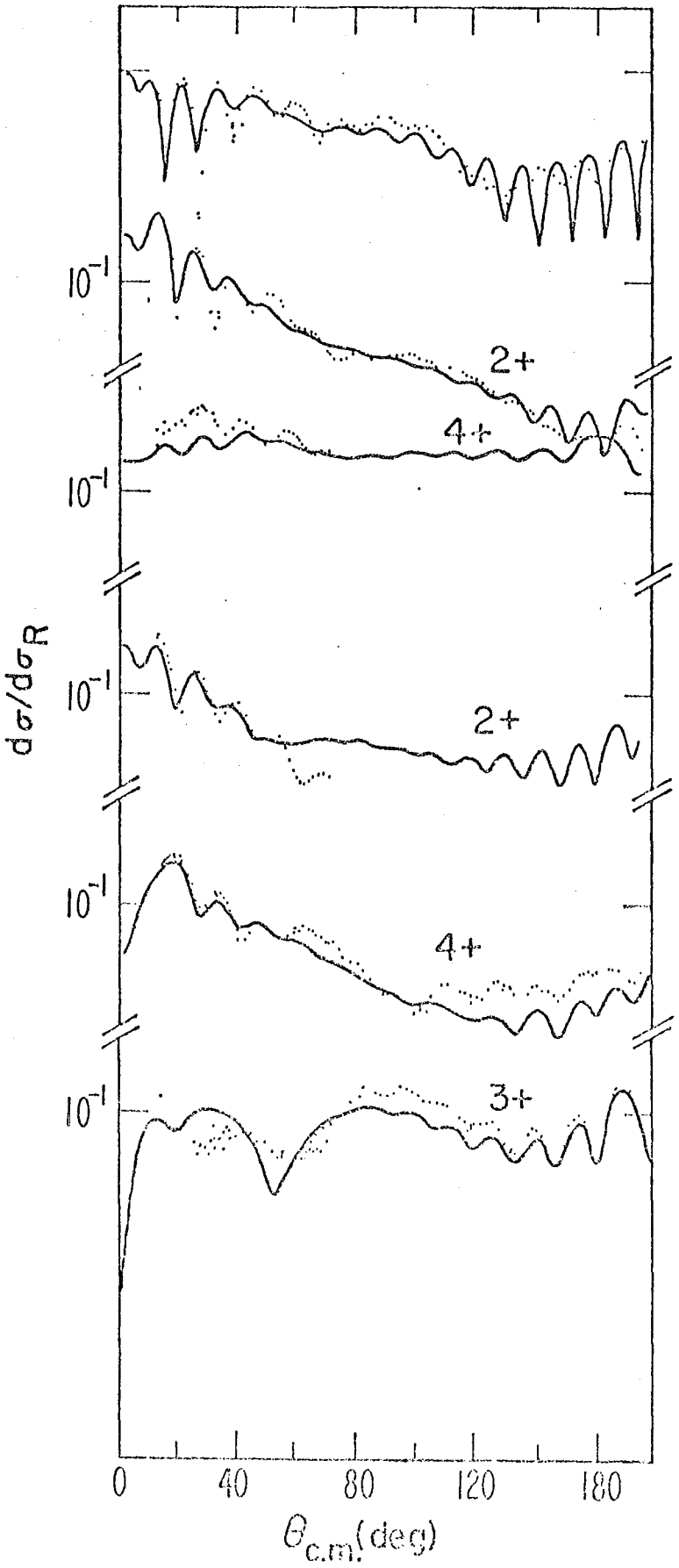

Fig. 16.

XBL 783-2452

where ReU_ℓ is the real part of the complex term U_ℓ. The quantities $|1 - U_\ell|^2$, $1 - |U_\ell|^2$, and $1 - ReU_\ell$ are of interest in analyzing the scattering process. Also of interest is $1 - ImU_\ell$. In Figs. 17 through 26, we plot various forms of the real and complex part of the scattering matrix vs. the laboratory energy and angular momentum. We plot $1 - ReU_\ell$ and $1 - ImU_\ell$ in Figs. 18 and 20 to 24, noting the main peak and "echo" peaks in Figs. 20, 21, 22. In Fig. 19b we plot $1 - |U_\ell|^2$ which gives a measure of the absorption into other channels. And in Fig. 19a we plot $|1 - U_\ell|^2$ which is the measure of the elastic scattering process. We plot $1 - |ReU_\ell|^2$ and $|1 - ReU_\ell|^2$ for simplicity in these two cases. We plot representative cases for W = 1 MeV and W = 0 as well as various values of ℓ and laboratory energy.

J. Structure of the S-Matrix and Resonance Decay Theory

1. Resonance Loops in the Complex S-Matrix Elements

We examine some of the qualitative properties of resonance alpha particle scattering. The structure of the complex S-matrix elements are examined for the dependence on energy and momentum. The resonance loops give information about the resonance capture and elastic and a few inelastic decay channels as well as compound nuclear formation. The reason we chose to apply this formalism to the ^{24}Mg case, rather than heavier targets such as ^{208}Pb, considered in Section II, is because we can achieve convergence rapidly in the coupled channel multipartial wave analysis.

We plot "Argand" diagrams for the real and imaginary matrix elements of the scattering matrix. We plot the dependence in the complex plane on both the laboratory energy and angular momentum.

The parameters used in our calculation using the SCATER2 code are

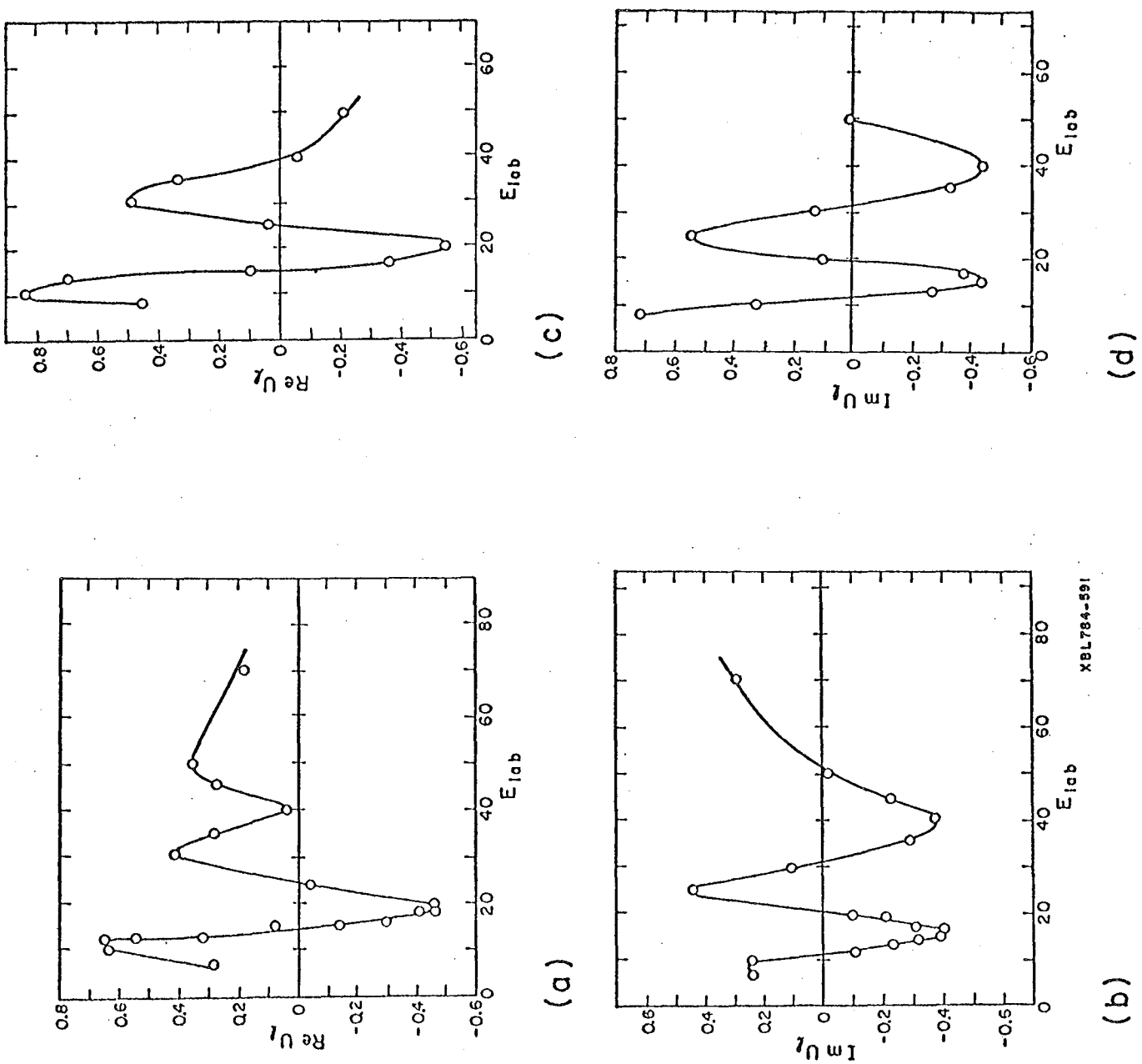

Fig. 17. (a) The real part of the scattering matrix elements are plotted vs. the laboratory energy, E_{lab}; (b) Comparison is made to the imaginary part of the matrix elements vs. E_{lab}. In both (a) and (b) W = -1.0 MeV. We can compare the plots in (a) and (b) to similar plots in (c) and (d) where W = 0 is chosen. All plots in Fig. 17 have $\ell = 0$.

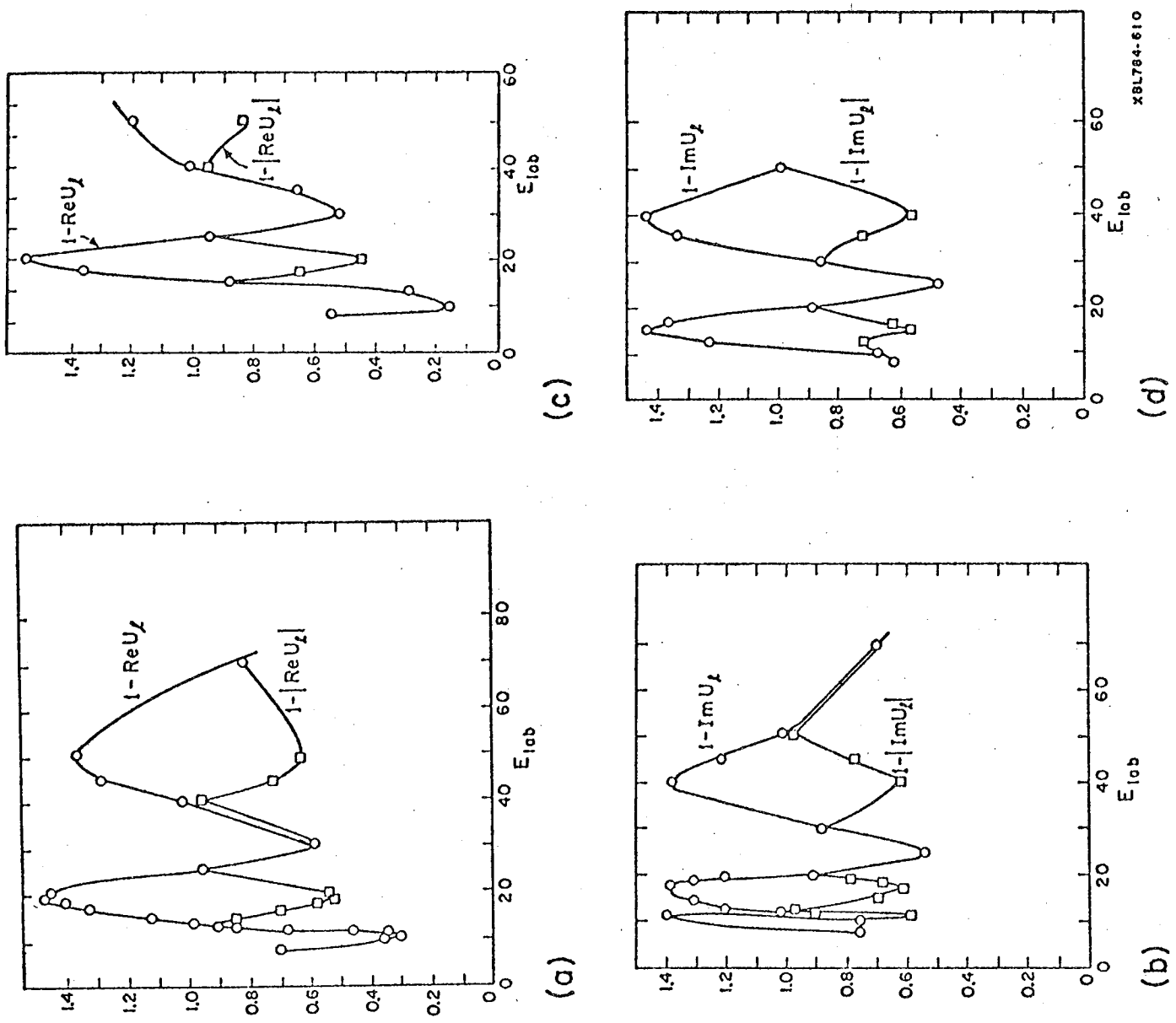

Fig. 18. (a) The quantities $1 - \mathrm{ReU}_\ell$ and $1 - |\mathrm{ReU}_\ell|$ are plotted vs. E_{lab}. (b) The quantities $1 - \mathrm{ImU}_\ell$ and $1 - |\mathrm{ImU}_\ell|$ are plotted vs. E_{lab}. In both (a) and (b), W = -1.0 MeV. Comparison of real and imaginary matrix elements vs. laboratory energy can be made. The quantity $(1 - \mathrm{ReU}_\ell)$ is proportional to the total cross section (see Eq. (161)). In (c) and (d) similar plots to (a) and (b) are made for W = 0. All plots in Fig. 18 have $\ell = 0$.

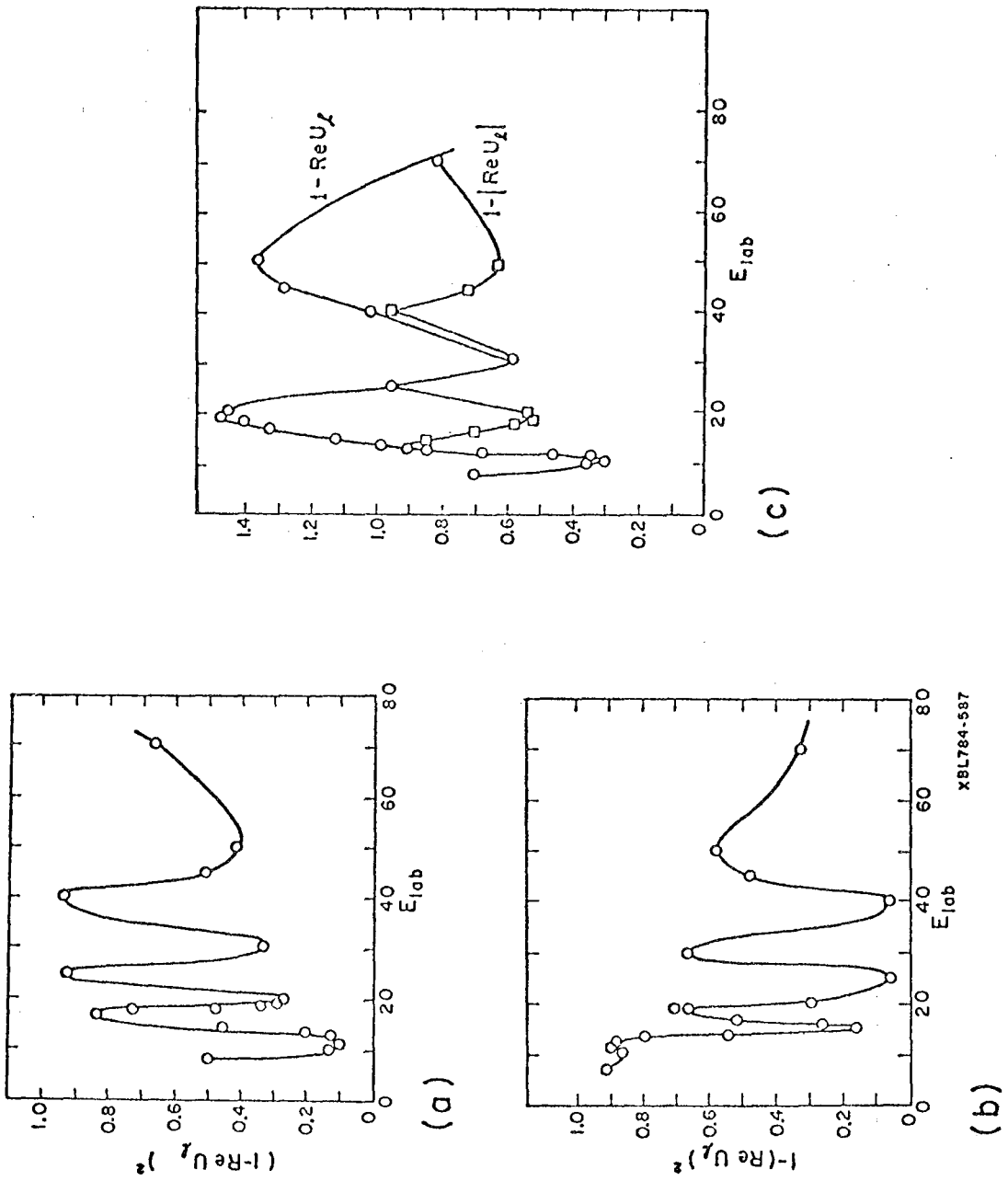

Fig. 19. (a) The quantity $(1 - \mathrm{ReU}_\ell)^2$ vs. E_{lab} is plotted. (b) The quantity $1 - (\mathrm{ReU}_\ell)^2$ vs. E_{lab} is plotted. The quantity $|1 - U_\ell|^2$ is the transmission coefficient which is proportional to the elastic cross section (see Eq. (159)). The quantity $(1 - |U_\ell|^2)$ is proportional to the reaction cross section (see Eq. (160)). We compare (a) and (b) to (c) where $1 - \mathrm{ReU}_\ell$ and $1 - |\mathrm{ReU}_\ell|$ are plotted vs. E_{lab}. (Note that Fig. 19c is the same as Fig. 18a.)

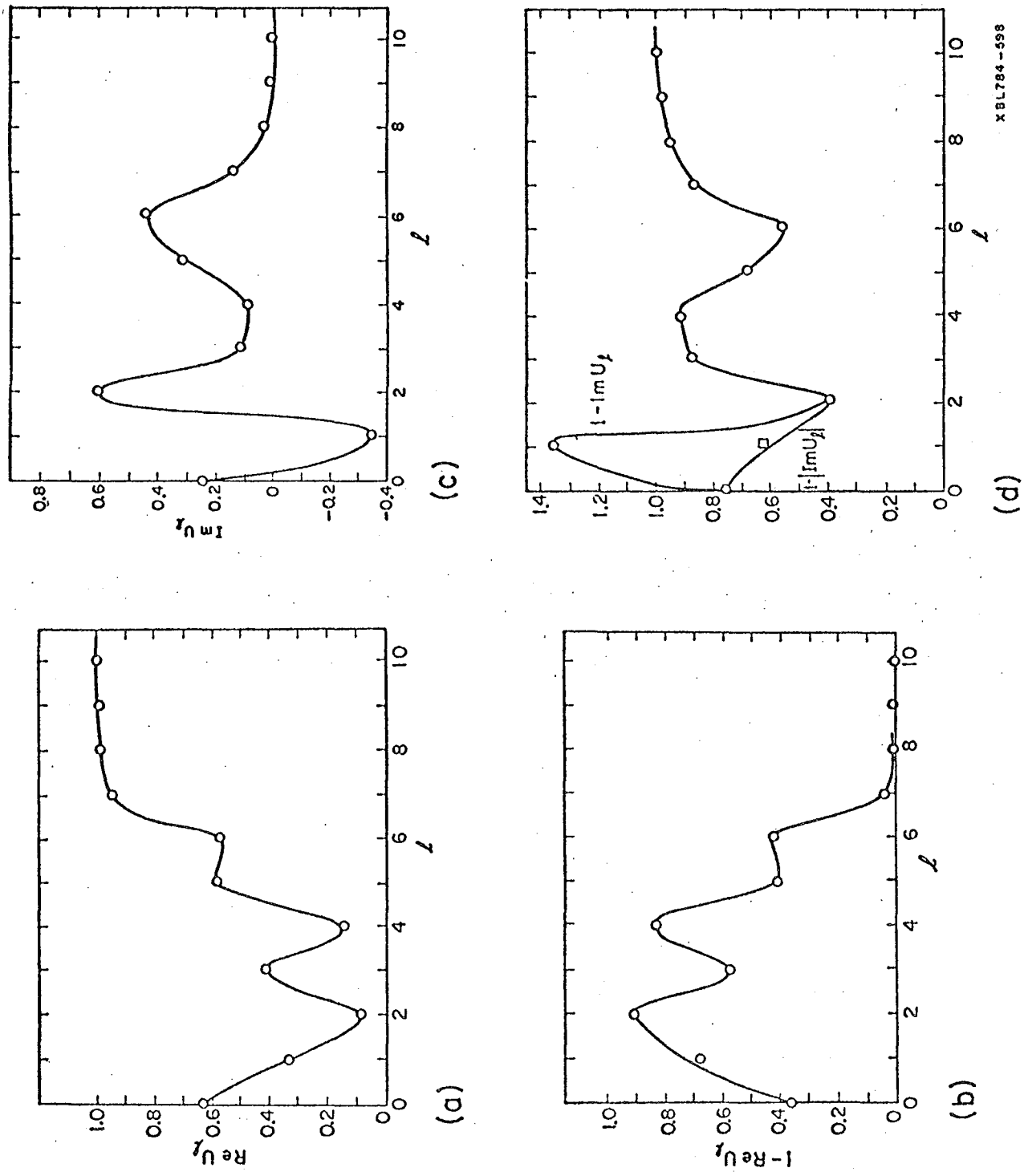

Fig. 20. Plots of forms of the real and imaginary parts of the scattering matrix are plotted vs. ℓ and compared. Both forms of ReU_ℓ or ImU_ℓ and $1 - ReU_\ell$ and $1 - ImU_\ell$ are examined. All plots are at laboratory energy E_{lab} = 10 MeV and W = -1.0 MeV.

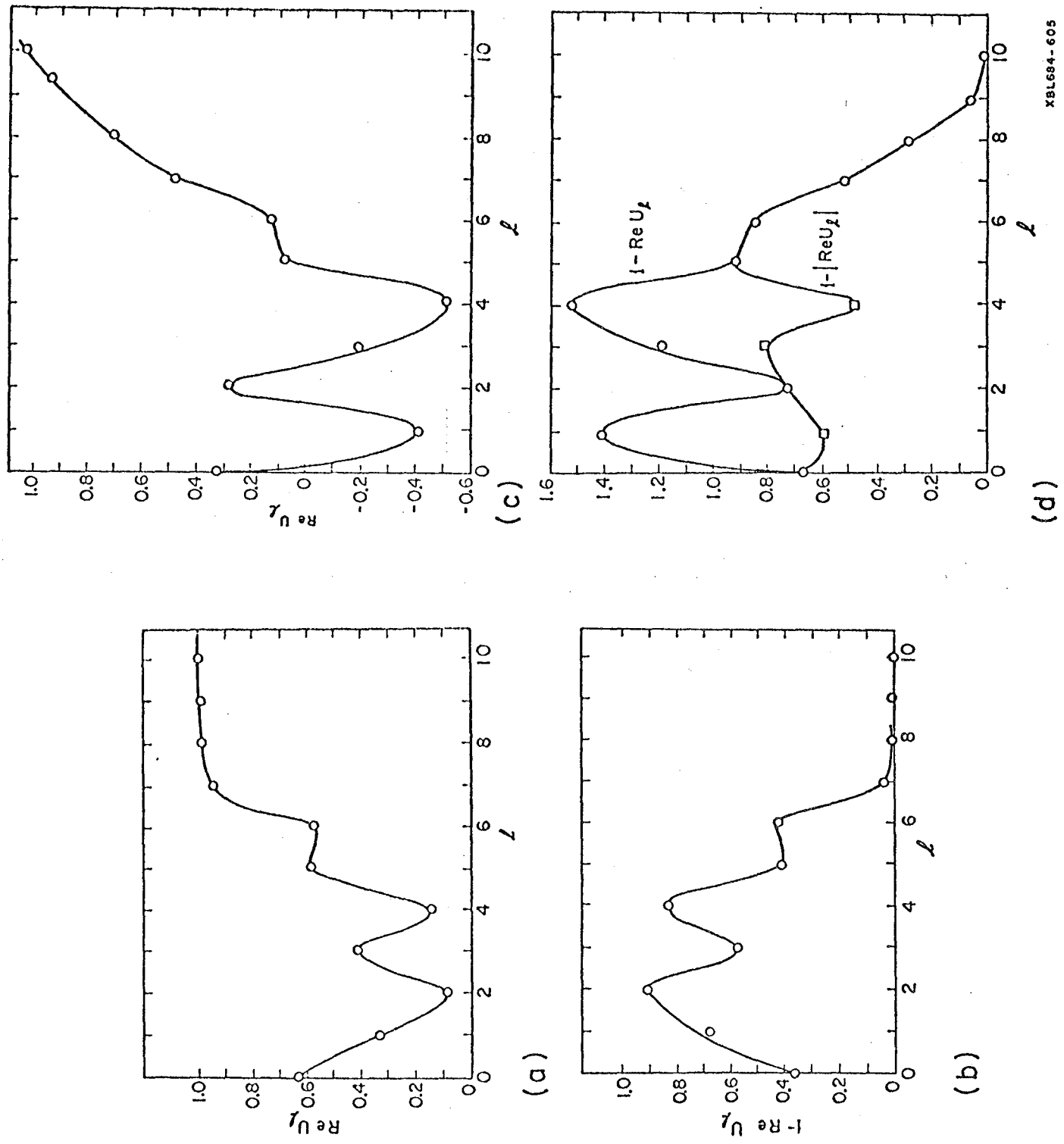

Fig. 21. Forms of the real part of the scattering matrix elements are plotted vs. ℓ. (a) and (b) have E_{lab} = 10 MeV and (c) and (d) have E_{lab} = 14 MeV, so that the effect of different energies can be seen. All have W = -1.0 MeV.

Fig. 22. (a) The real and (b) the imaginary part of the scattering matrix elements are plotted vs. the angular momentum, ℓ, at E_{lab} = 30 MeV and W = -1.0 MeV. These plots can be compared to Fig. 20(a) and (c), respectively, at E_{lab} = 10 MeV and W = -1.0 MeV to see the effect of energy. Comparison can also be made to Fig. 23(a) and (c) at E_{lab} = 70 MeV and W = -1.0 MeV. Fewer oscillations for the matrix elements vs. ℓ occur for larger E_{lab}.

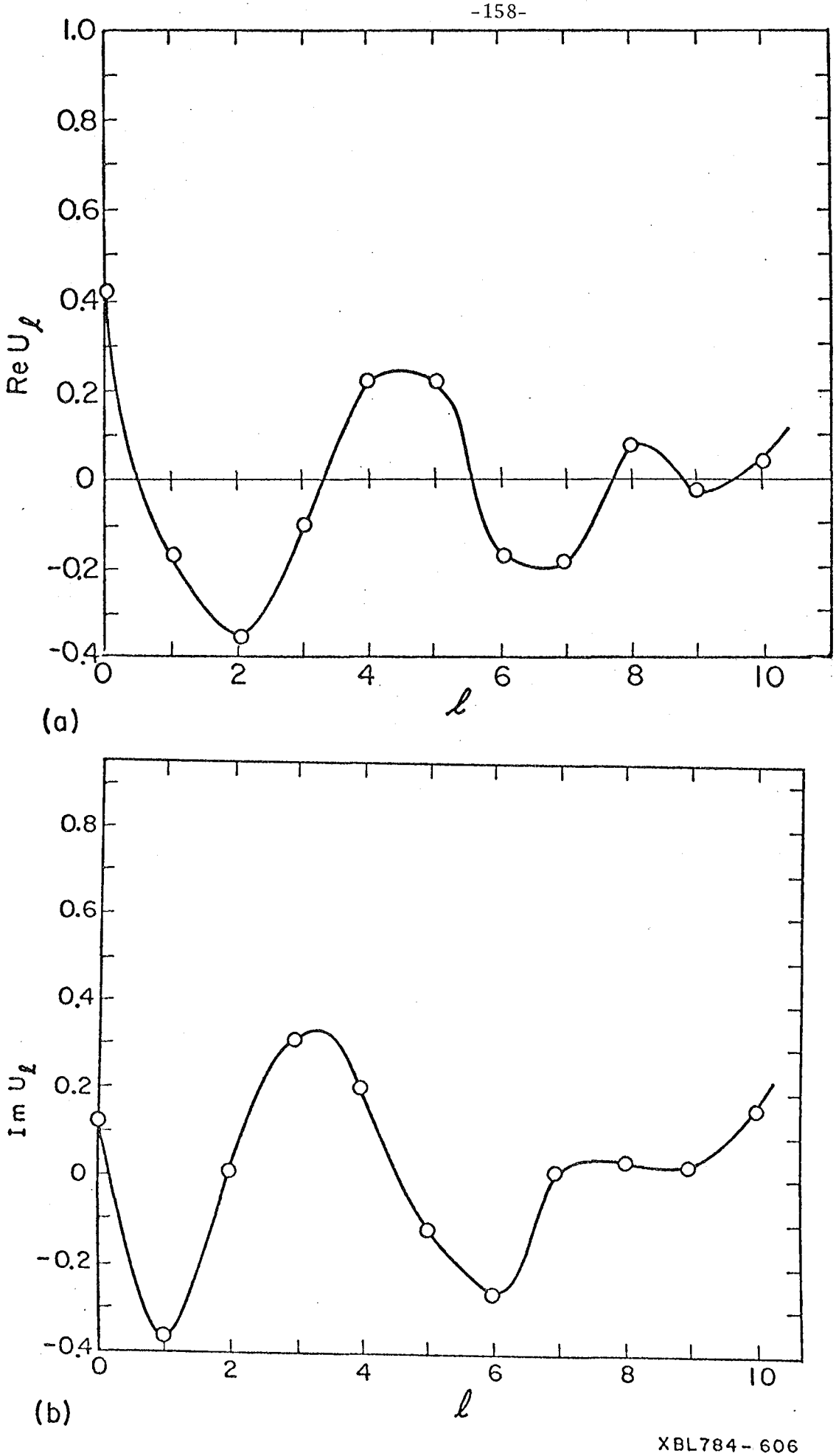
1.0
0.8
0.6
0.4
0.2
0
-0.2
-0.4
Re U_ℓ
0
2
4
6
8
10
ℓ
(a)
0.8
0.6
0.4
0.2
0
-0.2
-0.4
Im U_ℓ
0
2
4
6
8
10
ℓ
(b)
XBL784-606

Figure 22

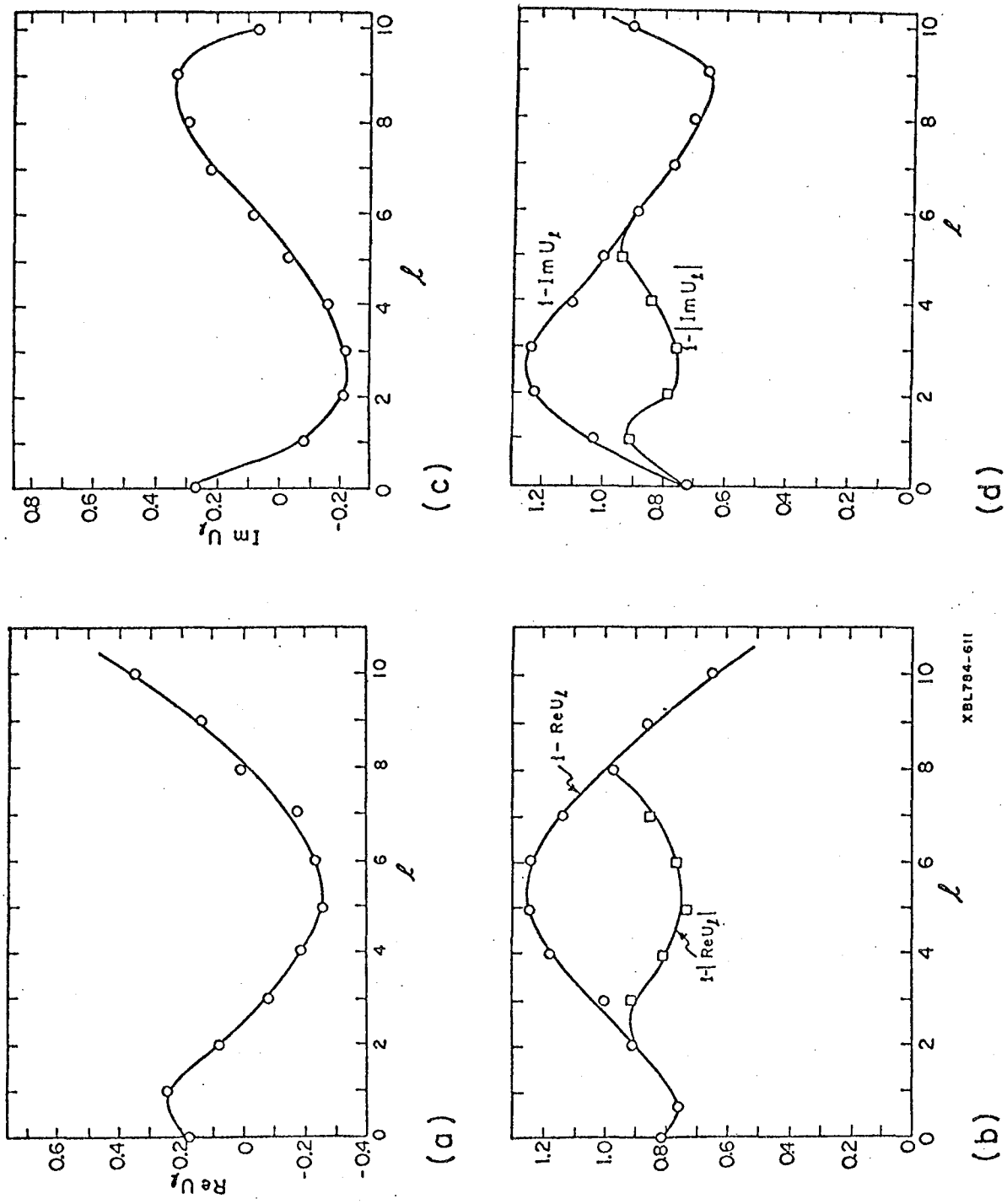

Fig. 23. We compare forms of the real matrix elements of the scattering matrix, (a) and (b), with the imaginary part (c) and (d), plotted vs. ℓ for large laboratory energy, E_{lab} = 70 MeV. Comparison of Fig. 23 with Fig. 20 (for E_{lab} = 10 MeV). In all cases W = -1.0 MeV.

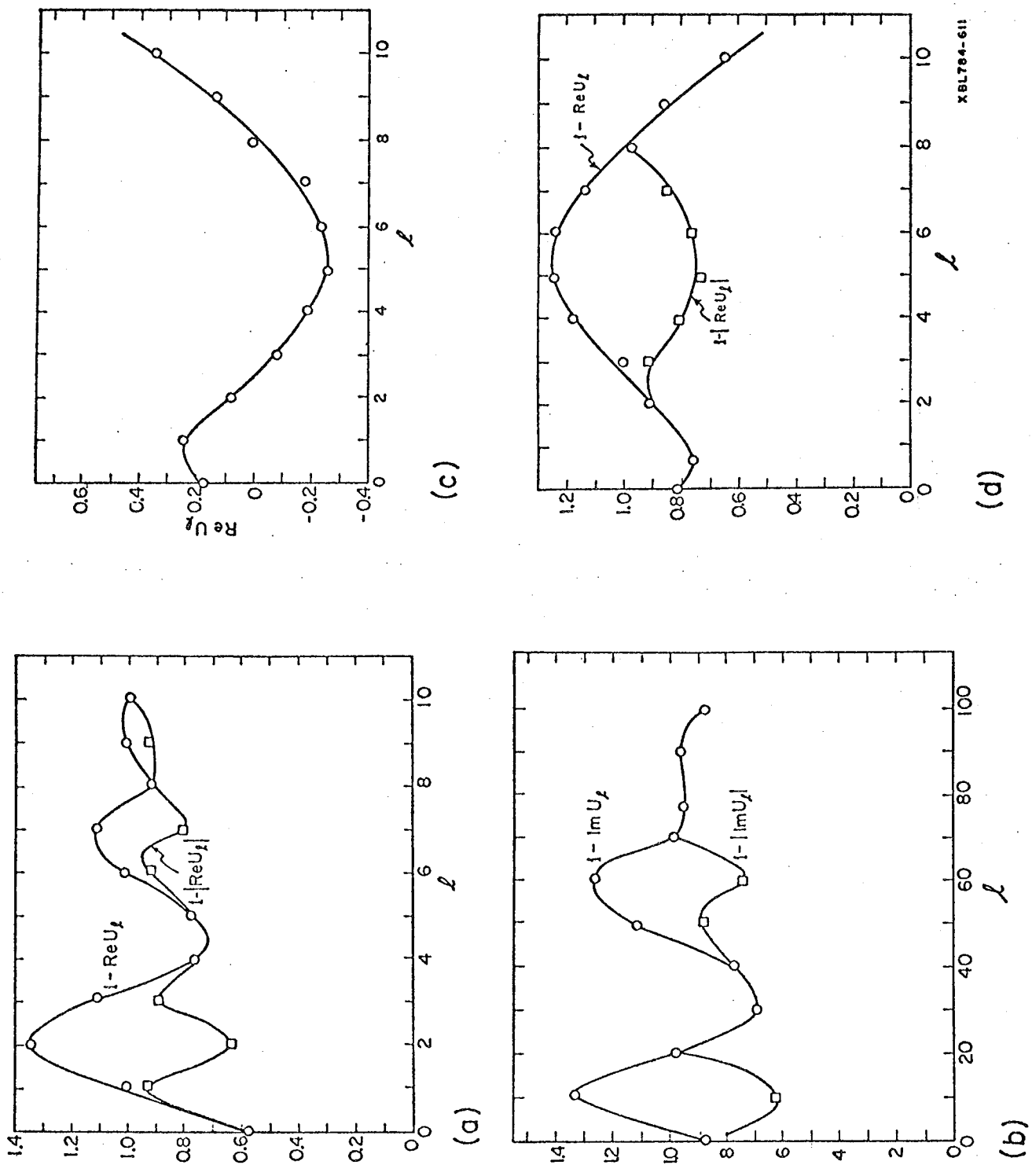

Fig. 24. In (a) plots of $1 - \mathrm{ReU}_\ell$ and $1 - |\mathrm{ReU}_\ell|$ vs. ℓ are compared to (b) plots of $1 - \mathrm{ImU}_\ell$ and $1 - |\mathrm{ImU}_\ell|$ vs. ℓ at E_{lab} = 30 MeV. One can compare the energy effect on (a) to (d), $1 - \mathrm{ReU}_\ell$ and $1 - |\mathrm{ReU}_\ell|$ vs. ℓ for E_{lab} = 70 MeV. (c) ReU_ℓ vs. ℓ is plotted at 70 MeV. In all cases W = -1.0 MeV.

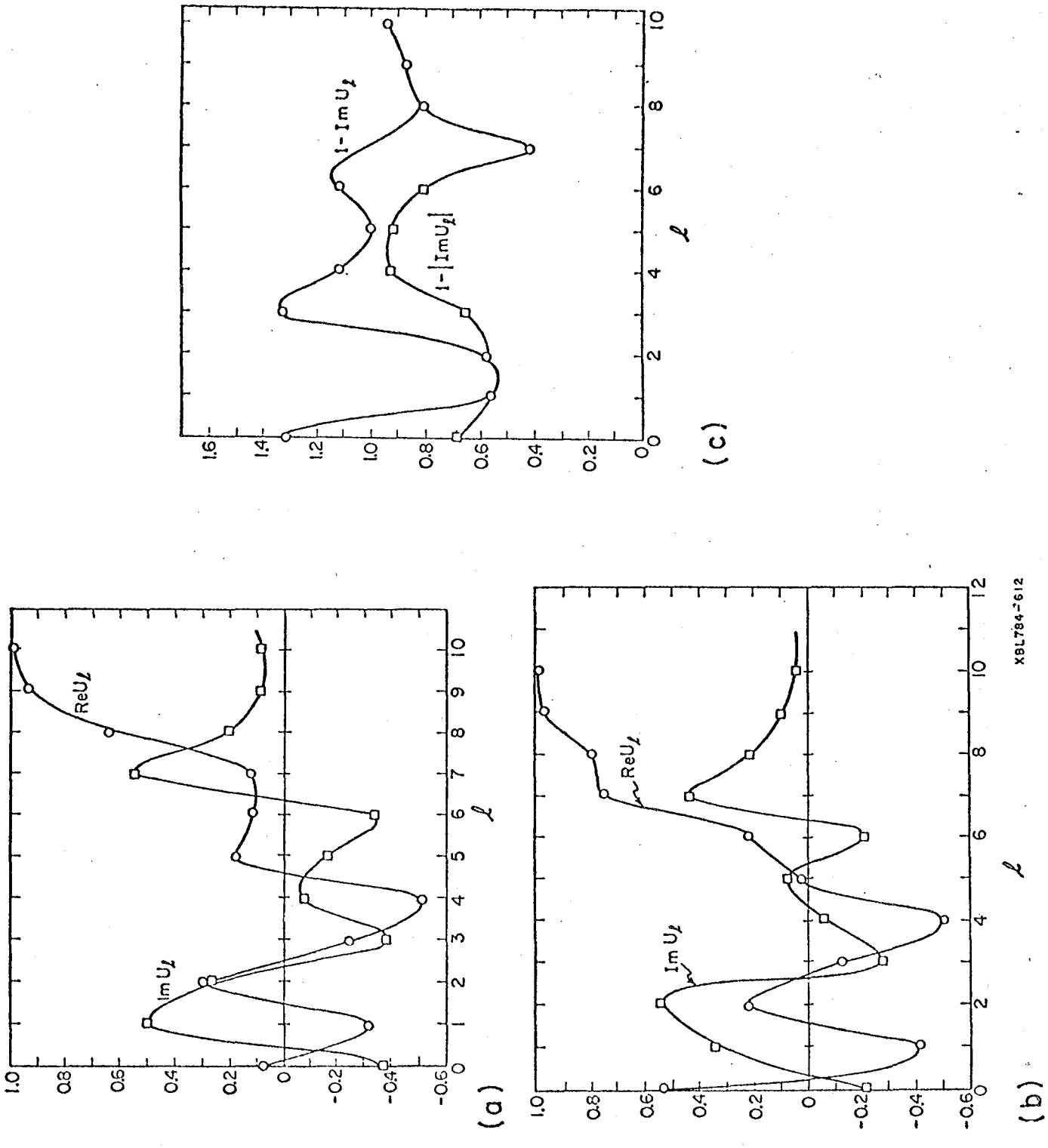

Fig. 25. Plots of ReU_ℓ and ImU_ℓ vs. ℓ are compared for (a) E_{lab} = 15 MeV and (b) E_{lab} = 14 MeV. The 14 MeV case can be compared to $1 - ImU_\ell$ and $1 - |ImU_\ell|$ vs. ℓ in (c). All plots are at W = -1.0 MeV.

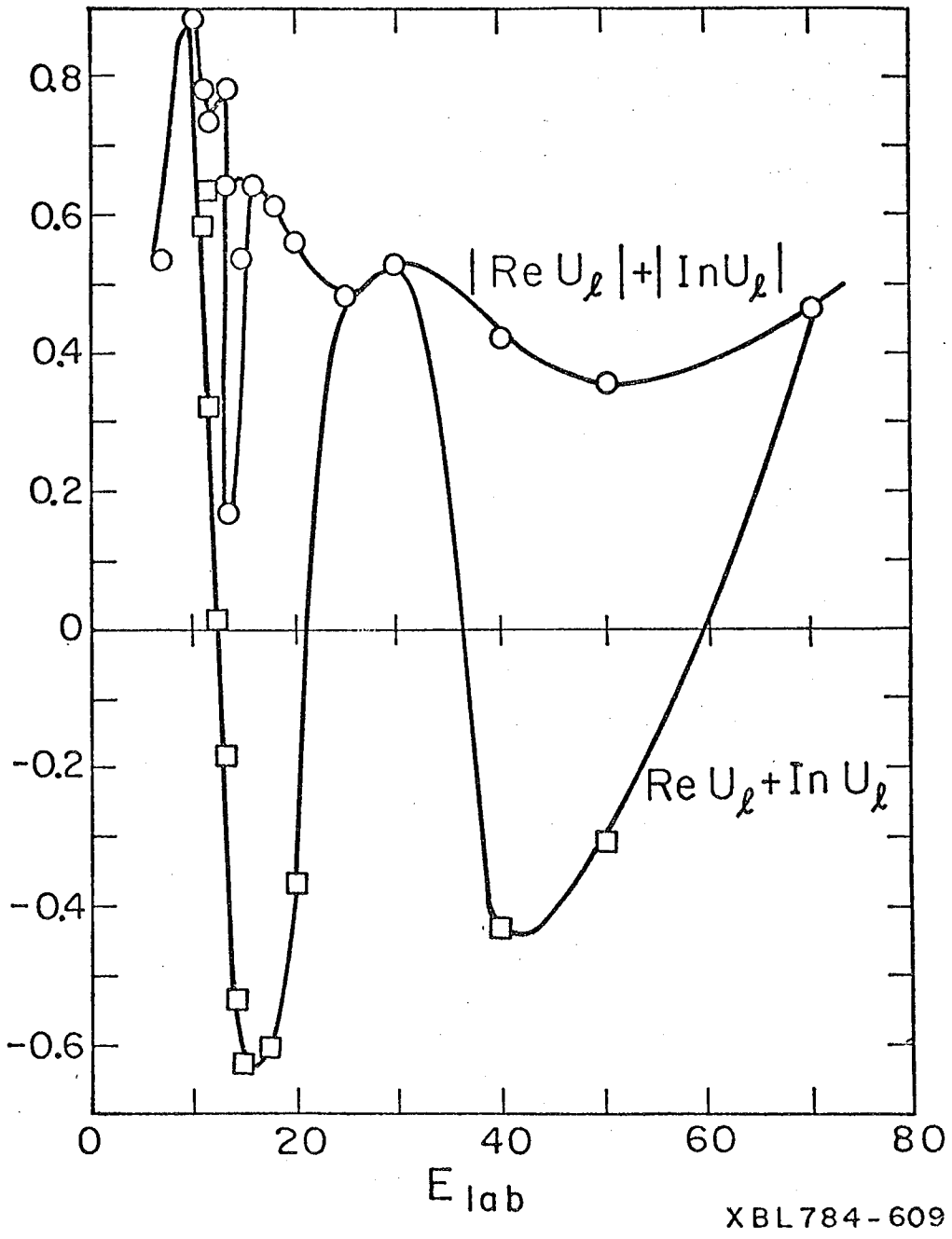

Fig. 26. The sum of the real and imaginary parts of the scattering matrix are plotted vs. E_{lab}. Also the sum of the absolute values of the real and imaginary parts of the scattering matrix are plotted vs. E_{lab} and compared to the direct sum. Both curves are for W = -1.0 MeV and $\ell = 0$.

given in Table 28. The target and projectile properties are listed as well as the deformation parameters and the ^{24}Mg energy levels. See also Tables 24, 25, 26 and 27 (pages 142, 144 twice, and 148, respectively).

In our first analysis we plot ImU_ℓ vs. ReU_ℓ for various E_{lab} values for 7.5 MeV $\leq E_{lab} \leq$ 70 MeV in the energy plane for each ℓ value. The first set of plots (Figs. 27a to 27k) are made for the imaginary part of the Woods-Saxon potential, W = -1.0 MeV and the second set (Figs. 28a to 28i) for W = 0. The third set of figures (Figs. 29a to 29e) are for ImU_ℓ vs. ReU_ℓ for various ℓ values from $0 \leq \ell \leq 10$ in the ℓ plane, for one for each energy in the range for E_{lab} from 8 MeV to 50 MeV. From the plots of ImU_ℓ vs. ReU_ℓ in the energy plane for various energies in MeV, and for the W = -1.0 MeV imaginary part of the potential, and various ℓ values from small to larger E_{lab} (but, in general, for smaller E_{lab}) the direction is predominantly clockwise in the "Argand" diagram, which is the hard sphere background which is shrunk from the unit circle due to channel coupling. Let us now examine Figs. 27a to 27k.

A resonance is present for counterclockwise rotation of the Argand plot for pole in the lower half energy plane. For $\ell = 0$ (Fig. 27a) between E_{lab} of 7.5 MeV and 70 MeV, the complex elements of U_ℓ loop twice around the origin in a clockwise direction for the hard sphere background. For $\ell = 1$ (Fig. 27b), the initial lower values of E_{lab} from 7.5 MeV to 12.5 MeV start in a counterclockwise direction, indicative of a resonance state, but for 12.5 MeV to 70 MeV, the complex elements U_ℓ loop in the clockwise direction again, once around from the background. For $\ell = 2$, from 7.5 to 70 MeV, it loops clockwise, indicating no predominate resonance is present, and for $\ell = 3$, for 7.5 to 17 MeV, the loop is in the counterclockwise direction, again indicating the presence of a resonance, and 17 to 70 MeV,

TABLE 28. The parameters used in the coupled channel calculation for the scattering of alpha particles off of the target, ^{24}Mg.

Elements	Radius and values	Deformation parameter	States	^{24}Mg energy levels	Eta	J	KS	K
M_T = 23.985 target mass	R_{min} = 0.05 f	$\beta(1) = 0.290$	1	0	2.229	0	0	0.271
		$\beta(2) = 0.350$	2	1.368	2.402	2	0	1.180
Z_T = 12 target atomic number	R_{max} = 15 f	$\beta(3) = 1.571$	3	4.120	2.922	4	0	0.970
	H = 0.1 step size	$\beta(4) = 0.120$	4	4.230	2.951	2	2	0.961
M_p = 4.0026 projectile mass		$\beta(5) = 0$	5	6.000	3.251	3	2	0.872
	$\ell_{1(min)} = 0$	$\beta(6) = 0$	6	5.220	3.564	4	2	0.795
Z_p = 2 projectile atomic number	$\ell_{2(max)} = 10$							

Fig. 27. The real and imaginary parts of the scattering matrix elements are plotted as ImU_ℓ vs. ReU_ℓ in the energy plane. Each labeled point denotes a laboratory energy in MeV from 7.5 MeV to 70 MeV. Consecutive values of angular momentum ℓ are represented.

(a) $\ell = 0$
(b) $\ell = 1$
(c) $\ell = 2$
(d) $\ell = 3$
(e) $\ell = 4$
(f) $\ell = 5$
(g) $\ell = 6$
(h) $\ell = 7$
(i) $\ell = 8$
(j) $\ell = 9$
(k) $\ell = 10$

All cases have the imaginary parts of the Woods-Saxon potential, W = -1.0 MeV. The predominant "motion" from small to larger energy for small ℓ is in the clockwise direction. Counterclockwise motion becomes more predominant for larger ℓ values.

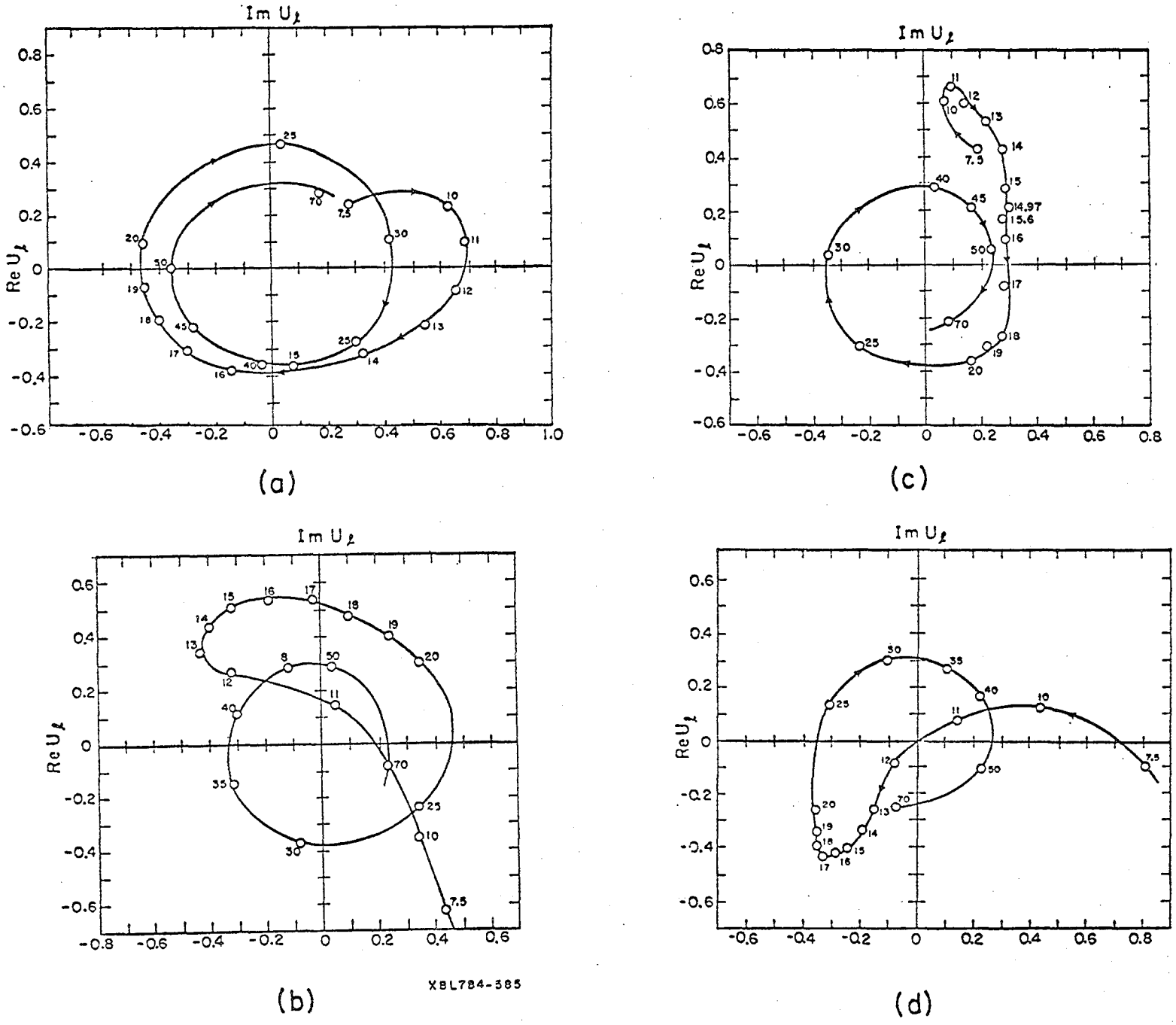

Figure 27 (a - d)

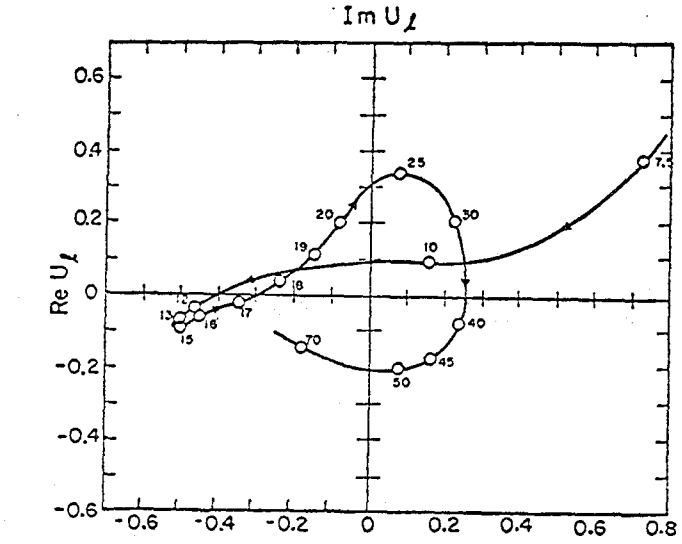
Im U_ℓ
Re U_ℓ
(e)

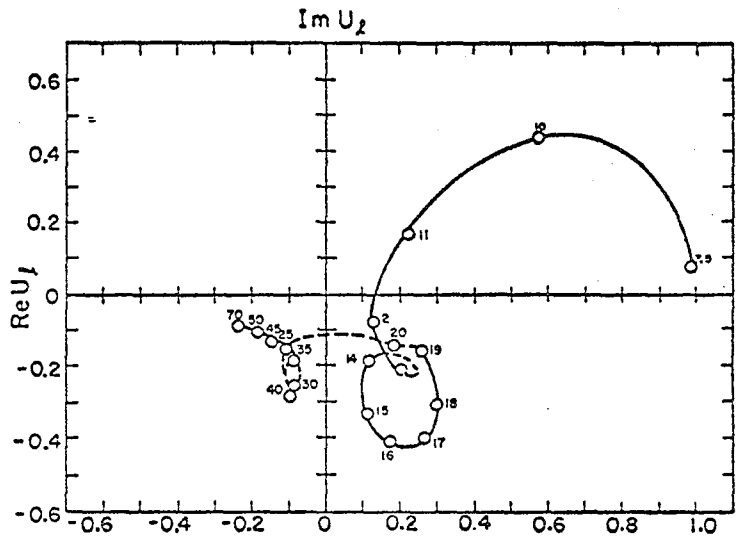
Im U_ℓ
Re U_ℓ
(g)

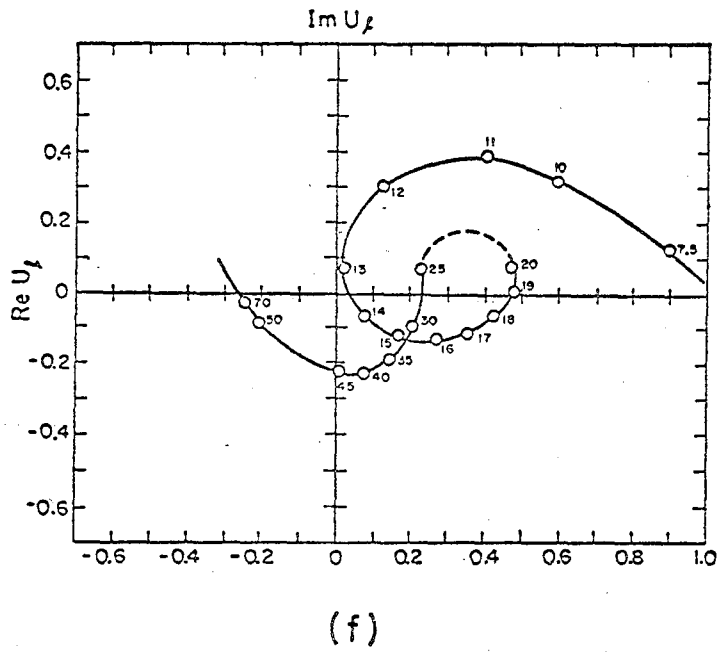
Im U_ℓ
Re U_ℓ
(f)

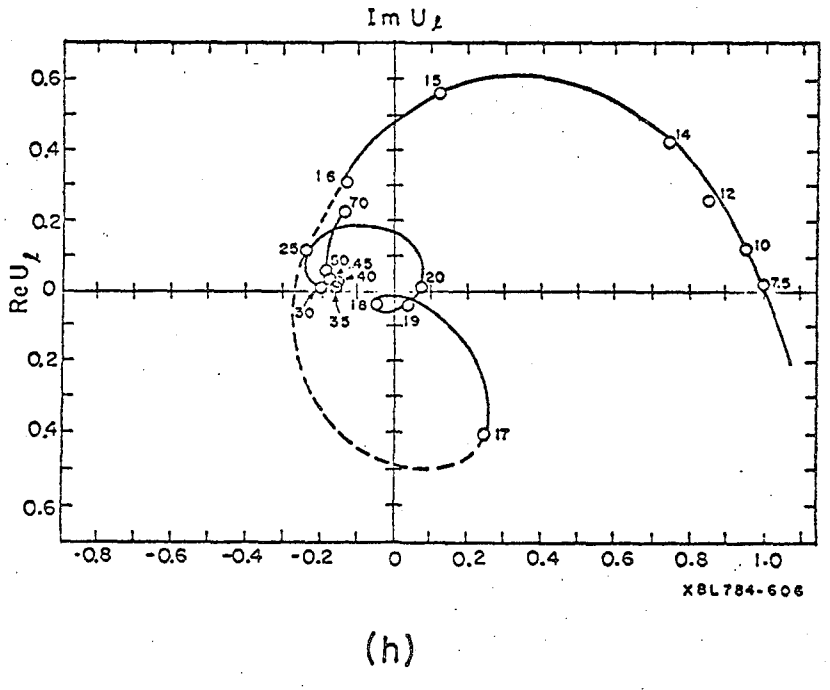
Im U_ℓ
Re U_ℓ
XBL784-606
(h)

Figure 27 (e - h)

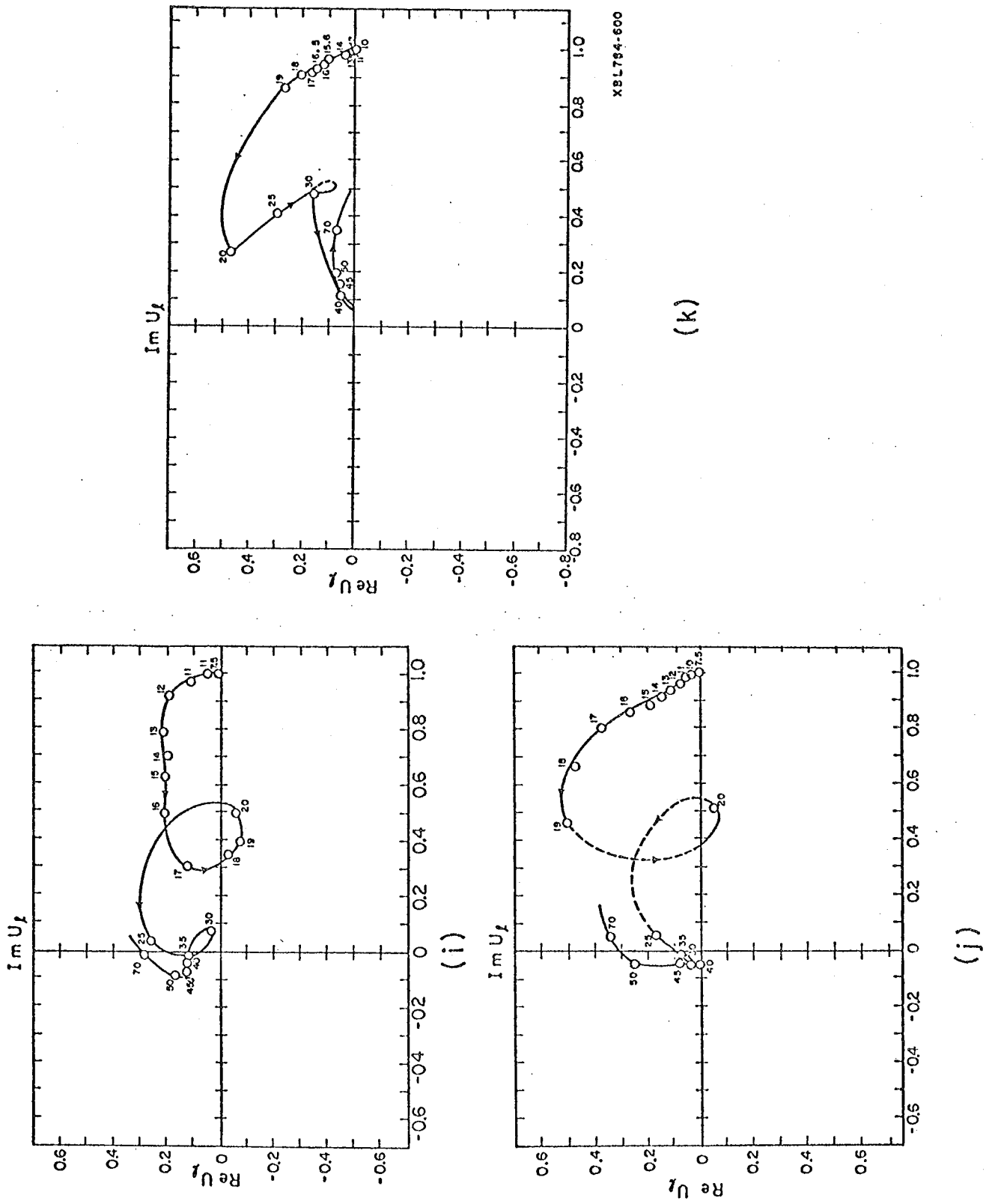

Figure 27 (i - k)

Fig. 28. The real and imaginary parts of the scattering matrix elements are plotted in the energy plane from 8 MeV to 50 MeV laboratory energy. Consecutive values of angular momentum ℓ are represented.

(a) $\ell = 0$
(b) $\ell = 1$
(c) $\ell = 2$
(d) $\ell = 3$
(e) $\ell = 4$
(f) $\ell = 5$
(g) $\ell = 6$
(h) $\ell = 9$
(i) $\ell = 10$

All cases have $W = 0$. Comparison between the same ℓ values of Fig. 27 and 28 can be made and give the effect of the inclusion of the imaginary part of the complex potential, W. Resonance loops are tighter as W gets larger but the trends are similar. (Because of this similarity $\ell = 7$ and $\ell = 8$ plots are omitted for $W = 0$.)

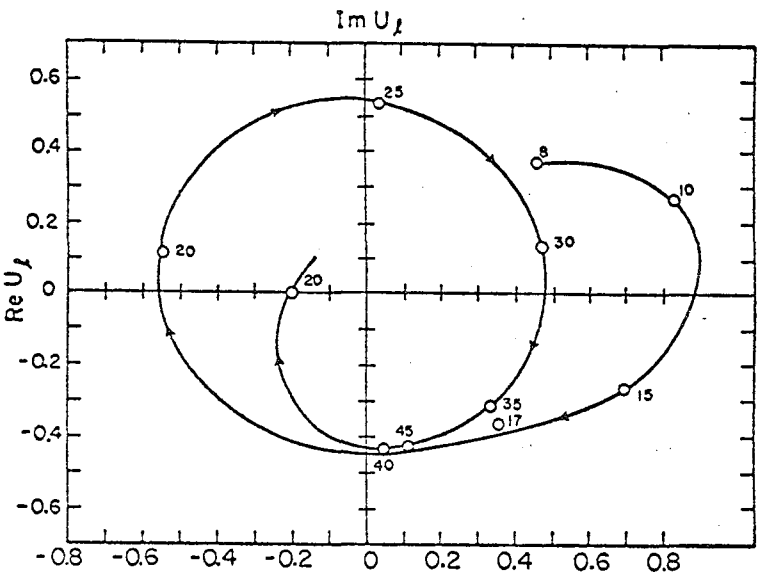
Im U_ℓ
Re U_ℓ
(a)

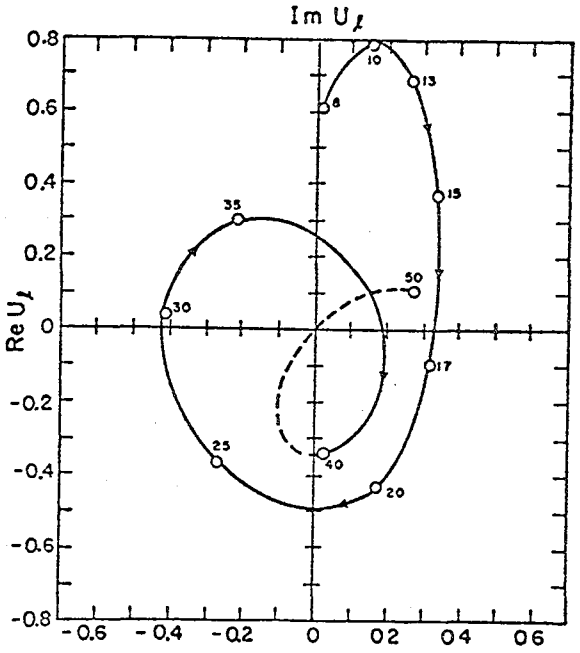
Im U_ℓ
Re U_ℓ
(c)

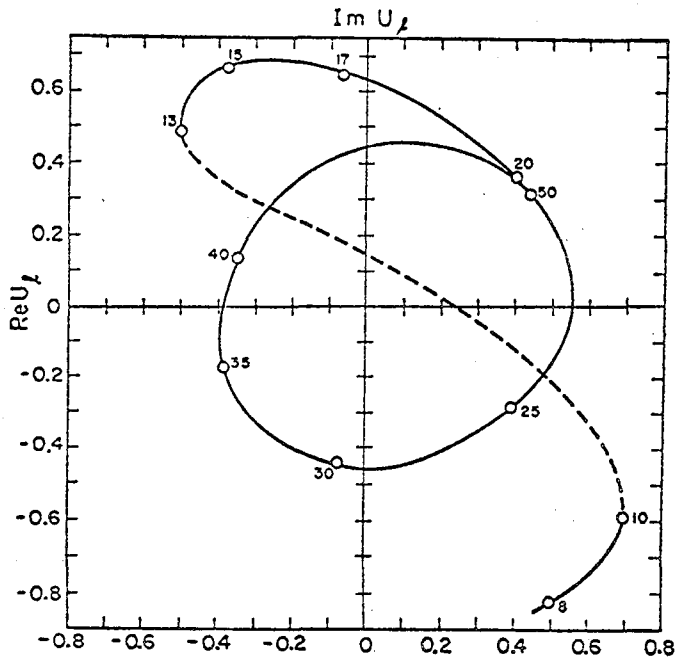
Im U_ℓ
Re U_ℓ
(b)

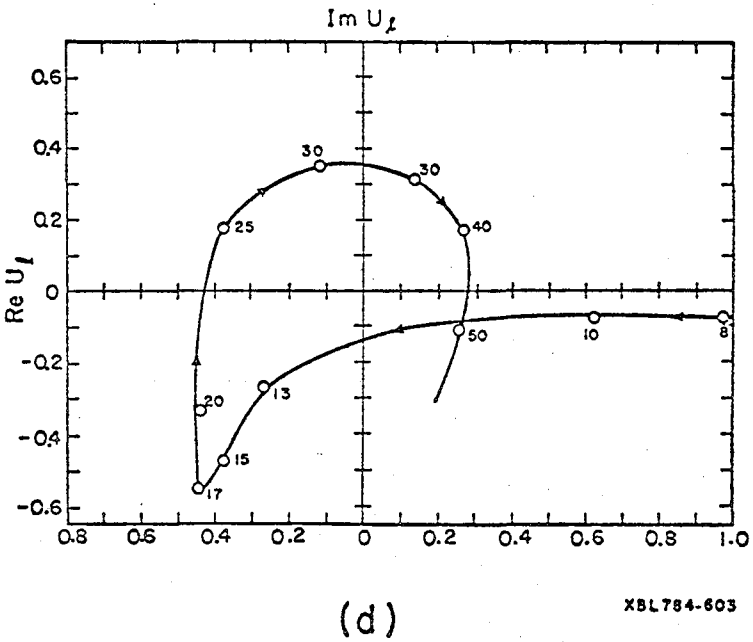
Im U_ℓ
Re U_ℓ
(d)
XBL784-603

Figure 28 (a - d)

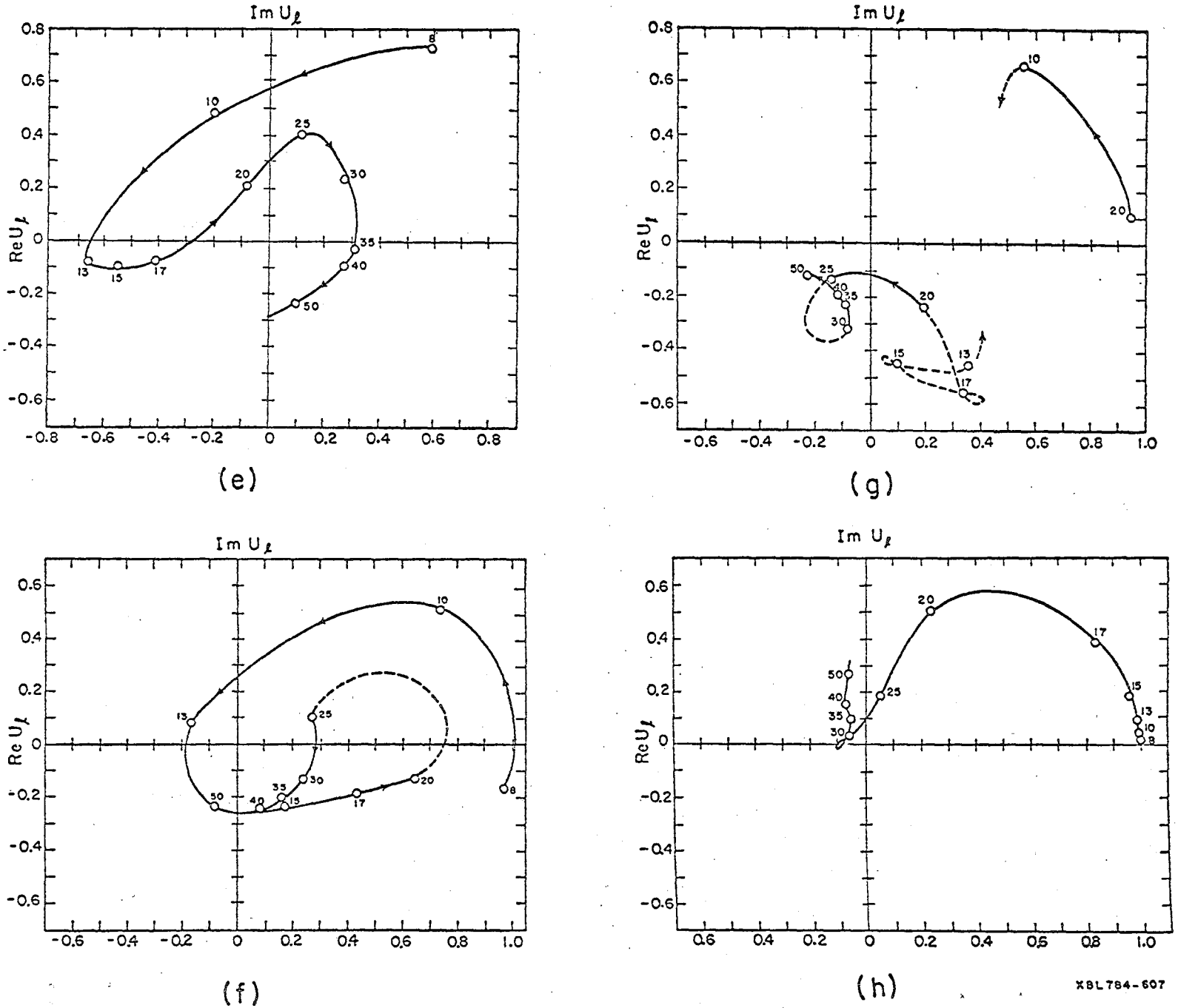

Figure 28 (e - h)

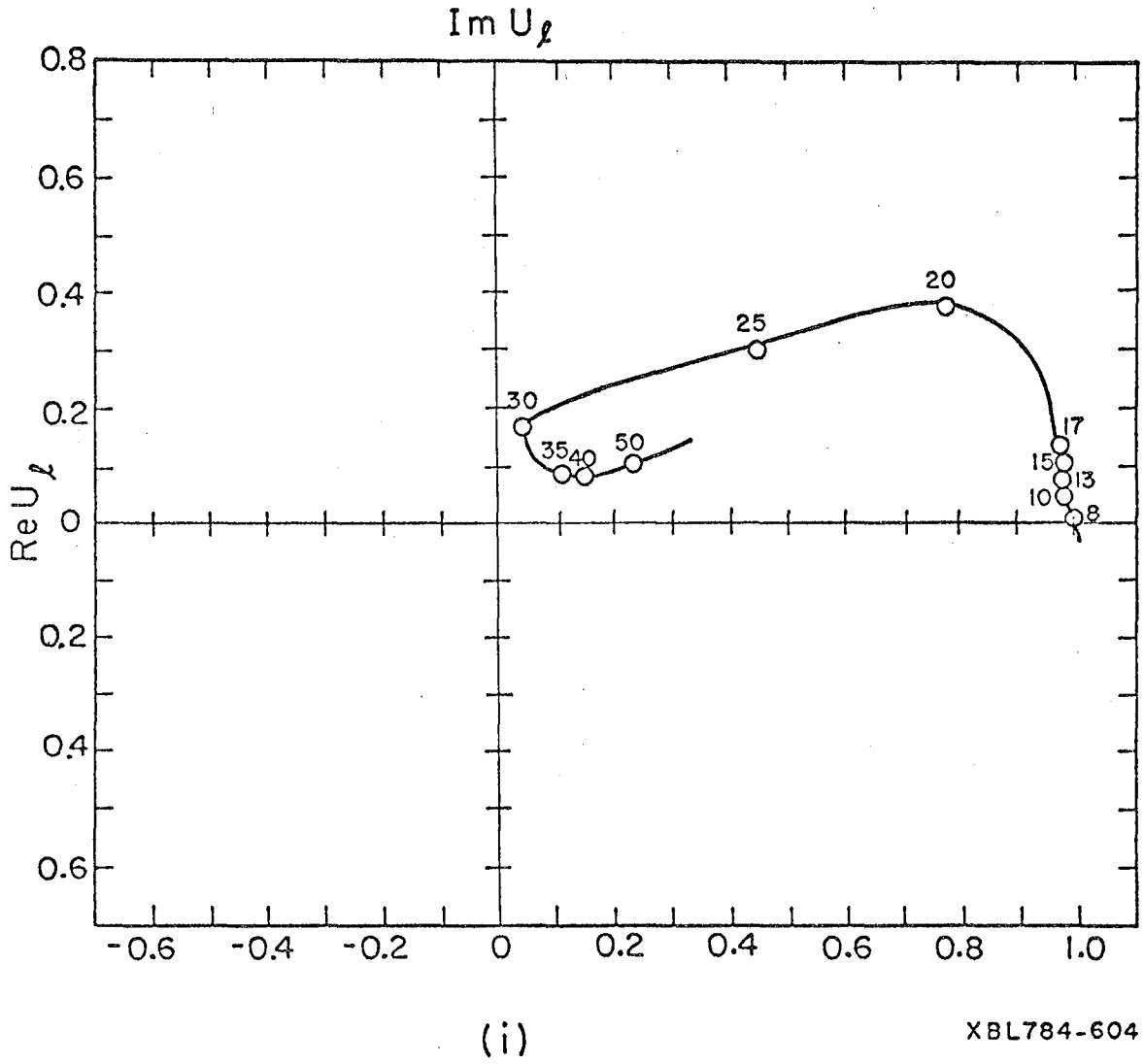
Im U_ℓ
Re U_ℓ
0.8
0.6
0.4
0.2
0
0.2
0.4
0.6
-0.6
-0.4
-0.2
0
0.2
0.4
0.6
0.8
1.0
30
25
20
17
15
13
10
8
35
40
50
(i)
XBL784-604

Figure 28 (i)

Fig. 29. The real and imaginary parts of the scattering matrix elements are plotted in the angular momentum plane. Each labeled point denotes a value of ℓ. Increasing values of the laboratory energy are given.

(a) E_{lab} = 7.5 MeV
(b) E_{lab} = 10 MeV
(c) E_{lab} = 14 MeV
(d) E_{lab} = 30 MeV
(e) E_{lab} = 70 MeV

For larger laboratory energy the "motion" from small to large ℓ values is clockwise. Resonance loops appear; for example, a resonance loop appears at $\ell = 8$ for E_{lab} = 70 MeV.

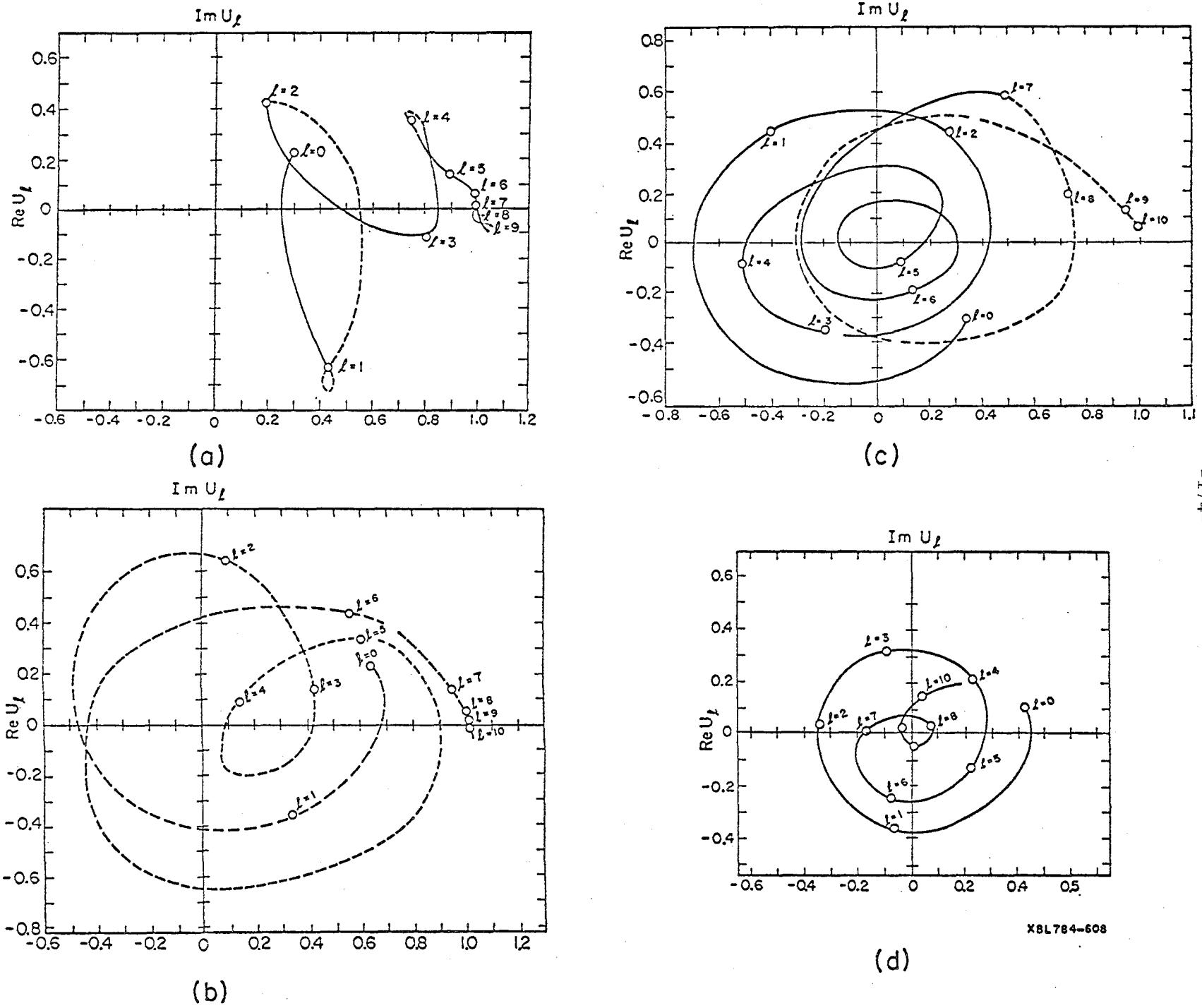
Im U_ℓ
Re U_ℓ
ℓ=0
ℓ=1
ℓ=2
ℓ=3
ℓ=4
ℓ=5
ℓ=6
ℓ=7
ℓ=8
ℓ=9
ℓ=10
(a)
(b)
(c)
(d)
XBL784-608

Figure 29 (a - d)

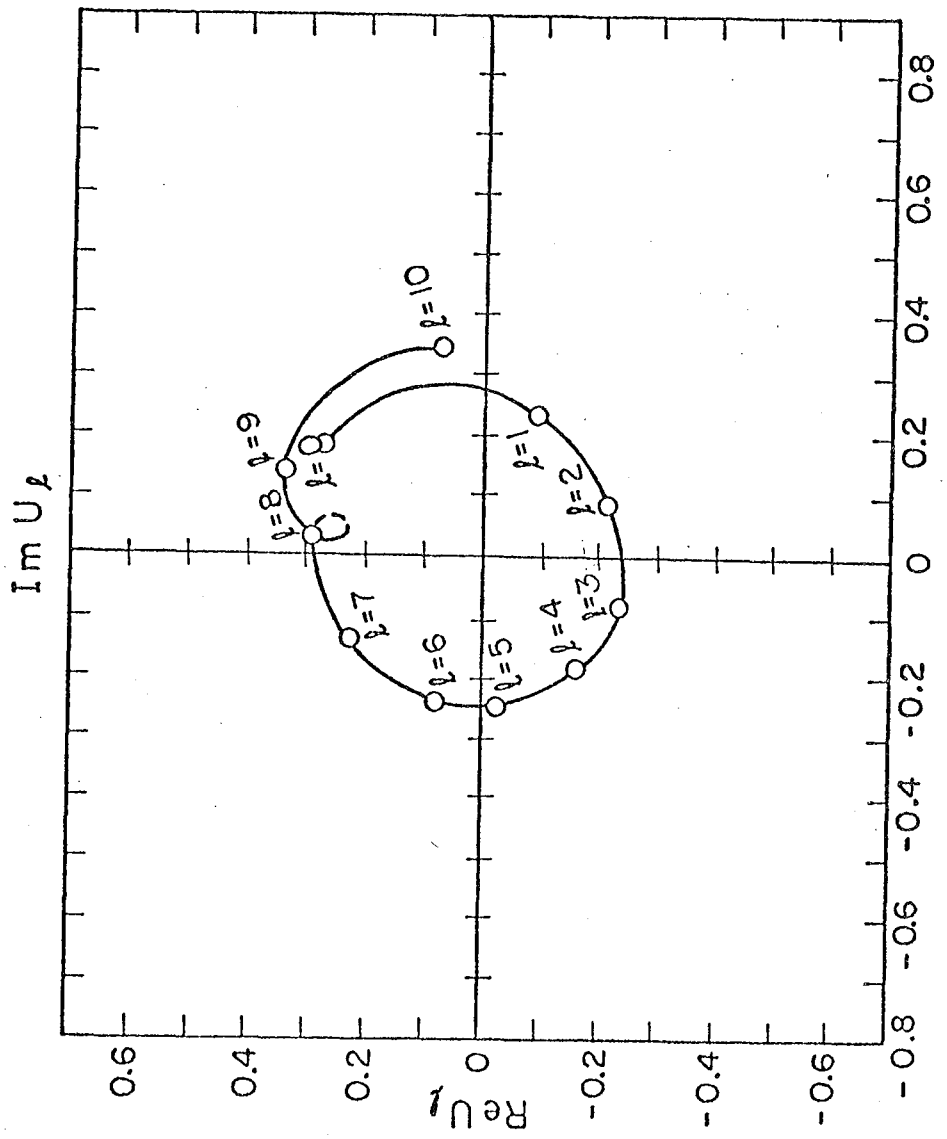
Im U_ℓ
Re U_ℓ
0.8
0.6
0.4
0.2
0
-0.2
-0.4
-0.6
-0.8
ℓ=0
ℓ=1
ℓ=2
ℓ=3
ℓ=4
ℓ=5
ℓ=6
ℓ=7
ℓ=8
ℓ=9
ℓ=10
XBL784-568
(e)

Figure 29 (e)

it loops once around the origin in clockwise direction. For $\ell = 4$, from 7.5 to 14 MeV, the Argand diagram moves counterclockwise, indicating a resonance; from 14 to 70 MeV it is clockwise around the origin almost once. For $\ell = 5$ (Fig. 27f) from 7.5 to about 22.5 MeV, the resonance plot proceeds counterclockwise but not encircling the origin, again indicating a resonance state, and at 25 MeV to 70 MeV, it loops one-half circle around origin in clockwise direction. In Fig. 27f we have a very clear-cut example of a resonance where there is no interference from higher energy resonance states. For this case, one-half the full energy width interval for full width at half maximum is given for about $\Gamma = 12.5$ MeV, giving a time delay of $\tau = 2.66 \times 10^{-24}$ sec. In Fig. 27i, for $\ell = 8$, we have a number of resonances (at least three); the first occurs from approximately 7.5 MeV to 14 MeV, a second occurs around 16 to 30 MeV, and a third from 30 to 45 MeV. For $\ell = 10$, the Argand plot from 7.5 to 20 MeV, the curve proceeds counterclockwise for a first resonance, and from 20 to 30 MeV, clockwise; and 30 to 40 MeV, counterclockwise for a second resonance, and 40 to 70 MeV, clockwise. Singularities occur at 20, 30 and 40 MeV. For $W = 0$ (Fig. 28i), $\ell = 10$, there exists a major resonance and all matter is counterclockwise for 8 MeV $< E_{lab} <$ 50 MeV.

In the strong absorption optical model the nuclear surface acts as though it has a reflective index and by changing the amount of absorption, W, the complex part of the potential is like changing the index of refraction.

The reason we proceed from a smaller complex part of the Woods-Saxon potential is in order not to "wash out" the resonance loops for which we are searching.[90] Since alpha particles are strongly absorbed, complex

parts of the potential should be larger, perhaps of the order of magnitude of 10 to 20 MeV.

K.W.McVoy calculates the energy-dependent resonance loops for compound nuclear states of the complex S-matrix elements for scattering of neutrons or medium-mass targets.[91-93] The loops exhibit similar forms to ours, although no Coulomb part of the potential is included and nuclear projectile spin is included. The loops move further in from the unit circle as the absorptive part of the nucleon potential is increased (in the range $W = 0$ to $W = 7$ MeV). The resonance loops become tighter for smaller A targets.[91]

The poles in the energy dependence of the Breit-Wigner approximation for entrance-channel partial width Γ_ℓ for elastic scattering is given by

$$S(E) = e^{2i\phi(E)} \left[1 - \frac{i\Gamma_\ell}{E - E_o + i\Gamma/2} \right] \qquad (162)$$

where $\phi(E)$ is the "background phase" of distant poles.[94] If the resonances are narrow and isolated, $\phi(E)$ will be nearly constant across the energy region. This will be an approximation in the case of broad resonances.

If $\phi(E)$ is approximately constant over the energy range, the complex numbers S(E) travel counterclockwise around a closed "resonance circle" of radius $\rho = \Gamma_e/\Gamma$ where Γ is the total width. Since, in practice $\phi(E)$ is not entirely constant, it tends to move S(E) in a clockwise direction and the resonance circle usually never closes. These "background phases" show up in the S-trajectory provided $\rho = \Gamma_e/\Gamma$, which is the fractional coupling of the resonance to the entrance channel, is near unity. However, if W(r) is increased until $\rho << 1$, so that the resonance is decoupled from the entrance channel, its resonance circle will shrink into insignificance and the corresponding peak will vanish from the cross section. At the resonance energy, S is most sensitive to absorption by other channels, where the particle is trapped longest in the well.

For nearly elastic scattering, the S-trajectory is compared to a main resonance circle at low energy which is followed by "echo" circles due to $\phi(E)$ at higher energy because there are resonances plus bound states in the partial waves.

The off-resonance behavior of S will be effected less by a large W which absorbs the resonance away, and the "echo" maximum will remain as a distinctive feature even in the non-elastic case. The non-elastic part of the cross section obtains its maximum when $\rho = 0.5$.

In the plots of ImU_ℓ vs. ReU_ℓ in the energy plane, large values of the partial wave, $\ell \sim 9$ and $\ell \sim 10$, and in the limit of small $E_{lab} \sim 7.5$ MeV, then $ReU_\ell(E)$ is about unity and $ImU_\ell(E)$ approaches zero, for both W = -1 MeV and zero. In the plots of ImU_ℓ vs. ReU_ℓ in the energy plane, for $\ell = 0$ and W = -1.0 MeV, then ImU_ℓ and ReU_ℓ approach zero as the energy approaches

zero. For $\ell = 1$ and 3 and low energy, the plot begins in the fourth quadrant, and for $\ell = 2$, 4 and low energy, the plot begins in the first quadrant. For $\ell \geq 5$, ReU_ℓ approaches unity and ImU_ℓ approaches zero.

For the plot of ImU_ℓ vs. ReU_ℓ, in the ℓ plane for small laboratory energy, for $\ell = 10$, then $ReU_\ell(E)$ approaches one and $ImU_\ell(E)$ approaches zero, but above the resonance at about $E_{lab} = 15$ MeV, then $\ell = 10$ moves toward the center for $ImU_\ell(E) < 1$ and $ReU_\ell(E) < 1$. At $E_{lab} = 30$ MeV $\ell = 10$, $ImU_\ell \sim 1.5$ and $ReU_\ell \sim 0.2$ on the unit circle. For the resonance pole in the upper half ℓ plane, the presence of resonance is indicated by clockwise motion and background by counterclockwise motion. Many resonances are present as indicated by the predominately clockwise motion in Figs. 29a to 29e. In the momentum or ℓ plane for $W = 0$, the pole appears in the upper half plane and bound states occurs on the positive imaginary axis. We have S-waves only for $W = 0$.

The positions of the poles and zeros in the complex energy plane can give us information about the resonance process. We can define a phase shift in terms of a phase angle to a pole or zero in the E plane from a point on the real axis. The S-matrix is proportional to a ratio of the form $(\xi^* - E)/(\xi - E)$, which can be expressed as $e^{2i\delta}$ and ξ^* is the complex conjugate of E. Here we consider the case where $W = 0$ so that the zeros from the numerator in the upper energy plane are in the same relative position as the poles in the lower half energy plane. As we move along the real energy axis and approach a pole-zero pair for our resonance, the phase increases rapidly and then more slowly away from resonances.

For the Argand plots of the S-matrix elements for energy dependence, we can define a rate of movement along the curve or differential length

along the curve as a curve interval per energy interval or differential energy curve element. Near a resonance, the phase shift δ increases and the differential curve element will increase. This occurs as the energy approaches and makes a transition through each resonance. This can readily be observed in Fig. 27h, for example. The curve moves very rapidly from 7.5 MeV to 19 MeV, particularly around 16 to 19 MeV. Then from 19 to 20 MeV it moves more slowly; from 25 to 70 MeV, away from the major resonance, it moves much more slowly. There is a second resonance, 20 MeV to 30 MeV, and then from 50 to 70 MeV, the now clockwise resonance motion resumes. Further detailed determinations would have to be performed to obtain a more detailed look at the third resonance occurring in the energy interval from 30 to 50 MeV.

The delay time of the compound resonance state is associated with the rate of change of the phase per energy interval. The further from the real axis in the lower half energy plane the pole is, the broader the resonances. Alpha decay resonances are narrow and the poles are near the real axis. The phase increases more rapidly near these poles giving a longer decay time for the smaller widths of the narrow resonances.

If we increase the depth of the real part of the Woods-Saxon, the pole in complex energy plane as well as the depth is increased; then the pole moves in the E plane up along negative imaginary energy axis, for $W \neq 0$. States that were formerly unbound then become bound. If the pole occurs above threshold, it represents a resonance; if it occurs below threshold, it represents a bound state. The resonances associated with the compound nuclear state are narrow (see Fig. 30). If no other inelastic channels were open then the pole would be on the imaginary axis.

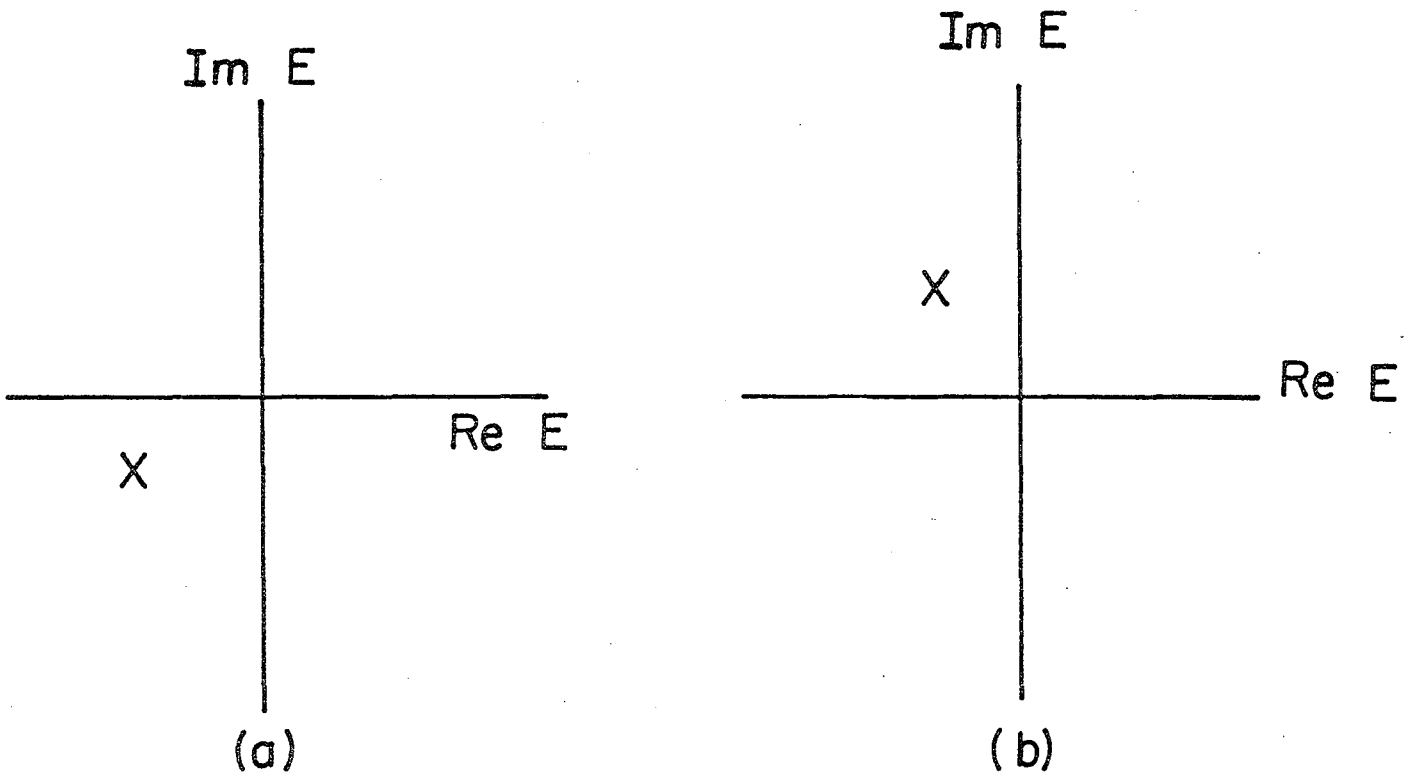

XBL 783-2448

Fig. 30. As the depth of the real part of the nuclear potential is increased, then the pole in the complex energy plane moves up the imaginary energy axis for (a), the unbound case, to (b) the bound case.

2. Critical partial wave conditions

A classical scattering quantity, the impact parameter for each partial wave is defined as $b_\ell = \ell/k$ for momentum $k = (\frac{1}{2} ME_\alpha)^{\frac{1}{2}}$ and the geometrical cross section is given by $\sigma_\ell = \pi b_\ell^2$. Projectile trajectories with $\ell > \ell_c$ remain "outside" the nucleus while those with $\ell < \ell_c$ are inside the nucleus. For smaller ℓ the trajectory enters the nucleus. We define ℓ_c as the critical angular momentum for a given center of mass energy, for which the effective potential is just surmounted.

For example, if we are examining the threshold for resonance capture of an alpha on the surface of ^{24}Mg, then for $E_{lab} = 15$ MeV, $E_{c.m.} \cong 13$ MeV, and referring to the potential plot in Fig. 2 we see that $\ell \sim 0$. The form of this plot for a medium-heavy nucleus ^{208}Pb would be similar for ^{24}Mg but the point of inflection would be effected or occur at a slightly different energy. The inflection point in the potential for the ^{24}Mg optical model parameters is at $\ell_c = 30$ and the critical angular momentum $E_{c.m.} = 45$ MeV, or $E_{lab} = 52.5$ MeV.

In the spherical approximation, we have the potential energy from the form given in the Fig. 2 caption. We can tailor-expand the nuclear part of the potential to eliminate the exponential and use the inflection point $\partial V/\partial r = 0$ condition and solve for ℓ_c, the critical momentum. In our calculation we set $\ell_{min} = 0$ and $\ell_{max} = 10$ in SCATER2 and we examine dependence of the complex S-matrix elements on different values of ℓ.

As in the N. Austern and J. S. Blair model,[81] in order to simplify the radial integrals which occur in the first-order processes, the angular momentum transfers are taken to be much smaller than the angular momentum that are important for the partial wave expansion, especially for other than tightly bound states.

For large real parts of the nuclear optical potential, for $\ell < \ell_c$, the projectile trajectory plunges deep into the nuclear interior.[81] Although effects of the inclusion of the imaginary part of the Woods-Saxon potential are evident, they are minimal when the long path length in the nuclear potential (due to the deep well) causes strong attenuation from the elastic flux. We use a well depth of -100 MeV (as indicated as realistic in arguments in Sections II and IV), which will mean that the dependence of the position and size of the S-matrix resonance loops will not be highly sensitive to W, the imaginary part of the potential.

Dependence on W is examined by K.W.McVoy[91] as well as in this section. We can see that there is an effect in going from W = 0 to W = -1.0 MeV, but the general form of the plots are similar for both plots of the complex S-matrix elements in the energy and angular momentum dependence.

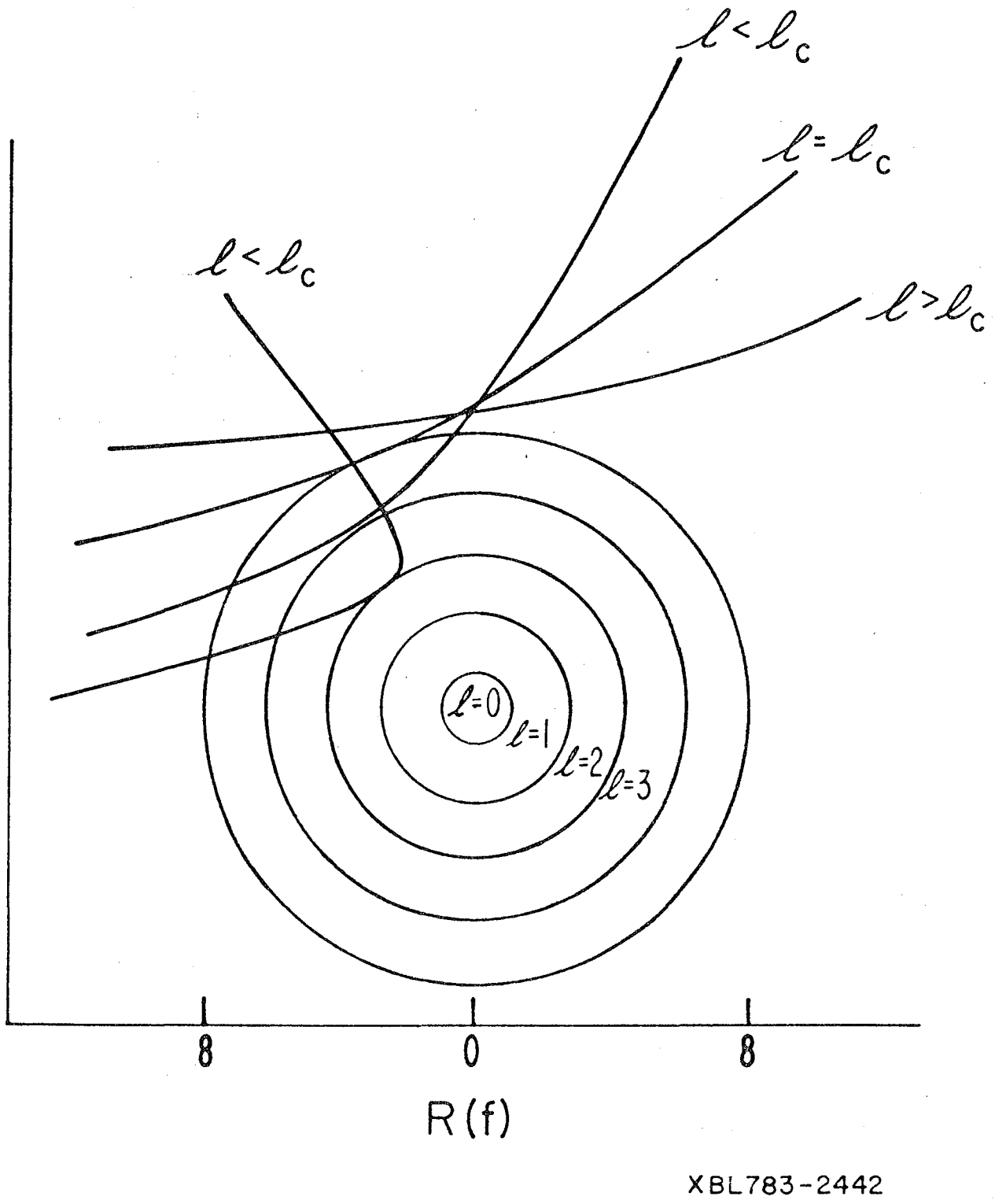

Fig. 31. The above shows a schematic of the ℓ value partial wave zones from which partial waves can be scattered. The outside circle marks the half-value of the nuclear parameters. Trajectories in the potential are also represented from various partial waves. The grazing trajectory is given by partial wave ℓ_c; the radius in Fermis, f.

3. Decay time and resonance loops in the S-matrix

We have been examining the structure of the S-matrix for the ^{24}Mg target, spin zero. We used the unified nuclear reaction theory to calculate the S-matrix pole in the vicinity of a sharp resonance. This resonance is identified with a metastable state of the compound nucleus. The decay time formalism can be used to calculate the lifetime and branching ratios to the ground state.[95,96]

In analogy to the work in high-energy physics for the scattering of nucleons off of nucleons, the residue of the pole gives the decay as reaction width. We can identify the partial decay width for alpha decay a resonance loop in the complex S-matrix for approximately elastic scattering. The S-matrix plots have a similar trend for both W = -1.0 MeV and W = 0, which may indicate that the resonance loops and curve shape in plot are due primarily to channel coupling or absorption into higher or other ℓ wave channels. Absorption represented by the complex part of the potential also effects the resonance. Further investigation would involve changing the value of W and also examining the S-matrix structure without coupling.

For the transition amplitude connecting the initial bound state and the final continuum state, F. T. Smith[97] has demonstrated that the lifetime of a metastable state is related to the scattering delay time which can be calculated from the scattering matrix. The widths of a metastable state are compared with the displacement of the pole of the scattering matrix from the real axis in the energy plane. This definition of the lifetime or resonance width depends on the use of the Breit-Wigner formula for the scattering matrix.

We examine the behavior of the complex matrix elements of the scattering matrix, calculated from the coupled channel resonant decay theory for small imaginary parts of the nuclear potential, because in the formation of the nuclear state, the alpha cluster is absorbed but is assumed to maintain its identity. If the imaginary term of the complex potential is large, the alpha particle may be rapidly absorbed at the nuclear surface and lose its four nucleon-cluster identity and these nucleons would "disperse" into the nuclear interior.

If the decay rate is very rapid, then the reaction is more likely to occur as a direct reaction and the compound nuclear state would not form. To best fit our model of compound nuclear state formation, the decay time should be for a medium or slow rate of decay.

In Section V.A.3, in Eq. (10), if the decay time Δt decreases, then the decay width $\Delta\Gamma$ becomes larger. If W, the complex part of the potential becomes larger, then the decay width reflects the increase in absorption and $\Delta\Gamma$ becomes smaller and the decay time longer. The existence of narrow resonances shows directly that long-lined compound systems, formed by the target nucleus and the incident nucleon, exists. We can estimate the decay width as

$$\lambda = \frac{1}{\hbar} P_\ell \gamma_\ell^2 \tag{163}$$

for nuclear penetrability,

$$P_\ell = e^{-\left[2\int_{R_i}^{R_f} \left(2\mu/\hbar^2 [E - V(r)]^{\frac{1}{2}} dr\right)\right]} \tag{164}$$

which gives us $P_\ell \sim 10^{-33}$. With the resonance occurring at $E_{1ab} \cong 15$ MeV, we estimate the residue of the pole to give $\gamma_\ell \sim 10^{28}$ so that $\lambda \sim 10^{23}$ 1/sec.

The decay half-life of the ground state is given by

$$t_{\frac{1}{2}} = \ell n\, 2/\lambda \tag{165}$$

(for $\hbar = 1$), then $t_{\frac{1}{2}} \sim 10^{-23}$ sec. We look at the manner in which this relates to compound nuclear formation.

4. A check on the compound nuclear model

Recall that the definition of the R-matrix function is given in terms of the radial wave functions

$$R = \frac{\hbar^2}{2m_\alpha r_c} \sum_\lambda \frac{u_\lambda^2(r_c)}{E_\lambda - E} = \sum_\lambda \frac{\gamma_\lambda^2}{E_\lambda - E} \tag{166}$$

where m_α is the mass of the projectile alpha, r_c is the channel radius, u_λ are the radial wave function, γ_λ are the reduced withds in a "single particle" potential, where

$$\gamma_\lambda = (\hbar^2/2mr_c)^{\frac{1}{2}}\, u_\lambda(r_c) \tag{167}$$

The energy E_λ is the strong resonance energy with a width Γ_λ. We can write the elastic cross section at a strong resonance,

$$\sigma_{e\ell} = \pi\lambda\!\!\!^{-2}(2\ell^2 + 1)\, \frac{\Gamma^2}{(E - E_\lambda') + \frac{1}{2}\Gamma^2} \tag{168}$$

for $\Gamma = 2\gamma_\lambda^2 P$ and $E_\lambda' = E_\lambda - \gamma_\lambda^2 S$, where the energy E_λ is shifted by a quantity which depends on the real part of the logarithmic derivatives of the outside wave functions and

$$\Gamma = 2\gamma_\lambda^2 P \tag{169}$$

where the quantity P is related to the imaginary part of the logarithmic

derivative. The real and imaginary parts of the logarithmic derivative can be written as

$$\mathcal{L}_\ell = S_\ell + iP_\ell \tag{170}$$

for

$$\mathcal{L}_\ell = (r\mathcal{O}'_\ell/\mathcal{O}_\ell)_{r=r_c} \tag{171}$$

and

$$\mathcal{L}^*_\ell = (r\mathcal{I}'_\ell/\mathcal{I}_\ell)_{r=r_c} \tag{172}$$

in terms of the outgoing $\mathcal{O}_\ell$ and incoming $\mathcal{I}_\ell$ waves. The quantity S_ℓ is called the shift and P_ℓ is called the penetration factor which is proportional to the fraction of incident particles on a sphere of radius $r=r_c$ which penetrates the sphere.[15]

Returning to the expression for the elastic cross section in terms of the scattering matrix,

$$\sigma_{e\ell} = \pi\lambda^2 \sum_\ell (2\ell+1)\,|1 - U_\ell|^2 \tag{173}$$

Equating the above equation with Eq. (168), we get

$$\sum_\ell (2\ell+1)\,|1 - U_\ell|^2 = (2\ell^2+1)\,\frac{\Gamma^2}{(E - E'_\lambda) + \frac{1}{2}\Gamma^2} \tag{174}$$

We can solve this quadratic equation for Γ. Let us consider the case for $\ell = 0$; then we have

$$|1 - U_o|^2\,[(E - E'_\lambda) + 0.5\,\Gamma^2] = \Gamma^2 \tag{175}$$

for resonance energy $E_{lab} = 14$ MeV and $V_o = -100$ MeV, and $W = -1.0$ MeV and $E = 25$ MeV, and from Fig. 17, we have $ReU_\ell = 0.32$. Then in terms of

the real part of the scattering matrix we have

$$\Gamma^2 = \frac{11|1-U|^2}{(1-0.5|1-U|^2)} \tag{176}$$

where we have $\Gamma \cong 0.82$ MeV.

Compound nuclear reactions will proceed more slowly than direct reactions because of the time involved in compound nuclear formation and resonant channel decay. If we consider the typical "nuclear period", the average time taken for a bound nucleon to cross the nucleus and considering E = 25 MeV to be a typical kinetic energy, then $\tau = 1/3\ A^{1/3} \times 10^{-22}$ sec. The corresponding width is about $\Gamma = 13/A^{1/3}$ MeV. For our ^{24}Mg case this gives us $\tau = 9.6 \times 10^{-23}$ sec and $\Gamma \cong 4.51$ MeV. The imaginary part of the nuclear potential is usually taken to be $W \sim 1$ to 10 MeV. The lifetime of the incident channel is the same order or less than the typical nuclear period, as we see from our calculation, Eq. (176).

The existence of narrow resonance shows directly that long-lived compound systems formed by the target nucleus and incident nucleus exist.

It should be noted that alpha decay involves strong interactions which proceed rapidly as opposed to weak interactions which proceed more slowly, of the order of magnitude $\tau \sim 10^{-9}$ sec. Alpha processes are hindered (see Section III) and the ^{212}Po alpha decay of $t_{1/2} = 3 \times 10^{-7}$ sec is the shortest alpha decay rate. In the region of the s-d shell (in the next section) alpha emission is often associated with other de-excitation processes, such as alpha emission occurring subsequently to beta decay as a delayed process.

We can analyze the observed energy resonance as single-particle alpha resonances; that is, as resonances involving the alpha particle which is already formed and has an identity in the nuclear interior.

We determined the theoretical time for an alpha to escape, in terms of its traversed time once around the nuclear interior as $\tau = 9.6 \times 10^{-23}$ sec. The time calculated in terms of the single-particle resonances gives $\tau = 2.66 \times 10^{-24}$ sec, implying that the alpha particle escapes before it traverses once around the nucleus. The reason actual alpha decay rates are much larger is because alpha formation involves a many-body problem and one must include the probability of formation, calculated in terms of a many-nucleon system, in terms of the frequency of nucleon collision as well as the barrier penetration probability after an identifiable alpha cluster has formed. The actual decay width is expressed as the product of reduced width (related to the formation time of the alpha particle) and the barrier penetration factor (which can be expressed as an exponential attenuation of an integral in the WKB approximation which depends on the barrier height and thickness). The reduced width relates to the spin orientation of the nuclear particles and the Pauli exclusion principle and is therefore expressable in terms of Clebsch-Gordon coefficients.

In looking at the one-level expression for decay rates, we have assumed that all resonances are isolated. This is not always the case. If we call the full width at half maximum, Γ (associated with the lifetime of the resonance and the Poincaré resonance), and D (associated with the natural period decay time), then we have two conditions. First, if $\Gamma < D$, then we have isolated resonances; and if $\Gamma \ll D$, these resonances

are very well separated. Second, if $\Gamma > D$, then the resonances are not well isolated and may overlap. Third, if $\Gamma \sim D$, there may be some overlapping of resonances. In our example calculation for ^{24}Mg, W = -1.0 MeV and $\ell = 5$ (Fig. 27f), we found Γ = 12.5 MeV and from before (page 188) D = 4.51 MeV, which would imply that our resonances are not completely separated so that background effects can occur. In our example case, the resonances appear quite isolated but there are other cases, W = -1.0 MeV, $\ell = 6$ (Fig. 27h) where overlapping resonances are apparent with at least two major resonances appearing.

5. General discussion of the alpha decay of nuclei in the first half of the s-d shell

Alpha emission occurs predominantly in elements heavier than lead but there are lighter alpha emitters. The predominant de-excitation process for light nuclei is γ and β decay, and in some cases, proton emission. In some light nuclei, alpha decay will result as a secondary process after another de-excitation process. Alpha particle resonance states occur, particularly in the deformed region between the Z (proton) and N (neutron) magic numbers of 8 and 20. Alpha decay occurs because the helium ion (four nucleons in the $1s_{1/2}$ shell with zero angular momentum) is an unusually stable entity. In the deformed region from Z, N of 10 to 14, alpha resonances occur where Z and N = 14 is about the center of this deformed region. Most models invoke an inert ^{16}O case with extra nucleon[8] excitation. The spectra of the nuclei in Fig. 32 display the 0^+, 2^+, 4^+, etc. rotational spectra. There are also levels such as the 3^+ (5.24 MeV) and 3^- (7.62 MeV) in ^{24}Mg, which may be explained as a particle-hole excitation.

Fig. 32. Energy levels of even-even nuclei in the 2s1d shell for ^{16}O, ^{20}Ne, ^{24}Mg, and ^{28}Si are displayed. Alpha resonances for ^{24}Ne and ^{24}Mg are also given. Ref. 98 gives spectra for A = 18 to 20 and Ref. 99 gives spectra for A = 21 to 44. We also utilized information from Ref. 100. The alpha decay from the ^{24}Mg to ^{20}Ne branch and ^{28}Si to ^{24}Mg branch are both about 0.01%.

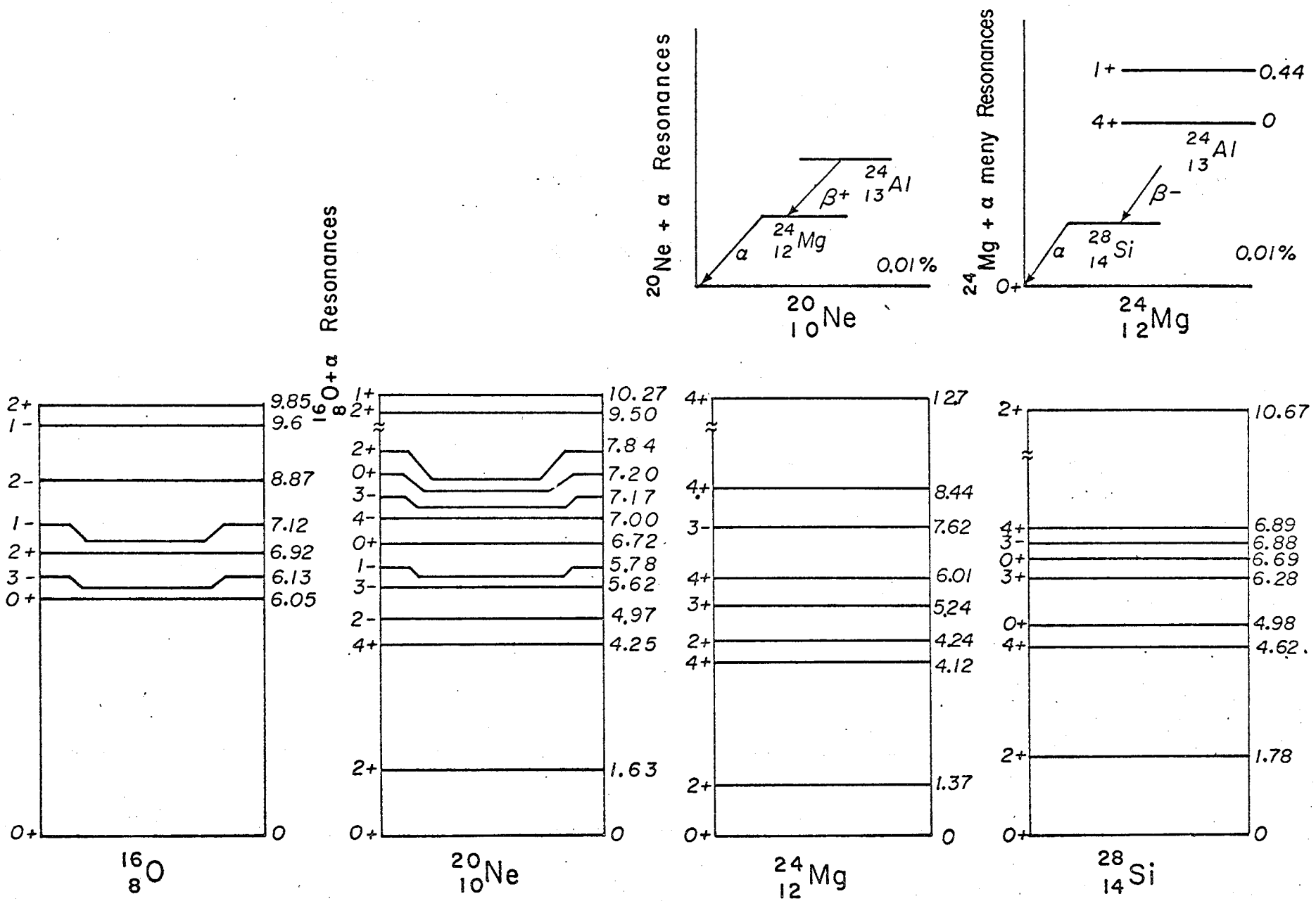
^{20}Ne + α Resonances
$^{24}_{13}$Al
β+
$^{24}_{12}$Mg
α
0.01%
$^{20}_{10}$Ne
^{24}Mg + α meny Resonances
1+ 0.44
4+ 0
$^{24}_{13}$Al
β−
$^{28}_{14}$Si
α
0.01%
0+
$^{24}_{12}$Mg
$^{16}_{8}$O+α Resonances
2+ 9.85
1− 9.6
2− 8.87
1− 7.12
2+ 6.92
3− 6.13
0+ 6.05
0+ 0
$^{16}_{8}$O
1+ 10.27
2+ 9.50
2+ 7.84
0+ 7.20
3− 7.17
4− 7.00
0+ 6.72
1− 5.78
3− 5.62
2− 4.97
4+ 4.25
2+ 1.63
0+ 0
$^{20}_{10}$Ne
4+ 12.7
4+ 8.44
3− 7.62
4+ 6.01
3+ 5.24
2+ 4.24
4+ 4.12
2+ 1.37
0+ 0
$^{24}_{12}$Mg
2+ 10.67
4+ 6.89
3− 6.88
0+ 6.69
3+ 6.28
0+ 4.98
4+ 4.62
2+ 1.78
0+ 0
$^{28}_{14}$Si
XBL785-986

Figure 32

CONCLUSION

We have examined a number of aspects of the alpha decay problem. Calculations have been made in terms of single-particle shell-model wave functions and collective rotational and vibrational states. Some aspects of the alpha decay theory which we have explored are

1) the relative alpha decay rate dependence on the optical model well depth and on the boundary condition matching radius,
2) the alpha cluster formation probability and properties of the barrier penetration,
3) effects of the relative alpha decay rate by electrostatic and nuclear channel coupling of vibrational and rotational excitations
4) alpha decay of even-even and odd-even isotopes is light, heavy and transuranium elements,
5) assumptions about the projection of the orbital angular momentum for $K_i = K_f$ or $m_\ell = 0$ on the nucleon surface,
6) some possible properties of intermediate "doorway" channel states,
7) compound and single particle resonance states.

Throughout the relatively long history of alpha theory and experiment spanning well over 50 years, this problem has been subjected to a number of types of analysis, each one found to be wanting, incomplete or inadequate. At present no comprehensive or complete model of alpha decay exists. This situation is certainly not due to a lack of diligence on the researcher's part, but on the difficulty of the problem. In order to

explore the various aspects of this complex problem, we have developed some graphic techniques in the form of Argand diagrams of the complex elements of the scattering matrix and through this type of analysis, it is hoped that we can better understand the complicated competing mechanisms that make up the alpha decay processes.

We shall now briefly review some of the nuclear systems which we have examined in detail, suggesting some areas for further investigation of this fascinating, unfolding mystery of nuclear matter in dynamic action.

We have made use of the coupled channel formalism for the alpha decay of even- and odd-mass medium-heavy and heavy nuclei to calculate the relative width of decay. We examined the effect of electromagnetic and nuclear coupling on the alpha decay of $\ell = 18$, ^{212m}Po and ^{212}Po ground state decay to the vibrational states of ^{208}Pb and also the ^{210}Pb decay to ^{206}Pb. The excitation of the collective states of the spherically symmetric ^{208}Pb in the macroscopic model and also the microscopic shell model wave functions for the alpha decay to ^{208}Pb and ^{206}Pb daughters were also considered. Our emphasis has been on the calculations involving ground-ground state decay without coupling due to phonon-phonon interactions. We could extend the model to include inward integration starting with a finite amplitude in the excited channels, which we did not do for purposes of the present calculation. This may augment the fit for larger nuclear radii for the ^{212m}Po to ^{208}Pb decay.

Alpha decay in spheroidal nuclei have been examined for the odd-mass parent nuclei, ^{253}Es and ^{255}Fm, to the $7/2^+$ ground state and rotational excited state rotational bounds. Properties on the nuclear surface and coupling to vibrational and rotational excitation on channel coupling has

been examined in detail because of the relative success we had with the model for even-even alpha decay. Although channel coupling improved the fit to the relative intensities to the ground and excited states of the daughter, an exact fit has not been obtained as we have discussed in detail in the text. It may prove useful to extend our coupled channel exploration to incorporate other coupled channel mechanisms thatn the coupling terms we used for the purpose of the present calculation.

We also examined the nuclear reaction or R-matrix unified theory which utilized the time-dependent method. It was hoped that we can calculate absolute alpha decay widths which are not being dependent on the nuclear radius. The new theory has the advantage that it is possible to calculate a reasonable fit to the ^{212}Po and ^{210}Po alpha absolute alpha widths but they are still dependent on the well-depth parameter. For the present calculation, we did not include channel coupling effects which can be included in the future. Also the optical model parameters utilized for the purpose of the present calculation did not contain a finite imaginary part of the potential, i.e., we used $W = 0$ only.

In recent years a major assumption about the mechanism of alpha decay process is that the most influential region of the nucleus on the alpha decay rate is due to effects occurring at the nuclear surface. It is assumed that the alpha particle is most likely to form on the surface and that the barrier penetration occurs, localized to the nuclear surface region, and has a significant effect on the alpha decay rate. The imaginary part of the Woods-Saxon potential in the DWBA approximation weights the surface region the most heavily. Also, channel coupling usually is designed to emphasize surface effects. In our R-matrix approach, we calculate the

absolute decay rate as a volume integral over the entire nucleus so that inclusion of $W \neq 0$ and coupling terms would certainly modify our boundary conditions and perhaps the final results. It may possibly be that a more realistic theory should emphasize surface effects but we feel that processes in the nuclear interior should not be neglected. These boundary conditions would attenuate the alpha wave $\varphi_\alpha(r)$ in the nuclear interior.

Further work utilizing the R-matrix formalism could be extended to coupling conditions which include octupole-octupole two-phonon surface vibrations. The RPA approximation would be reasonable since vibrational levels have greater spacing than the rotational levels. Since our present R-matrix calculation yields such promising results, certainly future work by this or other researchers is warranted.

We also exmained in detail, the qualitative structure of the S-matrix for the (α,α') scattering on the ^{24}Mg, 0^+ ground state nuclei with a view towards developing techniques to help elucidate certain aspects of the alpha decay mechanism. Channel coupling to the various predominantly rotational levels of the daughter has been included. The qualitative features of the complex S-matrix elements in the energy and momentum planes may yield information about nuclear surface and interior clustering phenomena.

We have developed a method to graphically represent and analyze the alpha decay process in terms of the scattering of alpha particles in elastic and a few inelastic channels and compound nuclear resonance decay. It is hoped that these high-powered techniques from high-energy nuclear scattering will give us a more comprehensive understanding of the alpha decay process and of nuclear structure, and allow us to calculate absolute

decay width reasonably independent of the nuclear optical model parameters.

We have discussed in detail the graphic interpretation of the information displayed in the Argand diagrams. From the behavior of the complex part of the S-matrix elements, we can gain a better understanding of the relationship of single-particle and compound nuclear resonance states. The use of the graphics of the Argand diagram plots can assist greatly in the interpretation and development of a better understanding of the alpha decay process. We can explore further the contributions to the lifetime of alpha resonance states from the time to form an alpha cluster and the time necessary for barrier penetration of the alpha cluster. We can further explore how resonances overlap and if there are other mechanisms involved in alpha decay than

1) cluster formation probability,
2) nuclear and electrostatic channel coupling,
3) barrier penetration probabilities,
4) compound nuclear resonances states, and
5) intermediate nucleon transfer reactions.

How each of these processes contributes to the branching ratios and decay probabilities will certainly further our understanding of the alpha decay process as well as our understanding of the mystery and complexity of the nuclear interior.

ACKNOWLEDGMENTS

The assistance and encouragement of Professor G. T. Seaborg and Professor J. Cerny is greatly appreciated. The continuing support, assistance and advice of Professor G. Chew has been significant towards the completion of this and other projects. The advice, assistance and encouragement of H. Mullins and Dr. D. Chew facilitated and was instrumental in the completion of this project. The conferences and suggestions of Professor J. O. Rasmussen, Dr. A. J. Soinski and Professor K. McVoy were most fruitful as were those with Dr. K. Harada. The use of the SCATER2 S-matrix code formulated by Dr. N. K. Glendenning and the advice of N. Brown and C. Quong in the use of this program led to some most interesting calculations.

The conferences and support of this work by Dr. H. Puthoff and R. Targ as well as J. Reynolds are significant to this project's completion as well as the support of Prof. P. Lieber and his encouragement and the support of the PF Foundation of New York and the Orb Foundation of London. The interest and comments of J. Oldham and B. Balanda were also helpful as well as the advice of Prof. O. Chamberlain, Prof. E. Teller, Prof. E. Wichman, and Prof. L. Alvarez. C. Frank's, L. Lizama's and G. Perry's assistance is also acknowledged. A very special acknowledgment for the continuing advice, support and patient encouragement is given to Dr. P. J. Webster and C. E. Webster. The excellent typing of the manuscript by Deberah Olson is greatly appreciated.

This work was performed under the auspices of the U.S. Department of Energy.

REFERENCES

1. A.J.Soinski, E.A.Rauscher, J.O.Rasmussen, and D.G.Raich, Nucl. Phys. A283, 413 (1977).
2. T.Tamura, Rev. Mod. Phys. 37, 679 (1965).
3. E.A.Rauscher, J.O.Rasmussen, and K.Harada, Nucl. Phys. A94, 33 (1967).
4. A.J.Soinski, R.B.Frankel, Q.O.Navarro, and D.A.Shirley, Phys. Rev. C2, 2379 (1970).
5. J.O.Rasmussen, Arkiv. Fysik 7, 185 (1953).
6. A.Bohr, P.O.Fröman, and B.R.Mottelson, Mat. Fys. Skr. Dan. Vid. Selk. 29, No. 10 (1975).
7. H.Feshbach, Ann. Phys. 5, 357 (1958).
8. A.M.Lane and R.G.Thomas, Rev. Mod. Phys. 30, 257 (1958).
9. K.Harada, Prog. Theoret. Phys. 26, 667 (1961).
10. K.Harada and E.A.Rauscher, Phys. Rev. 169, 818 (1968).
11. H.A.Bethe, Rev. Mod. Phys. 9, 69 (1937).
12. G.Gamow, Zeits F. Physic 52, 510 (1924).
13. R.G.Thomas, Phys. Rev. 97, 224 (1955).
14. H.J.Mang, Annl. Rev. Nucl. Sci. 14, 1 (1964).
15. M.A.Preston, Phys. Rev. 75, 90 (1949).
16. J.O.Rasmussen, in Alpha-, beta- and gamma-ray spectroscopy, edited by K.Siegbahn (North Holland Publ., Amsterdam, 1965), Chap. 11, p.701.
17. J.O.Rasmussen and B.Segall, Phys. Rev. 103, 1298 (1956).
18. H.J.Mang, Z. Phys. 148, 572 (1957).
19. J.K.Poggenburg, Ph.D. Thesis, Lawrence Radiation Laboratory Report UCRL-16187 (August 1965)(unpublished).

20. P.O.Froman, Mat. Fys. Skr. Dan Vid. Selsk. 1, No. 3 (1957).

21. N.K.Glendenning and K.Harada, Nucl. Phys. 72, 481 (1965).

22. I.Perlman, F.Asaro, A.Ghiorso, A.Larsh, and R.Latimer, Phys. Rev. 127, 917 (1962).

23. H.Feshbach, Ann. Phys. 19, 287 (1962).

24. L.McFadden and G.R.Satchler, Nucl. Phys. 84, 177 (1966).

25. H.V.Gillet, A.M.Green, and E.A.Sanderson, Phys. Lett. 11, 44 (1964).

26. W.T.Pinkston, Nucl. Phys. 37, 312 (1962).

27. W.W.True and W.T.Pinkston, Phys. Rev. 168, 1388 (1968), and private communication.

28. H.D.Zeh, Z. Phys. 175, 490 (1963).

29. J.O.Rasmussen, Nucl. Phys. 44, 93 (1963).

30. J.Blomqvist and S.Wahlborn, Ark. Phys. 16, No. 46 (1960).

31. R.G.Thomas, Prog. Theor. Phys. 12, 253 (1954).

32. A.M.Lane and E.D.Pendlebury, Nucl. Phys. 15, 39 (1960).

33. J.O.Rasmussen and E.R.Hansen, Phys. Rev. 109, 1656 (1958).

34. E.A.Rauscher, Lawrence Radiation Laboratory Report UCRL-11875 (January 1965)(unpublished).

35. A.Bohr and B.R.Mottelson, Mat. Fys. Skr. Dan Vid. Selsk. 27, No. 16 (1953).

36. H.J.Mang and J.O.Rasmussen, Mat. Fys. Skr. Dan. Vid. Selsk. 2, No. 3 (1962). The author appreciates the helpful discussions with J.O.Rasmussen on this interpretation.

37. I.Perlman and J.O.Rasmussen, Handbuch der Physik, Vol. 42 (Springer-Verlag, Berlin, 1957).

38. R.R.Chasman and J.O.Rasmussen, Phys. Rev. 115, 1257 (1959).

39. I.Ahmad, F.T.Porter, M.S.Freedman, R.F.Barnes, R.K.Sjoblom, Phys. Rev. C2, 390 (1971); I.Ahmad and J.Milstead, Nucl. Phys. A239, 1 (1975).

40. F.Asaro, S.G.Thompson, F.S.Stephens, and I.Perlman, Proceedings of the Internat'l Conf. on Nuclear Structure, Kingston, Jamaica, edited by D.A.Bromley and E.W.Vogt (Univ. of Toronto Press, Toronto, Canada, 1960), p.581.

41. I.Ahmad, private communication, 1974.

42. F.Asaro, S.Bjørnholm, and I.Perlman, Phys. Rev. 133, 3291 (1964).

43. A.J.Soinski, Thesis, Lawrence Berkeley Laboratory Report LBL-3411 (September 1974)(unpublished).

44. Z.Syzmanski, S.Wycech, C.Gustafson, I.Lamn, P.Moeller, and B.Nilsson, Nucl. Phys. A131, 1 (1969).

45. H.C.Pauli, Phys. Rep. 7C, 35 (1973).

46. L.S.Goodman, H.Diamond, and H.Stanton, 166th Annual Meeting of the ACS (Chicago 1973), Abstract No. NUCL 35.

47. M.Abramowitz, in Handbook of Mathematical Functions, edited by M.Abramowitz and I.A.Stegun (National Bureau of Standards, Washington D.C., 1964), p.537; and C.Fröberg, Rev. Mod. Phys. 27, 399 (1955).

48. A.J.Soinski, E.A.Rauscher, J.O.Rasmussen, and D.G.Raich, LBL Nuclear Science Annual Report, LBL-5057, 296 (1975).

49. J.O.Rasmussen and E.R.Hansen, Phys. Rev. 109, 1656 (1956).

50. A.Bohr and B.R.Mottelson, Mat. Fhys. Skr. Dan. Vid. Selsk. 22, No. 16 (1953).

51. Y.A.Ellis and M.R.Schmorak, Nucl. Data Sheets 8, 345 (1972).

52. J.K.Poggenburg, H.J.Mang, and J.O.Rasmussen, Phys. Rev. 181, 1697 (1969).

53. P.O.Fröman, Kgl. Danske Videnskab. Selskab. Mat.-Fys. Medd. Skrifter 1, No. 3 (1957).

54. L.A.Malov and V.G.Soloviev, Sov. J. Nucl. Phys. 5, 403 (1967).

55. F.A.Gareev, S.P.Ivanova, L.A.Malov, and S.G.Soloviev, Nucl. Phys. A171, 134 (1971).

56. J.O.Rasmussen and A.J.Soinski, private communication, Lawrence Berkeley Laboratory (1975).

57. H.J.Mang, Phys. Rev. 119, 1069 (1960).

58. H.Feshbach, A.K.Kerman, and R.H.Lemmer, Ann. Phys. 41, 230 (1967).

59. H.M.A.Rodi, A.A.Shihab-Eldon, and J.O.Rasmussen, Lawrence Berkeley Laboratory Report LBL-5071 (October 1976)(submitted to Phys. Rev.).

60. H.Casimir, Physica 1, 193 (1934).

61. H.J.Mang, Lawrence Berkeley Laboratory Report UCRL-8931 (October 1959)(unpublished).

62. M.L.Goldberger and K.M.Watson, Collision Theory (Wiley & Sons, New York, 1964).

63. M.L.Schiff, Quantum Mechanics (McGraw-Hill, New York, 1955), p.239.

64. D.H.Wilkinson, Proceedings of the Rutherford Conf. on Nuclear Structure (1961), p.339.

65. W.J.Thompson, G.E.Crawford, and R.H.Davis, Nucl. Phys. A98, 288 (1967).

66. S.G.Kadmenskii, V.E.Kalechits, and A.A.Martyov, Sov. J. Nucl. Phys. 14, 193 (1972).

67. M.Rotenberg and L.Wilets, Phys. Rev. 110, 1126 (1950).

68. M.Bohr, Nature 137, 344 (1936).

69. V.H.Weisskopf and E.P.Wigner, Z. Physik 63, 54 (1930).

70. G.Breit and E.P.Wigner, Phys. Rev. 49, 519 (1936).

71. G.Breit, Phys. Rev. 40, 127 (1932).

72. P.L.Kapur and R.E.Peierls, Proc. Roy. Soc. (London) A166, 277 (1938).

73. E.P.Wigner and L.Eisenbud, Phys. Rev. 72, 29 (1947).

74. T.Shibata, H.Ejiri, J.Chiba, S.Nagamiya, K.Nakai, R.Anholt, H.Bowman, J.G.Ioannou, E.A.Rauscher, and J.O.Rasmussen, Lawrence Berkeley Laboratory Report LBL-4398 Rev. (February 1978).

75. G.Breit, Phys. Rev. 58, 506 (1940).

76. A.S.Saperstein, Ann. Phys. 37, 209 (1966).

77. H.A.Weidenmüller, Ann. Phys. 28, 60 (1964).

78. C.Mahaux and A.A.Weidenmüller, Ann. Phys. 32, 259 (1965).

79. G.Breit, Rev. Mod. Phys. 23, 147 (1959).

80. N.K.Glendenning, Nucl. Phys. A117, 49 (1968) and private communication, Lawrence Berkeley Laboratory. The author appreciates the use of the program SCATER2.

81. N.Austern and J.S.Blair, Ann. Phys. 33, 15 (1965).

82. A.Springer, Lawrence Berkeley Laboratory, Ph.D. Thesis, UCRL-11708 (October 1964)(unpublished).

83. J.Wills, University of Washington, Ph.D. Thesis (1963)(unpublished).

84. S.G.Nilsson, Lawrence Berkeley Laboratory Report UCRL-18355 Rev. (September 1968)(unpublished).

85. D.A.Goldberg, S.M.Smith, and G.F.Bundzik, Phys. Rev. 10C, 1362 (1974).

86. E.A.Rauscher, A.J.Soinski, J.O.Rasmussen, Bull. Am. Phys. Soc. 23, 37 (1978).

87. H.Yukawa, Proc. Phys. Math. Soc. Japan 17, 48 (1935).

88. Proceedings International Conf. on Clustering Phenomena in Nuclei, International Atomic Energy Agency, Vienna (1969).

89. G.J.Wozniak, D.P.Shahel, J.Cerny, and N.A.Jelley, Phys. Rev. C14, 815 (1976).

90. J.O.Rasmussen, private communication (May 5, 1977).

91. K.W.McVoy, Ann. Phys. 43, 91 (1967).

92. K.W.McVoy, "Nuclear Resonance Reactions and S-Matrix Analyticity," Chapter 8 of Fundamentals in Nuclear Theory (International Atomic Energy Agency, Vienna, 1967).

93. K.W.McVoy, private communication, August 1978.

94. G.J.Goebel and K.W.McVoy, Nucl. Phys. A115, 504 (1968).

95. W.Tobocman, Phys. Rev. 174, 1115 (1968), and private communication (1968).

96. W.Tobocman, Phys. Rev. 173, 1047 (1968).

97. F.T.Smith, Phys. Rev. 118, 349 (1960).

98. F.Ajzenberg-Selove, Nucl. Phys. A190, 1 (1972).

99. P.M.Endt and C.Van der Leun, Nucl. Phys. A214, 1 (1973).

100. C.M.Lederer and V.S.Shirley, eds., Table of Isotopes, 7th edition (John Wiley & Sons, New York, 1978).

101. J.Bar-touv and I.Kelson, Phys. Rev. 142, 599 (1966).

102. W.H.Bassichis, C.A.Levinson, and I.Kelson, Phys. Rev. 136, B380 (1964).

103. J.Bar-touv and I.Kelson, Phys. Rev. 5B, 1035 (1965).

104. I.Kelson and C.A.Levinson, Phys. Rev. 134, B269 (1964).

105. J.W.Clark and T.P.Wang, Ann. Phys. 40, 127 (1966).

This report was done with support from the Department of Energy. Any conclusions or opinions expressed in this report represent solely those of the author(s) and not necessarily those of The Regents of the University of California, the Lawrence Berkeley Laboratory or the Department of Energy.